TESIS DE LA UNIVERSIDAD DE ZARAGOZA
2022
119

Carlos Mallor Turón

A Probabilistic Analysis Method for Fatigue Crack Growth in Metal Components: Application to the Damage Tolerance Assessment of Railway Axles

Director/es
Calvo Molina, Susana
Núñez Bruis, José Luis

ISSN 2254-7606

Prensas de la Universidad
Universidad Zaragoza

ISSN 2254-7606

Universidad Zaragoza
1542

Tesis Doctoral

A PROBABILISTIC ANALYSIS METHOD FOR FATIGUE CRACK GROWTH IN METAL COMPONENTS: APPLICATION TO THE DAMAGE TOLERANCE ASSESSMENT OF RAILWAY AXLES

Autor

Carlos Mallor Turón

Director/es

Calvo Molina, Susana
Núñez Bruis, José Luis

UNIVERSIDAD DE ZARAGOZA
Escuela de Doctorado

Programa de Doctorado en Ingeniería Mecánica

2022

Universidad Zaragoza
1542

Tesis Doctoral

A Probabilistic Analysis Method for Fatigue Crack Growth in Metal Components: Application to the Damage Tolerance Assessment of Railway Axles

Autor

Carlos Mallor Turón

Directores

Susana Calvo Molina

José Luis Núñez Bruis

Tutor

Miguel Ángel Martínez Barca

Escuela de Doctorado de la Universidad de Zaragoza
Programa de Doctorado en Ingeniería Mecánica

2022

A mi familia

«Es una verdad muy cierta que, cuando no está en nuestro poder discernir lo más verdadero, debemos seguir lo más probable». René Descartes. *Discurso del Método*, 1637.

Agradecimientos

Resulta paradójico, pero escribir los agradecimientos es quizás una de las partes más difíciles del trabajo, ya que hay que pensar en todas aquellas personas que de una forma u otra han colaborado a lo largo de la realización de la tesis, lo cual no es nada sencillo. Muchos y de diversa índole son los agradecimientos que quiero expresar, puesto que de la interacción con todas estas personas me llevo muchas de las experiencias más enriquecedoras en esta etapa de mi vida.

Mi más sincero agradecimiento a Susana Calvo y José Luis Núñez, directores de esta tesis, sin cuyos consejos, guía y permanente ánimo no hubiera sido posible la realización del presente trabajo. Quiero hacer especial énfasis en agradecer la oportunidad que me han dado, la confianza depositada para desarrollar el trabajo con total libertad, así como el interés mostrado por mis ideas y aportaciones.

Agradecer a Miguel Ángel Martínez, tutor de esta tesis por parte de la Universidad de Zaragoza, su total predisposición, profesionalidad y diligencia a la hora de ayudarme con todo lo relativo a la universidad.

A los compañeros del Instituto Tecnológico de Aragón, especialmente a todo aquel con el que haya dedicado tiempo a debatir sobre temas relacionados con esta tesis.

Cumplidas las formalidades:

A mis amigos de Híjar, los que siempre están ahí.

A mi amigo Alberto de Urrea, la universidad no hubiese sido lo mismo sin él.

A los amantes del esquí de montaña *Los sobrinos*, por alcanzar siempre la cima.

A mi primo Javi, por ser desde pequeños mi referente en la informática.

A mi hermana Marina, porque, aunque seamos diferentes me apoya (casi siempre).

A mis padres, por darme todo a su alcance en la vida.

A Raquel, porque las personas que te quieren te animan a crecer como persona.

Carlos, 17 de marzo de 2022.

Abstract

With the fast development of the railway industry, more and more challenges arise for the safety and reliability of critical components, among which fatigue is the primary problem. During service, the rolling stock undergoes extremely complex cyclic loads, which can lead to a number of fatigue problems. These difficulties seriously threaten the safety of railway operation and can even cause significant loss of life and property. Although scientists and engineers worldwide have made extraordinary efforts over the past centuries, there are still many challenges and uncertainties, especially in developing the next generation of means of transport.

This thesis intends to tackle a number of issues on the fatigue of railway axles. The topics include, but are not limited to, analytical, theoretical, and computational research on: (i) failure mechanisms, fatigue crack growth; (ii) modelling the fatigue process; (iii) probabilistic assessment methods of application to the railway axle problem; (iv) strengthening uncertainty propagation methodologies via first and second-order approximations; (v) fatigue performance and degradation characterized through stochastic moments and lifespan probability distributions; (vi) fatigue assessment and maintenance by means of periodic inspections; and (vii) identification and approval of the fatigue performance by means of methods with probabilistic foundations for the determination of inspection intervals and the associated probabilities of crack detection.

This thesis starts from the early developments of railway axles safety assessment and its evolution. It continues with an extension of widespread methods for probabilistic analysis of general-purpose especially suitable for the fatigue crack growth phenomenon in metal components. It then gives an extension of damage tolerance approaches with identification and particular emphasis on the characterization of its probabilistic aspects and their effects, resulting in a procedure for the determination of inspection intervals that is based on a probabilistic description of fatigue lifespan. And finally, it ends with a thorough illustration of the probabilistic methodology devised to be applied to the damage tolerance assessment of railway axles. On the whole, this thesis presents new probabilistic treatments and useful results for the maintenance planning of railway axles within the frame of damage tolerance.

In particular, to define inspection intervals that ensure a continuous and safe operation of a damage-tolerant railway axle, a reliable estimation of its life considering the potential fatigue crack growth is required. For fatigue life estimation, the NASGRO crack growth equation is ordinarily used in its deterministic standard form. Due to the uncertainties involved in the fatigue process, inspections must be devised not only considering the uncertainties in the performance of the inspection technique, but also based on a probabilistic lifespan prediction. To this end, the uncertainty propagation of fatigue crack growth life provides the probability distribution of the lifespan needed for probabilistic damage tolerance analysis and for structural integrity assessment and management.

Given these premises, this thesis presents a procedure for the determination of inspection intervals that uses a fatigue crack growth life estimation based on the lifespan probability distribution. In the course of the work, a new probabilistic formulation for fatigue crack propagation based on the NASGRO equation is developed. It provides a stochastic approach for predicting statistical moments of fatigue lifetime. The procedure basically uses the full second-order approach to approximate the first four moments of the fatigue crack growth life. The methodology efficiently estimates the expected value, first raw moment; the variance, second central moment; the skewness, third central standardized moment; and the kurtosis, fourth central standardized moment, of the underlying fatigue crack growth life distribution. These moments are obtained from the approximation via the Taylor series up to the quadratic terms, full second-order, of the NASGRO equation with respect to the random input variables taken into account. Subsequently, the location, scale and shape parameters of the particular Pearson distribution type automatically determined are estimated, making the statistical moments of the constructed lifespan distribution match the first four prescribed moments predicted by the probabilistic equations. Thereafter, the procedure devised extends the current damage tolerance principles in railway axles by means of improving the relevance of the crack growth simulation, replacing its deterministic estimation by a probabilistic one. Thereby, the damage tolerance assessment benefits from a better knowledge of the distribution of fatigue lifespan. As a result, it gives a more conservative recommendation for the definition of inspection intervals as it considers the effects of the process variables randomness in the fatigue lifespan, as it relies on a probabilistic fatigue propagation instead of on a deterministic one. The procedure developed extends the current state of the art in damage tolerance of railway axles, considering the fatigue crack growth from a probabilistic point of view.

The proposed reliability-based inspection planning method is discussed through a numerical example regarding the fatigue crack growth in a railway axle under stochastic considerations. The validity of the proposed method is verified by taking into account several input random variables whose variability, distribution type, and correlations are thoroughly grounded. The inspection intervals are further assessed in terms of the overall probability of detecting cracks in successive inspections and

in terms of probability of failure, considering the probability of detection curve of the non-destructive testing technique. The methodology presented enables an efficient and accurate quantification of the lifespan uncertainties via its probabilistic distribution. The probabilistic results are compared with Monte Carlo simulations to check the goodness of the first four moments predicted, as well as the quality of the probability density function constructed. It is proven that the probability density function of the lifespan is properly derived by the methodology, without knowing or assuming the output probability distribution beforehand. The procedure developed provides recommendation for the calculation and definition of practical inspection intervals and the associated inspection techniques that can be used in ensuring the continued safe operation of railway axles.

In summary, this thesis provides a probabilistic analysis method for fatigue crack growth in metal components. Moreover, it offers an efficient procedure for the definition of maintenance inspection intervals of railway axles, considering complex stochastic scenarios within the damage tolerance assessment. Approaches for the design and analysis of products with special consideration for the ecological and economic impacts associated with their manufacture and maintenance, strive for products which make the lowest possible environmental impact throughout its life cycle. The method provided is expected to have a positive and comprehensive effect on the optimization of maintenance intervals, thus promoting an efficient use of rail transport to carry people and freight. In this sense, it would also reduce the environmental impact of mankind associated with air pollution caused by transport, as it helps rail transport to become a more environmentally friendly alternative. As a final consideration, the novel operational framework in this thesis is expected to be an asset for a broad range of engineering problems dealing with random variables.

Keywords: Probabilistic fatigue crack growth; Fatigue life prediction; Damage tolerance; Railway axles; Uncertainty propagation; Statistical moments; NASGRO; Lifespan probability distribution; Pearson distribution family; Inspection intervals; Probability of detection.

Resumen

Con el rápido desarrollo de la industria ferroviaria, surgen cada vez más retos en la seguridad y la fiabilidad de componentes críticos, entre los cuales la fatiga es el problema principal. En servicio, el material rodante está sujeto a cargas cíclicas extremadamente complejas, que pueden dar lugar a una serie de problemas de fatiga. Estas dificultades amenazan seriamente la seguridad ferroviaria y pueden llegar a causar importantes pérdidas en términos de vidas y bienes. Aunque científicos e ingenieros de todo el mundo han realizado esfuerzos extraordinarios durante los últimos siglos, existen todavía muchos desafíos e incertidumbres, especialmente en el desarrollo de la próxima generación de medios de transporte.

Esta tesis pretende abordar una serie de cuestiones relativas a la fatiga en ejes ferroviarios. Los temas incluyen, entre otros, la investigación analítica, teórica y computacional acerca de: (i) mecanismos de fallo, crecimiento de grieta por fatiga; (ii) modelización del proceso de fatiga; (iii) métodos de evaluación probabilista de aplicación en ejes ferroviarios; (iv) refuerzo de las metodologías de propagación de incertidumbre mediante aproximaciones de primer y segundo orden; (v) rendimiento y degradación por fatiga caracterizados mediante momentos estocásticos y distribuciones de probabilidad de vida; (vi) evaluación de la fatiga y el mantenimiento mediante inspecciones periódicas; y (vii) identificación y validación del comportamiento a fatiga mediante métodos con base probabilista para la determinación de intervalos de inspección y probabilidades de detección de grieta asociadas.

Esta tesis parte de los primeros desarrollos en la evaluación de la seguridad de ejes ferroviarios y su evolución. Continúa con una extensión de los métodos habituales para el análisis probabilista de propósito general especialmente adecuados para el fenómeno de crecimiento de grieta por fatiga en componentes metálicos. A continuación, ofrece una extensión de los enfoques de tolerancia al daño con identificación y particular énfasis en la caracterización de sus aspectos probabilistas y sus efectos, lo que resulta en un procedimiento para la determinación de intervalos de inspección basado en una descripción probabilista de la vida a fatiga. Finalmente termina con una ilustración detallada de la metodología probabilista concebida para ser aplicada en la evaluación de tolerancia al daño de ejes ferroviarios. En su conjunto, esta tesis presenta nuevos tratamientos probabilistas y resultados útiles para la planificación del mantenimiento de ejes ferroviarios en el marco de tolerancia al daño.

En particular, para definir intervalos de inspección que garanticen un funcionamiento continuo y seguro de un eje ferroviario tolerante al daño, se requiere una estimación fiable de su vida considerando un potencial crecimiento de grieta por fatiga. Para la estimación de la vida a fatiga, normalmente se utiliza la ecuación de crecimiento de grieta de NASGRO en su forma estándar determinista. Debido a las incertidumbres en el proceso de fatiga, las inspecciones deben diseñarse no sólo considerando las incertidumbres en el buen funcionamiento de la técnica de inspección, sino también basándose en una predicción probabilista de la vida. Para ello, la propagación de incertidumbre en la vida en crecimiento de grieta por fatiga proporciona la distribución de probabilidad de la vida necesaria para el análisis probabilista de tolerancia al daño y para la evaluación y control de la integridad estructural.

Con estas premisas, esta tesis presenta un procedimiento para la determinación de intervalos de inspección que utiliza una estimación de la vida en crecimiento de grieta por fatiga basada en la distribución de probabilidad de la vida. Durante el trabajo, se desarrolla una nueva formulación probabilista para el crecimiento de grieta por fatiga basada en la ecuación NASGRO. Esta proporciona un enfoque estocástico para predecir los momentos estadísticos de la vida a fatiga. El procedimiento básicamente usa un enfoque de segundo orden completo para aproximar los cuatro primeros momentos de la vida a fatiga. La metodología estima eficientemente el valor esperado, primer momento; la varianza, segundo momento central; la asimetría, tercer momento central estandarizado; y la curtosis, cuarto momento central estandarizado, de la distribución subyacente de la vida a fatiga. Estos momentos se obtienen a partir de la aproximación mediante serie de Taylor hasta términos cuadráticos, de segundo orden completo, de la ecuación NASGRO con respecto a las variables aleatorias de entrada consideradas. A continuación, se estiman los parámetros de localización, escala y forma del tipo particular de distribución de Pearson determinada automáticamente, haciendo que los momentos estadísticos de la distribución de vida construida coincidan con los cuatro primeros momentos estimados por las ecuaciones probabilistas. A partir de ahí, el procedimiento ideado amplía los principios actuales de tolerancia al daño en ejes ferroviarios mediante mejoras en la relevancia de la simulación del crecimiento de la grieta, sustituyendo su estimación determinista por una probabilista. De esta forma, la evaluación de tolerancia al daño resulta beneficiada por un mejor conocimiento de la distribución de la vida a fatiga. Como resultado, ofrece una recomendación más conservadora para la definición de intervalos de inspección dado que considera los efectos de la aleatoriedad de las variables del proceso en la vida a fatiga, ya que se basa en crecimiento de grieta probabilista en lugar de uno determinista. El procedimiento desarrollado extiende el estado del arte actual en materia de tolerancia al daño en ejes ferroviarios, considerando el crecimiento de la grieta por fatiga desde un punto de vista probabilista.

El método propuesto para la planificación de inspecciones basado en fiabilidad se discute mediante un ejemplo numérico relacionado con el crecimiento de grieta por

fatiga en un eje ferroviario bajo consideraciones estocásticas. La validez del método propuesto se verifica teniendo en cuenta distintas variables aleatorias de entrada cuya variabilidad, tipo de distribución y correlaciones quedan exhaustivamente fundamentadas. Los intervalos de inspección se evalúan además en términos globales de probabilidad de detección de grieta en inspecciones sucesivas y en términos de probabilidad de fallo, considerando la curva de probabilidad de detección de la técnica de ensayo no destructivo. La metodología presentada permite una cuantificación eficaz y precisa de las incertidumbres en la vida a través de su distribución probabilista. Los resultados probabilistas se comparan con simulaciones de Monte Carlo para verificar la bondad de los cuatro primeros momentos estimados, así como la calidad de la función de densidad de probabilidad construida. Se comprueba que la función de densidad de probabilidad de la vida es derivada adecuadamente mediante la metodología, sin conocer ni suponer de antemano la distribución de probabilidad de salida. El procedimiento desarrollado proporciona recomendaciones para el cálculo y la definición de intervalos de inspección prácticos y las técnicas de inspección asociadas que se pueden utilizar para garantizar la operación continua y segura de ejes ferroviarios.

En resumen, esta tesis proporciona un método de análisis probabilista para el crecimiento de grieta por fatiga en componentes metálicos. Además, ofrece un procedimiento eficiente para la definición de intervalos de inspección en el mantenimiento de ejes ferroviarios, considerando escenarios estocásticos complejos dentro del enfoque de tolerancia al daño. Planteamientos de diseño y análisis de productos con especial consideración de los impactos ecológicos y económicos asociados a su fabricación y mantenimiento, se esfuerzan por conseguir productos que tengan el menor impacto ambiental a lo largo de su ciclo de vida. Se espera que el método proporcionado tenga un efecto positivo y global en la optimización de intervalos de mantenimiento, promoviendo así un uso eficiente del transporte ferroviario para mover personas y mercancías. En este sentido, también disminuiría el impacto medioambiental de la humanidad asociado con la contaminación atmosférica causada por el transporte, ya que ayuda a que el transporte ferroviario sea en una alternativa más respetuosa con el medio ambiente. Como consideración final, se espera que el novedoso marco operativo en esta tesis sea un recurso para una amplia gama de problemas de ingeniería que tratan con variables aleatorias.

Palabras clave: Crecimiento de grieta por fatiga probabilista; predicción de vida a fatiga; Tolerancia al daño; Ejes de ferrocarril; Propagación de incertidumbre; Momentos estadísticos; NASGRO; Distribución de probabilidad de vida; Distribuciones de Pearson; Intervalos de inspección; Probabilidad de detección.

Contents

Page

Agradecimientos **v**

Abstract **vii**

Resumen **xi**

Contents **xv**

Nomenclature **xix**

Background and Outline **1**

Chapter 1 State of the art **9**

1.1 Evolution of safety assessment of railway axles 9
1.1.1 The rise of railways 10
1.1.2 Railway accidents involving axle failure 13
1.1.3 Research on fatigue cracks in railway axles 17
1.1.4 Design, manufacture and maintenance of wheelsets 19
1.1.5 Safety assessment levels for railway axles 27
1.2 Fundamentals of damage tolerance 31
1.2.1 Damage concepts, behaviour and effects 31
1.2.2 Basics of fracture mechanics 33
1.2.3 Stress intensity factor evaluation 38
1.2.4 Material characterization 40
1.2.5 Stable fatigue crack propagation 43
1.2.6 Damage tolerance assessment of railway axles 46
1.3 Probabilistic aspects of damage tolerance 50
1.3.1 Probabilistic fatigue crack growth 51
1.3.2 Material scatter 54
1.3.3 Variable amplitude loading 58
1.3.4 Flying ballast impacts 60
1.3.5 Reliability of probability of detection 62
1.4 Probabilistic approaches in mechanical engineering 64
1.4.1 Simulation-based methods 66
1.4.2 Local expansion-based methods 66
1.4.3 Functional expansion-based methods 68
1.4.4 Most probable point-based methods 69

1.4.5 Frequentist . . . 69
1.4.6 Bayesian . . . 70
1.5 European initiatives related to rail transport . . . 70
1.5.1 European Green Deal . . . 71
1.5.2 European Year of Rail 2021 . . . 71
1.5.3 Europe's Rail Joint Undertaking . . . 73
1.6 Discussion of open points to be covered . . . 76

Chapter 2 Full second-order approach for the moments of functions of random variables 81
2.1 Introduction . . . 81
2.2 Abbreviations and conventions . . . 83
2.3 Linear combinations: matrix form . . . 88
2.3.1 Expected value . . . 90
2.3.2 Covariance matrix: variance and covariance . . . 90
2.4 Non-linear combinations: matrix form . . . 90
2.4.1 Expected value first-order . . . 93
2.4.2 Expected value second-order . . . 94
2.4.3 Covariance matrix: variance and covariance first-order . . . 95
2.5 Non-linear combinations: summation notation . . . 98
2.5.1 Expected value second-order . . . 100
2.5.2 Expected value first-order . . . 101
2.5.3 Variance second-order . . . 101
2.5.4 Variance first-order . . . 105
2.5.5 Third central moment *skewness* second-order . . . 106
2.5.6 Third central moment *skewness* first-order . . . 112
2.5.7 Fourth central moment *kurtosis* second-order . . . 112
2.5.8 Fourth central moment *kurtosis* first-order . . . 121

Chapter 3 Probabilistic fatigue crack growth methodology in the damage tolerance assessment of railway axles 123
3.1 Introduction . . . 123
3.2 Fatigue crack growth model . . . 127
3.2.1 Deterministic NASGRO equation . . . 127
3.2.2 Probabilistic NASGRO equations . . . 128
3.2.3 Stress intensity factor evaluation: weight functions . . . 131
3.3 Pearson distribution family fit from prescribed moments . . . 133
3.4 Use of probabilistic fatigue life estimation in defining inspection intervals for railway axles . . . 135
3.4.1 Steps of the damage tolerance analysis . . . 135
3.4.2 Probabilistic fatigue crack growth life . . . 137
3.4.3 Reliability-based inspection interval definition . . . 138
3.5 Performance of the non-destructive inspection methods . . . 142

Chapter 4 Application examples **147**
4.1 Introduction . . . 147
4.2 Case study definition: railway axle . . . 149
4.3 Random variables . . . 156
4.4 Putting It All Together (PIAT) . . . 161
4.4.1 Monte Carlo (MC) results . . . 162
4.4.2 Full Second Order Approach (FSOA) results . . . 164
4.4.3 Summary and comparison of the eight case scenarios . . . 168
4.4.4 Probability distribution reconstruction . . . 174
4.4.5 Definition of inspection intervals . . . 180
4.4.6 Probabilities of successful inspections . . . 184

Chapter 5 Conclusions and Outlook **195**
5.1 Conclusions . . . 195
5.2 Conclusiones . . . 198
5.3 Original contributions . . . 201
5.4 Aportaciones originales . . . 202
5.5 Future work . . . 203
5.6 Trabajo futuro . . . 206

Appendix A Full second-order approach assuming independence **209**
A.1 Abbreviations and conventions: moments of the joint distribution. . . 209
A.2 Non-linear combinations: summation notation assuming independence 214
A.2.1 Expected value second-order . . . 214
A.2.2 Expected value first-order . . . 214
A.2.3 Variance second-order . . . 214
A.2.4 Variance first-order . . . 216
A.2.5 Third central moment *skewness* second-order . . . 217
A.2.6 Third central moment *skewness* first-order . . . 225
A.2.7 Fourth central moment *kurtosis* second-order . . . 225
A.2.8 Fourth central moment *kurtosis* first-order . . . 245

Appendix B Variance of the sum of random variables **247**
B.1 Proof . . . 248

Appendix C Full second order approach application to NASGRO **249**
C.1 Taylor approximation up to second order . . . 250
C.2 First moment: expected value . . . 250
C.3 Second central moment: variance . . . 251
C.4 Third central moment: *skewness* . . . 253
C.5 Fourth central moment: *kurtosis* . . . 254

Bibliography **257**

Nomenclature

The following lists collect the main terminology used in this thesis. The meaning of each symbol is also detailed in the text where the symbol is used.

Acronyms and Abbreviations

C(T)	compact-tension
CCDF	complementary of the cumulative distribution function
CDF	cumulative distribution function
CPOD	cumulative probability of detection in successive inspections
CPOF	cumulative probability of failure in successive inspections
CPOND	cumulative probability of non-detection in successive inspections
Det.	deterministic
DTA	damage tolerance analysis
e.g.	exempli gratia
EPFM	elastic plastic fracture mechanics
Eq.	Equation
ERA	European railway agency
EU-Rail	Europe's rail joint undertaking
FCG	fatigue crack growth
FEM	finite element method
Fig.	Figure
FORM	first-order reliability method
FOSM	first-order second moment
FSOA	full second-order approach
GHG	greenhouse gas

i.e.	id est
LCC	life cycle cost
LEFM	linear elastic fracture mechanics
LPG	liquefied petroleum gas
M(T)	middle-tension
MC	Monte Carlo
MPI	magnetic particle inspection
MPP	most probable point
MT	magnetic particle testing
NDI	non-destructive inspection
NDT	non-destructive testing
PCC	Pearson correlation coefficient
PCE	polynomial chaos expansion
PDF	probability density function
PIAT	putting it all together
POD	probability of detection
POND	probability of non-detection
Pr. Eq.	probabilistic equation
Pr. Eqs.	probabilistic equations
r.v.	random variable
SF	survival function
SIF	stress intensity factor
SORM	second-order reliability method
SOSM	second-order second moment
UT	ultrasonic testing
vs.	versus
VT	visual testing
w/o	without

Latin alphabet

A	crack deepest point
a	crack depth / normal semiaxis
a_0	El-Haddad's parameter
a_1, a_2	real roots of the quadratic equation in the denominator of the integral of the Pearson solution
B	specimen thickness
B	crack surface point
b	crack width at the surface
C	parameter of the crack growth equation in the Paris region
c	crack tangential semiaxis
C_{th}^{m}	parameter for the ΔK_{th_0}–R relationship
C_{th}^{p}	parameter for the ΔK_{th_0}–R relationship
d	random variables number
da/dN	crack growth rate
e^{μ}	scale parameter of the log-normal distribution
f	Newman's crack opening function
f_N	probability density function of the random variable fatigue life N
$f(x;\alpha,\beta)$	probability density function for the standardized beta prime distribution
$f(x;\sigma)$	probability density function for the standardized log-normal distribution
$\mathcal{G}$	energy release rate
$\mathcal{G}_c$	critical energy release rate
$g_{,j}$	first partial derivative of g with respect to X_j $\left(=\frac{\partial g}{\partial X_j}\right)$
$g_{,jk}$	second partial derivative of g with respect to X_j and X_k $\left(=\frac{\partial^2 g}{\partial X_j \partial X_k}\right)$
g_{μ}	evaluation of $g(X)$ at P vector
K	stress intensity factor
K_c	critical stress intensity factor for static unstable crack growth
$\mathrm{Log}\mathcal{N}$	log-normal distribution
M	bending moment

$m(x,a)$	weight functions
N	mileage, number of equivalent km
$\mathcal{N}$	normal distribution
N	number of applied loading cycles
n	exponent of the crack growth equation in the Paris region
ns	steps number
n_{times}	number of times that the crack can be detected before a failure could occur
o_0, o_1, o_2	zeroth, first and second order terms of the Taylor approximation
P	applied load
P	mean value vector of X $(= (\mu_{X_1}, \mu_{X_2}, \ldots, \mu_{X_d}))$
p	parameter describing the sigmoidal shape of the crack growth equation in the threshold region
P_f	probability of failure
$p(x)$	Pearson probability density function
q	parameter describing the sigmoidal shape of the crack growth equation in the toughness region
R	stress ratio $(= \sigma_{min}/\sigma_{max})$
S_{max}	maximum applied stress
T_{ins}	periodicity of NDT inspections or inspection interval
W	specimen width
X	set of random variables $(= \{X_1, X_2, \ldots, X_d\})$
x	radial coordinate direction at the axle surface
Y	general shape function for stress intensity factors
Y	general multivariate function $(= g(X))$

Greek alphabet

α	plane stress/strain constraint factor
α, β	shape parameters of the beta prime distribution
β	reliability index EN 1990:2002
β_{1_Y}	square of skewness of Y $\left(= \text{Skew}\,(Y)^2\right)$
β_{2_Y}	kurtosis of Y $\left(= \text{Kurt}\,(Y) = \frac{\mu_{Y,4}}{\sigma_Y^4}\right)$
γ_{1_Y}	skewness of Y $\left(= \text{Skew}\,(Y) = \frac{\mu_{Y,3}}{\sigma_Y^3}\right)$
$\Gamma\,(x)$	gamma function $(= (x-1)\,!)$
Δa	crack depth increment at point a
Δb	crack depth increment at point b
ΔK	stress intensity factor range
E	Young's modulus
λ	location parameter of the log-normal and beta prime distributions
λ	failure rate
μ_{jk}	second central moment $(= \mu_2\,(X_j, X_k))$
μ_{jkl}	third central moment $(= \mu_3\,(X_j, X_k, X_l))$
μ_{jklm}	fourth central moment $(= \mu_4\,(X_j, X_k, X_l, X_m))$
μ_Y	expected value of Y $(= \text{E}\,[Y])$
μ_{Y_3}	third central moment of Y $\left(= \text{E}\left[(Y - \text{E}\,[Y])^3\right]\right)$
μ_{Y_4}	fourth central moment of Y $\left(= \text{E}\left[(Y - \text{E}\,[Y])^4\right]\right)$
ν	Poisson's ratio
σ	shape parameter of the log-normal distribution
σ	stress
σ_0	flow stress
σ_Y	standard deviation of Y $(= \text{SD}\,(Y))$
σ_Y^2	variance of Y $(= \text{Var}\,(Y))$
$\Phi\,(x)$	cumulative distribution function for the standard normal distribution
$\phi\,(x)$	probability density function for the standard normal distribution

Superscripts

B	above σ referring to the bending loading case
$B+I$	above σ referring to the bending plus interference loading cases
I	above σ referring to the interference loading case
i	step increment
m	minus
p	plus

Subscripts

a	below σ or K, referring to amplitude value
c	critical
def	below N referring to the definition of inspection intervals
eff	effective
fin	final
I, II, III	below K referring to the cracking mode
$\#i$	inspection number
ini	initial
$j, k, l, m,$ r, s, t, u	index from 1 to d random variables
m	below σ or K, referring to mean value
max	maximum
min	minimum
n	below μ, referring to n^{th} central moment
$POD\%$	below a referring to the crack depth at which the selected NDI gets a POD equal to the detection threshold
th	threshold
$th0$	threshold at $R = 0$

Background and Outline

Motivation

Nowadays, evidence of climate change is almost everywhere. There is scientific consensus that the climate is warming and that it is caused by human activities. Responding to these changes involves taking actions to limit the amount of warming via increasing energy efficiency, among other actions.

One of the challenges is related to mobility planning and management. To reduce the environmental impact due to air pollution caused by road vehicles, the entire transport system needs to be rethought. To tackle this issue, an approach may be to increase the use of rail transport to carry people and freight. However, the railway system has to be carefully managed and maintained in order to be a feasible alternative.

Railway axles have been widely adopted components for some two hundred years. They have played and still play an important role in scientific research, promoting the historical development of scientific and engineering knowledge about the fatigue of materials and structures. The fatigue of components became noticeable mainly as a result of some dramatic railway axle failures. It is significant to highlight, on one hand, that they are safety-critical components, whose failure can lead to catastrophic consequences. On the other one, there is an increasing need for optimizing the maintenance costs and operations related to the inspections during the railway axle service life.

Despite the vast amount of technical and scientific studies on the fatigue life prediction of railway axles, they are nowadays still designed against fatigue limits and mostly based on progressed experience. As a result of these approaches, although a high level of safety has been reached, it is difficult to go a step further in the attempt to optimise the design and the costs associated with their maintenance. For this reason, new trends in the design and management of railway axles against fatigue are moving towards damage tolerance assessment. This approach, a trend in the railway field, considers the progressive degradation and damage to the axle along its lifetime.

Fatigue and fracture mechanics approaches are frequently used to determine service life and inspection intervals. Several aspects contribute to reliable estimation of the fatigue lifetime of railway axles and, consequently, appropriate intervals planing. It is important to note that much of what happens in the real world, however, is not predictable with a hundred per cent certainty. There are uncertainties inherent to materials and components that cannot be quantified, and thus, there is an awareness that not all factors are well known and characterized. In fact, a structure may contain a number of flaws of various sizes. There is an inherent scatter in initial material quality and performance. The nature of the loads may be non-proportional comprising a spectrum of different amplitudes. In addition, the projected use of the component in the determination of applied stresses is inaccurate at best and subject to many discrepancies between predicted and actual usage. Owing to these complexities, fracture and fatigue crack growth should be viewed probabilistically rather than deterministically. All these factors have to be taken into account to determine a potential life distribution based on a combination of the aforementioned stochastic variables. All the previous aspects leave many points that are still open, consequently, further efforts are required in this field. In this sense, the development of advanced high-reliability technologies to maximize the service life, safety and availability of railway vehicles for its service, is of great importance.

In this context, the work in this thesis focuses on the probabilistic estimation of fatigue crack growth life to assess the railway axle reliability within the damage tolerance concept. Following the rigorous progress of previous researchers, it is necessary to investigate and develop probabilistic methodologies of general applicability in academia and industry. The quantification of uncertainty as a design strategy will replace the current design philosophy based on safety margins at least in state-of-the-art technological fields such as the railway axles.

Additionally, it should be noted that the actions in which this thesis is enclosed, such as the evaluation of the behaviour of materials and structural analysis of components, concerning safety, reliability or durability, are aligned with the current social challenge related to climate neutrality. In other words, the development of methodologies that help to extend the service life of a product by reducing the energy resources associated with its manufacture and maintenance, contribute to the protection of the environment.

In summary, the general motivation of the thesis is to contribute to the competitiveness of the railway sector and its environmental sustainability through the development of technologies that, through the integration of probabilistic simulation techniques and damage tolerance analysis concepts, allow predicting the functional behaviour and the service life of railway axles to improve the final performance of the products and to extend their life by making efficient use of materials and energy.

Objectives

The main objective of this thesis is the development of a novel computational methodology for the probabilistic analysis of fatigue crack growth in metal components that allows evaluating the reliability of an axle within the damage tolerance concept.

The specific objectives of this thesis are the following:

- Acknowledging the significance of replacing current traditional deterministic methods by probabilistic approaches for fatigue crack growth life estimation.
- Developing a probabilistic approach for the fatigue crack growth (FCG) in metal components on the basis of a well-supported deterministic FCG model.
- Determining the stress distribution on the crack by using numerical techniques based on the finite element method (FEM).
- Optimizing the calculation the stress intensity factor (SIF). Applying numerical methods based on FEM and SIF estimation based on efficient weight functions.
- Developing an efficient and general probabilistic FCG model. Checking the results by comparison with Monte Carlo (MC) method.
- Adopting a procedure for probability distribution fit based on the Pearson distribution family to reconstruct the underlying fatigue lifespan distribution.
- Combining probabilistic developments with reliability principles. Expanding damage tolerance techniques concerning reliability. Proposing damage tolerance strategies in relation to probability of detection (POD).
- Addressing the problem of inspection interval definition in the decision-making process of defining maintenance schedules of railway axles.
- Devising a reliability-based inspection planning that enables the optimization of maintenance costs selecting an appropriate inspection periodicity for axles.
- Ensuring higher reliability in the determination of the probability of failure by using the results of a probabilistic fatigue life estimation.
- Presenting different illustrative examples of the application of the devised probabilistic damage tolerance-based maintenance planning for railway axles thorough the consideration of different combinations of random input variables.
- Providing a tool that introduces a probabilistic approach to derive the probability of fatigue crack growth life as an output random property and ensure transferability from the probabilistic life estimation to real railways axles.

Outline

The outline of the thesis is as follows:

- In *Chapter 1 – State of the art*, the evolution of safety assessment of railway axles is briefly introduced. Subsequently, the fundamentals of the damage tolerance assessment are described. On this basis, probabilistic aspects of damage tolerance and different probabilistic approaches in mechanical engineering are reviewed. And finally, some European initiatives related to rail transport are outlined. Some gaps in our knowledge of the fatigue crack growth in the damage tolerance assessment of railway axles are identified and the need for optimizing the definition of inspection intervals of railway axles is emphasised.
- In *Chapter 2 – Full second-order approach for the moments of functions of random variables*, the derivation of the general method is presented in detail both in matrix form and summation notation. It offers a full second-order probabilistic formulation to predict the statistical moments, expected value, variance, skewness, and kurtosis, of an arbitrary model or system, using information about the input random variables distribution.
- In *Chapter 3 – Probabilistic fatigue crack growth methodology in the damage tolerance assessment of railway axles*, a novel, simple and stable procedure is introduced to the definition of inspection periodicities for railway axles. It is grounded on the use of probabilistic fatigue life estimation, considering the NASGRO equation and using weight functions for stress intensity factor evaluation. The procedure redefines the fatigue crack growth process from a deterministic to a probabilistic point of view. The overall procedure follows the steps of the damage tolerance analysis considering the probabilistic fatigue crack growth life adjusted using the Pearson distribution family. The distribution fit is done from prescribed moments provided by the full second-order approach derived in the previous chapter. In the end, the methodology provides a reliability-based inspection interval definition that is appropriate for scheduling the non-destructive inspection techniques frequently used in railway axles.
- In *Chapter 4 – Application examples*, the validation of the methods is done. The example considers a metal railway axle with an initial crack. The probabilistic analyses of the fatigue process consider several input random variables whose variability, distribution type, and correlations are thoroughly grounded when exemplifying the calculation workflow, promoting a deep understanding of their effects. Finally, all the ideas presented in the chapters of this thesis are put together, illustrating the course of reasoning for building a link between the full second-order approach applied to the fatigue crack growth process and the damage tolerance analysis of railway axles to define inspection intervals.

- In *Chapter 5 – Conclusions and Outlook*, the general conclusions of this study are drawn, the original contributions introduced in this research are stated and interesting possibilities for future work are discussed in the field of probabilistic fatigue. Special emphasis is placed on the major findings, consequential conclusions and open questions, as well as the need for further research. In summary, it is a celebration of my cumulative work and puts an end to this thesis.

Scientific production

The research developed in this thesis has been disseminated by the PhD candidate through the following journal articles and oral presentations in conferences.

- Journal publications indexed in the Science Citation Index Expanded (SCIE), included in the Journal Citation Reports (JCR) with Impact Factor (IF):

  1. **C. Mallor**, S. Calvo, J. L. Núñez, R. Rodríguez-Barrachina and A. Landaberea. Full Second-Order Approach for Expected Value and Variance Prediction of Probabilistic Fatigue Crack Growth Life. *International Journal of Fatigue*, 133: 105454, 2020.

  2. **C. Mallor**, S. Calvo, J. L. Núñez, R. Rodríguez-Barrachina and A. Landaberea. Uncertainty Propagation Using the Full Second-Order Approach for Probabilistic Fatigue Crack Growth Life. *International Journal of Numerical Methods for Calculation and Design in Engineering (RIMNI)*, 36: 37, 2020.

  3. M. Sánchez, **C. Mallor**, M. Canales, S. Calvo and J. L. Núñez. Digital Image Correlation Parameters Optimized for the Characterization of Fatigue Crack Growth Life. *Measurement*, 174: 109082, 2021.

- Journal publications indexed in the Emerging Sources Citation Index (ESCI):

  1. **C. Mallor**, S. Calvo, J. L. Núñez, R. Rodríguez-Barrachina and A. Landaberea. A Probabilistic Fatigue Crack Growth Life Approach to the Definition of Inspection Intervals for Railway Axles. *Frattura ed Integrita Strutturale - Fracture and Structural Integrity*, 59: 359–373, 2022.

- Journal publications indexed in INSPEC and Scopus:

    1. **C. Mallor**, S. Calvo, J. L. Núñez, R. Rodríguez-Barrachina and A. Landaberea. Propagation of Uncertainty in Fatigue Crack Growth for Probabilistic Life Estimation. *Procedia Structural Integrity*, 28: 619–626, 2020.

    2. **C. Mallor**, S. Calvo, J. L. Núñez, R. Rodríguez-Barrachina and A. Landaberea. On the Use of Probabilistic Fatigue Life Estimation in Defining Inspection Intervals for Railway Axles. *Procedia Structural Integrity*, 33: 391–401, 2021.

- International conferences:

    1. Oral presentation "Propagation of Uncertainty in Fatigue Crack Growth for Probabilistic Life Estimation". In: 1st Virtual European Conference on Fracture (VECF1), European Structural Integrity Society (ESIS), on-line, 29th of June 2020.

    2. Oral presentation "On the Use of Probabilistic Fatigue Life Estimation in Defining Inspection Intervals for Railway Axles". In: 26th International Conference on Fracture and Structural Integrity (IGF26), Italian Group of Fracture (IGF), on-line, 26th of May 2021.

- Iberian conferences:

    1. Compilation of proceedings "Uncertainty Propagation Using the Full Second-Order Approach for Probabilistic Fatigue Crack Growth Life". In: 1th Virtual Iberian Conference on Structural Integrity (VIbCSI1), Portuguese Structural Integrity Society and the Spanish Group of Fracture, Coimbra (Portugal), 2020.

- National conferences:

    1. **C. Mallor**, R. Rodríguez-Barrachina, J. L. Núñez, A. Landaberea and S. Calvo. Enfoque de Segundo Orden Completo para la Predicción del Valor Esperado y Varianza de la Vida a Fatiga en el Crecimiento de Grieta Probabilista. *Anales de Mecánica de la Fractura*. 36: 27-33, 2019. Presentación oral. En: Congreso del grupo Español de Fractura (GEF) edición 36, Sevilla, 3 a 5 de abril de 2019.

    2. M. Sánchez, S. Calvo, M. Canales, **C. Mallor** and R. Rodríguez-Barrachina. Método de Correlación Digital de Imágenes (DIC) para Medidas de Crecimiento de Grieta en Probetas No Estándar. *Anales de Mecánica de la Fractura*. 36: 46-51, 2019. Presentación oral. En: Congreso del grupo Español de Fractura (GEF) edición 36, Sevilla, 3 a 5 de abril de 2019.

- Universidad de Zaragoza conferences:

    1. Presentación oral “Metodología para el Análisis Probabilista del Crecimiento de Grieta por Fatiga en Componentes Metálicos. Avances y Resultados Provisionales”. En: VI Jornada de Doctorandos del Programa de Doctorado en Ingeniería Mecánica (PDIM), Zaragoza, 18 de junio 2019.
    2. Presentación oral “Metodología para el Análisis Probabilista del Crecimiento de Grieta por Fatiga en Componentes Metálicos. Avances y Resultados”. En: VII Jornada de Doctorandos del Programa de Doctorado en Ingeniería Mecánica (PDIM), Zaragoza, 18 de diciembre 2020.

1

State of the art

1.1 Evolution of safety assessment of railway axles

Modern railway axles are highly stressed safety-critical components, which are costly to maintain in service due, among other things, to the lack of adequate information on which to base rational inspection intervals. Railway axle failures may result in derailments, with serious damage for the rolling stock, the infrastructure, injuries to passengers, and it can lead to casualties in the most dramatic cases. Therefore, railway axle resistance to failure is a key issue in designing and properly maintaining railway wheelsets, to ensure high safety levels and, at the same time, to optimize life-cycle costs from an overall point of view. Railway axles are designed, manufactured and maintained so that they should not fail in service, typically targeting a lifetime up to 30–40 years of service what involves a mileage within the range 10^6–10^7 km depending on the usage, such as, freight, commuter or high-speed trains. The vast amount of km involves many wheelset turns, and therefore many reversals in the loads on the axle what clearly induces fatigue stress in the component due to the repetition of loading cycles. The increasing demand for higher axle loads at the turn of the 21st century presents quite new challenges with regard to safety issues that require further developments in operation, technology and regulation. The previous figures at a glance give the idea that there is room for improvement and optimization of such inspection intervals for railway axles maintenance. The design of a maintenance plan must maximise operational safety levels while minimising management costs.

In this section, an overview of the rise of the use of railways is given. Then, some remarkable examples of railway accidents involving axle failure in-service are described. Next, the fundamental research on early fatigue cracks in railway axles

that promoted the development and research on fatigue theories, is summarized and put into the contemporary context. Afterwards, the prevailing principles regarding design, manufacture and maintenance of wheelsets is broadly explained. Finally, the different safety assessment levels for railway axles are introduced to give the reader insight into the leading-edge railway safety technology.

1.1.1 The rise of railways

The development of railways has been an important driving force for technological progress. From the mid-eighties a dense rail network initiated from Europe, spread all over the world. It is definitely a milestone in human development. Railway systems steadily increased the volume of goods and number of passengers, becoming the predominant transport system within few decades. The speed of travel suddenly increased, leading to a significant reduction in travel times and immense benefits for trade and social interaction. The development of the railways was accompanied by influential advances in many fields, such as steel production and metal components manufacturing. However, the impressive progress involved for the first time, large metal components subjected to high stresses that changed cyclically over a long period of time in the case of axles. The characteristics of these cyclic loads and their effects on the initiation and propagation of cracks in a material, nowadays known as fatigue phenomenon, were completely unknown by that time.

The railway axle, simple component at first glance, has played a key role in the development of the understanding of fatigue. An example of a steel railway axle in a raw manufacturing stage and in a finished stage is shown in Fig. 1.1.

(a) Raw axle. (b) Finished solid axle.

Figure 1.1. Railway axle [1].

A pair of wheels mounted rigidly on a railway axle such that both rotate in unison is a wheelset, as the one presented in Fig. 1.2.

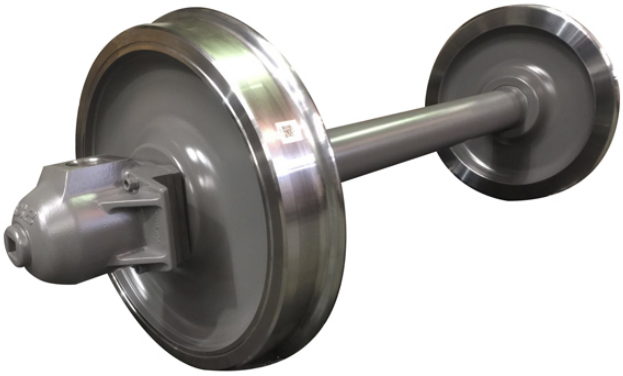

Figure 1.2. Wheelset for a freight wagon [2].

According to the European commission data [3], European countries have deployed, on an average, around 450 km of rail network per 1 million people and about 50 km of rail network per 1000 km^2. Spain in particular has developed about 350 km of rail network per 1 million people and around 30 km of rail network per 1000 km^2. The European railway density in km of railway per 1 million people population and the railway density in km of railway per 1000 km^2 of territory are presented in Fig. 1.3.

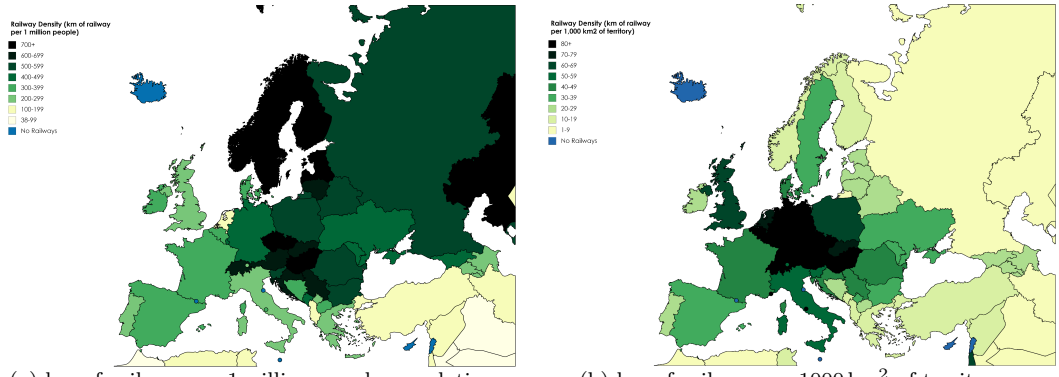

(a) km of railway per 1 million people population. (b) km of railway per 1000 km^2 of territory.

Figure 1.3. Railway density [3, 4].

It is possible to distinguish several networks in the Spanish railway system considering management or administration criteria. The most extensive and with most traffic corresponds to the general interest railway network, i.e. red ferroviaria de interés general (RFIG). In addition, there are regional rail networks, which run entirely through a certain region. The Spanish railway network is presented in Fig. 1.4.

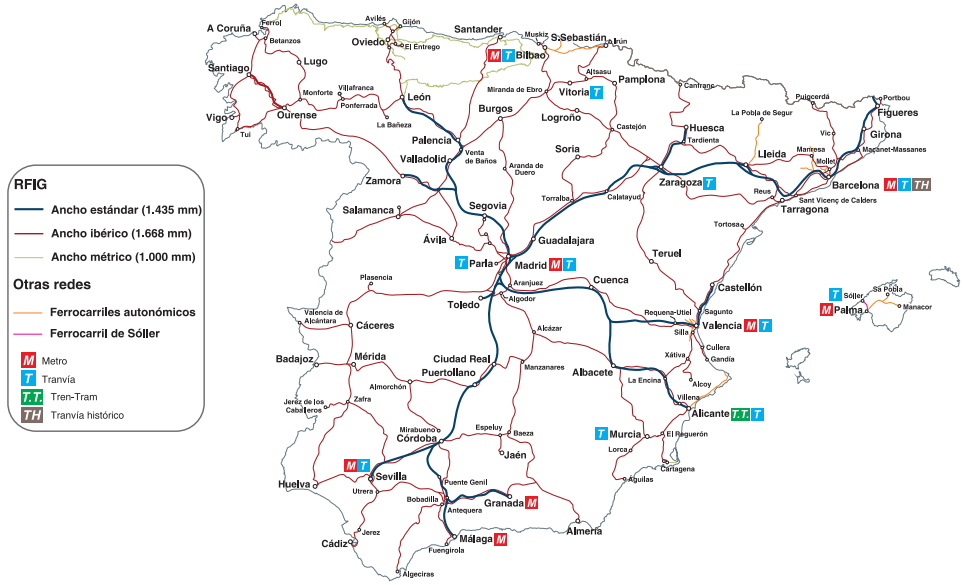

Figure 1.4. Spanish railway network according to its characteristics and managers (31-12-2019) [5].

The evolution of freight transport by rail in Spain in the period 1963-2019, is presented in Fig. 1.5 in million of tons. The freight transport in Spain reached 26 million tons in 2019. It is worth highlighting the growth over the last years in the freight transport carried out by private companies, as a result of the liberalization of the sector.

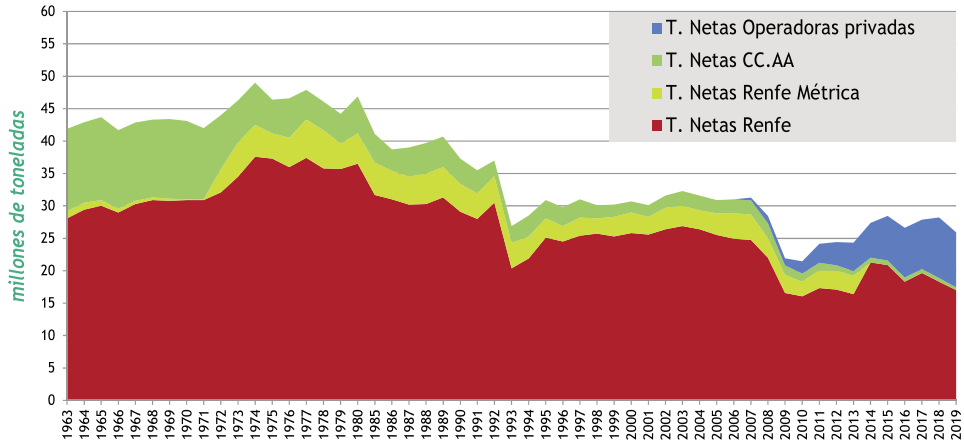

Figure 1.5. Evolution of freight transport by rail in Spain (1963-2019) [million tons] [5].

With the aforementioned figures in mind, is it possible to infer the importance of the rail transport as one of the most suitable forms, where the operation done by a railway company, provides service between train stations or freight customer facilities.

Railway axles are commonly operated over a service life of about 30 years or more which means a high number of loading cycles in the order of 10^9 cycles Smith [6] and Zerbst et al. [7]. The vast amount of cycles involves fatigue stresses due to the repetition. Therefore, railway axles are designed for a long term of operation.

The axles are one of the most essential components of rail systems, as their failure can lead to derailment and, potentially, a major loss of functionality and human casualties. Therefore, axle resistance to failure is a key issue in designing and adequately maintaining railway vehicles, to ensure high safety standards and, at the same time, to optimize life-cycle costs from a railway system point of view. In order to maintain the safety of rail systems, extensive research and experiments have been carried out in a prominent way, and many improvements have been made in the design method, manufacturing, and inspection techniques.

1.1.2 Railway accidents involving axle failure

Breaking railway axles, wheels and rails cause accidents with disastrous consequences for life and property. Axles are historically the weakest component of the wheelset. As aforementioned, railway axles are mechanical components whose failure may produce catastrophic consequences. The following accidents are examples of railway axle failures for which fatigue failure was the main mechanism.

The Versailles accident, France, on the 8th of May 1842. A train crashed between Versailles and Paris. The train was travelling to Paris when it derailed after one of the axles of the leading locomotive broke, and the carriages behind piled into it and caught fire from the engine. Many passengers, ranging between 60–100 or even more as reported in Smith [6] and Smith and Hillmansen [8], died in the fire. It was the deadliest train accident in the world at the time. It was the first railway accident in which major loss of life occurred, and therefore the bad news spread all around the globe. The Versailles railway accident is graphically represented in the lithograph of Fig. 1.6.

It was recognised that the fracture, which caused the railway axle to break, was unusual. The fracture surface was described as being significantly different from the usual appearance of broken iron by slow bending, acknowledged at that time. Nevertheless, it was clearly recognised that the failure occurred after a period of satisfactory service. Metal fatigue was poorly understood these days. This major accident caused by a broken railway axle was one of the key events, and perhaps the most important one, which initiated systematic research into the problem of strength and failure of engineering components.

Figure 1.6. Versailles derailment accident. Courtesy of Bibliothèque nationale de France [9].

The Viareggio accident, Italy, on the 29th of June 2009. A tragic derailment occurred in the Viareggio station. A freight train carrying tank wagons with liquefied petroleum gas (LPG) derailed after a sudden break of the leading axle of the first wagon. After the derailment, the tank wagon overturned and was ripped open by a sharp-edged object and leaked LPG which caught fire, burning a large area around the railway station and killing 32 people Bracciali [10]. This accident is one of the most tragic railway disasters which happened in Europe in the last decades.

An impressive picture of the Viareggio railway accident is shown in Fig. 1.7. From the image it is possible to conceive of the magnitude of the disaster.

Figure 1.7. Viareggio derailment accident [10].

As mentioned, this accident was caused by the fracture of an axle induced by fatigue. An image of the railway axle broken is shown in Fig. 1.8. In the close-up of the broken axle cross-section in Fig. 1.8b, the typical macroscopic progression marks on a fatigue fracture surface are clearly perceivable. These marks are result of the

successive positions of the advancing crack front. Note that these crescent-shaped marks radiate outward from the origin of the crack until the final fracture. The crack origin is approximately located at 4 o'clock of the axle, using as analogy the axle cross-section as a clock. Note also that the marks are often referred to as progression marks, marker bands, or beach marks.

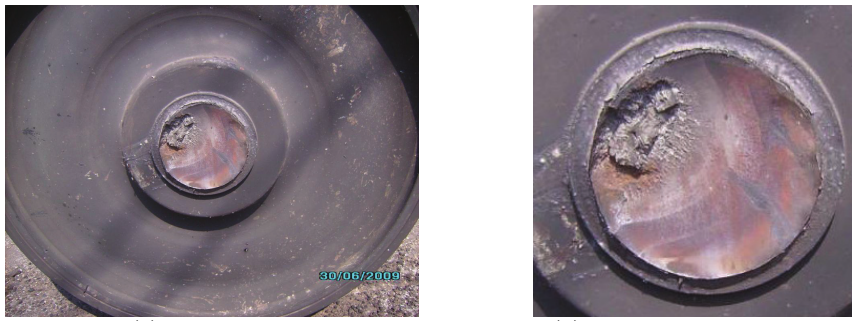

(a) Broken axle. (b) Close-up of the fracture.

Figure 1.8. Cause of the Viareggio accident [10].

Despite almost two hundred years of development, statistics say that broken axles still represent a quite common event. Very interesting reports prepared by the European railway agency (ERA) [11] over the past years provide insight into number of broken axles. These statistics can be found in the reports of ERA on railway safety regarding railway safety performance in the European Union. The data of broken axles collected from 2006 to 2014 is shown in Fig. 1.9.

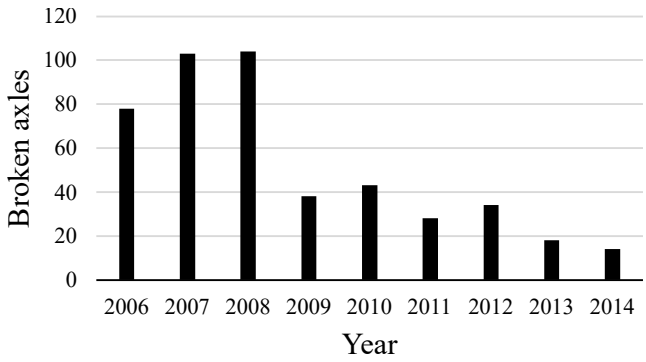

Figure 1.9. Precursors to accidents (EU-28, 2006-2014) [11].

As accidents on railways are rare, the monitoring of all events occurring on railways is an essential tool. Despite gradual improvements in the broken axle data quality, the data may not yet be fully comparable between member states, so certain caution should be exercised when interpreting these data. In any case, it gives insight into the relevance of broken axles in Europe. Note that Fig. 1.9 accounts for all types of train usage, that is, freight, commuter, high-speed trains, etc.

Focusing on freight wagons only, the European Commission set up a Task Force (TF) to discuss the aforementioned axle failures and propose measures on maintenance of freight wagons and in particular of wheelsets. The TF was made up of experts in the field of freight wagon maintenance and railway axles. The population of freight wagon axles at these years was estimated to be 1.6 million in service, running 50 billion km/year what implies an average of 30 000 km/year as the typical travel of a freight axle. The TF released a deliverable [12], which collected the information of a survey about the situation of freight axles failures in the European Union considering the period 2006-2009. A total of 38 cases were reported as shown in Table 1.1.

Table 1.1. Causes and number of axle failures on freight wagons.

Cause	Number	Percentage
Hot axle boxes	30	79 %
Fatigue and corrosion	2	5 %
Fatigue and metallurgic fault	3	8 %
Fatigue (with no further information)	3	8 %

For the sake of clarity, hot axle box is the term used when an axle bearing overheats on a piece of railway rolling stock. Analysing the collected data, the failures caused due to hot axle boxes represent about the 80 % of all failures while fatigue is the other identified cause representing about the 20 %. Moreover, fatigue seems to appear in conjunction with factors such as corrosion or a metallurgic default. Therefore, to improve the previous figures, ensuring that maintenance is adequate is one of the main aspects that must be systematically evaluated.

The axle failure records a number of episodes per year that is still too high. Although, a minor of the total traffic intensity is attributable to freight transport, it has an important portion on the axle failures. Therefore, research actions must focus on the freight sector with particular reference to the transport of dangerous goods. The essential question posed by the recent accidents concerns not only the identification of the cause of the failure in the axle but also the reasons why the progression of the fatigue crack was not discovered during non-destructive inspection (NDI) before the catastrophic failure.

Since railway wheelsets are safety critical components and their failures can cause derailments, deaths and injuries, as mentioned, and since wheelsets cannot be duplicated, safety can only be obtained through a rigorous and adequate inspection plan with the use of NDI. These maintenance schedules must complement the best operating practices already adopted in the railway sector, providing a higher level of safety. Wheelset maintenance is expensive, time-consuming, complex to organize, involves large capital and human resources, but it has been done for almost two hundred years and there seems to be no other way to ensure rolling stock safety.

1.1.3 Research on fatigue cracks in railway axles

The historical development of scientific and engineering knowledge about fatigue of materials and structures, dates back from the early decades of the 19th century. The fatigue of components became noticeable over the industrial revolution, mainly as a result of the development of the railway industry and some dramatic failures as described in the Subsection 1.1.2. Fatigue failures were frequently associated with steam engines, locomotives and pumps as this type of failure was rather commonplace. Over that period, fatigue was recognized as a fracture phenomenon occurring after numerous loading cycles where a single load of the same magnitude would not cause any damage.

A synopsis of the timeline of fatigue research is provided below [13, 14]. The following provides a brief, not exhaustive overview on the most important milestones and their relevance in railway axles in order to form the necessary background and knowledge of the fatigue phenomenon.

- In 1837, Albert published the first article on fatigue, including the first known fatigue test results of conveyor chains used in mines which had failed in service.
- In 1842, Rankine recognised the importance of stress concentrations in his investigation of the strength of railway axle failures.
- In 1843, Glynn reported the fatigue of an axle of a locomotive tender, that is, a rail vehicle hauled by a steam locomotive containing its fuel, being coal very often. A sketch describing the fracture surface was included in the investigation, and reproduced in Fig. 1.10. At that time the fracture shown was described as an annular smooth zone produced by a constant process, extending for some mm in depth all round the axle. The drawing clearly shows a circumferential crack surrounding the final brittle fracture.

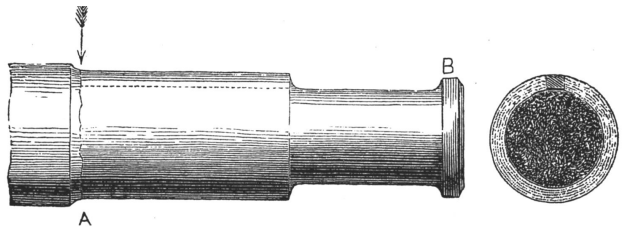

Figure 1.10. Glynn's drawing of a fatigue failure in an axle.

- In 1848, James and Galton published results of tests on large iron bars subjected to alternating loads as there were known from railway axles. In the series of experiments, it was shown that the repeated application and removal of a load could cause failure at loads well below of the static breaking load.

It can be observed that by the middle of the century, engineers knew of the effects of fluctuating stresses on the strength of metals. Over these years, many disastrous rail accidents due to fatigue occurred, for instance, the well-known Versailles accident in 1842 were the axle of a locomotive broke as described in Subsection 1.1.2. A broader insight into the phenomenon of fatigue was gained in the following years:

- In 1854, Braithwaite reported on common service fatigue failures such as railway axles. The term *fatigue* was mentioned for the first time in the investigations, and from then on, the term fatigue was coined and widely used.
- In the 1858-1870 period, Wöhler conducted a series of experiments concerning fatigue in railway axles. In order to know the loads magnitude and characteristics, the service loads of railway axles were measured with original deflection gages as diagrammed in Fig. 1.11.

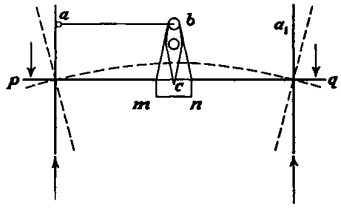

Figure 1.11. Whöler's device for recording deflections of axles in service [14].

Then, knowing the magnitudes of the maximum forces acting, the strength of axles under constant reversal of the stresses was investigated. The experiments were conducted on small-scale axle-like specimens, loaded by steady rotating bending in the purpose-built machine shown in Fig. 1.12. This test-rig reproduced the stress fluctuations previously measured. For a detailed description of the measuring device and the testing machine, the reader is referred to [14].

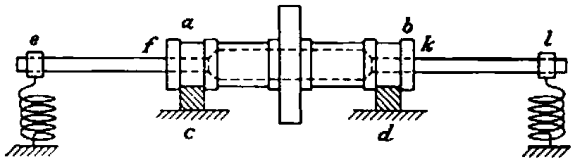

Figure 1.12. Whöler's fatigue testing machine [14].

Wöhler drew the following conclusions regarding the fatigue of materials from the systematic studies performed. The material can be induced to fail by many repetitions of stresses, even if all of them are lower than the static strength. The stress amplitudes are decisive for the destruction of the cohesion of the material, so, it was concluded that cyclic stress range is more important than peak stress. The concept of endurance limit was also introduced, thus making an essential contribution to fatigue avoidance by design. This implicitly

suggested design for finite fatigue life, taking into consideration even the scatter of fatigue life, or in other words, the probability of failure. The effect of the stress concentration of sharp corners was studied. This scenario takes place in axle transitions where different diameters in different sections are used. It was observed that the use of transition radii mitigated the effect. It is important to note that this practice is still in use in the railway axle manufacturing. Additionally, the discontinuity of stiffness between the axles and the wheels press-fitted, was identified as an important region in fatigue assessment.

It can be concluded that these early investigations were of a fundamental nature. For each kind of test, several machines and measuring instruments were envisioned and designed ad-hoc. Over these years, failure of railway axles was a matter of concern and also a design challenge that drove a continuous motivation. Works of the time proposed many theories and ideas on the cause of the failure of railway axles, and the matter was widely discussed in scientific gatherings. It was during these debates when the term fatigue was coined to describe the sudden fracture of a component which, at least visibly, was performing properly, right up to the moment of failure. It can be stated that these early investigations on railway axles formed the basis of knowledge on which fatigue in materials science is grounded.

The problems of the early days of railway technology were overcome long ago. However, increasing demands and higher axle loads aimed nowadays account for quite new challenges with respect of material and technology as well as safety issues.

1.1.4 Design, manufacture and maintenance of wheelsets

Nowadays, the general structural reliability analysis of components when applied to the particular case of railway rolling stock is supported on three main pillars: (i) design, (ii) manufacture, and (iii) maintenance. They are included in the diagram of Fig. 1.13 for having a better view.

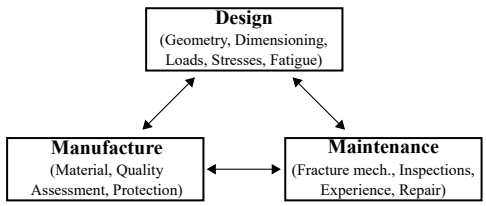

Figure 1.13. Reliability of structural components.

The continued efforts, research and development carried out on rolling stock, show that the developments are fundamentally driven and governed by three factors: (i) operation, (ii) technology, and (iii) regulation. These are shown in Fig. 1.14.

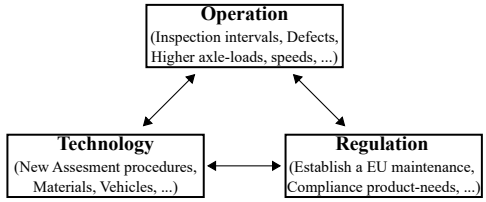

Figure 1.14. Current developments in the railway field.

In this framework, the reliability of structural components can be further investigated in the different lines of research associated to the design, manufacture and maintenance as presented in the exploded view in Fig. 1.15, that shows the reciprocal relationships among the various parts.

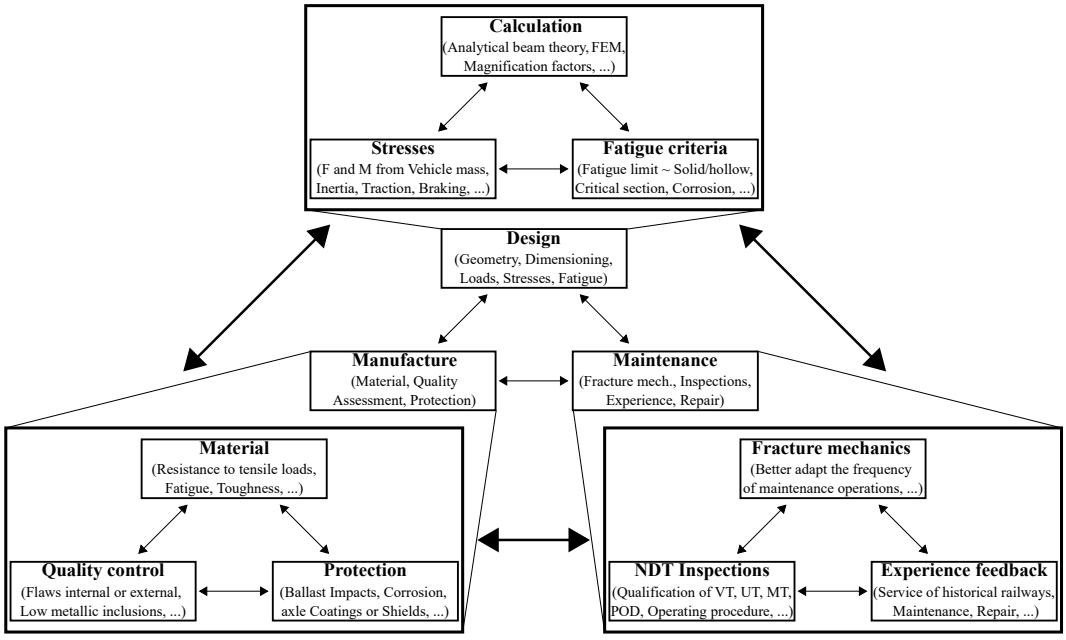

Figure 1.15. Exploded view of reliability of the wheelsets: design, manufacture, and maintenance.

Design. The design of rolling stock is based on three fundamental parameters: (i) calculation, (ii) stresses, and (iii) fatigue limits. Railway axles are designed to have a theoretically *infinite life* according to EN 13103-1:2017 standard [15], considering that fatigue limits are derived at 10^7 cycles of load. For axles, the design calculations currently employed are based on the beam theory and nominal stress method following the procedure thoroughly described in EN 13103-1:2017 standard [15] that is of application for both non-powered axles and powered axles. The schematic of forces for the calculation of the bending moment is shown in Fig. 1.16. The forces and moments considered include the mass of the vehicle, global bending given a defined distribution of loads acting at the bearing journals and at the

contact points between wheels and rails, inertia of masses when cornering, bending plus axial load, and from traction and braking actions, torsion. Briefly, there are different specific permissible stresses at various locations on the axle associated with the different steel grades. The stress thresholds, derived from uni-axial fatigue tests done in the laboratory on test pieces representative of the component and the material, are set with generous safety factors. The axle is divided into sections bounded by geometrical discontinuities and at each end of those sections, the calculated stresses must be below the permissible stresses. Additionally, fatigue stress concentration factors are considered and included in nomograms according to geometrical ratios. On the other hand, wheels are calculated by the finite element method in order to determine the principal stresses under conventional loads following the procedure described in EN 13979-1:2020 [16] and CEN-TS 13979-2:2011 [17] standards.

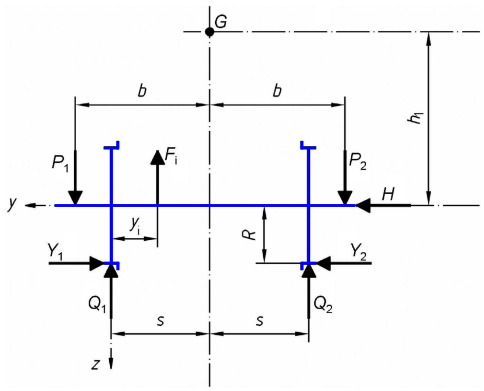

Figure 1.16. Forces for calculation of bending moment in a railway wheelset (in blue) [15].

Manufacture. The manufacture of rolling stock is based on three fundamental aspects: (i) material, (ii) quality control, and (iii) protection. The wheelset production process involves the wheel production, the axle production and the assembly of both. The wheel and axle production processes are quite similar, consisting in four main steps: (i) forging, (ii) heat treatment, (iii) machining, and (iv) finishing. The differences are basically related on the particularities of each component.

Among the different wheel types, solid wheels are the standard for freight applications. The wheel production process can be summarized as follows:

- forging: press-forming press, wheel rolling, dishing press,
- heat treatment: rim chilling where after the austenization of the wheel, a rapid local cooling-down affecting only the tread of the wheel is performed to increase the tread hardness, which is the area subjected to wear in service,
- machining: turning, boring,

- optionally shot-peening or cold-rolling of the web area in order to increase its strength against fatigue,
- inspection and verification: dimension control, MPI, UT,
- finish: painting, protection.

Railway axles are produced according to following particular process:

- forging: press-forming press,
- heat treatment: depending on the steel grade, railway axles can be normalized or double normalized, to obtain a fine pearlitic-ferritic structure or can be quenched and tempered, to obtain a bainitic/annealed martensitic fine structure,
- rough machining: centring, turning, drilling,
- finish machining: turning, grinding,
- optionally, cold rolling of seats or whole axle to increase the fatigue strength, molybdenum coating in the seats to improve the fretting fatigue resistance, or sand blasting which is also used in maintenance, to remove painting,
- inspection and verification: dimension control, MPI, UT,
- finish: painting, protection.

Then in wheelsets production, wheels are mounted on to the axle seats by an interference fit. The most extended method for the assembly is by using a press. An alternative method is via shrink fit by heating the wheel before the assembly.

Regarding the materials in use for rolling stock, according to EN 13260:2020 standard [18], the steels grades EA1N, EA1T and EA4T are the standard materials, being EA1N (normalized) and EA1T (tempering quenched) low strength carbon steels while EA4T (tempering quenched) is a low-alloyed steel of fairly medium to high strength. The chemical composition of these steel grades is defined through the maximum percentage contents of the various elements as described in EN 13261:2020 standard [19].

Additionally, the verification of the fatigue characteristics is essential in order to have a wheelset designed correctly. The performance of a railway axle in service depends upon these characteristics. The fatigue limit values defined for wheelsets in EN 13260:2020 standard [18], are used for the calculation of the maximum permissible stresses that are referred to in the design rules in EN 13103:2017 standard [15] as explained above in the first main pillar of reliability, i.e. design.

For the axle product, the fatigue limits are assessed in tests made on full size test pieces, in order to predict the behaviour of the axle under in-service stresses. These fatigue limits apply to different axle areas. The limits applying to the wheelsets that

depend mostly on the assembly, are defined in EN 13260:2020 standard [18], and the fatigue limits applying to the axle body are included in EN 13261:2020 standard [19]. In the case of body axle, a fatigue limit F_1 is defined on the body surface for solid axles, and F_2 on the bore surface in the case of a hollow axle. In the case of assembly related aforementioned, it is necessary to define one fatigue limit for solid axles, F_3 under the press-fit surfaces, and two fatigue limits for hollow axles, F_4 under the press-fit zone, excluding the connecting rod, and F_5 under the connecting rod press-fit. These fatigue limits shall be tested in three test pieces verifying that there is no crack after 10^7 cycles of load. The values to be achieved are given in Table 1.2.

Table 1.2. Fatigue limits values in [MPa] from standards [18, 19].

Steel grade	F_1	F_2	F_3	F_4	F_5
EA1N/EA1T	200	80	120	110	94
EA4T	240	96	145	132	113

Maintenance. The maintenance of railway axles relies on three main concepts: (i) fracture mechanics, (ii) non-destructive testing (NDT) inspections, and (iii) experience feedback. Nowadays, inspection intervals can be carried out both during service and during maintenance steps. Those inspections, based on return of limited experience, are not entirely ruled by any international standard since there is little or no standardisation of maintenance operations. However, prescriptions have been established, mainly for freight rolling stock. Particularly, EN 15313:2016 standard [20], related to the wheelset maintenance, implements special maintenance actions for freight wagon axles of type A and B as a function of their loading. Table 1.3 shows the maintenance intervals and maintenance actions that have to be applied to guarantee safe operating conditions for these type of axles according to axle load.

These values have been derived from the experience gained by users in European applications. The axle integrity shall be assessed by NDT in compliance with the requirements specified in the maintenance plan. For type A axles, the mileage is limited to 400 000 km or equivalent time in service, between medium or heavy maintenance. For type B axles, inside design limits, but its use must be checked case by case considering wagon parameters and permitted infrastructure axle load.

The periodicity of NDT of the axle must be defined taking into account the design, the type of application, and the service experience. The informative Annex J of EN 15313:2016 standard [20] presents a general rule applicable to axles. It states that the general rule for axles conforming to the requirements of European standards is to perform NDT during medium or heavy maintenance of railway wheelsets. This represents the highest level of security. Additionally, the standard itself remarks that the inspection interval can be further adapted based on service experience, and more specifically on the results of the NDT, and may result in an increase or a decrease of the inspection interval. From here, it can be observed that this is an open point in the

Table 1.3. Special maintenance actions for freight wagon axles according to axle load [20].

Axle type	**Axle load M (t)**	**Additional criteria**	**Corresponding additional maintenance action**
For type A-I; A-II; A-III(1) axles operated from 20 t up to 21 t axle load in standard maintenance plan and re-classified back to 20 t operation:		Re-integrate axle in standard maintenance plan with UT of the wheel seat at the next reprofiling, medium or heavy maintenance level of the wheelset	
Type A-I; A-II; A-III(1)	21 < M	Not covered by this EN	Scrap
Type A-III (2)	20 < M ≤ 20,6	Inside design limits, validated by service	No special requirements
Type A-III (2)	20,6 < M ≤ 21	Limited mileage between medium or heavy maintenance: 400,000 km or the equivalent time in service	NDT with mounted wheels – UT at wheel seat – UT or MT at transition radii
Type A-III (2)	21 < M ≤ 22	Limited mileage between medium or heavy maintenance: 200,000 km or the equivalent time in service	
Type B	22,5 < M ≤ 23,5	Inside design limits but use to be checked case by case in accordance with wagon parameters and permitted infrastructure axle load	No special requirements

standards, and therefore the responsibility of setting the specific values of inspection intervals lies in the maintenance service. Consequently, the axle inspection processes are aimed at an ad-hoc approach identifying appropriate NDT practices. Annex J further details that for type A or B axles mounted on freight wagons, the following requirements apply: (i) to perform NDT on all the axle sections during medium maintenance, and (ii) to perform NDT by magnetic particle inspection (MPI) on the full axle surface during heavy maintenance.

For clarity, the previous maintenance actions on wheelsets are enclosed in Table 1.4, where the acronyms stand for, visual testing (VT), ultrasonic testing (UT), and magnetic particle testing (MT).

Table 1.4. Main maintenance actions of wheelsets.

Type	Action	NDT
Wheels reprofiling	off-vehicle maintenance	VT
Medium maintenance	off-vehicle maintenance w/o changing wheels	UT and/or MT on axle sections
Heavy maintenance	off-vehicle maintenance w/ changing wheels	MT on the full axle surface

In summary, the EN 15313:2016 standard [20] contains general instructions but does not provide sufficiently clear guidance on how to implement maintenance activities at a practical operational level. It is worth keeping in mind that wheelset maintenance is expensive, time-consuming, complex to organize and involves large capital and human resources.

As mentioned, the current design and operation of rolling stock is based on many years of experience. Designers establish design cases based on practice and customer specifications without explicitly establishing any link of these studied cases with actual system behaviour. At the same time, current standards do not rigorously specify how to determine the material properties used in the design, but rather use empirical methods based on experience with traditional materials. The subjective nature of this approach, however, leads to satisfactory results since over the past years the safety of these systems has been proved. The limitation of this design methodology lies in the fact that the wheel and axle design and its associated maintenance strategy and inspection periods involve such uncertainties that it is almost impossible to optimize them. The new design requirements aim to a reduction of weight and life cycle cost (LCC) for a given level of safety. The first condition can be met reducing the level of dynamic loads and should be done through an optimization process, the second of them involves the increase in service life, what can be achieved through the proper exploitation of the materials used and the optimization and improvement of non-destructive inspection practices. A scientific approach to the inspection interval definition complementary to the empirical approach is required in order to establish the highest level of safety. These new challenges in the design strategy of rolling stock give way to the development of new numerical and experimental methodologies based on fracture mechanics and non-destructive inspection techniques within the approach of damage tolerance analysis (DTA).

No unique scheme exists on how to apply fracture mechanics to different components. One of the most important aspects is the time taken for a detected crack to extend to its critical size. If this time is known, and it is sufficiently large, a design concept based on inspection intervals can be applied in a viable way. If it is rather small, the concept has to aim at avoiding crack initiation. Below, a number of different options of fracture mechanics application in design according to Zerbst et al. [21] are enumerated. These are:

(i) damage tolerant design;
(ii) fail-safe design (redundant design, crack arrest, leak-before-break);
(iii) periodic proof testing;
(iv) periodic removal of cracks; and
(v) durability design using a fracture mechanics based fatigue endurance curve.

In a railway axle, knowing that the time for a crack to nucleate and grow should be sufficiently large ZERBST et al. [22], a design concept based on damage tolerance seems reasonable. Damage tolerance, as its name suggests, entails allowing subcritical flaws to be in a structure for a certain period. Note that damage tolerance does not mean that a crack detected during an inspection is considered acceptable even when its size is far from being critical. In some cases this is a possible option, but it must be handled with care in safety relevant components as it is the case of railway axles.

As mentioned, the fatigue fracture of materials is caused by the nucleation and propagation of cracks under cyclic loading. The crack size scale for initial and final cracks is illustrated in Fig. 1.17. However, structures can withstand a considerable load in presence of cracks or yet failed parts are considered to be damage tolerant.

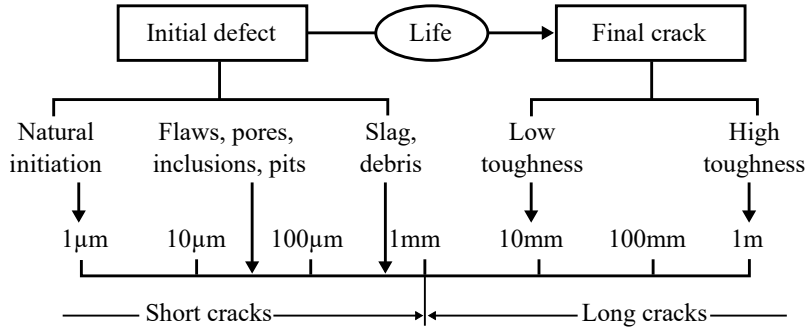

Figure 1.17. Several initial and final crack sizes delimiting crack propagation life.

The initial defect length can vary from 1 µm to ≈1 mm, depending on the defects existing in the material. The final crack length is usually of some millimetres. The distinction between short and long cracks is sometimes taken as ≈1 mm in length.

The general stages within the lifetime of a component are illustrated in Fig. 1.18.

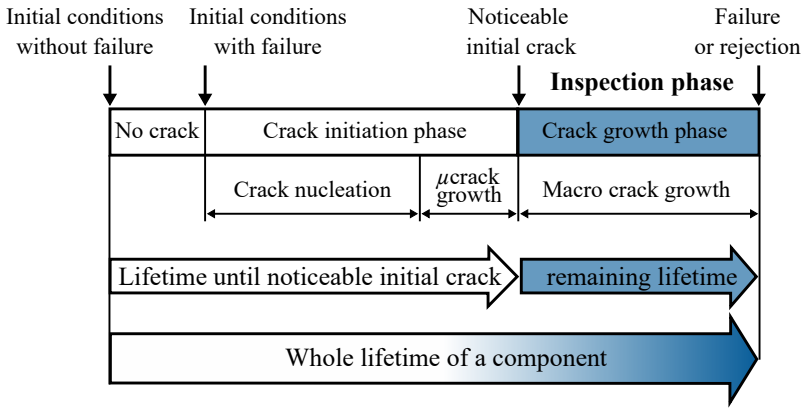

Figure 1.18. Stages of lifetime.

The ideal initial conditions would be to not have a single failure, but in reality components have initial defects that arise naturally. From the initial defect, flaws, pores, inclusions, pitting, etc., the crack nucleates and initiates until it reaches a certain size that is considered to be noticeable. This process consists of the crack nucleation phase and the micro-crack growth phase. The lifetime up to this stage is referred to as the lifetime until the initial crack is noticeable. The next phase, often referred to as crack growth or crack propagation, spans from the initial crack under consideration to the final crack size for failure, or rejection of the component. The process is the macro-crack growth and the length of this phase is known as the remaining lifetime, as it is the lifetime that the component can be inspected by non-destructive techniques within a damage tolerance assessment scheme. As introduced above, the determination of inspection intervals is possible by combining methods of structural durability together with fatigue approaches and fracture mechanics concepts. In the following sections, some of the most important aspects regarding this evolving approach, are further revised.

The very aim of fatigue crack propagation is then to establish the relationship of crack propagation as a function of a loading parameter under complex service conditions. Some factors that influence the crack propagation rate are: (i) the component size and geometry; (ii) loading conditions; and (iii) the microstructure of materials, aside from environmental aspects such as corrosion and temperature.

1.1.5 Safety assessment levels for railway axles

The existing design and operation of railway axles is based on a two-stage safety concept comprising *safe life* and *damage tolerance* approaches. These safety levels are illustrated in Fig. 1.19, which is taken from an extended review on safe life and damage tolerance aspects of railway axles by Zerbst et al. [22]. It also includes an additional stage *in-service damage indication systems* with further options that offer potential for establishing a third stage safety concept. For completeness, Fig. 1.19 also indicates the maturity of the technologies in the three stages, by using a two-level scale as follows: (*) state of the art, and (**) present and future development.

Primary safety level: Safe life design. In Europe, railway axles are designed according to EN 13103-1:2017 standard [15] for trailing, i.e. non-powered and for driving, i.e. powered axles. Summarizing, the design is based on the static stresses with dynamic effects being included as magnification factors in a way that the resulting loading represents the worst possible case-scenario. This differs from the reality because all loads are assumed to act simultaneously. The maximum permissible stress in the axle is given by fatigue limits of the material under consideration, and also it additionally depends on the type of axle, solid or hollow, and the axle section, that is, under press-fits, body axle, etc. Moreover, if the axle is exposed to corrosion

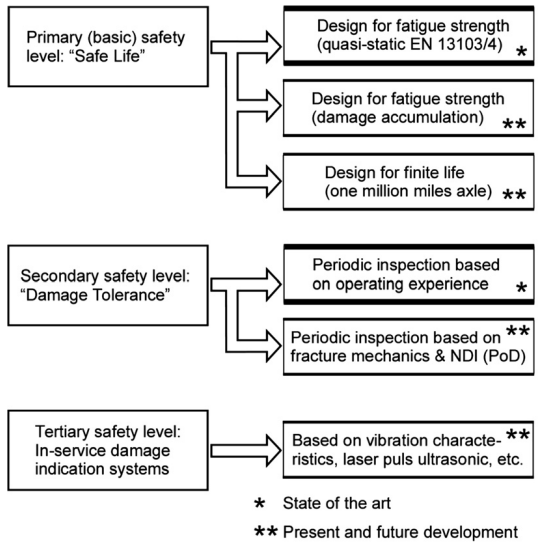

Figure 1.19. Components of a safety assessment system for railway axles [22].

reductions of the allowable stress is indicated. The main problem in designing railway axles is the incompatibility between the two targets: low wheelset mass, and low design stress. Both are wanted, but each can only be obtained to the detriment of the other. This design issue is sometimes addressed using smaller wall thickness in hollow axles, mass reduction, and using higher-strength steel, obviously, with higher stress properties. This is, however, problematic in terms of crack susceptibility and crack propagation. Additionally, changes in the dimensions of a railway axle also depend on the overall geometry of the boogie. The existing methodology in railway axle standards is discussed by Grubisic and Fischer [23] and Sonsino [24] where its replacement by a methodology taking into account damage accumulation is suggested. The approach proposed by Beretta and Regazzi [25] for railway axle design, is based on the FKM guidelines [26], where the fatigue assessment considers the damage sum criteria derived from the concepts of damage accumulation originally proposed by Miner [27]. In particular, two approaches are proposed by the guidelines: (i) the Haibach model, similar to the original Miner's rule but with two regions of the fatigue curve defined, the *finite life* region and the *infinite life* one; and (ii) the Miner-Konzequent method. The discussion on the allowable damage sum indexes relative to the safe life assessment of railway axles is still open.

Secondary safety level: Damage tolerance design. The primary safety level based on a traditional safe life design, has several limitations as it is unable to take into account the deterioration of the axles during service, such as paint detachment, pitting from corrosion or damage from ballast impacts. These issues are discussed in depth in the following sections. All these types of damage could act as fatigue crack initiation mechanisms, causing final fracture of the component. Although, the

existence of such cracks in railway axles is not acceptable, it seems that it is not possible to totally avoid them, at least based on the current technology. To overcome these limitations, a secondary level of safety is introduced in the railway axle safety assessment, based on periodic in-service inspections. The very aim of the damage tolerance approach is to detect potential cracks before they become critical.

There are several alternatives to determine the appropriate inspection periodicity that are: (i) based on feedback experience, and (ii) based on fracture mechanics principles. The former alternative uses the limited knowledge of the inspections periodicities performed so far by the different managers for the different applications. In addition, the current regulations and recommendations regarding the distance between inspections described in Section 1.1.4 are considered. It is worth to remark here, that there is a lack of standards regarding specific inspections of railway axles, but only guidelines about the freight wagons. Moreover, the applicable standards are generic and open to interpretation when it comes to damage and repair procedures. In consequence, the responsibility is totally demanded to the constructor and the maintenance service. Given this scenario, it is trivial that it is not possible to determine an optimal inspection interval beforehand since there is not any information that relates the actual state of the component and the likely crack propagation until the next inspection. The latter alternative based on fracture mechanics approach, assumes that a crack is present in the axle, and it can grow during service. The primary result is the crack depth versus time or number of loading cycle characteristics and, based on this, the residual lifetime, i.e. the time or number of loading cycles the assumed initial crack would need to become critical. By an appropriate analysis, the residual lifetime can be calculated, and consequently, an adequate inspection plan can be defined, in order to ensure safety. It provides an assured level of safety for the axles of a fleet of trains by quantifying in-service inspection intervals. This approach is commonly used in aerospace engineering, mechanical engineering, and civil engineering as exemplified by Jones [28], to manage the extension of cracks in structure through the application of the principles of fracture mechanics. The sustainment tools needed to assess in-service cracking issues in rolling stock are similar to those needed for aircraft structures in that both need to address issues related to the growth of cracks from small material discontinuities in complex geometries and under complex variable amplitude load spectra. It is worth noting here that crack nucleation and early crack propagation are not an issue of damage tolerance analysis. Instead, the presence of a sufficiency large crack size is postulated. What matters is the largest crack that could escape detection under in-service conditions. The details of the current state-of-the-art methodologies developed within the frame of damage tolerance assessment applied to railway axles are given in the next section. Note that the discussion of this relatively new methodology when compared with what is prescribed by the current standards, safe life design, and with the damage accumulation alternative, is still open.

It is envisioned that inspection periods should not be established only on the basis of experience but also on the basis of a given fracture mechanics methodology. However, it should be kept in mind that fatigue, fracture and in general any material degradation process, are inherently stochastic phenomena. Randomness in the microstructure and in the properties of the material, in the in-service loads or in the manufacturing process itself, considerably affect the dispersion over the lifetime of the component. In practice, the effects inherent to these uncertainties are covered by the use of safety factors and the use of conservative assumptions. Such approaches are therefore deterministic and aim to ensure an acceptable level of safety in the structure by keeping the probability of failure low enough to meet industry standards.

Deterministic analyses in the field of damage tolerance unfortunately cannot help in assessing the degree of conservatism of a given structural design subjected to so many sources of uncertainty in service. This type of analysis also seems inappropriate for assessing the contributions of each of these random parameters from a stochastic point of view and, of course, is insufficient when scheduling a maintenance plan.

In an effort to overcome these limitations, probabilistic approaches to fracture mechanics have received increased attention in recent years in the field of damage tolerance. One of the objectives of this thesis is to tackle the limitations on the current state of the art by establishing a stochastic approach to the problem, quantifying the uncertainties associated with it and providing the probabilistic lifespan knowledge that would be an essential asset for a precise calculation inspection periodicities according to the damage tolerance point of view.

Tertiary safety level: In-service damage indication systems. For completeness, in the extended review on the safety levels of railway axles by Zerbst et al. [22], is added that there is also some work in progress on a tertiary safety level in order to detect axles containing fatigue cracks during train operation. The challenge is to detect the crack when the train is moving or during stops. These types of initiatives are often classified as condition monitoring processes, where a certain parameter is controlled representing the condition of the component in order to identify a significant change which is indicative of a developing fault. The principles which are under investigation include inspections based on high energy laser pulse ultrasonics as in Morgan et al. [29] and Ngigi et al. [30], monitoring the vibration characteristics of the axle described by Verhelst [31], and based on new sensor systems adapted to rotating axles in hollow or solid axles to inspect online during service as investigated in Prager and Grzeszkowski [32]. All these recent ideas for a third safety level are, as mentioned, in early stages of development and as one of the main drawbacks is that they are nowadays only capable of detecting fairly large cracks.

The existing and potential innovative safe life and damage tolerance methods applied to railway axles has been summarized. In the following, aspects such as damage tolerance or probabilistic considerations are discussed in detail.

1.2 Fundamentals of damage tolerance

Damage tolerance is the ability of a component or structure to sustain constant and/or varying loads in the presence of fatigue cracks, corrosion defects, impacts, metal inclusions, or any damage induced by accidental loads until such damage is detected through inspections. In this section, the focus will be on fatigue cracks. Damage tolerance analysis for fatigue cracks uses fracture mechanics to describe the fatigue crack growth process, the residual strength or life, and combined with the definition of a periodic inspection plan, provides a certain level of safety. That means that fatigue cracks are allowed to appear as long as they can be detected with a certain probability before they reach their critical size. The rationale of the basic elements of damage tolerant methodology are introduced below. The concept of crack growth behaviour, from an initial flaw to failure, is introduced. The basics of fracture mechanics, stress intensity factors, material characterization, and life prediction methodology are presented. Finally, the general scheme for a damage tolerance analysis of railway axles is reviewed and summarized.

1.2.1 Damage concepts, behaviour and effects

A schematic of the typical crack growth behaviour in a structural component is shown in Fig. 1.20. It illustrates the crack evolution from an initial damage size a_{ini} to a damage size that causes structural failure and loss of safety. The x-axis measures the number of loading cycles applied, N, or the equivalent elapsed time during which loading is applied, or an equivalent distance travelled, for instance, mileage in km. The y-axis measures the corresponding length or depth of a crack, a, in the given component, typically in mm. It is inferred from Fig. 1.20, that when the crack is short, it grows very slowly. As the crack becomes longer, the crack growth rate increases until the crack reaches the critical size, when fracture of the structural element occurs. While the sub-critical crack growth process occurring may take a lot of years of service, e.g. 20–30 years, the fracture process is almost immediate.

The crack grows as a result of the cyclic loading that is applied to the structure. Any crack will grow a given increment Δa in a given number of loading cycles ΔN. Such process is driven by the crack growth rate da/dN. When the crack length reaches a critical value, the growth becomes unstable, thereby inducing failure. When the crack reaches the critical length, the number loading cycles reach the structural life limit. The structural life limit is a measure of the maximum allowable service time, or number of accumulated service cycles or distance travelled, associated with driving the crack from its initial length to the critical length. The main aim of the damage tolerant approach is to ensure that cracks do not reach levels that could impair the safety of the component during the expected lifetime.

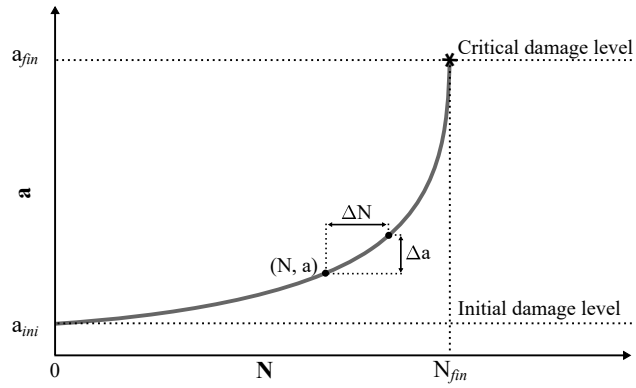

Figure 1.20. Schematic of crack growth behaviour for a typical crack.

There are several parameters observed that have an effect in the crack growth life as summarized by MIEDLAR et al. [33]. The most important of these are: (i) geometrical properties of the structure and the initial crack size a_{ini} and shape, (ii) the loading history, and (iii) the material properties.

Geometrical properties - a measure of quality. The effects of the properties of the structure, component dimensions and expected crack location are significant in crack growth behaviour. The structural properties involve such things as crack configuration, load transfer through joints, holes size, parts thickness, etc. A substantial amount of experimental work is required to characterize some of these geometrical effects on life. Moreover, the effect of initial crack size is notable. Given a configuration and loading, the smaller the initial crack size, the longer the life.

Stress history - a measure of usage and location. The magnitude and sequence of loadings are noted to have a significant effect on the rate at which cracks grow. The stress history describes the magnitude and sequence of stresses at one location that results from the sequence of loadings acting on components. For instance, as a railway travels different missions and different manoeuvres such as curves, over crossovers, through switches, rail joints, etc, it experiences different amplitude loadings.

Material properties - a measure of material resistance to cracking. It is shown experimentally that for the same loading condition, i.e. the same number and amplitude of stress cycles, cracks grow faster in certain metal alloys than in others. The crack growth rate da/dN for each material can be measured experimentally through testing. Given the same load and geometric conditions, the material having the slower growth rate characteristics will have a longer life.

To sum up, these main parameters are in the realm of: geometry, quality, and initial crack size; usage, varying loading history; and material properties. Given this concepts, the crack length will be the measure of damage and the crack growth rate will define the rate of damage accumulation.

1.2.2 Basics of fracture mechanics

Fracture mechanics is the field of mechanics which studies the propagation of cracks in a material. This discipline uses methods of analytical solid mechanics to calculate the driving force on a crack and those of experimental solid mechanics to characterize the resistance of the materials to fracture.

A comparison of the traditional approach to structural design with the fracture mechanics approach is presented in the diagrams of Fig. 1.21. In the traditional approach in Fig. 1.21a, the calculated design stress is compared with the flow properties of likely suitable materials. A material is assumed to be appropriate if its strength is greater than the expected stresses. Frequently, this approach uses safety factors on stress, combined with assuming a minimum tensile property of the material, to prevent brittle fracture. The fracture mechanics approach in Fig. 1.21b has three variables, rather than the two in the traditional approach. In this case, the flaw size is an additional structural variable, the fracture toughness replaces strength as the critical material property, and the consideration of the applied stress remains. This approach quantifies the critical combinations of these three basic variables.

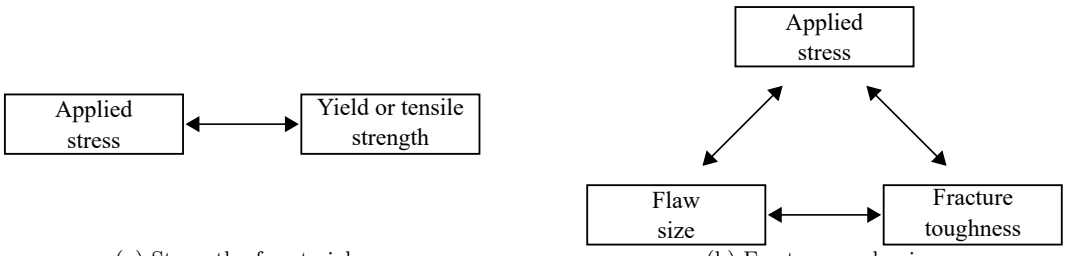

(a) Strength of materials. (b) Fracture mechanics.

Figure 1.21. Traditional strength of materials approach and fracture mechanics approach [34].

There are two alternative approaches to fracture analysis [34]: (i) the energy criterion, and (ii) the stress intensity approach. These two approaches are equivalent in certain circumstances. Both are discussed below, but the focus will be on the SIF approach.

The energy criterion. The energy approach states that crack extension occurs when the energy available for crack growth is enough to overcome the resistance of the material. The material resistance may include the surface energy, plastic work, or other types of energy dissipation associated with a propagating crack.

Griffith [35] was the first to propose the energy criterion for fracture, but Irwin [36] is primarily responsible for developing the current version of this approach. The energy release rate $\mathcal{G}$ is defined as the rate at which energy is transformed as a material undergoes fracture. At the moment of fracture $\mathcal{G} = \mathcal{G}_c$, which is the critical energy release rate, that is related to the fracture toughness.

A crack in an infinite plate subjected to a remote tensile stress is shown in Fig. 1.22.

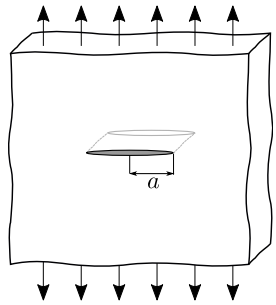

Figure 1.22. Through-thickness $2a$ crack in an infinite plate subjected to a remote tensile stress.

For that configuration, the energy release rate is given by Eq. (1.1), where E is Young's modulus, σ the remotely applied stress, and a is the half crack length.

$$\mathcal{G} = \frac{\pi\sigma^2 a}{E} \tag{1.1}$$

At fracture, the critical combinations of stress and crack size for failure are described in Eq. (1.2), where $\mathcal{G} = \mathcal{G}_c$, a_c is the critical crack size, and σ_f is the failure stress.

$$\mathcal{G}_c = \frac{\pi\sigma_f^2 a_c}{E} \tag{1.2}$$

The energy release rate, $\mathcal{G}$, is the driving force for fracture, while $\mathcal{G}_c$ is the resistance of the material to fracture. To draw an analogy to the strength of materials approach of Fig. 1.21a, the applied stress can be viewed as the driving force for plastic deformation, while the yield strength is a measure of the material's resistance to deformation.

The tensile stress analogy is also useful for illustrating the concept of similitude. A yield strength value measured with a test specimen should be applicable to a large structure knowing that the yield strength does not depend on specimen size as long as the material is homogeneous. One of the fundamental assumptions of fracture mechanics is that fracture toughness, $\mathcal{G}_c$ in this case, is independent of the size and geometry of the cracked body. Therefore, a fracture toughness measurement on a specimen should be applicable to a structure. Provided that this assumption is valid, all configuration effects are taken into account by the driving force $\mathcal{G}$. The similitude assumption is valid when the material behaviour is predominantly linear elastic.

The stress intensity approach. The stress intensity factor (SIF), K, is used in fracture mechanics to predict the stress state, i.e. stress intensity, near the tip of a crack caused by a remote load or residual stresses [34]. The SIF, is a measure of the severity of a crack in an elastic solid and is closely related to the stress field in the vicinity of the crack front. In linear elastic fracture mechanics (LEFM) there is a direct relationship between the SIF and the $\mathcal{G}$ which governs the criticality of a crack.

The magnitude of K depends on specimen geometry, the size and location of the crack, and the magnitude and the distribution of loads on the material. It can be written as in Eq. (1.3), where $f(a/W)$ is a specimen geometry dependent function of the crack length, a, and the specimen width, W, and σ is the applied stress.

$$K = \sigma\sqrt{\pi a}\ \ f(a/W) \tag{1.3}$$

Theoretically, the stress ahead of a sharp crack tip becomes infinite and cannot be used to describe the state around a crack. When the plastic zone at the tip of the crack is small relative to the crack length the stress state at the crack tip is the result of elastic forces within the material and is termed LEFM and can be characterised using the stress intensity factor K. The stress intensity factors have the bizarre units of stress $\times$ length$^{1/2}$, e.g. MPa$\sqrt{\text{m}}$. Although the load on a crack can be arbitrary, Irwin [37] found that any state could be reduced to a combination of three independent stress intensity factors for the various modes illustrated in Fig. 1.23.

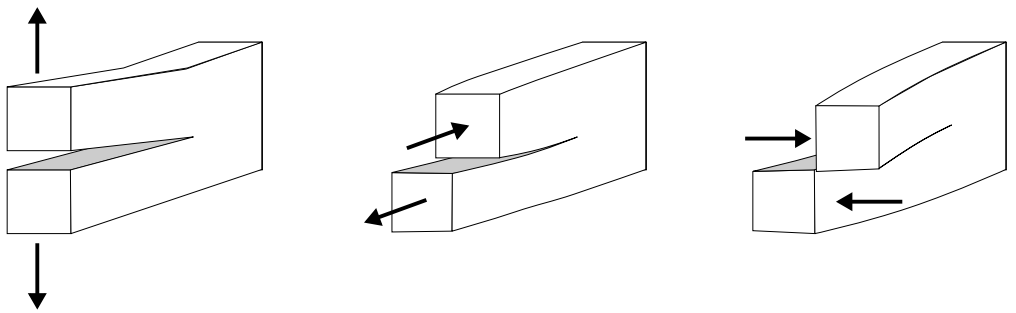

(a) Mode I: opening. (b) Mode II: in plane shear. (c) Mode III: out-of-plane shear.

Figure 1.23. The three modes of loading that can be applied to a crack.

The three modes are described as follows:

- Opening mode I in Fig. 1.23a: a tensile stress normal to the plane of the crack,
- Sliding mode II in Fig. 1.23b: a shear stress acting parallel to the plane of the crack and perpendicular to the crack front, and
- Tearing mode III in Fig. 1.23c: a shear stress acting parallel to the plane of the crack and parallel to the crack front.

An element near the tip of a crack in an elastic material is shown in Fig. 1.24.

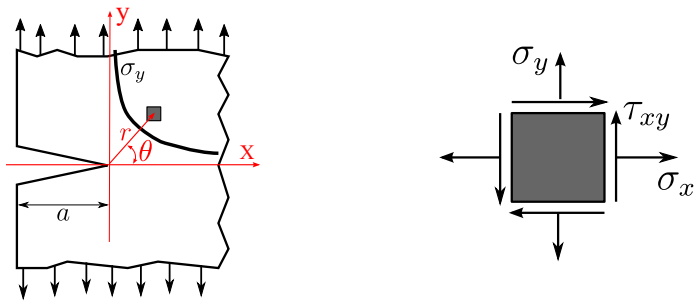

(a) Sharp crack. (b) Components of stress.

Figure 1.24. Ideally sharp crack in a linear elastic domain.

Linear elastic theory predicts that the stress distribution σ_{ij} near the crack tip, in polar coordinates (r, θ) with origin r = 0 at the crack tip, has the form in Eq. (1.4), where K is the stress intensity factor and f_{ij} is a dimensionless quantity that varies with the load and geometry.

$$\sigma_{ij}(r,\theta) = \frac{K}{\sqrt{2\pi r}} f_{ij}(\theta) + \text{ higher order terms} \tag{1.4}$$

Detailed expressions for the singular stress fields for the three types of cracking mode are gathered in Table 1.5. Note that in these expressions ν is the Poisson's ratio.

Table 1.5. Stress fields ahead of a crack tip in a linear elastic, isotropic material.

σ_{ij}	Mode I	Mode II	Mode III
σ_x	$\frac{K_{\mathrm{I}}}{\sqrt{2\pi r}} \cos\frac{\theta}{2}\left[1-\sin\frac{\theta}{2}\sin\frac{3\theta}{2}\right]$	$-\frac{K_{\mathrm{II}}}{\sqrt{2\pi r}} \sin\left(\frac{\theta}{2}\right)\left[2+\cos\left(\frac{\theta}{2}\right)\cos\left(\frac{3\theta}{2}\right)\right]$	0
σ_y	$\frac{K_{\mathrm{I}}}{\sqrt{2\pi r}} \cos\frac{\theta}{2}\left[1+\sin\frac{\theta}{2}\sin\frac{3\theta}{2}\right]$	$\frac{K_{\mathrm{II}}}{\sqrt{2\pi r}} \cos\left(\frac{\theta}{2}\right)\sin\left(\frac{\theta}{2}\right)\cos\left(\frac{3\theta}{2}\right)$	0
σ_z	0 (plane stress) $\nu(\sigma_x+\sigma_y)$ (plane strain)	0 (plane stress) $\nu(\sigma_x+\sigma_y)$ (plane strain)	0
τ_{xy}	$\frac{K_{\mathrm{I}}}{\sqrt{2\pi r}} \cos\frac{\theta}{2}\sin\frac{\theta}{2}\cos\frac{3\theta}{2}$	$\frac{K_{\mathrm{II}}}{\sqrt{2\pi r}} \cos\left(\frac{\theta}{2}\right)\left[1-\sin\left(\frac{\theta}{2}\right)\sin\left(\frac{3\theta}{2}\right)\right]$	0
τ_{xz}	0	0	$-\frac{K_{\mathrm{III}}}{\sqrt{2\pi r}} \sin\left(\frac{\theta}{2}\right)$
τ_{yz}	0	0	$\frac{K_{\mathrm{III}}}{\sqrt{2\pi r}} \cos\left(\frac{\theta}{2}\right)$

The corresponding equations for the displacement relationships for modes I, II, and III can be found in [34]. Note that each stress component is proportional to a single constant, K. If this constant is known, the entire stress distribution at the crack tip can be computed with the equations in Table 1.5. This constant, i.e. the SIF, completely characterizes the crack tip conditions in a linear elastic material.

If the material fails locally at some critical combination of stress and strain, then it follows that fracture must occur at a critical value of stress intensity, K_c. Thus

K_c is an alternate measure of fracture toughness. For instance, in mode I, failure occurs when $K_I = K_{\mathrm{Ic}}$. In this case, K_{I} is the driving force for fracture and K_{Ic} is a measure of material resistance. As with $\mathcal{G}_c$, the property of similitude should apply to K_{Ic}. That is, K_{Ic} is assumed to be a size-independent material property. Comparing Eqs. (1.1) and (1.3) results in the relationship between K_{I} and $\mathcal{G}$ in Eq. (1.5).

$$\mathcal{G} = \frac{K_{\mathrm{I}}^2}{E} \tag{1.5}$$

This same relationship holds for $\mathcal{G}_c$ and K_{Ic}. Thus the energy and stress intensity approaches to fracture mechanics are essentially equivalent for linear elastic materials.

Similarly, small flaws may result in crack growth when subjected to cyclic loading, i.e. fatigue. For long cracks, the rate of growth is largely governed by the stress intensity factor range ΔK from the maximum and minimum K, i.e. K_{max} and K_{min}, experienced by the crack due to the applied stress range $\Delta\sigma$. The cyclic stress range $\Delta\sigma\,(= \sigma_{max} - \sigma_{max})$ and the cyclic stress intensity factor range $\Delta K\,(= K_{max} - K_{max})$ are illustrated in Fig. 1.25 for a growing crack. Note also that the figure represents the amplitude and the mean values for the stress, σ_a and σ_m respectively, and for the corresponding SIF, K_a and K_m accordingly. Fast fracture will occur when the stress intensity exceeds the fracture toughness of the material. The prediction of crack growth is at the heart of the damage tolerance mechanical design discipline.

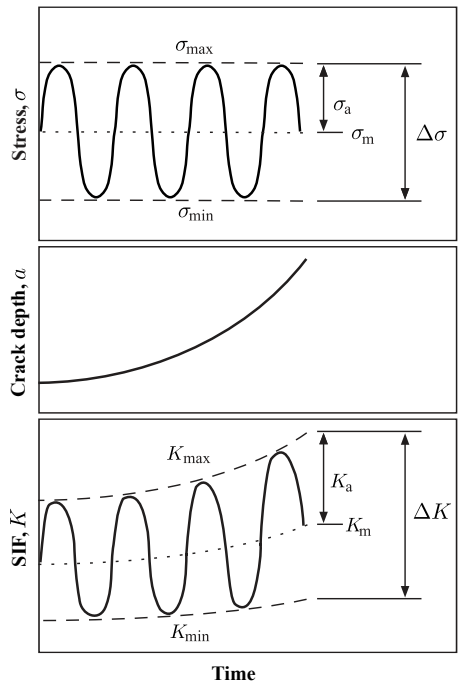

Figure 1.25. Definition of several σ and K values for a growing crack a under cyclic fatigue loading.

In railway applications, the fracture mechanics approach has not yet become a standard procedure. Nevertheless, to switch from an experience-based approach, as defined in current axle design standards, to a safe planning of maintenance inspections as well as for a damage-tolerant design for railways axles, fracture mechanics seems to be a mandatory tool to be taken into account.

1.2.3 Stress intensity factor evaluation

Regarding crack growth prediction, an accurate determination of the SIF is a key factor. For this purpose, the initial crack size and shape must be defined first. It is well established that in railway axles the cracks nucleated on the surface have a semicircular or semielliptical shape Zerbst et al. [22]. This type of cracks are among the most common ones found in several structural components, thus widely investigated and documented in the literature. Since the SIF is a key parameter to estimate stress and displacement fields ahead of a crack tip, various alternatives have been explored to calculate it for any given geometry and load combination. The SIF at the crack tip, as commonly defined by Eq. (1.6), contains σ, which is the characteristic stress, a, that is the characteristic crack dimension, and the geometry factor Y which is a dimensionless constant that depends on the geometry and the mode of loading. Note that Y can be a function of crack length a as well as other geometrical features and is also known as shape function.

$$K = \sigma\sqrt{\pi a}\ Y \tag{1.6}$$

The careful estimation of the SIF, which is a crucial operation in the frame of the damage tolerant assessment, is so related to an accurate evaluation of the shape function Y, given the shape and dimension of the crack relatively to the component. It is possible to estimate the Y factor through the application of available ready-made solutions, by extensive stress analysis using the FEM or by adopting the so-called weight functions. Below, the focus is on the ready-made solutions given an example for the sake of understanding while the other methods are tacked further on.

There are collections of ready-made Y factor solutions such as [38, 39]. The most widely used solutions for obtaining the SIFs for semi-elliptical surface cracks in plates of finite-thickness were obtained using the FEM by Raju and Newman [40] and Shiratori and Miyoshi [41]. The former obtained data for tensile and bending loads and presented their results through an empirical equation. The latter obtained results for constant, linear, parabolic, and cubic crack surface stress distributions. However, the solutions presented in those works are limited to specific loading conditions, and therefore they have limited applicability.

For illustrative purposes, the well-known standard test specimen for the measurement of fatigue crack growth rates is the compact-tension (C(T)) specimen defined in the ASTM E647 standard [42] and reproduced in Fig. 1.26.

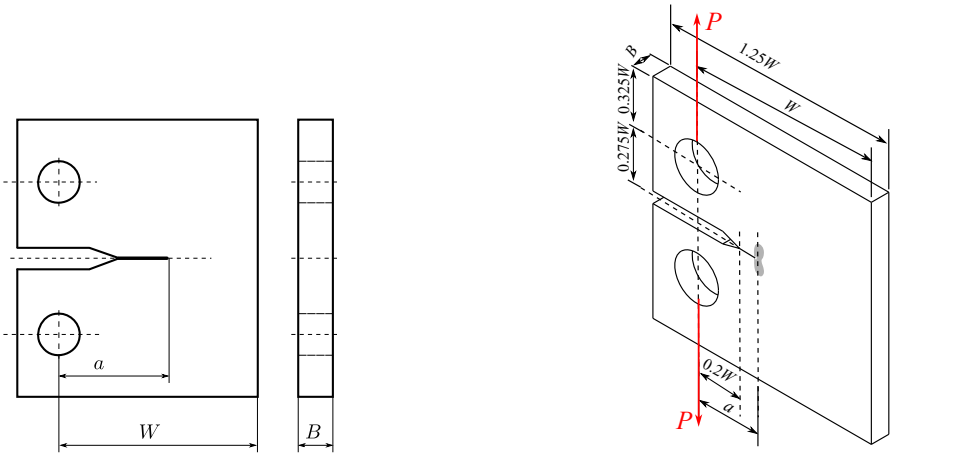

(a) Geometry and main dimensions. (b) Three dimensional view and applied load.

Figure 1.26. Compact-tension C(T) specimen for measurement of fatigue crack growth rates [42].

The SIF solution for standard C(T) specimen under tension loading is shown in Eq. (1.7), according to Bower [39], where P is the applied load, B is the thickness of the specimen, a is the crack length, and W is the width of the specimen.

$$K_{\mathrm{I}} = \frac{P}{B}\sqrt{\frac{\pi}{W}}\left[16.7\left(\frac{a}{W}\right)^{1/2} - 104.7\left(\frac{a}{W}\right)^{3/2} + 369.9\left(\frac{a}{W}\right)^{5/2} - 573.8\left(\frac{a}{W}\right)^{7/2} + 360.5\left(\frac{a}{W}\right)^{9/2}\right] \tag{1.7}$$

As an example of the weight functions approach, Shen and Glinka [43] used the results of Shiratori and Miyoshi [41] to generate weight functions for semi-elliptic surface cracks in finite-thickness plates. Similar works for different crack geometry ratios were developed by Wang and Lambert [44, 45].

The works carried out for the determination of SIF in railway axles is noteworthy. Carpinteri et al. [46, 47] analysed the propagation of a surface crack in a cylindrical axle subjected to rotational bending using a two-parameter theoretical model and assuming that the crack front presents a semi-elliptical shape. In Carpinteri et al. [48] the SIF is determined in axles under tension and bending. Subsequently, Madia et al. [49, 50] based on the research of Carpinteri et al. [47] developed a new approach to include the effect of axle-wheel interference fit in the crack growth analysis because of its negative effect on the remaining life estimation. These studies also investigated the FCG in different axle geometries and crack positions.

The FEM methodology applied for the evaluation of SIF provides really accurate results, but with a high computational cost. It should not be forgotten that these factors have to be constantly re-evaluated as the crack size and shape evolves, so the FEM methodology seems inflexible when it comes to easily generalize the results in geometry. Therefore, it is necessary to generate faster and more flexible numerical tools, which can be based on the weight functions developed by the aforementioned authors. These functions are first-order tensors that depend only on the cracked body geometry and by using the superposition principle any loading configuration can be represented by considering the application of the corresponding tensile, compressive, shear, stresses directly on the crack faces.

1.2.4 Material characterization

A key factor in the damage tolerance analysis is the material characterization in fracture. Fracture mechanics analyses rely on crack growth material data curves as the ones presented in Fig. 1.27, where Fig. 1.27a shows the crack growth curve in terms of crack size a vs. the number of cycles N, and Fig. 1.27b shows the crack growth rate da/dN vs. the stress intensity factor range ΔK in a double logarithmic scale. Both curves are explained below in detail. This figure consists of two different but related representations of synthetic crack growth data with example units for the sake of better illustration.

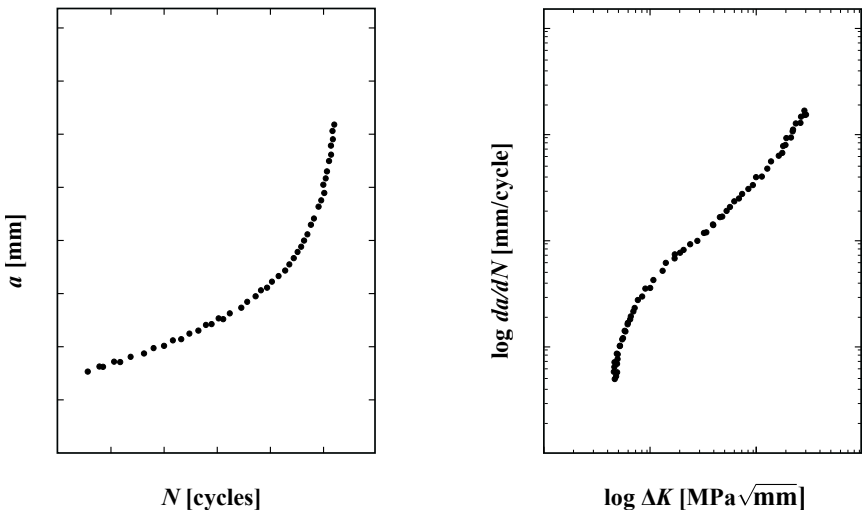

(a) a–N. (b) da/dN–ΔK.

Figure 1.27. Typical experimental fatigue crack growth data.

The da/dN–ΔK curve. Fatigue crack growth models require a significant amount of basic experimental material characterization. Raw fatigue crack growth datasets come in the form of the a–N relationship as in Fig. 1.27a. The compact-tension (C(T)) or middle-tension (M(T)) specimens defined in the ASTM E647 standard [42], tested under constant amplitude loading are the most frequently used geometrical configurations to map the relationship between the crack length, a, and the number of loading cycles, N. In order to use such data for subsequent fatigue life predictions, the set of $[N, a]$ points from the fatigue crack growth experiments has to be transformed into the set of $[\Delta K, da/dN]$ pairs as it is represented in Fig. 1.27b. Therefore, the two curves presented in Fig. 1.27 show the original and transformed fatigue crack growth data sets measured in a given experimental campaign. It is clear that the conversion technique is relevant for further fatigue crack growth analysis, and therefore it is standardized. Note that the lifespan, that is, the period of time that the crack takes to grow until final fracture, mainly depends on the first stages of crack propagation, while final regime plays a minor role as its growth rate da/dN is really fast.

The fracture toughness, K_c. Fracture toughness is a mechanical property that measures the resistance of a material to fracture. It is the critical stress intensity factor of a sharp crack where propagation of the crack suddenly becomes rapid and unlimited, i.e. the final regime. This parameter characterizes the intensity of stress field in the material local to the crack tip when rapid crack extension takes place. As in some other microstructurally sensitive material properties, fracture toughness is strongly dependent on the plane stress or plane strain conditions of the crack tip constraint due to component thickness. The typical thin and thick plates thickness effects on fracture toughness are illustrated in Fig. 1.28. The critical value of stress intensity factor in mode I loading measured under plane strain conditions is known as the plane strain fracture toughness, denoted K_{Ic}.

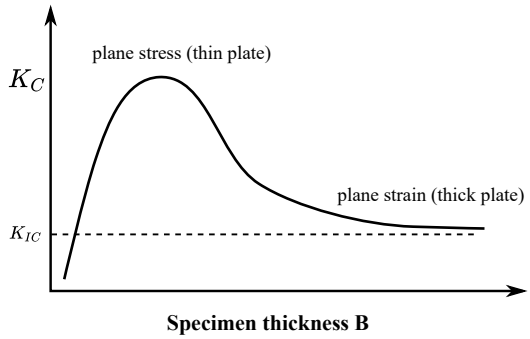

Figure 1.28. Variation of fracture toughness with specimen thickness.

The threshold stress intensity factor range, ΔK_{th}. The threshold stress intensity factor range, or also referred to as fatigue crack growth threshold, is defined as the asymptotic value of the stress intensity factor range ΔK at which the

fatigue crack growth rate da/dN of long cracks approaches zero. The experimental determination of fatigue crack growth threshold values is measured by reducing gradually the load until the crack growth rate reaches a very small value. Notice that only one threshold value per specimen can be determined for a given stress ratio. For instance, the ΔK_{th0} is the threshold SIF range measured using a stress ratio of $R = 0$. Thus, the complete characterization of the threshold behaviour of a material is time-consuming and expensive.

The determination of the da/dN–ΔK curve by experimental tests is addressed in the ASTM E647 standard [42] and in the ASTM E399 standard [51]. The ASTM E647 standard [42] is the standard which currently governs the fatigue crack growth test procedure covering the determination of fatigue crack growth rates from near-threshold to controlled instability providing results defined by the theory of linear elasticity, and transformation methods such incremental polynomial and secant methods, while the ASTM E399 standard [51] describes the determination of the fracture toughness K_{Ic} of metallic materials under predominantly linear-elastic plane-strain conditions. Innovative methodologies that do not need extensometers are becoming more and more frequent nowadays. One such example is obtaining the fatigue crack growth curve by using experimental full-field non-contact measurement techniques like the digital image correlation presented in Sánchez et al. [52] in combination with numerical post-processing methods.

Recently, some authors have investigated the effect of specimen geometry and loading conditions on the da/dN–ΔK curve. Varfolomeev et al. [53], investigating EA4T railway steel, found different da/dN–ΔK curves in region II, and even more pronounced differences in Region I for different types of specimens. The reason for these discrepancies in the results was considered to be due to plasticity-induced crack closure phenomenon. Beretta et al. [54] studied the effects of scale on the fatigue limit and crack growth rate for high strength steels used in the manufacture of high speed axles. The tests performed on micro-cracked specimens were compared with tests performed on full-scale axles showing that the results obtained on axles are less conservative. It is also pointed out in Beretta and Carboni [55] that the inspection intervals of safety-critical components should be calculated based on algorithms capable of describing the crack growth rate under service loads.

There are some other relevant aspects that have an effect in fatigue crack growth such as the importance of the stress ratio, mean stress effects, overloads, crack opening-closure mechanisms, and also some important practices such fatigue precracking before testing. Since this subsection is devoted to giving a brief overview of the fundamental material characterization in fracture mechanics, the reader is referred to [34] where all the aforementioned topics are broadly explained. The use of both the fracture toughness and the crack propagation threshold within the fatigue crack grow models is addressed in the next subsection.

1.2.5 Stable fatigue crack propagation

When the crack dimensions are larger than the plastic radius at the crack tip, the LEFM is applicable, otherwise, the elastic plastic fracture mechanics (EPFM) is required [34]. The former case is referred to as *long cracks*, and the latter case is referred to as *short cracks*. In the railway axles case, the focus is only on the LEFM approach briefly described in Subsection 1.2.2, since, in general, the dimension considered, for cracks included in a railway axle, corresponds to long cracks, with dimension of a few millimetres Zerbst et al. [56].

The earliest hypothesis that the fatigue crack growth rate, da/dN, was related to the stress intensity factor range of a load cycle, ΔK, was postulated by Paris et al. [57]. The typical plot of the crack growth rate with respect to the stress intensity range, da/dN–ΔK, is presented in Fig. 1.29 on log scales. This curve would fit the typical experimental fatigue crack growth in Fig. 1.27b.

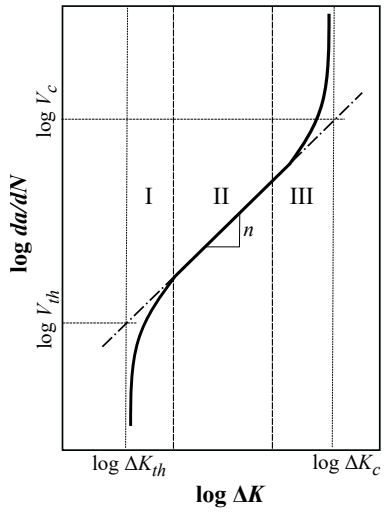

Figure 1.29. Typical crack growth rate vs. the stress intensity range.

At intermediate ΔK values, the curve is approximately linear, but the crack growth rate deviates from the linear trend at high and low ΔK levels. The three distinct regimes that are present in the previous sigmoidal curve can be explained as follows.

- Region I: At low growth rates, near the ΔK_{th} the growth is slow. Below this, there is no growth.
- Region II: At mid-range of growth rates, the behaviour corresponds to a linear zone where there is stable or steady growth.
- Region III: At high growth rates, there is a fast unstable growth until final fracture.

Paris and Erdogan [58] approximated the intermediate crack growth region II with a power law relationship, presented in Eq. (1.8), where a is the crack length, da/dN is the fatigue crack growth rate for a single load cycle N, n is an empirical constant representing the slope on a log-log scale, C is an intercept constant, and ΔK is the SIF range from the maximum and minimum K, i.e. K_{max} and K_{min}.

$$\frac{da}{dN} = C\,(\Delta K)^n \tag{1.8}$$

Paris and Erdogan were pioneers in proposing such an empirical expression to solve FCG problems fitting the intermediate linear region or regime II. The Eq. (1.8) is known nowadays as the Paris and Erdogan equation. The approach developed is based on a similarity concept: if the stress state at the crack front and its shape matches at a given time period for two different geometries and loading conditions, then the crack growth rate observed for the two cracks should be the same for that time period. This assumes that the crack growth rate of the material is a function of the SIF. The concept of similitude, when applicable, provides the theoretical basis for fracture mechanics. Similitude implies that the crack-tip conditions are uniquely defined by a single loading parameter, the SIF.

A variety of empirical FCG equations similar to the Paris-Erdogan equation were developed to represent all or some of the regions of the fatigue crack growth rate curve. Over the years, several improvements have been done in order to obtain a better accuracy and to include a variety of factors that represent effects that affect the crack growth rate such as the stress ratio, overloads, or the crack opening-closure phenomenon. Some of these crack propagation equations are collected in Table 1.6. Note that the material constants C, n, p, q, in the set of equations do not have the same numerical values or even units.

Table 1.6. Proposed fatigue crack growth rate models based on the stress intensity factor range.

Author reference	Region(s) / Effect(s)	Equation
Paris and Erdogan [58]	II	$\frac{da}{dN} = C(\Delta K)^n$
Allen et al. [59]	I, II	$\frac{da}{dN} = C(\Delta K)^n \left(1 - \frac{\Delta K_{th}}{\Delta K}\right)^p$
Forman et al. [60]	II, III / Stress ratio R	$\frac{da}{dN} = C\left(\frac{\Delta K^n}{(1-R)K_c - \Delta K}\right)$
McEvily and Groeger [61]	I, II, III	$\frac{da}{dN} = C\,(\Delta K - \Delta K_{th})^2 \left(1 + \frac{\Delta K}{K_c - K_{\max}}\right)$
Walker [62]	II / Stress ratio R	$\frac{da}{dN} = C\left(\frac{\Delta K}{(1-R)^{1-p}}\right)^n$
Elber [63]	II / Crack opening-closure	$\frac{da}{dN} = C\,(K_{\max} - K_{\mathrm{op}})^n$
Forman and Mettu [64] (NASGRO†)	I, II, III / Most generalized	$\frac{da}{dN} = C\left(\frac{1-f}{1-R}\Delta K\right)^n \frac{\left(1 - \frac{\Delta K_{th}}{\Delta K}\right)^p}{\left(1 - \frac{K_{max}}{K_c}\right)^q}$

† NASGRO or also known as Forman-Newman-De Koning (FNK) [65].

The state-of-the-art and most common expression to describe fatigue crack growth in all three regions is the NASGRO equation [34]. It is a general equation that covers the lower growth rate near the threshold ΔK_{th} and the increased growth rate approaching the fracture toughness K_c, as well as allowing for the mean stress effect by including the stress ratio R and also the crack closure via the Newman's crack opening function f. The different elements of the crack growth rate NASGRO equation were developed by Forman and Newman of NASA, Shivakumar of Lockheed Martin, de Koning of NLR and Henriksen of ESA and was initially documented by Forman and Mettu [64]. The three different regimes differentiated in Fig. 1.29 are denoted on the NASGRO equation presented in Eq. (1.9).

$$\frac{da}{dN} = \underbrace{C\left(\frac{1-f}{1-R}\Delta K\right)^n}_{Regime\ II} \frac{\overbrace{\left(1-\frac{\Delta K_{th}}{\Delta K}\right)^p}^{Regime\ I}}{\underbrace{\left(1-\frac{K_{max}}{K_c}\right)^q}_{Regime\ III}} \tag{1.9}$$

The NASGRO equation contains six material constants: C, n, p, q, K_c and ΔK_{th}. It should be noted here that the ΔK_{th} is not an actual material constant since it depends on the R ratio. According to the NASGRO formulation, for a particular material, the fatigue crack growth rate depends only on the loading parameters ΔK and R. Thus, all the above expressions assume elastic similarity of the growing crack, none of these equations incorporate a history dependence and are therefore strictly valid only for constant stress intensity loading [34]. However, many of these equations were developed with variable amplitude loads in mind. Although there are many situations where similarity is a good assumption for variable amplitude loading, the potential for history effects must always be taken into account. The NASGRO equation is adopted in the most recent research carried out on railway axles, e.g. Beretta and Carboni [55], Zerbst et al. [66] and Beretta and Villa [67].

These equations can be integrated to infer the fatigue life. It means integrating numerically the da/dN curve in order to estimate the number of cycles N, for the propagation of a crack from an initial defect size at to the final crack size at fracture. The integration is done numerically, especially when the fatigue problem deals with random load sequences or a sequence of loading blocks. In the case of a three-dimensional body, such as a railway axle, the integration of the FCG curve is carried out separately at the surface crack tip and at the deepest point of the crack front in order to predict the change in crack shape, usually keeping a semi-elliptical shape.

1.2.6 Damage tolerance assessment of railway axles

The basic ingredients for damage tolerance analysis are described in the previous subsections. This subsection will show how fatigue crack growth is considered in a damage tolerance analysis of an actual structure, a railway axle. The general scheme for a damage tolerance analysis of railway axles is given in the form of a stepwise procedure. Thereafter, the various options of the target information pursued are summarized. Finally, a number of typical inspection intervals for different railway applications are reviewed and presented to illustrate the application of damage tolerance analysis.

According to Zerbst et al. [66], the aim of a damage tolerance analysis of railway axles is either:

- to specify requirements for NDI which crack size has to be detected with high probability when the inspection interval T_{ins} is fixed by an existing maintenance scheme, or
- to determine inspection intervals, T_{ins}, according to a certain cumulative probability of detection in successive inspections (CPOD).

The input parameters and the working steps of a damage tolerance analysis of railway axles are shown schematically in Fig. 1.30.

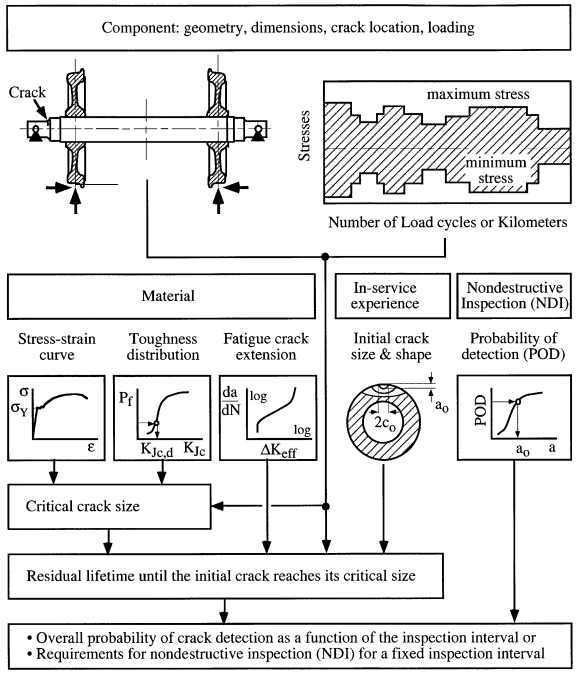

Figure 1.30. General scheme of a damage tolerance analysis of a railway axle [66].

As result of this procedure, it is possible to obtain the two aforementioned results:

- requirements for NDI for a fixed inspection interval, T_{ins}, or
- overall CPOD as a function of the inspection interval, T_{ins}.

The input parameters and basic steps of a damage tolerance analysis of railway axles are presented in detail in Fig. 1.31. They comprise the initial crack depth and shape, the applied loading including the bending, the load spectra, and the press-fit stresses, material properties, primary the da/dN–ΔK curve describing FCG process.

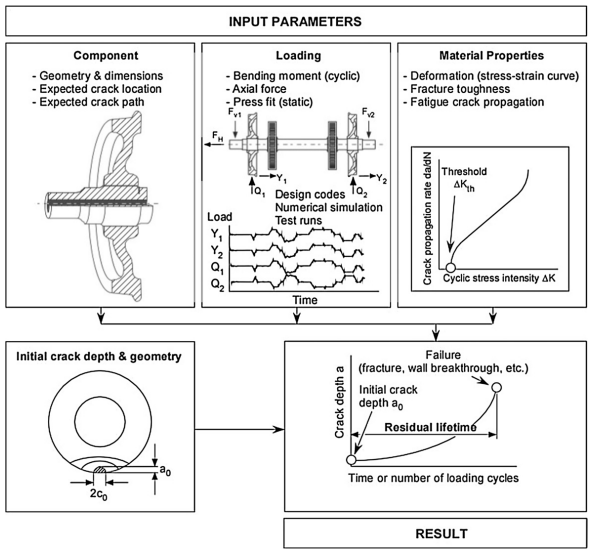

Figure 1.31. Inputs and basic steps of a damage tolerance analysis of a railway axle [7, 22].

There are two basic options of a damage tolerance analysis and both use the fatigue crack growth life results from the procedure in Fig. 1.31. What differentiates the two assessment options is the target information as shown in Fig. 1.32. Note that the two options aforementioned are denoted as option A and option B.

As it is thoroughly explained by Zerbst et al. [7, 22], the aim in option A is to specify the crack size which has to be detected by NDT with high probability. Starting from the number of loading cycles at failure, one inspection interval is subtracted. This way a crack depth a_d is determined which has to be found in an inspection. On the other hand, the aim in option B is to specify the overall probability of detection, CPOD as a function of the inspection interval. This option is based on the residual lifetime within which a number of inspections will be carried out depending on the inspection interval. When more than one inspection is planned within the residual lifetime, the instantaneous probability of detection (POD) increases from inspection to inspection due to the crack extension.

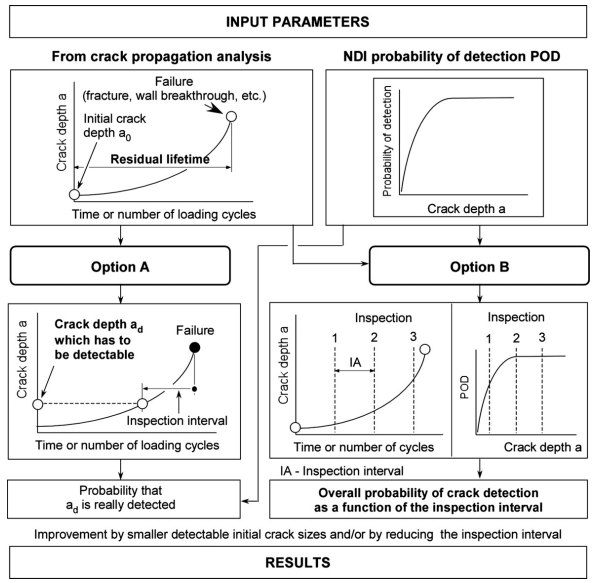

Figure 1.32. Two options of a damage tolerance analysis of a railway axle [7, 22].

The typical inspection intervals for different railway applications are collected and compared in terms of distance run and time in Table 1.7. Although operators tend to minimise the maintenance costs, they are required to operate in a way that should follow the indication of the standards, where applicable, e.g. the EN 15313:2016 standard [20] outlined in Subsection 1.1.4. Standards provide the operator a minimum requirement to follow in order to guarantee the safe service of the train. Operators should assure that, the method followed is as effective, and no less safe, than the method that is recommended in the requirements of the standard.

Table 1.7. Typical basic inspection and service frequency for railway wheelsets [68, 69].

Km	High Speed Train	3,000 to 20,000	30,000 40,000	90,000 200,000	180,000 200,000	500,000	500,000	1,800,000[2] 1,600,000[3]	4,000,000 (on condition)	1,800,000[2] 1,600,000
	Commuter Train	16,000	48,000	240,000		150,000 to 250,000	750,000	1,500,000	1,500,000 to 2,000,000	1,500,000
	Freight Train	50,000	100,000	200,000 to 600,000	200,000			1,500,000		1,500,000
	Distance-based inspection	Visual inspection*	Instrumented inspection*	NDT inspection*	Wheel tread reprofiling	Wheel tread reprofiling	Gear Unit Oil change	Wheel substitution[1] & bearing (unit)	Gear Unit bearing substitution	Wheel substitution[1]
Months	*Time-based inspection*									
	Freight Train	12	24	48 to 96	48			360		360
	Commuter Train	1	3	12		12	24	48	48-60	48
	High Speed Train	2 0.25	4 2.5	18 7.5	18 15	40	40	160[3] 150[2]	400	160[3] 150[2]

[1] Target values (depends on material / freight wagons influenced by tread braked wheels)
[2] China High Speed Train
[3] EU High Speed Train
*brake disc included

Focusing on freight train application, the NDT inspections are typically carried out in about 200 000–600 000 km or equivalently around 48–96 months. These figures at a glance give the idea that there is room for improvement and optimization of such inspection intervals, T_{ins}, for freight railways.

The general point of view conveyed by all authors who are advancing the development of damage tolerance methodologies is the importance of objectively quantifying the level of reliability of new designs in a way that ensures high component safety. It is clear that one hundred percent reliability and safety cannot be guaranteed, however a deterministic analysis cannot help in the assessment of design reliability since it does not take into account the different sources of uncertainty that have an effect in the crack growth process. There is some progress along these lines for the development of stochastic models in the railway sector. For example, the works by Beretta and Carboni [55] and Beretta and Villa [67] use approaches based on Monte Carlo simulations in order to obtain the life distribution, or the investigations by Zerbst et al. [7] that analyse the influence of the material parameter C on fatigue life by quantifying how its variation affects the fatigue dispersion. These investigations are usually time-consuming because, among other things, of the use of MC simulations. However, some interesting investigations proposed numerical methods based on the probabilistic finite element method, that is more efficient than the MC method. For instance, it is worth highlighting the works by Bea [70], Núñez [71], Grasa [72], Calvo [73] and Prados-Privado [74] that investigated different damage models regarding fatigue cracks. Therefore, it seems relevant to investigate these new perspectives when applied to the damage tolerance assessment of railway axles.

In general, it is important to highlight the multidisciplinarity of this field, which involves: (i) numerical activities for probabilistic evaluation of fatigue crack growth in railway axles and the sensitivity of the random variables that affect the growth process, (ii) experimental campaigns in order to characterize the fracture mechanics behaviour of the materials and components, (iii) the design and optimization of non-destructive testing methodologies that improve the probability of crack detection, and (iv) an overall new approach to establish inspection intervals in railway axles. Therefore, to improve the component LCC, huge research efforts on these lines are required to improve the reliability and to reduce component and maintenance costs.

1.3 Probabilistic aspects of damage tolerance

In addition to many highly technical writings on both pure and applied mathematics, Laplace published a popular work entitled *A Philosophical Essay on Probabilities* [75] in 1814. In its introduction, Laplace states: 'Strictly speaking it may even be said that nearly all our knowledge is problematical, and in the small number of things which we are able to know with certainty, even in the mathematical sciences themselves, the principal means for ascertaining truth, induction, and analogy, are based on probabilities.' For centuries, the importance of uncertainties in making the right decisions to solve a problem has been acknowledged. Indeed, engineering, like other aspects of life, is about making the right decisions based on data that may not be sufficiently well defined. The proper management of uncertainties makes the difference between a profitable and sustainable product and an ordinary one. In this context, it is necessary to develop applications and analysis tools that consider the stochastic nature of engineering problems, following Laplace, since its essay struck a chord in the concluding chapter stating: 'the theory of probabilities is, essentially, only common sense reduced to calculation and thereby it supplements most happily the ignorance and the weakness of the human mind.'

When applying the laws of mechanics to practical design and damage tolerance assessment problems, other considerations than those of pure mechanics often appear. In many cases, neither the fatigue laws, material data, loading conditions, crack size and shape, nor the probability of crack detections are known with any precision. Traditionally in mechanical engineering this is addressed by applying safety factors. Depending on the particular conditions and how safety-critical the component is, the safety factor is chosen in such a way as to ensure enough safety. In some cases this is prescribed by norms and standards, but this is not the case in the context of fracture assessments of railway axles. There are, however, further issues with this deterministic design philosophy. In the case when the input parameters and the output parameters are variable, the problem of selecting a representative safety factor value arises. In some standards the values are prescribed while in other cases the choice is left to the engineer. Therefore, in some advanced applications, a probabilistic approach is preferred, as supported in the following subsections.

In the context of liberalization of rail in Europe, more and more initiatives are promoted for the assessment of safety standards to determine the levels of safety, reliability and availability of rolling stock and in particular associated with railway axles. Thanks to the opening of the railway market and competition, the reduction of total life cycle cost of the whole wheelset became a driving topic for railway research. This also requires the optimization of axle inspection intervals, which in some cases involves a very high cost. To this aim, the different parameters explained above, involve aspects such as fatigue laws in crack propagation, material parameters, service

load cases, impacts, NDT techniques, etc., that due to their inherent uncertainties, they have to be addressed from a probabilistic perspective, and therefore they must be expressed in probabilistic terms.

Even when the traditional approach is used, probabilistic considerations are of help. Whilst probabilistic modelling has been used extensively in design, reliability, and safety considerations in many branches of engineering, this is not generally the case for most structures and components in damage tolerance assessment. To some extent this issue highly depends on tradition. Deterministic analyses in the field of damage tolerance unfortunately cannot help in assessing the underlying degree of conservatism of a given structural design with many sources of uncertainties, under operational conditions which are themselves known with some degree of uncertainty. Such analyses also appear inappropriate to assess the contributions of the many parameters involved in such problems, from a stochastic view point. In addition, they are insufficient to assist the decision-making process of scheduling the maintenance of structures as it is the case of a railway axle.

In the following, some of the most remarkable probabilistic features in damage tolerance are discussed. The revision and summary focuses on the probabilistic nature of fatigue crack growth, on material variability during crack propagation, on variable loading conditions in service, on damages produced by impacts, and finally on reliability issues of detection of flaws when using non-destructive techniques.

1.3.1 Probabilistic fatigue crack growth

As the initial flaws and cracks in structural materials result from manufacturing and environmental effects, they are inherently random. In addition, the cracks propagate in and between material grains boundaries, which are highly random due to the processes that initiate them. The scatter of the material fatigue resistance to cyclically applied loads, fatigue crack growth, is stochastic in nature. The scatter is often the reason for the differences between a deterministic prediction of fatigue lives and those observed in tests or in service. Therefore, it is necessary to develop probabilistic analyses even if the macrostructure is considered deterministic. Scatter in the microstructure, in the crack nucleation and small crack growth, in long crack growth, as well as uncertainties in service loads and material properties, considerably affect the fatigue crack growth life dispersion. When evaluating the reliability under fatigue crack growth, these random factors and uncertainties must be considered.

The inherently stochastic character of fatigue crack growth is clearly justified with the experimental tests, where the measurements quite naturally exhibit statistical variations. The scatter in fatigue data was discussed as early as 1926 by Mayer [76, 77], but it was only after the large replicate experiments at constant amplitude loading performed in 1979 by Virkler et al. [78] that the intrinsic stochasticity of

fatigue crack growth was investigated in detail. The geometry of the specimen used in Virkler's investigation was a 25.4 mm thick Center-Cracked-Tension (CCT) panel of 2024-T3 aluminium alloy. Nowadays, it is known as middle-tension (M(T)) specimen as described in ASTM E647 standard [42]. Its geometry is shown in Fig. 1.33.

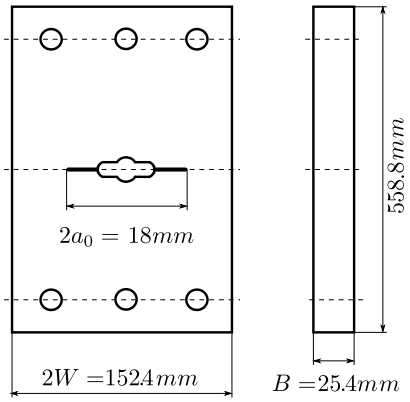

Figure 1.33. Virkler's M(T) test specimen [78].

The fatigue crack growth results for the 68 identical specimen tested by Virkler at constant amplitude loading are shown in Fig. 1.34.

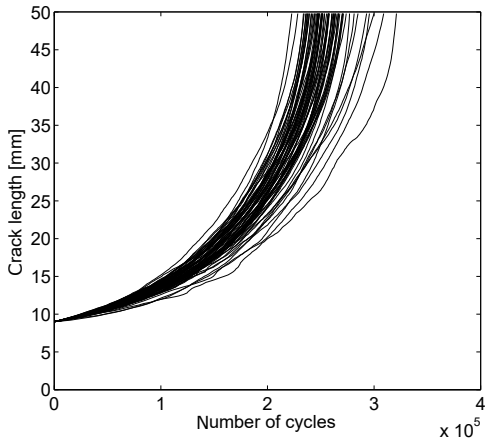

Figure 1.34. Virkler's experiments [78]: the 68 curves of crack length vs. number of cycles.

As can be observed from the data, the behaviour of crack growth is random, even when very carefully controlled experiments are performed with identical specimens. The curves of different specimens intermingle, and it is result of the two main random effects that can be distinguished Ortiz and Kiremidjian [79]: (a) each curve has an irregular shape, high frequency stochasticity; and (b) the mean crack growth curve of each experiment is different, low frequency stochasticity. This intrinsic stochasticity of fatigue crack growth is due to variability of material properties, material inhomogeneities, and also due to the inherent variability of the manufacturing process.

It was hypothesized that the collection of the final number of cycles, N_{fin}, for a final crack size, a_{fin}, is best described by the log-normal distribution. Thus, the histogram of $\ln(N_{fin})$ follows a bell-shaped curve. To demonstrate it, the experimental fatigue crack growth results (N_{fin}, a_{fin}) from the Virkler experiments are considered at the final crack size, that is at $a_{fin} \approx 50\,\text{mm}$. The resultant histogram obtained and the fitted log-normal probability density function (PDF) are shown in Fig. 1.35.

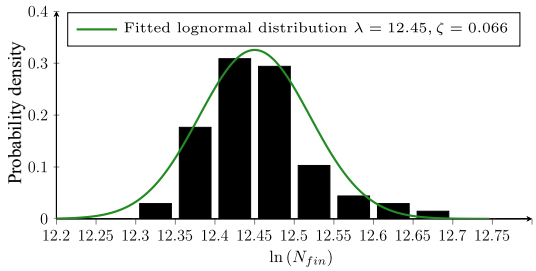

Figure 1.35. Histogram and probability density function fit from the Virkler's data [78].

The concept of a random phenomenon can be explained considering a repetitive experiment with a set of possible outcomes, such as the final number of cycles above. If the experiment is performed repeatedly with all conditions controlled and identical results are obtained, the phenomenon observed is called *deterministic*. If, on the other hand, the results are not identical, it is called *random* and a real value known as *probability of the event* can be associated with each of the results of this experiment, so that: the probability is related to the relative frequency of occurrence of the event for a large number of realizations of the experiment, it is bounded between zero and one, the sum of the probabilities of all possible events in a particular experiment is equal to one, all possible outcomes of an experiment are contained in the sample space, and any real variable defined in this space is known as a *random variable*.

As shown in the previous literature, fatigue crack growth is stochastic in nature. The randomness in components such as railway axles under fatigue conditions is inherent to at least three aspects. Firstly, it is clearly justified with the experimental tests, where the measurements quite naturally exhibit statistical variations as shown in Cervello [80], Novosad et al. [81], Beretta and Carboni [82] and Mädler et al. [83]. Secondly, the railway axles are under variable loading and a many cycles during their operation which means scattering of loads as shown in [84] and in Pokorný et al. [85] and Pokorný et al. [86]. The third reason is the fact that geometrical dimensions may have some variations that could significantly affect the functioning of a component as discussed by Traupe and Landaberea [87]. These aspects determine the complexity and the way to address any calculation, estimation or experimental analysis related to the fatigue process in railway axles application. This is one of the reasons why fatigue crack growth is difficult to predict as it involves intrinsically model parameters that are subject to uncertainty.

In the current state of practice the effects of these inherent uncertainties are mostly covered by the use of empirically based factors sometimes called safety factors and by the use of conservative assumptions. Such approaches are therefore most often deterministic. They are expected to ensure an acceptable safety level for the structure of interest, e.g. the probability of occurrence of individual lives shorter than the target life, albeit undefined, needs to be kept small enough to meet standards and requirements. The next subsections give an even deeper understanding of the main sources of uncertainties in railway axles applications.

1.3.2 Material scatter

The series of fatigue crack growth experiments performed by Virkler introduced in the previous Subsection 1.3.1, revealed that no matter how precise the experimental measurements are, the final number of cycles required for a crack to propagate from the precisely determined initial length to the final size, vary significantly.

A reason for the above problem is the dispersion of material fatigue resistance to cyclically applied loads, which is related to the scatter in the microstructure, in the crack nucleation and that is why the growth of small and long cracks may differ from one specimen to another. Therefore, one of the main obstacles to full probabilistic modelling is the difficulties in obtaining data of sufficient statistical quality.

To use the NASGRO equation, all the involved empirical constants must be estimated as described in the ASTM E647 standard [42] and in the ASTM E399 standard [51], as explained in Subsection 1.2.4. Firstly, the least square fit of the threshold data is carried out for the considered material to estimate the values of the material constants ΔK_{th}, C_{th}^{p}, and C_{th}^{m}. The same statistical technique is applied to crack propagation curves at $R = 0$ to estimate parameters C, n, p, q of the NASGRO equation. Besides, the K_c is measured according to the aforementioned methodology. It is important to highlight that the fitting procedure is statistical in essence on top the fact that all the experimental measurements are stochastic themselves.

It is well-known that the amount of crack extension per number of applied load cycles, i.e. the crack growth rate da/dN, fluctuates around the least-squares regression line. However, in the NASGRO model, several parameters are used to fit the experimental data accurately. The set of empirical constants in the NASGRO model are able to represent the scattered FCG data. It is assumed that the intra-specimen variability can be described by the probability distributions of these crack propagation parameters that at the same time are obtained via statistical fitting. Statistical analysis of various sets of fatigue crack growth data from experiments have been published in the literature such as in the section II of [88]. It should be noted that the availability of experimental data results in the railway axles field is quite limited.

In terms of application to railway axles, overloads and small loads influence on the fatigue crack growth are investigated in detail by Maierhofer et al. [89], where an improved NASGRO fatigue crack growth approach is calibrated for two common material grades for railway axles, namely EA4T and EA1N. These two effects are overlaid by statistical scatter and variability, which may be attributed to scatter within a single batch, inter-batch variability and inter-laboratory variability.

The investigation carried out by Maierhofer et al. [89] is based on experiments on small-scale fracture mechanics specimens from dedicated test bars. Depending on the purpose of each experiment, different parameters were obtained: the threshold stress intensity factor range at $R = 0$, ΔK_{th0} for long cracks, C_{th}^{p}, and C_{th}^{m}; the parameter C using the natural logarithm $\ln(C)$, n, and p; the statistical variability of the crack growth parameters of individual specimens during the experiments characterized via their statistical moments, empirical mean value and the empirical standard deviation; and the Pearson correlation coefficient (PCC) and statistical confidence for the pairs of parameters, n-$\ln(C)$ and n-ΔK_{th0}. Note however that an experimental full-scale validation of the previous results adopting real load spectrum is still missing.

Despite the importance of the richness of the parameters characterized, it is important to highlight the paramount relevance of the correlations investigated between the model parameters. It turns out that n and $\ln(C)$ are highly correlated, while no statistically significant correlation is found for n and ΔK_{th0}. Especially the former is indispensable for probabilistic crack growth assessment. The random variables n and C can be thought as a bivariate Normal–Log-normal distribution as they are highly correlated. The Pearson's correlation coefficient obtained by Maierhofer et al. [89] is $\mathrm{PCC}_{n,\ln(C)} = -0.968$ for EA1N steel grade.

The probabilistic FCG model presented by Wei [90] considers several input parameters of the NASGRO model for the EA1N and EA4T steels. For instance, the ΔK_{th0} is considered to belong to a normal distribution, C is assumed to follow a log-normal distribution while n is considered as constant. It is important to remark here that this consideration is bad practice as it is clearly discussed by Annis [91]. As the author argues, fixing either n or C seems at a glance like a reasonable solution, and it does reduce the over-prediction of scatter. While this is an obvious improvement, the error remains wildly unacceptable because the standard deviation of C or n is arbitrarily adjusted, i.e. manipulated until a believable result is achieved.

A statistical distribution for the sigmoidal crack growth rate function is presented in Paolino and Cavatorta [92]. It proposes a statistical description of crack growth rate curves considering: C as a log-normal distribution, n as normal distribution, $\log C$ and n as jointly normal distribution using a correlation coefficient PCC, ΔK_{th0} belonging to a log-normal distribution, and K_{Ic} as a log-normal distribution. It also states that the above assumptions are not the only ones possible, and therefore alternative statistical distributions can be adopted and their suitability evaluated.

Beretta and Carboni [55] proposed an approach based on Monte Carlo simulations in order to obtain the life distribution of solid round bars. Two sources of scatter are considered: (i) the dispersion of ΔK_{th0} data in the near-threshold regime, and (ii) the scatter along the Paris region. Considering the first source of scatter, i.e. the threshold region, two assumptions are made. One considers that the ΔK_{th0} belongs to a normal and the other assumes a log-normal distribution. The second source of scatter is considered as the parameter C as belonging to a log-normal distribution, while the slope parameter n is kept constant. It is important to remark here that this consideration is bad practice as aforementioned explained based on Annis [91]. Note also that the parameters $\log C$ or n with ΔK_{th0} are considered as independent.

Regarding the random variable threshold stress intensity factor range at $R = 0$, ΔK_{th0}, there is not a clear consensus about what probability distribution is most suitable. As shown, it is considered normal in Wei [90], log-normal in Paolino and Cavatorta [92] and both normal and log-normal in Beretta and Carboni [55].

A random variable approach for the analysis of fatigue crack growth is presented by Beretta and Villa [67]. The article deals with the analysis of a probabilistic description of crack growth based on the NASGRO equation. It addresses a description of Virkler's crack growth data, which shows a correlation between the parameters n, $\log C$, and ΔK_{th0}, but unlike Maierhofer et al. [89], in this case only the PCC is looked at, not whether the correlation is statistically significant or not. In contrast to Maierhofer's paper, it indicates that there is a two-to-two correlation between the three variables. The analysis is then applied to a set of crack growth data obtained from a steel applied in the manufacturing of railway axles. The same kind of analysis was performed and in this case, the parameters n and $\log C$ show a very high correlation, while ΔK_{th0} shows a weaker dependence on the other parameters. The authors conclude that a reasonable approximation could be obtained by assuming a bi-variate Gaussian distribution for n and $\log C$, considering ΔK_{th0} as an independent variable.

As for the correlation between the parameters n, C, and ΔK_{th0}, there is clear consensus on the correlation of the first two, i.e. n and C, but there is not so clear consensus on the significance of the correlations of these with the third ΔK_{th0}.

To better understand the correlation between the parameters n and C, it is advisable to review an article on probabilistic life prediction by Annis [91]. Many analysis tackle probabilistic life prediction by replacing constants with probability distributions. The problem arises when the statistical relationships among the parameters are ignored or given little attention. The simple substitution of distributions for constants will indeed produce a non-deterministic result, but the corresponding probabilities are sometimes inaccurate. The article claims that probabilistic life prediction is not as easy as it looks at first glance. It explores the Paris equation to illustrate many statistical realities that are often ignored by otherwise careful engineers.

One such important issue is that the Paris law parameters behave in tandem. A schematic plot of crack growth rate vs. stress intensity on a log-log grid is shown in Fig. 1.36. It shows why C and n are jointly distributed. When the slope, n, is shallow the intercept, C, must be larger for the resulting line to go through the data. Similarly, a steeper slope requires a smaller intercept. Note that in this schematic the intercept is $C = \log(da/dN) = -10$, at $\log(\Delta K) = 0$.

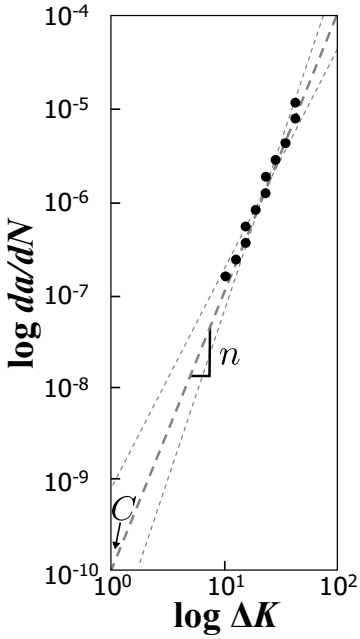

Figure 1.36. Schematic showing why C and n parameters are correlated. [91].

The main outcome of the article is that in the event of a fatigue crack growth equation used for a probabilistic analysis, the key to obtaining realistic predictions is to consider the correlation between the parameters C and n. Therefore, these calculations should correctly model and implement the multivariate joint probability distribution of the two parameters.

The discussion by Zerbst et al. [7] provides damage tolerance options applied to railway axles and factors influencing the residual lifetime as well as the required inspection interval. These comprise material properties such as the scatter of the $da/dN - \Delta K$ curve, the fatigue crack propagation threshold ΔK_{th} and the toughness of the material.

It analysed the influence of the material parameter C on fatigue life by quantifying how its variation affects the fatigue dispersion. Usually an upper bound curve to the $da/dN - \Delta K$ data is applied. The authors found that considering 95 % upper to a 5 % lower bound of C corresponded to a variation in residual lifetime of a factor of three.

It is worth highlighting the dispersion found in the ΔK_{th} parameter and its dependence on the experimental characterization technique used. This effect is relevant because the scatter in the fatigue crack propagation threshold if taken into account will introduce a significant dispersion in the residual lifetime analysis. Additionally, the paper provides an example of how the difference between threshold values can have an effect on the predicted residual lifetime of an axle. The ΔK_{th} value including scatter was identified to be problematic for the analysis because the residual lifetime sensitively responded to even small variations in threshold.

These studies among others, constitute the first steps for subsequent approaches for the analysis of the variability in the fatigue crack growth process in railway axles. Statistical fatigue crack growth data is rare and thus should be obtained from new scheduled tests, which are costly and time-consuming. Another limitation of the available statistical fatigue crack growth data is the fact that the materials tested often come from a single production batch, while in practice, the materials used by manufacturers come continuously from different suppliers. Therefore, the resistance of material to fatigue crack propagation will vary from batch to batch. On the other hand, the same by nomenclature material tested in different laboratories by using a standard experimental set-up comes from variety of suppliers and therefore, it is more representative in terms of batch to batch variability.

The statistical variability of the parameters among specimens during the experiments can be characterized via their statistical moments as the empirical mean value, the empirical variance, etc. In addition, these parameters can be tested for possible correlations. In any crack growth prediction or simulation methodology, it is important to consider the relationships among the random parameters in terms of probability in addition to the statistical moments of the parameters individually. Notice that disregarding the inherent correlations between random parameters could lead to incorrect results. In consequence, taking account of the correlations between parameters is of major importance for a proper probabilistic analysis. Taking advantage of the previous experimental material scatter measurements, inspection intervals for railway axles may be determined on the sound basis of probabilistic fatigue crack growth calculations.

1.3.3 Variable amplitude loading

The methods for analysing constant amplitude fatigue loading conditions are fairly well established, although a number of uncertainties remain. Constant amplitude loading refers to either constant stress amplitude, σ_a, or constant stress intensity amplitude, K_a, as depicted in Fig. 1.25. Variable amplitude fatigue loading introduces additional difficulties that are not fully understood. Some relevant aspects of variable amplitude loading are discussed below.

Similitude of crack tip conditions, which involves a unique relationship between da/dN, ΔK, and R, is usually valid for constant amplitude loading. Real structures, however, seldom fit to this ideal. A typical structure experiences a spectrum of stresses over its life. In such cases, the crack growth rate at any moment depends on the current loading conditions. Accordingly, only cyclic stresses levels where $da/dN > 0$ contribute to fatigue, and therefore are considered for the crack growth extension. Cyclic stress levels where $da/dN = 0$ do not contribute to fatigue crack growth, however, the total number of cycles should include all cycles, even those that do not contribute to fatigue damage. Of course, the da/dN is also a function of crack size, so it must be continually recomputed during the life calculation.

Several researchers have addressed the question of whether variable amplitude loading effects may play an important role in railway axles, but the results are still unclear. The effect of variable amplitude load is tackled in Zerbst et al. [66] using the NASGRO equation and a real loading sequence, not finding a clear load interaction effect. Similar results are obtained by Beretta and Carboni [93] for a high speed traffic loading sequence. However, Sander and Richard [94] disagree with this conclusion based on their own investigations of railway axles with block loading sequences. In a study by Beretta and Carboni [82], a negligible interaction effect for EA1N steel test specimens is found, but significant crack growth retardation in full-scale axles which experienced the same loading sequence is inferred. This result might be the consequence of a different crack closure behaviour due to a different constraint situation shifting the threshold ΔK_{th} to higher values in the axles, i.e. the variable amplitude effect, by its nature, would be a ΔK_{th} effect. Another result that points into this direction is provided by Luke et al. [95], where a negligible load history effect at high ΔK levels but strong retardation at lower ΔK is observed. Notice that in the investigation by Zerbst et al. [66], any loading sequence effect was found in calculations performed with threshold values equal to zero, what implies that the linear region II is extrapolated for $\Delta K < \Delta K_{eff}$. However, for different ΔK_{th} values, this investigation shows some sequence effects that depend on the ΔK_{th} used. To sum up, there are still challenges to be investigated in the research area of variable amplitude loading in order to objectively quantify the reliability of wheelsets.

The current state of the art of FCG analysis of railway axles seems to neglect any load sequence effect but uses stress spectra obtained by cycle counting methods, e.g. a rainflow algorithm. It is important to acknowledge that railway axles are subjected to load sequences of varying amplitude, so these complex loads must be considered when determining the evolution of the SIF during the crack growth process in order to calculate a reliable prediction of fatigue life. Although in the railway sector there is no standard defining the random load supported by axles under service conditions, different research efforts have attempted to quantify the effects of the randomness of the load on fatigue life. Several examples of railway axle load spectra, which are a key part of variable amplitude fatigue analysis, are provided below.

The load spectrum in a freight train from the UIC B 169/RP 36 report [84] is shown in Fig. 1.37. The stress collectives from representative traffics with heavy loads were measured in Germany on wheelsets with an axle load of 22.5 t. The amplitude and frequency values scaled for 660 000 km and for 15 000 km are shown in tabular form.

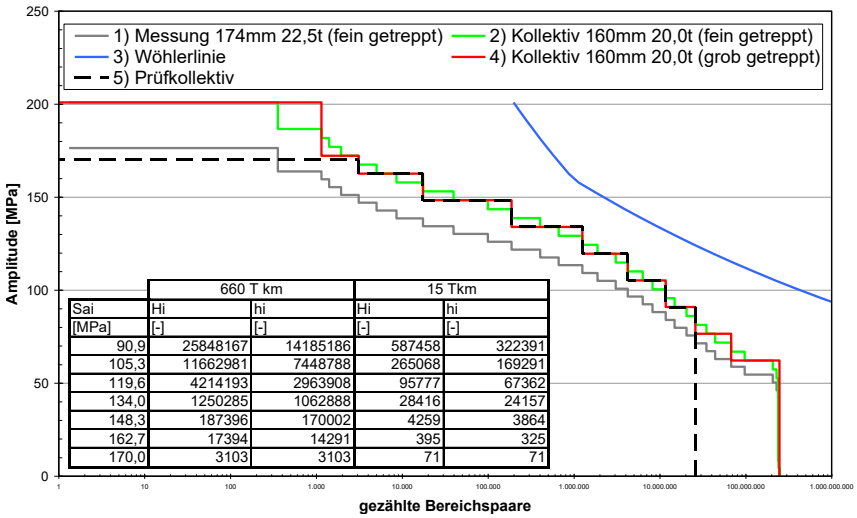

	660 T km		15 Tkm	
Sai	Hi	hi	Hi	hi
[MPa]	[-]	[-]	[-]	[-]
90,9	25848167	14185186	587458	322391
105,3	11662981	7448788	265068	169291
119,6	4214193	2963908	95777	67362
134,0	1250285	1062888	28416	24157
148,3	187396	170002	4259	3864
162,7	17394	14291	395	325
170,0	3103	3103	71	71

Figure 1.37. Stress spectrum in a freight train [84].

An exhaustive list of stress spectra in railway axles can be found in the following investigations: Beretta and Regazzi [25], Mädler et al. [83], Pokorný et al. [86], Beretta and Carboni [93], Luke et al. [95], Beretta et al. [96], Watson and Timmis [97], Regazzi et al. [98] and Traupe et al. [99].

1.3.4 Flying ballast impacts

The phenomenon of flying ballast is especially important in high-speed rail operations. Nonetheless, ballast particles away from the track bed might cause damage to freight axles. This subsection briefly identifies the potential and hazard consequences of ballast impacts in the current railway system.

According to Zerbst et al. [22] and Watson [100], the occurrence of impact damaged axles can be estimated to be 5 % for freight axles. As shown in Fig. 1.38, the mean value depth of the detected impact notches is about 0.8 mm. The distribution of impact craters is described by a Weibull distribution but can also be approximated by a log-normal distribution. A 2 mm crack corresponds to the 95 % percentile of the Weibull fit. That is, the upper bound approximates to depth a of 2 mm. Ballast impacts are a rather typical issue but are found to be larger than those of typical corrosion pits. Of course a ballast-induced notch is not a crack, although there is some chance of developing small fatigue cracks from these sharp edges.

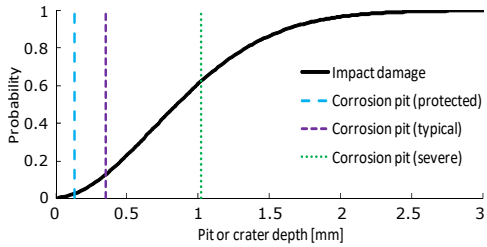

Figure 1.38. Depth of impact craters and comparison with corrosion pits [100].

The histogram of impact depths is as shown in Fig. 1.39 according to Watson [100] and Gravier et al. [101].

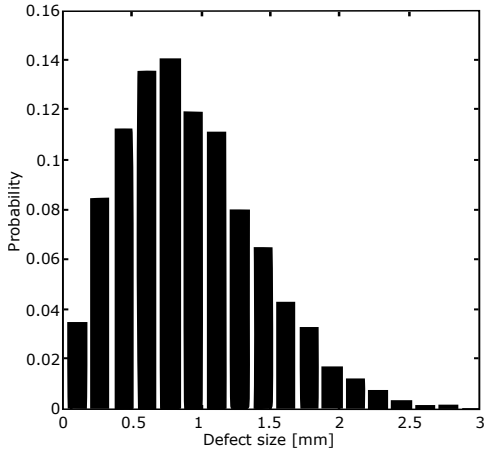

Figure 1.39. Typical histogram of impact depth [102].

Despite the *infinite life* methodology adopted for railway axles design, notable accidents have occurred in the past as shown in Subsection 1.1.2. The current methodology is unable to consider the deterioration of the axles during service, such as paint detachment shown in [103], pitting from corrosion as by Beretta et al. [104], or damage from ballast impacts such investigations by Gravier et al. [101, 105]. Some examples of these are damages shown in Fig. 1.40.

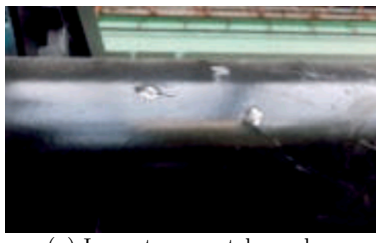

(a) Impact or scratch marks.

(b) Paint damage and oxidation.

Figure 1.40. Different damages of an in-service railway axle [103].

These initial flaws can act as the initiation of a fatigue crack that could become similar to the transition crack shown in Fig. 1.41, causing final fracture of the axle.

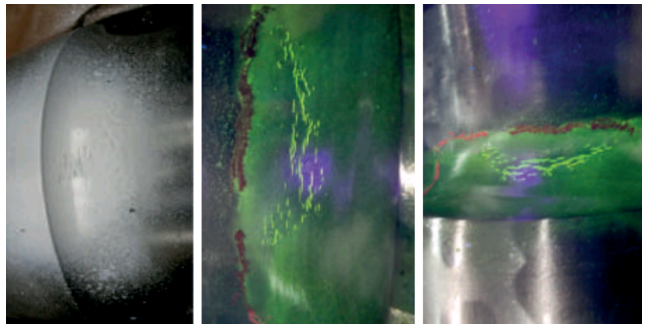

Figure 1.41. Transition fatigue crack [103].

In damage tolerance analysis, the initial crack size is usually defined by the NDT detection limit. However, railway service experience has also to be taken in consideration. Ballast impacts occur particularly on high speed tracks in snowy seasons, in tunnels and after a track renewal. That impacts are seldom but when they occur they can leave sharp angled notches of up to 2 mm in depth as described in Gravier et al. [101]. Because such an incidence could happen right after a maintenance inspection, seems reasonable to consider this size as likely initial crack size even if the NDT methods in use were able to detect cracks smaller than 2 mm.

1.3.5 Reliability of probability of detection

Railway axles are subjected to deterioration during service such as contact fatigue, friction fatigue, thermal fatigue, fatigue caused by rotating bending and/or torsional oscillations, abrasion wear and tear, corrosion and loss of paint, damage from ballast impacts, or impacts during maintenance. To detect such damages and prevent catastrophic failures of the safety-critical axles, it is necessary to perform periodic NDI of the vehicle in service. This issue dates back to the steam age when a railway worker checked the integrity of train wheels and axles via tapping them with a hammer and listening to the sound made to determine the integrity of them. The worker was able to tell from the note heard whether the wheelset was fine or not. The rudimentary role of the *wheeltapper* was quite common and of crucial importance in the 19th century. This *tap test* was the first way to inspect wheelsets in service, and it can be thought to be the precursor of ultrasonic testing. Nowadays, the most common methods for inspecting railway axles are: visual testing (VT), ultrasonic testing (UT), and magnetic particle testing (MT). Such inspections are planned at predetermined intervals, and so far are based on the experience of the operators or the manufacturers. Determining the inspection interval based on the experience is a clear inconsistency when aiming for the highest safety at the lowest cost.

The NDT performance is a statistical matter Zerbst et al. [56], and the characteristic adopted for evaluating its performance is the POD vs. crack size curve, commonly referred to as POD curve. The probability of detection (POD), as the name suggests, is stochastic in nature. The probability of detection that is typical of a given methodology and test method shows the capacity of detection of an inspection technique in regard to discontinuity size. However, in real situations, POD curves do not have an ideal behaviour. The typical shape of the POD vs. crack size curve is shown in Fig. 1.42.

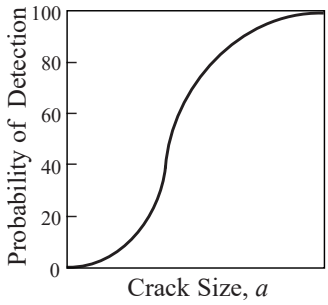

Figure 1.42. Probability of crack detection POD as a function of crack size a.

Commonly, such a curve is explicitly expressed as a function of a characteristic linear dimension of the flaw, for instance: diameter, crack length, crack depth, etc. However, it is important to note that it is also function of many other physical and operational parameters such as: the NDT method, the particular material, the complexity of the geometry, the flaw shape, and environmental and human influence. This, in fact, means that the POD curve obtained in laboratory when using certain fixed conditions and operators, is of limited application to other cases due to its intrinsic variability.

The statistical nature of NDT derives from the experimental evidence that repeated inspections of same flaws do not necessarily result in consistent indications. The probability of detecting a flaw increases with its size and may not reach a 100 %, or it would refer to an unrealistically large crack size. Note also that the scatter of POD values for a given size can be significant. Because of the high effort and cost involved in this kind of characterizations, only a few curves are available. The POD vs. crack size relationships for various NDT methods widely adopted in the railway axle field were obtained by Benyon and Watson [106]. Additional POD curves can be found in the following investigations: Wei [90] and Watson et al. [107]. Some examples of investigations that rely on these curves are the following: Zerbst et al. [22, 56, 66, 108], Pokorný et al. [86] and Carboni and Beretta [109].

In the damage tolerance context, non-destructive inspection refers to the in-service testing which besides the performance of the NDT method used, refers to a number of additional variable factors aforementioned such as the automation, the operator skills with respect to the test method and the complexity of component inspected.

1.4 Probabilistic approaches in mechanical engineering

It is currently recognised that the statistical nature of the mechanical properties of solid materials, the scattering of loads and uncertainties inherent to geometrical parameters, affect their structural behaviour, and therefore probabilistic numerical approaches for reliability assessment and durability prediction are needed. Probabilistic analyses are a useful complement to deterministic analyses that can be used in the design of components or structures and to support the decision-making process of defining maintenance inspections. Those applications still deserve some developments via the extension of the prevailing numerical methodologies. One such area is damage tolerance in the railway sector, where no systematic and detailed probabilistic analysis is provided so far, especially to define in service inspection intervals in train axles for crack detection.

Nowadays, probabilistic methods are of great importance in research and developments in engineering, which is challenged by new technologies and rapidly changing needs and values in the society. Contemporary needs related to, for example, life cycle analysis, product optimization, assessment of existing structures, etc., still give room to new developments in order to establish accurate and practically applicable probabilistic engineering methods to support them.

This section provides a description of methods dealing primarily with probabilistic and statistical approaches to contemporary structural problems encountered in diverse technical disciplines such as aerospace, civil, marine, mechanical, and nuclear engineering. The description aims to maintain a healthy balance between generality of techniques and discussion of problem-specific alternatives, presenting a number of ideas among different probabilistic approaches in mechanical engineering.

Essentially, probabilistic analyses focus upon the quantitative characterization and reduction of uncertainties in both computational and real world applications. They try to determine how likely certain outcomes are if some aspects of the system are not exactly known, i.e. predicting the effects of random variability. There are two major types of probabilistic approaches. The first one is the forward propagation of uncertainty, where the various sources of uncertainty are propagated through the model to predict the overall uncertainty in the system response. The second one is the inverse assessment of model uncertainty and parameter uncertainty, where the model parameters are calibrated simultaneously using test data.

There have been a number of investigations on the first approaches and a majority of uncertainty analysis techniques are developed for it. On the other hand, the second approaches are gaining attention in the engineering design community. Many methods are being researched or are currently in use to predict the random variability of an output variable. Some of these methods include the following:

- Methodologies for forward uncertainty propagation:
  - Simulation-based methods:
    - Monte Carlo (MC) simulations;
    - importance sampling;
    - adaptive sampling; and
    - Latin hypercubes.
  - Local expansion-based methods:
    - Taylor series;
    - perturbation method; and
    - first-order second moment (FOSM) method.
  - Functional expansion-based methods:
    - Neumann's expansion;
    - orthogonal or Karhunen-Loeve expansions;
    - polynomial chaos expansion; and
    - wavelet expansions.
  - Most probable point-based methods:
    - first-order reliability method (FORM); and
    - second-order reliability method (SORM).
- Methodologies for inverse uncertainty quantification:
  - Frequentist;
  - Bayesian:
    - modular Bayesian approach; and
    - fully Bayesian approach.

Although this thesis focuses on local expansion-based methods via Taylor series and checks its performance by comparison with simulation-based methods, namely the Monte Carlo method, the other probabilistic approaches listed are also briefly described in the following subsections. Due to the complex mathematical calculations in probabilistic approaches, in fact, sometimes intractable when handled in detail, the target here is to promote a deeper understanding of the methods considered rather than to provide a collection of equations.

1.4.1 Simulation-based methods

As it can be inferred from its name, simulation-based methods are probabilistic methods that rely on a simulation modelling and analysis. This is a broad class of computational algorithms where a system is mathematically modelled, and therefore computer-based simulations are able to provide information about its behaviour. Existing probabilistic simulation-based methods include Monte Carlo (MC) simulations, importance sampling, adaptive sampling, Latin hypercubes, etc. Below, the MC method is briefly summarized.

The MC method is well known and used in many fields of engineering for solving problems of random variables providing a probabilistic interpretation [110]. The essential idea consists of generating input variability via repeated random sampling and to evaluate a deterministic model obtaining many deterministic results that interpreted as a whole, form a probability distribution. Afterwards the response can be analysed in the desired statistical terms, e.g. expected values and variances. Using MC, the failure probability can be estimated when there are multiple random variables. This analysis is easy to perform, since it merely involves incorporating a random number generator into a deterministic model. Each MC simulation is referred to as a realization. Notice that, MC analysis is very inefficient, however, as numerous trials are required for convergence. In short, it provides non-deterministic results via brute force. Nevertheless, MC simulations are often improved by importance sampling. In this case, samples are not generated based on their distribution function, but on some arbitrary function and then weighted with their probability. For example, sampling techniques like Latin hypercube sampling can be used in order to ensure that the whole random space is captured.

There are some attempts to obtain the life distribution in the railway sector based on the MC method such as in the works by Beretta and Carboni [55], Beretta and Villa [67] and Giannella [111]. The accuracy of the statistical moments calculated in this thesis are checked by comparison with MC simulations.

1.4.2 Local expansion-based methods

Local expansion-based methods are probabilistic methods based on the local approximation of a function of random variables using math expansions such as the well-known Taylor series. In general, the function has to met some conditions such as being sufficiently differentiable in the vicinity of the objective, or having certain finite quantities as statistical moments. This is a broad class of methods where a function is approximated, thus representing its behaviour in the vicinity of the evaluation point. These linear or linearised methods have advantages when dealing with relatively small input variability and its accuracy tend to be better in cases when outputs

that do not have high non-linearities. Well-established probabilistic local expansion-based methods include Taylor series, the perturbation method, the first-order second moment (FOSM) method etc. Below, the FOSM method is outlined.

Generally, it may not be feasible to calculate the expected value and the variance of the response by means of the direct use of the expectation operator on the function which relates the random input and output variables if that function is not simple. In such cases, approximation techniques such as the FOSM are resorted to address the stochastic problem. The FOSM method is a probabilistic method to determine stochastic moments of a function with random input variables by using Taylor expansions, provided that the function is sufficiently differentiable and that the moments of the input variables are known. The objective is to determine the effect of the input random variables on the randomness of the function based on them.

The simplest version of the FOSM is illustrated in Fig. 1.43. It represents a function $Y = g(X)$ with only one random input variable X assumed to be normally distributed and the first-order Taylor series approximation of $g(X)$, that is, a linear equation, that is used to map the input randomness onto the y-axis.

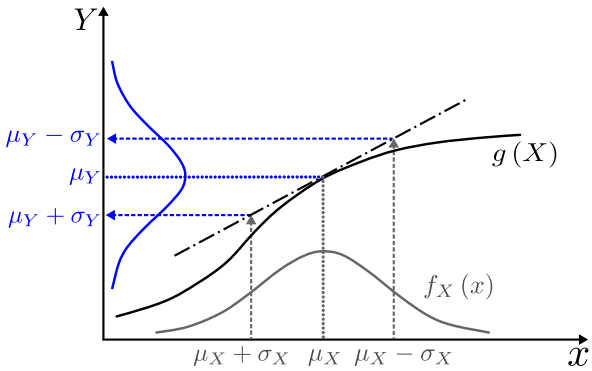

Figure 1.43. FOSM on a function with one random input variable.

The real output shape mapped on y-axis would be in some extent distorted and the distribution would be asymmetric, certainly not normal. When using a first-order Taylor series, the linear mapping provides a normal distribution for Y as represented. In order to enable the estimation of a non-symmetric or non-normal symmetric form that takes into account the effect of the non-linear function, a second-order Taylor approximation is thoroughly investigated in this thesis.

The FOSM method derives its name from the fact that it uses a first-order Taylor approximation of the function and uses only the first and second moments of the random input variables to determinate the expected value and the variance of the response. As a curiosity, it is worth mentioning that the term *moment* in statistics comes from physics. Pearson [112] adopted the word for probability distributions as an allusion to *moment of inertia*, a term common in physics, which describes

the mass distribution of a body in terms of its resistance to changes in angular momentum. Using the physical analogy, if the probability density function indicated the density of a beam, the expected value would be the position of its center of mass, and the variance would be its moment of inertia. However, this physical analogy is less intuitive for higher order moments.

Once the FOSM has been applied, it is common practice to check its results against the MC. Both methods are approximations in their essence, which one is more suitable, will depend on the requirements of problem considered. Probabilistic structural analysis is conditioned mainly by two characteristics, the efficiency and the accuracy. The FOSM method is a low-cost technique in terms of computation time while the MC is an expensive method. If the differences between the results provided are small enough, both methods are considered to be equally accurate and thus the use of the FOSM is recommended for applications that require fast estimations such as technical tools used in design or as an aid to the decision making process of defining periodic inspections of maintenance.

There are several examples in the literature where the Taylor series, the perturbation method, and the FOSM methods are employed to estimate stochastic distributions in the fatigue-related problems such as in the remarkable works by Bea [70], Núñez [71], Grasa [72], Calvo [73] and Calvo et al. [113].

1.4.3 Functional expansion-based methods

Functional expansion-based methods are probabilistic methods that rely on representing the r.v.s using a polynomial basis that is orthogonal to the distribution of the random vector. Depending on the distribution of the random vector, different types are distinguished. Existing probabilistic functional expansion-based methods include Neumann's expansion, orthogonal or Karhunen-Loeve expansions, polynomial chaos expansion (PCE), wavelet expansions, etc. Below, the PCE method is described.

The PCE method is an approach for representing a random variable in terms of a polynomial function of other random variables. The polynomials are selected to be orthogonal with respect to the joint probability distribution of these random variables. PCE is able to estimate the evolution of uncertainty in a dynamical system when there is probabilistic uncertainty in the system parameters.

An example where the PCE is used to estimate fatigue crack propagation in structures with random parameters is the work by Qiu and Zhang [114].

1.4.4 Most probable point-based methods

Most probable point (MPP)-based methods are probabilistic methods that use a response function that depends on the probabilistic distributions of the input variables. Each particular combination of input variables values has certain probability of occurrence based on the input distributions. Since each input variable combination gives a particular response value, the probability of obtaining a target response is equal to the probability of obtaining the associated input combination. Existing probabilistic MPP-based methods include the first-order reliability method (FORM) and the second-order reliability method (SORM). Below, these methods are addressed.

For FORM and SORM, the limit state function, which is a condition of a structure beyond which it no longer fulfils a relevant criteria, is approximated at the MPP. The limit state function divides the random space into a safety and a failure regions. The MPP is the point on the function with the highest probability density and with the smallest distance to the expected values of the inputs. The MPP is searched, then the limit state function is approximated at the MPP by a linear, first-order function FORM, or a quadratic, second-order function SORM, and finally the probability of failure is obtained. The MPP is calculated using optimization techniques.

An example of a univariate approximation at MPP for higher-order reliability analysis for predicting fatigue failure probability of components subject to random loads, material properties, and geometry is presented in Rahman and Wei [115].

1.4.5 Frequentist

Frequentist methods are probabilistic methods of inverse uncertainty quantification that use frequentist inference and probability, which treats "probability" in equivalent terms to "frequency" and draws conclusions from sample-data by means of emphasizing the frequency or proportion of findings in the data. Frequentist methods are considered to be the philosophical rival of Bayesian statistics. Well-established frequentist methods include statistical hypothesis testing and confidence intervals.

Given some experimental measurements of a system and some simulation results from a model, inverse uncertainty quantification estimates the discrepancy between the experiment and the model, often called bias correction, and estimates the values of unknown parameters in the model if there are any, frequently called parameter calibration. In regression analysis, the standard error of parameter estimates is readily available, which can be expanded into a confidence interval. This method is of great importance since it is typically implemented in a model updating process.

An example of frequentist statistical modelling technique for analysis of in-service stresses for fatigue life analysis in railways is given by Wang [116].

1.4.6 Bayesian

Bayesian methods are probabilistic methods of inverse uncertainty quantification in which Bayes' theorem is used to update the probability for a hypothesis as more evidence or information becomes available. Whereby the probability that a hypothesis is true is inferred based on both observed evidence and the prior probability that the hypothesis was true. They combine common-sense knowledge with observational evidence to eliminate complexity in a model by considering only meaningful relationships and disregarding the influences of all other variables on outputs. Prevailing Bayesian methods include modular and fully Bayesian approaches.

Several methodologies for inverse uncertainty quantification exist nowadays under the Bayesian framework. It is result of the use of Markov chain-based techniques. Bayesian methods allow to satisfactorily combine various sources of information into a common complex model.

There are many examples in the literature where Bayesian approaches are used, for instance, a comparison of frequentist and Bayesian methods for analysis of in-service stresses for fatigue life analysis in railways is given by Wang [116]. An additional example of a probabilistic estimation in a cyclic loading fatigue crack propagation application for the failure forecast method using Bayesian inference is provided by O'Dowd et al. [117].

The components of most mechanical structures are designed to be very reliable. Failures are so uncommon that any approach based on observed frequencies is, in general, out of the question. Therefore, any estimation of the probability of failure must be based on some form of modelling in which statistical information about parameters, such as crack dimension, loading, material data, etc., is combined by the methods of mathematical statistics. The models are therefore probabilistic in the sense that the variability of the different quantities is assumed to be random, while the governing equations are purely deterministic. Thus, a probabilistic treatment cannot replace deterministic modelling, but is an extension of the deterministic modelling to consistently take into account the uncertainties of the quantities involved.

1.5 European initiatives related to rail transport

Rail transport has had a revival in recent years or decades in its competition with cars and aeroplanes, due to road congestion and rising fuel prices, as well as governments investing in rail as a means of reducing CO_2 emissions in the context of concerns about global warming. In the following, some European initiatives related to rail transport are described.

1.5.1 European Green Deal

The European Green Deal is an integral part of the strategy of the European commission to implement the United Nation's 2030 agenda and associated sustainable development goals. The European Green Deal [118] presented in December 2019 strives to make Europe the first climate-neutral continent, setting out a clear vision of how to achieve climate neutrality in Europe by 2050. Transport accounts for a quarter of the EU's greenhouse gas (GHG) emissions. To achieve climate neutrality, a 90 % reduction in transport GHG emissions is therefore needed by 2050.

The transformation of the railway system will be pivotal to achieve the European Green Deal objectives by offering both decarbonised and time/cost-competitive transport solutions for passengers as well as for freight cargo.

The EU has raised its 2030 climate ambition, committing to cutting emissions by at least 55 % by 2030. The Fit for 55 package [119], adopted in July 2021, includes proposals for supporting a faster roll-out, relative to prior objectives, of sustainable transport solutions such as the railway.

1.5.2 European Year of Rail 2021

2021 was the European Year of Rail, an European Commission initiative as part of the EU's efforts under the European Green Deal to achieve climate neutrality by 2050 [120]. This initiative was an opportunity to highlight the benefits of rail as a sustainable, smart and safe means of transport. In the following, some benefits highlighted over the 2021 European Year of Rail are summarized.

The benefits of rail are not only for holidaymakers and commuters. Businesses and freight carriers can shift to rail and benefit from low-cost, increasingly competitive offers to transport their goods all over Europe and reducing their carbon footprint at the same time. The length of railway lines in use in km in the USA, the EU, China, and Russia are shown in Fig. 1.44, ready to meet any need.

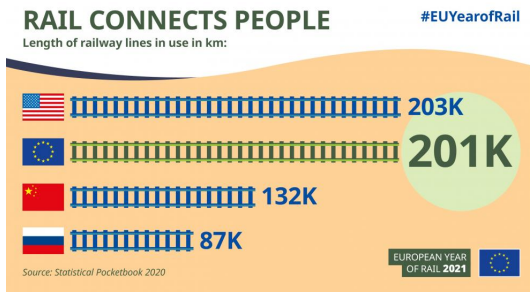

Figure 1.44. Length of railway lines in use in km [120].

Rail is one of the most sustainable forms of transport. Rail is green and sustainable because it is largely electrified and emits far less CO_2 than any equivalent travel by road or air. It accounts for only 0.4 % of GHG emissions from EU transport as it is shown in Fig. 1.45, while all EU transport accounts for 25 % of the EU's total emissions. Additionally, it is the only transport means that between 1990-2017 has consistently reduced its emissions and energy consumption, while increasingly using renewable energy sources. Increased use of rail is necessary to fulfil European climate objectives. Nevertheless, there are still some steps that can be taken to further improve the climate footprint of rail.

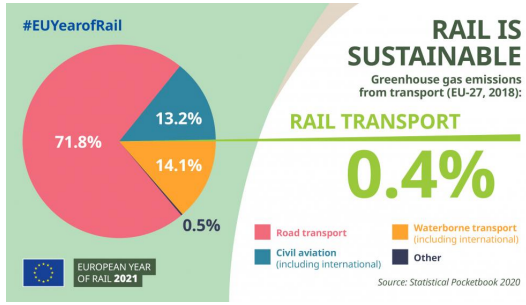

Figure 1.45. Greenhouse gas (GHG) emissions from transport (EU-27, 2018) [120].

Rail is affordable, comfortable and safe. It is the safest land transport means with the lowest incidence of fatal accidents as shown in Fig. 1.46. When railways are adequately taken care of, i.e. regularly serviced, maintained, replaced when needed, etc., an accident almost never happens.

Figure 1.46. Fatalities per billion passengers/km (2011-2015) [120].

Finally, some other interesting facts and figures about rail transport that were emphasised during the 2021 European Year of Rail [120] are: more than 916 000 people work in the EU railway sector, 21 % of the workforce in the EU rail sector are women, more than 9100 km of high-speed rail network in Europe, and 75 % of total train-kilometres are travelled by electricity-powered trains.

To recap, rail transport can be a good alternative to on-road vehicles. However, in order for them to be a feasible alternative, they have to be carefully maintained and managed. In the end, re-thinking the way people and goods are moving all over the world is urgent to combat and try to reverse the damages caused by climate change.

1.5.3 Europe's Rail Joint Undertaking

The Europe's rail joint undertaking (EU-Rail) is the European partnership on railway research and innovation established under Horizon Europe. It continues the achievements of the Shift2Rail Joint Undertaking (S2R) [121] developed under the Horizon 2020 initiative, that was the first European rail initiative to research and innovate (R&I) solutions to accelerate the integration of new and advanced technologies into innovative rail solutions. After the promotional European Year of Rail in 2021, concisely described in Subsection 1.5.2, this EU-Rail partnership aims to accelerate research and development in innovative technologies and operational solutions supporting the fulfilment of European Union policies and objectives relevant for the railway sector and supporting the competitiveness of the rail sector and the European rail supply industry [122].

The objectives of EU-Rail are devoted to addressing the EU policy objectives, rail sector vision, and the challenges inherent to the transformation of the rail system. Specifically, this initiative target the following goals:

(i) meeting evolving customer requirements;

(ii) improved performance and capacity;

(iii) reduced costs;

(iv) more sustainable transport;

(v) harmonised approach to evolution and greater adaptability;

(vi) reinforced role for rail in European transport and mobility; and

(vii) improved EU rail supply industry competitiveness.

It should be noted here that the fundamentals of this thesis are aligned with the general objectives aforementioned, especially with improving performance, reducing railway axle maintenance costs, and therefore making the railway a means of transport more sustainable what at the same time reinforces the EU transport and mobility competitiveness.

To achieve the previous objectives, five areas of priority for EU-Rail are determined:

(i) European rail traffic management and supporting its key role in a multi-modal transport system.

  (a) delivering a European rail traffic management system to achieve dynamic capacity management, improved performance, and cost efficiency;

  (b) providing systems for real time management of the network; and

  (c) supporting the key role of rail in future transport and mobility systems.

(ii) Digital and Automated Train Operations.

  (a) delivering an adaptable and scalable track-side and on-board architecture and associated solutions; and

  (b) delivering scalable automation in train operations.

(iii) Sustainable and digital assets.

  (a) solutions to reduce the environmental footprint, improve accessibility, and increase resilience of the rail system; and

  (b) innovative solutions to minimise asset life costs.

(iv) Competitive digital green rail freight.

  (a) developing and integrating new operational and technological solutions to make rail freight more competitive; and

  (b) fully digitalising operations to support rail freight in the logistics value chain.

(v) Smart solutions for low density lines, cost-efficient regional lines.

  (a) to adapt solutions to the whole rail network, supporting competitiveness of the whole sector.

Once again, the essentials in thesis are aligned with the priorities aforementioned, particularly with the actions to develop solutions for reducing the environmental footprint of the rail system by reducing railway axle maintenance costs what helps to extend their useful life providing technological solutions to make rail more competitive.

These priorities will ensure a fast transition to more attractive, user-friendly, competitive, affordable, easy to maintain, efficient and sustainable European rail system. Moreover, they are devoted to delivering a sustainable and resilient rail system by developing a zero-emission and climate resilient infrastructure, applying circular economy to the rail sector, piloting the use of innovative technologies, designs and materials in the full life-cycle of rail systems.

To improve the competitiveness of the rail freight transport, in addition to the safety analysis, an overall assessment of the LCC should be done as an essential part of the approval process when introducing new developments. The LCCs should cover not only the acquisition costs but also the maintenance and operational costs over the entire lifetime of the wheelsets.

Due to its enormous importance in relation to passenger safety and public economy, several research activities have been carried out in the field of design and maintenance of railway wheelsets throughout Europe. Below, some remarkable examples are summarized. The WIDEM project "Wheelset Integrated Design and Effective Maintenance" [123] investigated damage accumulation assumptions for the safe service life concept as well as NDT methods. The EURAXLES research project "Minimizing the risk of fatigue failure of railway axles" [124] aimed at reducing the LCC of wheelsets. The measures investigated included the integration of appropriate risk analysis methods into the design concept, the improvement of corrosion protection systems, and advancements in NDT methods. The WOLAXIM innovation project "Whole Life Rail Axle Assessment and Improvement" [125] aimed at providing three new methods for crack detection and corrosion assessment in railway axles. One method was for the exposed body of the axles, intended primarily for freight wagons. A second method was specifically for the hollow axles of high speed trains, improving the speed of the inspections. The third method aimed to enhance the measurement of corrosion in axles. Another example is the SUSTRAIL project "The sustainable freight railway: Designing the freight vehicle track system for higher delivered tonnage with improved availability at reduced cost" [126], that contributed to make the rail freight system regain position and market share. The proposed solution was based on an improvement in both freight vehicle and track components in a holistic approach to achieve a higher reliability and increased performance. The approach pursued innovations in rolling stock and freight vehicles, targeting an increase in speed and axle-load, combined with innovations in the track components. One last example may be the FR8RAIL project "Development of Functional Requirements for Sustainable and Attractive European Rail Freight" [127], submitted as part of the Shift2Rail Joint Undertaking (S2R) [121] developed under the Horizon 2020 initiative. The main aim was the development of functional requirements for a sustainable and attractive European rail freight meeting an ambitious 10 % reduction in the costs of freight transport by rail.

1.6 Discussion of open points to be covered

Among all the factors related to the design, operation, and maintenance of railway axles, the following points are still under discussion, and are taken into account during the research activity throughout this thesis.

Reliability engineering is a comparatively new discipline in scientific terms that emphasises the probability that a component will perform a required function safely under specific conditions for a certain time. Reliability engineering is then the study of the longevity and failure of a component based on four attributes which are: probability, proper operation, a given environment, and time. Early contributions introducing probabilistic ideas to the problem of structural reliability were those by Mayer [76, 77]. This work revealed general basic probabilistic methods as it was observed that component strength and loading conditions are random variables, and therefore there is an associated probability of failure. These probabilistic fundamental ideas were further developed establishing the theory of the FOSM method for reliability analysis by Cornell [128, 129]. This method has been widely used for many years by those engaged in the probabilistic analysis of structures. Recent research has contributed with new perspectives on the analysis of components in practical applications, taking advantage of the FOSM method. Thereby, it enables some new perspectives in the FCG analysis of components.

As mentioned, fatigue life prediction is essential for the design and maintenance planning of components such as railway axles. Consequently, a probabilistic approach that considers input statistical distributions and provides an output response distribution will be more useful than a deterministic one. Addressing the problem from a probabilistic point of view that is also efficient and precise is, therefore, a challenge. In some applications it is enough to obtain certain statistics of the response distribution, for instance, the expected value, the variance, or higher-order moments.

Over recent decades, probabilistic FCG methods are becoming popular. Some approaches consist in acquiring S-N diagrams from specimens, considering the variability of fatigue life, and then providing probabilistic fatigue S-N curves for the component integrity assessment as in Beretta and Regazzi [25] and Wu et al. [130]. Many other probabilistic models are based on deterministic crack growth equations such as the Paris' law by Paris and Erdogan [58]. For example, several probabilistic studies founded on the Paris' law are presented by Bea [70], Akama and Ishizuka [131], Bea et al. [132], Hillmansen and Smith [133], Hong et al. [134], Náhlík et al. [135], Wang et al. [136], Yasniy et al. [137] and Zhu et al. [138], being the model most frequently used. In recent years, new advances considering the complete crack growth curve have been made due to the increasing importance of considering the early stages of crack growth for a proper lifespan estimation. A modified version of the Paris' law,

the NASGRO equation by Forman and Mettu [64], represents the state of the art in the FCG field, being commonly used in railway axles evaluation. The NASGRO equation is commonly applied in the evaluation of railway axles as in investigations by Beretta and Carboni [55], Beretta and Villa [67], Náhlík et al. [135] and Mallor et al. [139]. Some probabilistic approaches use the MC method on the NASGRO equation to quantify the material uncertainties and loading conditions in the fatigue behaviour of railway axles as the ones in Beretta and Carboni [55] and Beretta and Villa [67]. Additionally, a comparison of the fatigue life calculation in railway axles according to the Paris' law and to the NASGRO equation is performed in Náhlík et al. [135]. In this article, for both models, several material parameters levels are considered to quantify how they affect the dispersion of the fatigue life.

It is worth highlighting the works made in the field of FCG life estimation according to the Paris' law using Markov chains and B-models by Bea [70], in the fatigue crack nucleation stage based on the Coffin-Manson damage model by Núñez [71], in the extension of the finite element method applied to bio-mechanics by Grasa [72], in the multiaxial fatigue assessment based on the virtual strain energy damage model of Liu by Calvo [73], and in the use of Markov chains and B-models applied to dental implants by Prados-Privado [74]. The probabilistic developments proposed in this thesis can be framed as a continuation of some research lines initiated by the previous researchers throughout their theses at the *Universidad de Zaragoza*.

It is important to note that so far few attempts have been made to apply the FOSM method considering the NASGRO model. A statistical description of the NASGRO model applying the FOSM method is derived by Corbetta et al. [140]. This study indicates that the first-order expansions provided are not sufficient to correctly describe the variability of the NASGRO law. The authors discard the use of second or higher-order expansions alleging that it could produce very complicated formulation making the method not viable in practice. For that reason, in that article, some simplifications are made regarding the probability relationships among random variables to overcome the difficulty. However, it remains unclear whether the FOSM or a higher-order version, have the potential to be successfully applied. It would thus be of interest to check the validity of the second or higher-order expansions to describe the probabilistic FCG based on the NASGRO model.

The probabilistic FCG strategies above provide certain statistics of the response distribution, such as the expected value and the variance. Then, the problem is further analysed according to these statistics. One such interesting analysis is to construct the whole PDF of fatigue crack growth life. The PDF can be used to describe the relative likelihood that the value of the lifespan would be equal to a particular value. Generally, the random output variable is assumed to follow a common probability distribution, such as the normal or the log-normal distribution, and subsequently the parameters of the distribution are estimated considering the

statistics of the response as constraints. An illustrative example of the previous strategy is shown by Mallor et al. [139] where the full second-order approach provides the expected value and the variance of the random output variable lifespan and then the normal and the log-normal PDFs are constructed according to these two statistics of the life. The article highlights some drawbacks regarding the need of assuming in advance a probability distribution of two parameters, since only the expected value and the variance of the underlying lifespan probability distribution are calculated, and also that the accuracy or similarity between the constructed PDFs and the results of the MC method can be improved. A general methodology that considers the statistics of the response and automatically provides an appropriate PDF of the response distribution will be more useful than a predefined one. It would thus be of interest to explore some alternatives to overcome the limitations aforementioned to contribute to a better knowledge of the distribution of fatigue life.

As shown in the previous literature, the uncertainty propagation in fatigue crack growth life has studied for many years. The investigations usually aim at providing the probability distribution of the lifespan which, in railway axles, is a fundamental aspect for the maintenance planning to keep the probability of failure as small as possible, as far as it is economically viable. Addressing the problem in an efficient and precise manner is, therefore, a challenge. The construction of a PDF under moment constraints has historically been of great interest. In some cases, the probability distribution manifests asymmetry or presents a characteristic heaviness of the tails relative to the rest of the distribution or both. Therefore, the need to manage the shape of the constructed PDF arises. The shape of the constructed distribution can be handled by means of its moments related to skewness and kurtosis. Early contributions considered this topic, devising a family of distributions, the Pearson family by Pearson [141], which has the appeal of encompassing several well-known distributions. This distribution has a rich flexibility in shape, covering a wide skewness-kurtosis region. Furthermore, the location, scale, and shape parameters of a particular Pearson distribution can be estimated in terms of the first four moments, that is: the expected value, first raw moment; the variance, second central moment; the skewness, third central standardized moment; and the kurtosis, fourth central standardized moment. As a consequence, the Pearson family has been used for modelling purposes by those engaged in the probabilistic analysis of structures. However, an overall treatment of the uncertainty propagation in fatigue crack growth life based on the NASGRO equation combined with the versatile Pearson distribution family is missing. To the best of the authors' knowledge, the work presented in this thesis is the first attempt to develop an effective, efficient and practical uncertainty propagation approach that is capable of predicting the first four moments of the lifespan distribution according to the NASGRO equation and using them to construct a probability density function based on the Pearson distribution family.

Nowadays, the definition of inspection intervals in railway axles based on fracture mechanics is an active topic of research. Several examples are the remarkable research by Zerbst et al. [7, 22], Beretta and Carboni [55], Mädler et al. [83], Luke et al. [95], Beretta et al. [96], Náhlík et al. [135], Broek [142] and Cocheteux and Pouillart [143]. In these investigations, despite the different initial and final crack sizes, they all use the FCG lifespan for the subsequent inspection planning. A reliable FCG life estimation is therefore key aspect as highlighted in Carboni and Cantini [144]. It would thus be of interest to improve the procedures for FCG lifespan estimation considering its stochastic nature to better define periodicities. As mentioned, to obtain a probabilistic FCG life estimation, a promising strategy is to construct the probability distribution of the lifespan of the axle as a result of the randomness of the inputs, using the Pearson distribution family based on prescribed statistical moments. These moments can be estimated by applying the full second-order approach FSOA to the fatigue crack growth NASGRO model [64] as in Mallor et al. [139, 145–148], and further explained throughout this thesis.

As shown, a number of investigations have studied the FCG process and the stochastic life prediction. Moreover, in-service loading is complex, and the experimental information is quite limited, so that to solve probabilistic FCG problems, hypotheses are generally assumed that may imply important limitations and restrictions. Several papers consider the Paris' law or the NASGRO equation. Most of the works use statistical methods that sometimes, as in the MC method, its application implies a high computational cost and the methodology becomes not suitable for practical applications where the computational efficiency is a crucial issue.

With this background in mind, this thesis investigates the FCG based on the NASGRO model from a probabilistic point of view. Moreover, it explores an efficient procedure for the definition of inspection intervals of maintenance in railway axles considering complex stochastic scenarios within the damage tolerance approach. In the meantime, a new probabilistic formulation of the FCG phenomenon based on the NASGRO equation is pursued. For this purpose, a generalized extension of the FOSM to a full second-order approach (FSOA) is aimed and analysed in combination with the NASGRO model. It is worth noting that the use of methodologies that help to extend the service life of a product by reducing the energy resources associated with its maintenance, contributes to the protection of the environment. The outcomes in this thesis are expected to have a positive and comprehensive effect on the optimization of maintenance intervals, thus promoting an efficient use of rail transport to carry people and freight. In this sense, it would also decrease the environmental impact of mankind due to air pollution caused by road transport, as it helps rail transport to become a more environmentally friendly alternative. The novel framework in this thesis is expected to be an asset in a broad range of engineering problems dealing with random variables. As noted above, the research developed in this thesis has been disseminated through the journal articles by Mallor et al. [139, 145–148].

2

Full second-order approach for the moments of functions of random variables

2.1 Introduction

The relationship between the input random variables and the output random variables, called error propagation, uncertainty propagation or stochastic moment approximation, can be explicitly derived and understood, being important for a comprehension of its underlying approximative character. Its objective is to determine the effect of the input variables randomness on the randomness of the function based on them. This chapter is devoted to bridging the gap between these approximation methods and researchers in the world of uncertainty modelling and propagation.

The full second-order approach (FSOA) for statistical moments prediction, derived in this thesis, is able to determine the stochastic moments of a general function, such as: the expected value, first raw moment; the variance, second central moment; the skewness, third central standardized moment; and the kurtosis, fourth central standardized moment, based on the Taylor series approximation. The main idea in this thesis is to apply this approach to predict the moments of the underlying distribution according to the probabilistic fatigue crack growth life based on the NASGRO equation.

The first-order second moment (FOSM) method, summarised in Subsection 1.4.2, derives its name from the fact that it uses a first-order Taylor approximation of the function and uses only the first and second moments of the input r.v.s to determinate the expected value and the variance of the response. When the second-order Taylor

is used, it is named as second-order second moment (SOSM) method, requiring up to second-order moments of the input r.v.s for the expected value estimation, but for the variance up to fourth-order moments. The moments of the input r.v.s required to approximate the first to the fourth order moments are given in the Table 2.1.

Table 2.1. Moments of random input variables required using first-order (FO) and second-order (SO).

Moment to approximate		Moment required	
Ordinal	Significance	FO	SO
1	Expected value (Raw)	1	1, 2
2	Variance (Central)	1, 2	1, 2, 3, 4
3	Skewness (Central Normalised)	1, 3	1, 2, 3, 4, 5, 6
4	Kurtosis (Central Normalised)	1, 4	1, 2, 3, 4, 5, 6, 7, 8

In this thesis the method is referred as full second-order approach (FSOA), not naming the order of the moments of the input random variables needed for computation as it depends on the order of the moment to approximate.

This chapter is organized as follows. Firstly, a series of abbreviations and conventions are presented to compact the math derivations. Secondly, the most general propagation of uncertainty for linear combinations in matrix form is derived. This includes the expected value and the covariance matrix, that is, the variance and the covariance calculations. In the third place, the propagation of uncertainty for non-linear combinations is derived in matrix form. This derivation relates the previous most general case to the approximation of non-linear functions through Taylor series, including the derivation of the expected value first and second-order and the covariance matrix of first-order, i.e. the variance and the covariance. Finally, the FSOA for the first to fourth moments of functions of random variables is derived using summation notation. It presents the expressions involving tensors of different orders in a simple and comprehensible way. The first to fourth moments are related by definition to the expected value, the variance, the skewness, and the kurtosis of the random output variable. Then from these second-order approximations the simpler first-order expressions are also derived.

2.2 Abbreviations and conventions

First a series of abbreviations and conventions are presented to compact the math derivations:

- General function evaluation at the mean values vector of the random variables:

$$g_\mu = g\left(\mu_{X_1}, \mu_{X_2}, \ldots, \mu_{X_d}\right) \tag{2.1}$$

- One index j after comma means first partial derivative of the general function with respect the random variable X_j evaluated about the mean values vector.

$$g_{,j} = \left.\frac{\partial g}{\partial X_j}\right|_{\left(\mu_{X_1}, \mu_{X_2}, \ldots, \mu_{X_d}\right)} \tag{2.2}$$

- Two indexes jk after comma mean second partial derivative of the function with respect the random variables X_j, X_k evaluated about the mean values vector. If both indexes are different the derivatives are called *second mixed partial derivatives.*

$$g_{,jk} = \left.\frac{\partial^2 g}{\partial X_j \partial X_k}\right|_{\left(\mu_{X_1}, \mu_{X_2}, \ldots, \mu_{X_d}\right)} \tag{2.3}$$

- The n$^{\text{th}}$ moment, also known as n$^{\text{th}}$ raw moment, of a continuous r.v. X_j with probability density function $f_X(x_j)$ is denoted as $\mu'_{j,n}$ and calculated by:

$$\mu'_{j,n} = \mathrm{E}\left[X_j^n\right] = \int_{-\infty}^{\infty} x_j^n f_X(x_j) dx_j \tag{2.4}$$

  - Remarks:
    - Note that the above definition refers to univariate moments.
    - The first raw moment of a continuous random variable X_j is called the expected value $\mu'_{j,1}$, more commonly denoted as μ_j or $\mathrm{E}[X_j]$:

$$\mu_j = \mathrm{E}[X_j] = \int_{-\infty}^{\infty} x_j f_X(x_j) dx_j \tag{2.5}$$

- The n$^{\text{th}}$ moment about the mean, or n$^{\text{th}}$ central moment, of a continuous random variable X_j is referred to as:

$$\mu_{j,n} = \mathrm{E}\left[(X_j - \mathrm{E}[X_j])^n\right] = \int_{-\infty}^{\infty} \left(x_j - \mu_{X_j}\right)^n f_X(x_j) dx_j \tag{2.6}$$

  - Remarks:
    * Notice that the above definition refers to univariate moments.
    * The first central moment of a r.v. always equals to 0. Not to be confused with the first raw moment, i.e. the expected value.

$$\mu_{j,1} = \mathrm{E}\left[(X_j - \mathrm{E}[X_j])^1\right] = \mathrm{E}[X_j] - \mathrm{E}[X_j] = 0 \tag{2.7}$$

    * Note that the expected value operator is linear in the sense that:

$$\mathrm{E}[X_j + X_k] = \mathrm{E}[X_j] + \mathrm{E}[X_K] \tag{2.8}$$

    * The second central univariate moment of a continuous r.v. is its variance:

$$\begin{aligned} \mu_{j,2} &= \mathrm{Var}(X_j) \\ &= \mathrm{E}\left[(X_j - \mathrm{E}[X_j])^2\right] \\ &= \mathrm{E}\left[{X_j}^2 - 2X_j\,\mathrm{E}[X_j] + \mathrm{E}[X_j]^2\right] \\ &= \mathrm{E}\left[{X_j}^2\right] - 2\,\mathrm{E}[X_j]\,\mathrm{E}[X_j] + \mathrm{E}[X_j]^2 \\ &= \mathrm{E}\left[{X_j}^2\right] - \mathrm{E}[X_j]^2 \end{aligned} \tag{2.9}$$

- The normalized or standardized n^{th} central moment is the n^{th} central moment divided by the standard deviation raised to the n^{th} power, i.e. σ^n. The normalized n^{th} central moment of a continuous random variable X_j is calculated by:

$$\frac{\mu_{j,n}}{\sigma_j^n} \tag{2.10}$$

  - Remarks:
    * Note that the above definition refers to univariate moments.
    * The normalized first central univariate moment of a continuous r.v. always equals to 0 and the second equals to 1.
    * The normalized third central univariate moment of a continuous r.v. is called skewness:

$$\gamma_1 = \frac{\mu_{j,3}}{\sigma_j^3} \tag{2.11}$$

    * Usually, the square of the skewness is denoted by β_1.

$$\beta_1 = \gamma_1^2 \tag{2.12}$$

* The normalized fourth central univariate moment of a continuous r.v. is called kurtosis:

$$\beta_2 = \frac{\mu_{j,4}}{\sigma_j^4} \tag{2.13}$$

* The kurtosis of a normal distribution is equal to 3. In practice to provide the comparison to the normal distribution, the excess kurtosis is defined as the kurtosis minus 3 denoted as γ_2, making a normal distribution to have zero excess kurtosis:

$$\gamma_2 = \beta_2 - 3 \tag{2.14}$$

- The moments of the joint distribution of $X = \{X_1, X_2, \ldots, X_d\}$ random variables are defined similarly. For d random variables, the number of non-trivial n^{th} order mixed or often called cross central moments can be calculated as:

$$\frac{(n+d-1)\,!}{n!\,(d-1)\,!} - d \tag{2.15}$$

Non-trivial means that the cross central moments that involve only one variable are excluded.

The n$^{\text{th}}$ central multivariate moments of continuous r.v.s are denoted with consecutive indexes, two for the 2$^{\text{nd}}$ central moment μ_{jk}, three indexes for the 3$^{\text{rd}}$ central moment μ_{jkl}, and four indexes for the 4$^{\text{th}}$ central moment μ_{jklm} and so on. Note that the presence of up to four indices does not imply that more than two r.v.s are involved. Each index runs from 1 to d random variables.

– 2$^{\text{nd}}$ central moment: *Covariance*

The covariance is a measure of the joint variability of two r.v.s.

The number of random variables d must be at least two for the concept of covariance to be non-trivial. The second mixed central moment for two continuous random variables X_j and X_k, where $j \neq k$, is called covariance, and it is denoted by:

$$\mu_{jk} = \operatorname{Cov}(X_j, X_k) = \int_{-\infty}^{\infty}\int_{-\infty}^{\infty} \left(x_j - \mu_{X_j}\right)\left(x_k - \mu_{X_k}\right) f_X(x_j, x_k)\, dx_j dx_k \tag{2.16}$$

Note that the variance is a special case of the covariance in which the two variables are identically the same.

$$\mu_{jj} = \operatorname{Cov}(X_j, X_j) = \int_{-\infty}^{\infty} \left(x_j - \mu_{X_j}\right)^2 f_X(x_j)\, dx_j = \operatorname{Var}(X_j) \tag{2.17}$$

In analogy to the variance Eq. (2.9), the covariance between two r.v.s can be expressed as the expected value of their product minus the product of their expected values:

$$\begin{aligned}\operatorname{Cov}(X_j, X_k) &= \mathrm{E}\left[(X_j - \mathrm{E}[X_j])(X_k - \mathrm{E}[X_k])\right] \\ &= \mathrm{E}\left[X_j X_k - X_j \mathrm{E}[X_k] - \mathrm{E}[X_j] X_k + \mathrm{E}[X_j]\mathrm{E}[X_k]\right] \\ &= \mathrm{E}[X_j X_k] - \mathrm{E}[X_j]\mathrm{E}[X_k] - \mathrm{E}[X_j]\mathrm{E}[X_k] + \mathrm{E}[X_j]\mathrm{E}[X_k] \\ &= \mathrm{E}[X_j X_k] - \mathrm{E}[X_j]\mathrm{E}[X_k]\end{aligned} \tag{2.18}$$

– 3rd central moment: *Coskewness*

The third central moment is a measure of the distribution symmetry or lack of symmetry. Any symmetric distribution will have a third central moment of 0.

The number of random variables d must be at least two for the concept of coskewness to be non-trivial. For two continuous random variables X_j and X_k, where $j \neq k$, the two non-trivial third mixed central moments are:

$$\begin{aligned}\mu_{jjk} = \mu_3(X_j, X_j, X_k) &= \int_{-\infty}^{\infty}\int_{-\infty}^{\infty} \left(x_j - \mu_{X_j}\right)^2 \left(x_k - \mu_{X_k}\right) f_X(x_j, x_k)\, dx_j dx_k \\ \mu_{jkk} = \mu_3(X_j, X_k, X_k) &= \int_{-\infty}^{\infty}\int_{-\infty}^{\infty} \left(x_j - \mu_{X_j}\right) \left(x_k - \mu_{X_k}\right)^2 f_X(x_j, x_k)\, dx_j dx_k\end{aligned} \tag{2.19}$$

The special case in which the same variable is considered three times leads:

$$\mu_{jjj} = \mu_3(X_j, X_j, X_j) = \int_{-\infty}^{\infty} \left(x_j - \mu_{X_j}\right)^3 f_X(x_j)\, dx_j \tag{2.20}$$

The normalized or standardized μ_{jjj} dividing by the standard deviation raised to the third power σ_j^3 is known as skewness. The skewness is denoted as γ_1, $\operatorname{Skew}(X)$ or $S(X_j, X_j, X_j)$.

$$S(X_j, X_j, X_j) = \frac{\mu_{jjj}}{\sigma_j^3} \tag{2.21}$$

In the same sense, the other mixed joint third central moments standardized using their respective standard deviations are called coskewness. They are related to skewness as covariance is related to variance.

It is common to refer to the square of the skewness γ_1^2 as β_1.

– 4^{th} central moment: *Cokurtosis*

The fourth central moment is a measure of the combined weight, heaviness, of the tails relative to the rest of the distribution.

The number of random variables d must be at least two for the concept of cokurtosis to be non-trivial. For two continuous random variables X_j and X_k, where $j \neq k$, the three non-trivial fourth mixed central moments are:

$$\begin{aligned}
\mu_{jjjk} &= \mu_4\left(X_j, X_j, X_j, X_k\right) = \int_{-\infty}^{\infty}\int_{-\infty}^{\infty}\left(x_j - \mu_{X_j}\right)^3\left(x_k - \mu_{X_k}\right) f_X\left(x_j, x_k\right) dx_j dx_k \\
\mu_{jjkk} &= \mu_4\left(X_j, X_j, X_k, X_k\right) = \int_{-\infty}^{\infty}\int_{-\infty}^{\infty}\left(x_j - \mu_{X_j}\right)^2\left(x_k - \mu_{X_k}\right)^2 f_X\left(x_j, x_k\right) dx_j dx_k \\
\mu_{jkkk} &= \mu_4\left(X_j, X_k, X_k, X_k\right) = \int_{-\infty}^{\infty}\int_{-\infty}^{\infty}\left(x_j - \mu_{X_j}\right)\left(x_k - \mu_{X_k}\right)^3 f_X\left(x_j, x_k\right) dx_j dx_k
\end{aligned} \tag{2.22}$$

The special case in which the same variable is considered four times leads:

$$\mu_{jjjj} = \mu_4\left(X_j, X_j, X_j, X_j\right) = \int_{-\infty}^{\infty}\left(x_j - \mu_{X_j}\right)^4 f_X\left(x_j\right) dx_j \tag{2.23}$$

The normalized or standardized μ_{jjjj} dividing by the standard deviation raised to the fourth power σ_j^4 is known as kurtosis. The kurtosis is denoted as β_2, $\text{Kurt}\left(X\right)$ or $K\left(X_j, X_j, X_j, X_j\right)$.

$$K\left(X_j, X_j, X_j, X_j\right) = \frac{\mu_{jjjj}}{\sigma_j^4} \tag{2.24}$$

The other mixed fourth central moments standardized using their respective standard deviations are called cokurtosis. They are related to kurtosis as coskewness is related to skewness and covariance to variance.

Some authors refer to the excess Kurtosis, γ_2, which is defined as kurtosis minus 3 to make it comparable to the normal distribution. The reason not to subtract off 3 in the presented math is that the fourth central moment generalizes better.

The description of the 5^{th} to 8^{th} moments of the joint distribution is given in Appendix A.

2.3 Linear combinations: matrix form

This section presents the most general propagation of uncertainty for linear combinations in matrix form. This includes the expected value and the covariance matrix, that is, the variance and the covariance calculations. Throughout this section, boldfaced letters are used to refer to random vectors or matrix.

A set of d_X input random variables $\{X_1, X_2, \ldots, X_{d_X}\}$ can be expressed as a d_X-dimensional vector $\mathbf{X}$, where d_X is the input random variables number:

$$\mathbf{X} = \begin{bmatrix} X_1 & X_2 & \cdots & X_{d_X} \end{bmatrix}^\top = \begin{bmatrix} X_1 \\ X_2 \\ \vdots \\ X_{d_X} \end{bmatrix} \tag{2.25}$$

A set of d_Y multivariate, also referred to as multi-variable, functions $\{Y_1, Y_2, \ldots, Y_{d_Y}\}$ can be expressed as a d_Y-dimensional vector function where d_Y is the output multivariate functions number:

$$\mathbf{Y}(\mathbf{X}) = \begin{bmatrix} Y_1 & Y_2 & \ldots & Y_{d_Y} \end{bmatrix}^\top = \mathbf{g}(\mathbf{X}) = \begin{bmatrix} g_1(\mathbf{X}) & g_2(\mathbf{X}) & \ldots & g_{d_Y}(\mathbf{X}) \end{bmatrix}^\top = \begin{bmatrix} g_1(\mathbf{X}) \\ g_2(\mathbf{X}) \\ \vdots \\ g_{d_Y}(\mathbf{X}) \end{bmatrix} \tag{2.26}$$

Consider the multi-input multi-output system in Fig. 2.1.

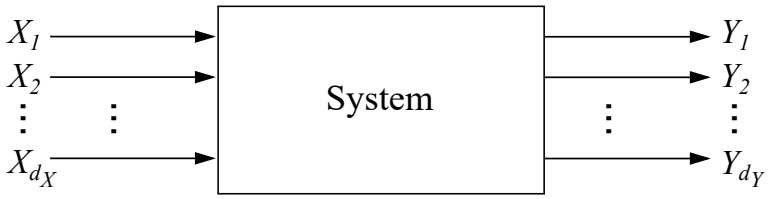

Figure 2.1. Multi-variable vector-valued function.

Assuming that the $\{Y_1, Y_2, \ldots, Y_{d_Y}\}$ functions are linear combinations of a set of d_X random variables $\{X_1, X_2, \ldots, X_{d_X}\}$ with combination coefficients $\mathbf{A}$, which is a $(d_Y \times d_X)$-matrix of combination coefficients:

$$\mathbf{A} = \begin{bmatrix} A_{11} & A_{12} & \cdots & A_{1d_X} \\ A_{21} & A_{22} & \cdots & A_{2d_X} \\ \vdots & \vdots & \ddots & \vdots \\ A_{d_Y 1} & A_{d_Y 2} & \cdots & A_{d_Y d_X} \end{bmatrix} \tag{2.27}$$

In matrix notation:

$$\mathbf{Y}(\mathbf{X}) = \mathbf{A}\mathbf{X} \tag{2.28}$$

The mean value vector of the random variables vector $\mathbf{X}$ is denoted as $\boldsymbol{\mu}_X$:

$$\boldsymbol{\mu}_X = \mathrm{E}[\mathbf{X}] = P = \begin{bmatrix} \mu_{X_1} & \mu_{X_2} & \cdots & \mu_{X_{d_X}} \end{bmatrix}^\top = \begin{bmatrix} \mu_{X_1} \\ \mu_{X_2} \\ \vdots \\ \mu_{X_{d_X}} \end{bmatrix} \tag{2.29}$$

We introduce the symmetric $\boldsymbol{\Sigma}_X$ input covariance $(d_X \times d_X)$-matrix which contains all variances and covariances of $\mathbf{X}$:

$$\boldsymbol{\Sigma}_X = \begin{bmatrix} \sigma^2_{X_1} & \sigma_{X_1X_2} & \cdots & \sigma_{X_1X_{d_X}} \\ \sigma_{X_2X_1} & \sigma^2_{X_2} & \cdots & \sigma_{X_2X_{d_X}} \\ \vdots & \vdots & \ddots & \vdots \\ \sigma_{X_{d_X}X_1} & \sigma_{X_{d_X}X_2} & \cdots & \sigma^2_{X_{d_X}} \end{bmatrix} = \begin{bmatrix} \mu_{11} & \mu_{12} & \cdots & \mu_{1d_X} \\ \mu_{21} & \mu_{22} & \cdots & \mu_{2d_X} \\ \vdots & \vdots & \ddots & \vdots \\ \mu_{d_X1} & \mu_{d_X2} & \cdots & \mu_{d_Xd_X} \end{bmatrix} \tag{2.30}$$

The mean value vector of the vector function $\mathbf{Y}(\mathbf{X})$ is denoted as $\boldsymbol{\mu}_Y$:

$$\boldsymbol{\mu}_Y = \mathrm{E}[\mathbf{Y}] = \begin{bmatrix} \mu_{Y_1} & \mu_{Y_2} & \cdots & \mu_{Y_{d_Y}} \end{bmatrix}^\top = \begin{bmatrix} \mu_{Y_1} \\ \mu_{Y_2} \\ \vdots \\ \mu_{Y_{d_Y}} \end{bmatrix} \tag{2.31}$$

We additionally introduce the symmetric $\boldsymbol{\Sigma}_Y$ output covariance $(d_Y \times d_Y)$-matrix which contains all variances and covariances of the output random variables $\mathbf{Y}(\mathbf{X})$:

$$\boldsymbol{\Sigma}_Y = \begin{bmatrix} \sigma^2_{Y_1} & \sigma_{Y_1Y_2} & \cdots & \sigma_{Y_1Y_{d_Y}} \\ \sigma_{Y_2Y_1} & \sigma^2_{Y_2} & \cdots & \sigma_{Y_2Y_{d_Y}} \\ \vdots & \vdots & \ddots & \vdots \\ \sigma_{Y_{d_Y}Y_1} & \sigma_{Y_{d_Y}Y_2} & \cdots & \sigma^2_{Y_{d_Y}} \end{bmatrix} \tag{2.32}$$

The covariance matrix $\boldsymbol{\Sigma}_Y$ is the matrix whose (i,j)-th entry is the covariance:

$$\boldsymbol{\Sigma}_{Y_{ij}} = \mathrm{Cov}\,(Y_i, Y_j) = \mathrm{E}\left[(Y_i - \mu_{Y_i})(Y_j - \mu_{Y_j})\right] \tag{2.33}$$

In matrix notation:

$$\boldsymbol{\Sigma}_Y = \mathrm{E}\left[(\mathbf{Y} - \mathrm{E}[\mathbf{Y}])\,(\mathbf{Y} - \mathrm{E}[\mathbf{Y}])^\top\right] \tag{2.34}$$

2.3.1 Expected value

The expected value vector of $\mathbf{Y}(\mathbf{X}) = \mathbf{A}\mathbf{X}$ for a random vector $\mathbf{X}$ with mean vector $\mathrm{E}[\mathbf{X}]$ is given by:

$$\begin{aligned} \boldsymbol{\mu}_Y &= \mathrm{E}[\mathbf{Y}] \\ &= \mathrm{E}[\mathbf{A}\mathbf{X}] \\ &= \mathbf{A}\,\mathrm{E}[\mathbf{X}] \end{aligned} \tag{2.35}$$

2.3.2 Covariance matrix: variance and covariance

The covariance matrix of $\mathbf{Y}(\mathbf{X}) = \mathbf{A}\mathbf{X}$, whose mean vector is $\mathbf{A}\,\mathrm{E}[\mathbf{X}]$, is given by:

$$\begin{aligned} \boldsymbol{\Sigma}_Y &= \mathrm{E}\left[(\mathbf{A}\mathbf{X} - \mathbf{A}\,\mathrm{E}[\mathbf{X}])(\mathbf{A}\mathbf{X} - \mathbf{A}\,\mathrm{E}[\mathbf{X}])^\top\right] \\ &= \mathrm{E}\left[\mathbf{A}(\mathbf{X} - \mathrm{E}[\mathbf{X}])(\mathbf{X} - \mathrm{E}[\mathbf{X}])^\top\mathbf{A}^\top\right] \\ &= \mathbf{A}\,\mathrm{E}\left[(\mathbf{X} - \mathrm{E}[\mathbf{X}])(\mathbf{X} - \mathrm{E}[\mathbf{X}])^\top\right]\mathbf{A}^\top \\ &= \mathbf{A}\,\mathrm{Cov}(\mathbf{X})\mathbf{A}^\top \\ &= \mathbf{A}\boldsymbol{\Sigma}_X\mathbf{A}^\top \end{aligned} \tag{2.36}$$

The previous derivation is the most general equation for propagation of uncertainty from one set of variables on another. In other words, it provides the effect of input random variables on the uncertainty of functions based on them. The output uncertainties are quantified in terms of the covariances of the output random variables.

2.4 Non-linear combinations: matrix form

This section derives the propagation of uncertainty for non-linear combinations in matrix form. This derivation relates the previous most general case to the approximation of non-linear functions through Taylor series, including the derivation of the expected value first and second-order and the covariance matrix of first-order, i.e. the variance and the covariance calculations.

When $\{Y_1, Y_2, \ldots, Y_{d_Y}\}$ is a set of d_Y functions which are non-linear combinations of $\mathbf{X}$, the uncertainty propagation can be performed by means of a linearisation of $\mathbf{Y}(\mathbf{X})$ through its Taylor series approximation about the vector of the means of the random variables $\boldsymbol{\mu}_X$. The second-order Taylor expansion of the i-th $(i = 1, \cdots, d_Y)$

component from the general case, that is, for any of the d_Y multivariate functions $\{Y_1, Y_2, \ldots, Y_{d_Y}\}$ is:

$$Y_i(\mathbf{X}) \approx \underbrace{g_i(\boldsymbol{\mu}_X)}_{o_0} + \underbrace{[\boldsymbol{\nabla}_{g_i}(\boldsymbol{\mu}_X)]^\top(\mathbf{X}-\boldsymbol{\mu}_X)}_{o_1} + \underbrace{\frac{1}{2}(\mathbf{X}-\boldsymbol{\mu}_X)^\top \mathbf{H}_{g_i}(\boldsymbol{\mu}_X)(\mathbf{X}-\boldsymbol{\mu}_X)}_{o_2} \tag{2.37}$$

Remarks:

- The zeroth, first, and second-order terms are denoted as o_0, o_1 ,and o_2 respectively.
- $\boldsymbol{\mu}_X$ is the mean value vector of the random variables vector $\mathbf{X}$.
- $g_i(\boldsymbol{\mu}_X)$ is the *model response*, that is, the multivariate function $Y_i(\mathbf{X})$ evaluated at the mean value vector $\boldsymbol{\mu}_X$.
- $[\boldsymbol{\nabla}_{g_i}(\boldsymbol{\mu}_X)]^\top$ is the transpose of the gradient vector of the multivariate function $Y_i(\mathbf{X})$ evaluated at the mean value vector $\boldsymbol{\mu}_X$.
- $\mathbf{H}_{g_i}(\boldsymbol{\mu}_X)$ is the Hessian matrix of the multivariate function $Y_i(\mathbf{X})$ evaluated at the mean value vector $\boldsymbol{\mu}_X$.

It has only been expressed the i-th the component as the quadratic order term o_2 can not be expressed in matrix form, as it requires tensor notation. The zeroth and first terms, what means the first-order Taylor approximation of the vector-valued function $\mathbf{Y}(\mathbf{X})$, can be written in matrix form:

$$\mathbf{Y}(\mathbf{X}) \approx \mathbf{g}(\boldsymbol{\mu}_X) + \mathbf{J}_g(\boldsymbol{\mu}_X)(\mathbf{X}-\boldsymbol{\mu}_X) \tag{2.38}$$

Remarks:

- Recall that $\mathbf{g}(\boldsymbol{\mu}_X) = \big[g_1(\boldsymbol{\mu}_X), g_2(\boldsymbol{\mu}_X), \ldots, g_{d_Y}(\boldsymbol{\mu}_X)\big]^\top$ is a compressed notation for the vector of the *model response*, that is, the vector-valued function $\mathbf{Y}(\mathbf{X})$ evaluated at the mean value vector $\boldsymbol{\mu}_X$.
- $\mathbf{J}_g(\boldsymbol{\mu}_X)$ is the Jacobian matrix of the vector-valued function $\mathbf{Y}(\mathbf{X})$ evaluated at the mean value vector $\boldsymbol{\mu}_X$.

The gradient $(d_X \times 1)$ column-vector $\boldsymbol{\nabla}_{g_i}(\boldsymbol{\mu}_X)$ of the multivariate function $Y_i(\mathbf{X})$ evaluated at the mean value vector $\boldsymbol{\mu}_X$ is defined as (column vector convention adopted):

$$\boldsymbol{\nabla}_{g_i}(\boldsymbol{\mu}_X) = \begin{bmatrix} \frac{\partial g_i}{\partial X_1} & \frac{\partial g_i}{\partial X_2} & \cdots & \frac{\partial g_i}{\partial X_{d_X}} \end{bmatrix}^\top = \begin{bmatrix} \frac{\partial g_i}{\partial X_1} \\ \frac{\partial g_i}{\partial X_2} \\ \vdots \\ \frac{\partial g_i}{\partial X_{d_X}} \end{bmatrix} \tag{2.39}$$

The Jacobian is the generalization of the gradient for a vector-valued function of several variables. The Jacobian matrix $\mathbf{J}_g(\boldsymbol{\mu}_X)$ defined over the vector-valued function $\mathbf{Y}(\mathbf{X})$ gives:

$$\mathbf{J}_g(\boldsymbol{\mu}_X) = \begin{bmatrix} \frac{\partial g_1}{\partial X_1} & \frac{\partial g_1}{\partial X_2} & \cdots & \frac{\partial g_1}{\partial X_{d_X}} \\ \frac{\partial g_2}{\partial X_1} & \frac{\partial g_2}{\partial X_2} & \cdots & \frac{\partial g_2}{\partial X_{d_X}} \\ \vdots & \vdots & \ddots & \vdots \\ \frac{\partial g_{d_Y}}{\partial X_1} & \frac{\partial g_{d_Y}}{\partial X_2} & \cdots & \frac{\partial g_{d_Y}}{\partial X_{d_X}} \end{bmatrix} \tag{2.40}$$

Then the Jacobian matrix of the vector-valued function $\mathbf{Y}(\mathbf{X})$ evaluated at the mean value vector $\boldsymbol{\mu}_X$, is defined to be a $(d_Y \times d_X)$-matrix, whose (i,j)-th entry is $\mathbf{J}_g(\boldsymbol{\mu}_X)_{ij} = \frac{\partial g_i}{\partial X_j}$, with $i = 1, 2, \ldots, d_Y$ and $j = 1, 2, \ldots, d_X$. This matrix reduces to a row-vector $(1 \times d_X)$-vector when $d_Y = 1$, which equals to the transpose of the gradient:

$$[\boldsymbol{\nabla}_{g_1}(\boldsymbol{\mu}_X)]^\top = \begin{bmatrix} \frac{\partial g_1}{\partial X_1} & \frac{\partial g_1}{\partial X_2} & \cdots & \frac{\partial g_1}{\partial X_{d_X}} \end{bmatrix} \tag{2.41}$$

In Eq. (2.37) appears the transposed gradient as it is only one component $Y_i(\mathbf{X})$ of the vector-valued function while in Eq. (2.38) appears the Jacobian as it considers all components of the vector-valued function $\mathbf{Y}(\mathbf{X})$.

As $\mathbf{Y}(\mathbf{X})$ is a d_Y-dimensional vector of multivariate functions, a vector-valued function, the collection of second partial derivatives in the quadratic term is a third-order tensor $((d_X \times d_X) \times d_Y)$ denoted as $\mathbf{Q}_g(\boldsymbol{\mu}_X)$. The notation Q indicates quadratic term.

$$\mathbf{Q}_g(\boldsymbol{\mu}_X) = (\mathbf{H}_{g_1}(\boldsymbol{\mu}_X), \mathbf{H}_{g_2}(\boldsymbol{\mu}_X), \ldots, \mathbf{H}_{g_{d_Y}}(\boldsymbol{\mu}_X)) \tag{2.42}$$

This third-order tensor is a collection of d_Y Hessian matrices $\mathbf{H}_{g_i}(\boldsymbol{\mu}_X)$, with $i = 1, 2, \ldots, d_Y$, that is, one for each function $\{Y_1, Y_2, \ldots, Y_{d_Y}\}$. These Hessian matrices of the multivariate functions $Y_i(\mathbf{X})$ are evaluated at the mean value vector $\boldsymbol{\mu}_X$. The Hessian matrices are defined to be a $(d_X \times d_X)$-matrix, whose (j,k)-th entry is $\mathbf{H}_{g_i}(\boldsymbol{\mu}_X)_{jk} = \frac{\partial^2 g_i}{\partial X_j \partial X_k}$, with $j = 1, 2, \ldots, d_X$ and $k = 1, 2, \ldots, d_X$. The third-order tensor is presented in Fig. 2.2.

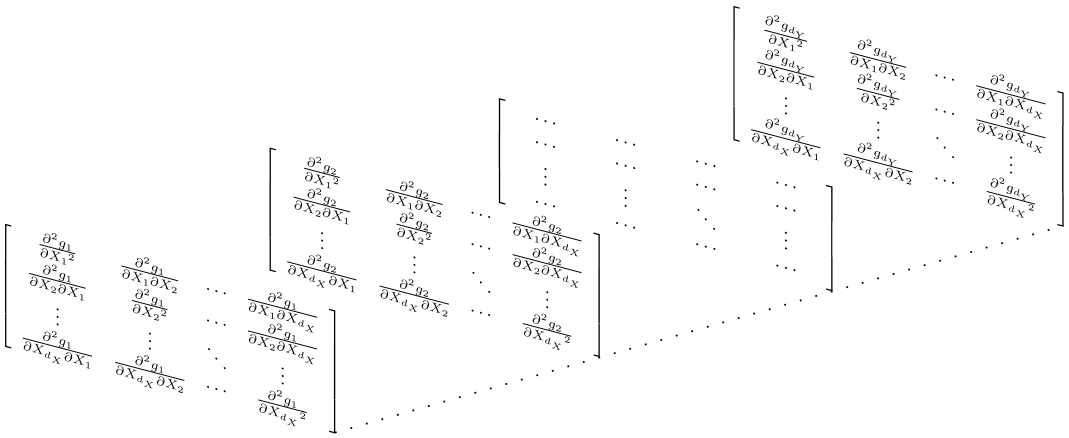

Figure 2.2. $\mathbf{Q}g(\boldsymbol{\mu}_X)$ third-order tensor.

This tensor leads to the usual Hessian $(d_X \times d_X)$-matrix when $d_Y = 1$.

$$\mathbf{H}_{g_1}(\boldsymbol{\mu}_X) = \begin{bmatrix} \frac{\partial^2 g_1}{\partial {X_1}^2} & \frac{\partial^2 g_1}{\partial X_1 \partial X_2} & \cdots & \frac{\partial^2 g_1}{\partial X_1 \partial X_{d_X}} \\ \frac{\partial^2 g_1}{\partial X_2 \partial X_1} & \frac{\partial^2 g_1}{\partial {X_2}^2} & \cdots & \frac{\partial^2 g_1}{\partial X_2 \partial X_{d_X}} \\ \vdots & \vdots & \ddots & \vdots \\ \frac{\partial^2 g_1}{\partial X_{d_X} \partial X_1} & \frac{\partial^2 g_1}{\partial X_{d_X} \partial X_2} & \cdots & \frac{\partial^2 g_1}{\partial {X_{d_X}}^2} \end{bmatrix} \tag{2.43}$$

2.4.1 Expected value first-order

The expected value vector of the first-order Taylor approximation $\mathbf{Y}(\mathbf{X}) \approx \mathbf{g}(\boldsymbol{\mu}_X) + \mathbf{J}_g(\boldsymbol{\mu}_X)(\mathbf{X} - \boldsymbol{\mu}_X)$ is given by:

$$\begin{aligned} \boldsymbol{\mu}_Y &\approx \mathrm{E}\left[\mathbf{g}(\boldsymbol{\mu}_X) + \mathbf{J}_g(\boldsymbol{\mu}_X)(\mathbf{X} - \boldsymbol{\mu}_X)\right] \\ &\approx \mathrm{E}\left[\mathbf{g}(\boldsymbol{\mu}_X)\right] + \mathrm{E}\left[\mathbf{J}_g(\boldsymbol{\mu}_X)(\mathbf{X} - \boldsymbol{\mu}_X)\right] \\ &\approx \mathrm{E}\left[\mathbf{g}(\boldsymbol{\mu}_X)\right] + \mathrm{E}\left[\mathbf{J}_g(\boldsymbol{\mu}_X)\right] \underbrace{\mathrm{E}\left[(\mathbf{X} - \boldsymbol{\mu}_X)\right]}_{0} \\ &\approx \mathbf{g}(\boldsymbol{\mu}_X) \end{aligned} \tag{2.44}$$

Remarks:

- The linearity of the expectation operator is applied.
- Note that the evaluated $\mathbf{J}_g(\boldsymbol{\mu}_X)$ is a matrix of scalar values.
- The first central moment of a r.v. always equals to 0. Not to be confused with the first raw moment which is the expected value.

- Recall that $\mathbf{g}(\boldsymbol{\mu}_X) = \left[g_1(\boldsymbol{\mu}_X), g_2(\boldsymbol{\mu}_X), \ldots, g_{d_Y}(\boldsymbol{\mu}_X)\right]^\top$ is a compressed notation for the vector of the *model response*, that is, the vector-valued function $\mathbf{Y}(\mathbf{X})$ evaluated at the mean value vector $\boldsymbol{\mu}_X$.
- $\boldsymbol{\mu}_Y$ is also a vector. The i-th component of this vector is equal to the i-th component of the output vector computed by the functions g_i at the mean value vector $\boldsymbol{\mu}_X$. $\mathrm{E}[\mathbf{Y}] = \boldsymbol{\mu}_Y$ is thus the computation of the model at mean value vector.

The first-order expected value approximation of a function $Y_1 = g_1(\mathbf{X})$ is:

$$\mu_{Y_1} \approx g_1(\boldsymbol{\mu}_X) \tag{2.45}$$

Using the abbreviations and conventions introduced in Section 2.2 to compact the math derivations and omitting the index $i = 1$ leads to:

$$\mathrm{E}[Y] = \mu_Y \approx g_\mu \tag{2.46}$$

2.4.2 Expected value second-order

The expected value i-th component of the second-order Taylor approximation of the i-th ($i = 1, \cdots, d_Y$) component from the general case $Y_i(\mathbf{X}) \approx g_i(\boldsymbol{\mu}_X) + [\boldsymbol{\nabla}_{g_i}(\boldsymbol{\mu}_X)]^\top(\mathbf{X} - \boldsymbol{\mu}_X) + \frac{1}{2}(\mathbf{X} - \boldsymbol{\mu}_X)^\top \mathbf{H}_{g_i}(\boldsymbol{\mu}_X)(\mathbf{X} - \boldsymbol{\mu}_X)$ is given by:

$$\begin{aligned}
\mu_{Y_i} &\approx \mathrm{E}\left[g_i(\boldsymbol{\mu}_X) + [\boldsymbol{\nabla}_{g_i}(\boldsymbol{\mu}_X)]^\top(\mathbf{X} - \boldsymbol{\mu}_X) + \frac{1}{2}(\mathbf{X} - \boldsymbol{\mu}_X)^\top \mathbf{H}_{g_i}(\boldsymbol{\mu}_X)(\mathbf{X} - \boldsymbol{\mu}_X)\right] \\
&\approx \mathrm{E}\left[g_i(\boldsymbol{\mu}_X)\right] + \mathrm{E}\left[[\boldsymbol{\nabla}_{g_i}(\boldsymbol{\mu}_X)]^\top(\mathbf{X} - \boldsymbol{\mu}_X)\right] + \mathrm{E}\left[\frac{1}{2}(\mathbf{X} - \boldsymbol{\mu}_X)^\top \mathbf{H}_{g_i}(\boldsymbol{\mu}_X)(\mathbf{X} - \boldsymbol{\mu}_X)\right] \\
&\approx \mathrm{E}\left[g_i(\boldsymbol{\mu}_X)\right] + \mathrm{E}\left[[\boldsymbol{\nabla}_{g_i}(\boldsymbol{\mu}_X)]^\top\right] \underbrace{\mathrm{E}\left[(\mathbf{X} - \boldsymbol{\mu}_X)\right]}_{0} + \mathrm{E}\left[\frac{1}{2}(\mathbf{X} - \boldsymbol{\mu}_X)^\top \mathbf{H}_{g_i}(\boldsymbol{\mu}_X)(\mathbf{X} - \boldsymbol{\mu}_X)\right] \\
&\approx \mathrm{E}\left[g_i(\boldsymbol{\mu}_X)\right] + \frac{1}{2}\left(\underbrace{\mathrm{E}\left[(\mathbf{X} - \boldsymbol{\mu}_X)\right]^\top}_{0} \mathbf{H}_{g_i}(\boldsymbol{\mu}_X) \underbrace{\mathrm{E}\left[(\mathbf{X} - \boldsymbol{\mu}_X)\right]}_{0}\right. \\
&\qquad \left. + \operatorname{tr}\left(\mathbf{H}_{g_i}(\boldsymbol{\mu}_X) \operatorname{Cov}\left((\mathbf{X} - \boldsymbol{\mu}_X), (\mathbf{X} - \boldsymbol{\mu}_X)\right)\right)\right) \\
&\approx g_i(\boldsymbol{\mu}_X) + \frac{1}{2} \operatorname{tr}\left(\mathbf{H}_{g_i}(\boldsymbol{\mu}_X) \operatorname{Cov}(\mathbf{X}, \mathbf{X})\right) \\
&\approx g_i(\boldsymbol{\mu}_X) + \frac{1}{2} \operatorname{tr}\left(\mathbf{H}_{g_i}(\boldsymbol{\mu}_X) \boldsymbol{\Sigma}_X\right) \\
&\approx g_i(\boldsymbol{\mu}_X) + \frac{1}{2} \langle \mathbf{H}_{g_i}(\boldsymbol{\mu}_X), \boldsymbol{\Sigma}_X \rangle_F
\end{aligned} \tag{2.47}$$

Remarks:

- Note that the evaluated $\mathbf{H}_{g_i}(\boldsymbol{\mu}_X)$ is a matrix of scalar values.
- The expectation of a quadratic form $\mathrm{E}[\mathbf{X}^\top \mathbf{A}\mathbf{X}] = \mathrm{E}[\mathbf{X}]^\top \mathbf{A}\,\mathrm{E}[\mathbf{X}] + \mathrm{tr}(\mathbf{A}\boldsymbol{\Sigma}_{\mathbf{XX}})$ where $\mathbf{X}$ is a vector of d_Y-random variables, $\mathbf{A}$ is a d_Y-dimensional symmetric matrix. Note that the operator $\mathrm{tr}(\ )$ denotes the trace.
- Recall the covariance property $\mathrm{Cov}(X + a, Y + b) = \mathrm{Cov}(X, Y)$.
- The trace of a square matrix which is the product of two equal-sized matrices is equal to the sum of entry-wise products of their elements, similarly to a dot product of vectors.
- $\langle , \rangle_F$ Frobenius inner product for matrix. The operation is a component-wise inner product of two matrices as though they are vectors. The dot product, often called in this context the inner product, is the sum of the products of the corresponding entries of two sequences of numbers.

The previous derivation for a i-th component, expressed in index version (omitting the index i) equals to:

$$\mathrm{E}\,[Y] = \mu_Y \approx g_\mu + \frac{1}{2}\sum_{j=1}^{d}\sum_{k=1}^{d} g_{,jk}\mu_{jk} \tag{2.48}$$

2.4.3 Covariance matrix: variance and covariance first-order

Starting from the covariance in matrix notation:

$$\boldsymbol{\Sigma}_Y = \mathrm{E}\left[(\mathbf{Y} - \mathrm{E}[\mathbf{Y}])\,(\mathbf{Y} - \mathrm{E}[\mathbf{Y}])^\top\right] \tag{2.49}$$

The covariance matrix of $\mathbf{Y}(\mathbf{X}) \approx \mathbf{g}(\boldsymbol{\mu}_X) + \mathbf{J}_g(\boldsymbol{\mu}_X)(\mathbf{X} - \boldsymbol{\mu}_X)$, whose mean vector is $\mathbf{g}(\boldsymbol{\mu}_X)$, is given by:

$$\begin{aligned}
\boldsymbol{\Sigma}_Y &\approx \mathrm{E}\left[\Big(\mathbf{g}(\boldsymbol{\mu}_X) + \mathbf{J}_g(\boldsymbol{\mu}_X)(\mathbf{X} - \boldsymbol{\mu}_X) - \mathbf{g}(\boldsymbol{\mu}_X)\Big)\Big(\mathbf{g}(\boldsymbol{\mu}_X) + \mathbf{J}_g(\boldsymbol{\mu}_X)(\mathbf{X} - \boldsymbol{\mu}_X) - \mathbf{g}(\boldsymbol{\mu}_X)\Big)^\top\right] \\
&\approx \mathrm{E}\left[\Big(\mathbf{J}_g(\boldsymbol{\mu}_X)(\mathbf{X} - \boldsymbol{\mu}_X)\Big)\Big(\mathbf{J}_g(\boldsymbol{\mu}_X)(\mathbf{X} - \boldsymbol{\mu}_X)\Big)^\top\right] \\
&\approx \mathrm{E}\left[\Big(\mathbf{J}_g(\boldsymbol{\mu}_X)(\mathbf{X} - \boldsymbol{\mu}_X)\Big)\Big((\mathbf{X} - \boldsymbol{\mu}_X)^\top \mathbf{J}_g(\boldsymbol{\mu}_X)^\top\Big)\right] \\
&\approx \mathrm{E}\left[\mathbf{J}_g(\boldsymbol{\mu}_X)(\mathbf{X} - \boldsymbol{\mu}_X)(\mathbf{X} - \boldsymbol{\mu}_X)^\top \mathbf{J}_g(\boldsymbol{\mu}_X)^\top\right] \\
&\approx \mathbf{J}_g(\boldsymbol{\mu}_X)\,\mathrm{E}\left[(\mathbf{X} - \boldsymbol{\mu}_X)(\mathbf{X} - \boldsymbol{\mu}_X)^\top\right]\mathbf{J}_g(\boldsymbol{\mu}_X)^\top \\
&\approx \mathbf{J}_g(\boldsymbol{\mu}_X)\,\mathrm{Cov}(\mathbf{X})\mathbf{J}_g^\top(\boldsymbol{\mu}_X) \\
&\approx \mathbf{J}_g(\boldsymbol{\mu}_X)\boldsymbol{\Sigma}_X\mathbf{J}_g^\top(\boldsymbol{\mu}_X)
\end{aligned} \tag{2.50}$$

Remarks:

- The matrix multiplication transposed equals to the multiplication of the matrices transposed reversing the order of the factors.

- Note that the evaluated $\mathbf{J}_g(\boldsymbol{\mu}_X)$ is a matrix of scalar values.

The previous derivation is the most general equation for the propagation of uncertainty from one set of variables onto another using a first-order Taylor approximation. In other words, it provides the effect of input random variables on the uncertainty of functions based on them approximated though Taylor. The output uncertainties are quantified in terms of the covariances of the output random variables.

The Eq. (2.50) can be interpreted as it is depicted in Fig. 2.3.

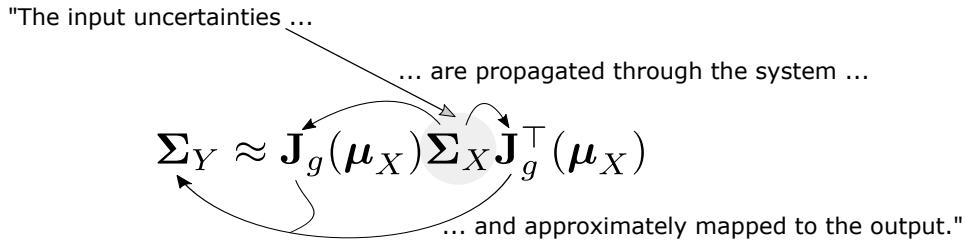

Figure 2.3. Interpretation of the error propagation law in its matrix form.

In the interpretation of the previous figure, the input uncertainties have a role in the covariance matrix of the input random variables, $\boldsymbol{\Sigma}_X$, and also in the mean value vector for evaluation of the Jacobian matrix of the output functions $\mathbf{J}_g(\boldsymbol{\mu}_X)$. Then the Jacobian matrix, that can be thought as the system, is used to transform the rows and columns of the covariance matrix of the input random variables, providing the covariance matrix of the output random variables, $\boldsymbol{\Sigma}_Y$, i.e. it is used to map the input randomness onto the output randomness.

Note this is equivalent to the matrix expression for the linear case Eq. (2.36) with $\mathbf{J}_g(\boldsymbol{\mu}_X) = A$.

Now it is possible to evaluate the dimensions of the matrices involved:

$$\begin{aligned} \boldsymbol{\Sigma}_Y &\approx \mathbf{J}_g(\boldsymbol{\mu}_X)\boldsymbol{\Sigma}_X\mathbf{J}_g^\top(\boldsymbol{\mu}_X) \\ (d_Y \times d_Y) &\approx (d_Y \times d_X)(d_X \times d_X)(d_X \times d_Y) \end{aligned} \tag{2.51}$$

And using the corresponding matrices:

$$\begin{bmatrix} \sigma^2_{Y_1} & \sigma_{Y_1Y_2} & \cdots & \sigma_{Y_1Y_{d_Y}} \\ \sigma_{Y_2Y_1} & \sigma^2_{Y_2} & \cdots & \sigma_{Y_2Y_{d_Y}} \\ \vdots & \vdots & \ddots & \vdots \\ \sigma_{Y_{d_Y}Y_1} & \sigma_{Y_{d_Y}Y_2} & \cdots & \sigma^2_{Y_{d_Y}} \end{bmatrix} \tag{2.52}$$

$$\approx \begin{bmatrix} \frac{\partial g_1}{\partial X_1} & \frac{\partial g_1}{\partial X_2} & \cdots & \frac{\partial g_1}{\partial X_{d_X}} \\ \frac{\partial g_2}{\partial X_1} & \frac{\partial g_2}{\partial X_2} & \cdots & \frac{\partial g_2}{\partial X_{d_X}} \\ \vdots & \vdots & \ddots & \vdots \\ \frac{\partial g_{d_Y}}{\partial X_1} & \frac{\partial g_{d_Y}}{\partial X_2} & \cdots & \frac{\partial g_{d_Y}}{\partial X_{d_X}} \end{bmatrix} \cdot \begin{bmatrix} \mu_{11} & \mu_{12} & \cdots & \mu_{1d_X} \\ \mu_{21} & \mu_{22} & \cdots & \mu_{2d_X} \\ \vdots & \vdots & \ddots & \vdots \\ \mu_{d_X1} & \mu_{d_X2} & \cdots & \mu_{d_Xd_X} \end{bmatrix} \cdot \begin{bmatrix} \frac{\partial g_1}{\partial X_1} & \frac{\partial g_2}{\partial X_1} & \cdots & \frac{\partial g_{d_Y}}{\partial X_1} \\ \frac{\partial g_1}{\partial X_2} & \frac{\partial g_2}{\partial X_2} & \cdots & \frac{\partial g_{d_Y}}{\partial X_2} \\ \vdots & \vdots & \ddots & \vdots \\ \frac{\partial g_1}{\partial X_{d_X}} & \frac{\partial g_2}{\partial X_{d_X}} & \cdots & \frac{\partial g_{d_Y}}{\partial X_{d_X}} \end{bmatrix}$$

Evaluating the first element of the output covariance matrix, i.e. the variance term, the first-order variance approximation of a function $Y_1 = g_1(\mathbf{X})$ is:

$$\begin{aligned} \sigma^2_{Y_1} &\approx \left(\frac{\partial g_1}{\partial X_1}\right)^2 \mu_{11} + \frac{\partial g_1}{\partial X_2}\frac{\partial g_1}{\partial X_1}\mu_{21} + \ldots + \frac{\partial g_1}{\partial X_{d_X}}\frac{\partial g_1}{\partial X_1}\mu_{d_X1} \\ &\quad + \frac{\partial g_1}{\partial X_1}\frac{\partial g_1}{\partial X_2}\mu_{12} + \left(\frac{\partial g_1}{\partial X_2}\right)^2 \mu_{22} + \ldots + \frac{\partial g_1}{\partial X_{d_X}}\frac{\partial g_1}{\partial X_2}\mu_{d_X2} \\ &\quad + \quad \ldots \quad + \quad \ldots \quad + \quad \ldots \quad + \quad \ldots \\ &\quad + \frac{\partial g_1}{\partial X_1}\frac{\partial g_1}{\partial X_{d_X}}\mu_{1d_X} + \frac{\partial g_1}{\partial X_2}\frac{\partial g_1}{\partial X_{d_X}}\mu_{2d_X} + \ldots + \left(\frac{\partial g_1}{\partial X_{d_X}}\right)^2 \mu_{d_Xd_X} \\ &\approx \sum_{j=1}^{d_X}\left(\frac{\partial g_1}{\partial X_j}\right)^2 \mu_{jj} + \sum_{j=1}^{d_X}\sum_{\substack{k=1 \\ k\neq j}}^{d_X}\frac{\partial g_1}{\partial X_j}\frac{\partial g_1}{\partial X_k}\mu_{jk} \\ &\approx \sum_{j=1}^{d_X}\sum_{k=1}^{d_X}\frac{\partial g_1}{\partial X_j}\frac{\partial g_1}{\partial X_k}\mu_{jk} \end{aligned} \tag{2.53}$$

Using the abbreviations and conventions introduced in Section 2.2 to compact the math derivations and omitting the index $i = 1$ leads to:

$$\mathrm{Var}\,(Y) = \sigma^2_Y \approx \sum_{j=1}^{d}\sum_{k=1}^{d} g_{,j}g_{,k}\mu_{jk} \tag{2.54}$$

The first-order covariance approximation of the functions $Y_1 = g_1(\mathbf{X})$ and $Y_2 = g_2(\mathbf{X})$ is:

$$\begin{aligned}
\sigma_{Y_1Y_2} \approx & \frac{\partial g_1}{\partial X_1}\frac{\partial g_2}{\partial X_1}\mu_{11} + \frac{\partial g_1}{\partial X_2}\frac{\partial g_2}{\partial X_1}\mu_{21} + \ldots + \frac{\partial g_1}{\partial X_{d_X}}\frac{\partial g_2}{\partial X_1}\mu_{d_X 1} \\
& + \frac{\partial g_1}{\partial X_1}\frac{\partial g_2}{\partial X_2}\mu_{12} + \frac{\partial g_1}{\partial X_2}\frac{\partial g_2}{\partial X_2}\mu_{22} + \ldots + \frac{\partial g_1}{\partial X_{d_X}}\frac{\partial g_2}{\partial X_2}\mu_{d_X 2} \\
& + \quad \ldots \quad + \quad \ldots \quad + \quad \ldots \quad + \quad \ldots \\
& + \frac{\partial g_1}{\partial X_1}\frac{\partial g_2}{\partial X_{d_X}}\mu_{1d_X} + \frac{\partial g_1}{\partial X_2}\frac{\partial g_2}{\partial X_{d_X}}\mu_{2d_X} + \ldots + \frac{\partial g_1}{\partial X_{d_X}}\frac{\partial g_2}{\partial X_{d_X}}\mu_{d_X d_X} \\
\approx & \sum_{j=1}^{d_X}\frac{\partial g_1}{\partial X_j}\frac{\partial g_2}{\partial X_j}\mu_{jj} + \sum_{j=1}^{d_X}\sum_{\substack{k=1 \\ k\neq j}}^{d_X}\frac{\partial g_1}{\partial X_j}\frac{\partial g_2}{\partial X_k}\mu_{jk} \\
\approx & \sum_{j=1}^{d_X}\sum_{k=1}^{d_X}\frac{\partial g_1}{\partial X_j}\frac{\partial g_2}{\partial X_k}\mu_{jk}
\end{aligned} \tag{2.55}$$

Using the abbreviations and conventions introduced in Section 2.2 to compact the math derivations and renaming the general functions as $Y_1 = g(\mathbf{X})$ and $Y_2 = h(\mathbf{X})$ leads to:

$$\mathrm{Cov}\,(Y_1, Y_2) = \sigma_{Y_1Y_2} \approx \sum_{j=1}^{d}\sum_{k=1}^{d} g_{,j}h_{,k}\mu_{jk} \tag{2.56}$$

2.5 Non-linear combinations: summation notation

This section presents the complete mathematical derivation of the full second-order approach for the first to fourth moments of functions of random variables using summation notation. It presents the expressions involving tensors of different orders in a simple and comprehensible way. The summation notation makes it is easier to work with expressions involving tensors of different orders. The first to fourth moments are related by definition to the expected value, the variance, the skewness, and the kurtosis of the random output variable. Then from these second-order approximations the simpler first-order expressions are also derived.

In this section, for the sake of brevity, the math derivation for every moment, begins with the second-order Taylor approximation and then the first-order is obtained from the second-order omitting the non-linear terms. Additionally, the equations in summation notation that have an equivalent in matrix form, are related to previously derived ones in Section 2.4.

A multi-input single-output system is considered, that is, a system with only one output random variable $\mathbf{Y}(\mathbf{X}) = \left[Y_1\right]^\top = \mathbf{g}(\mathbf{X}) = \left[g_1(\mathbf{X})\right]^\top$ simply denoted as Y as shown in Fig. 2.4.

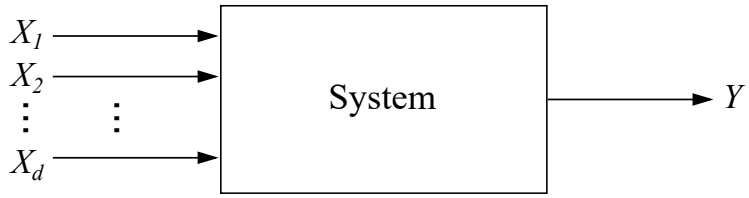

Figure 2.4. Multi-variable real-valued function.

Note that from the system in Fig. 2.1, Y_1 is simply denoted as Y and the d_X input random variables number is simply denoted as d.

To derive a complete second-order approach for obtaining the stochastic moments of an arbitrary general function $Y = g\left(X_1, X_2, ..., X_d\right)$ of d random variables about the mean value of each one, vector $\boldsymbol{\mu}_X = \mathrm{E}[\mathbf{X}] = P = \left[\mu_{X_1} \quad \mu_{X_2} \quad \dots \quad \mu_{X_{d_X}}\right]^\top$. The function is approximated using the second-order Taylor expansion about the vector of the means of the random variables:

$$\begin{aligned} Y \approx g\left(\mu_{X_1}, \mu_{X_2}, \dots, \mu_{X_d}\right) + \sum_{j=1}^{d} \left.\frac{\partial g}{\partial X_j}\right|_{\left(\mu_{X_1}, \mu_{X_2}, \dots, \mu_{X_d}\right)} \left(x_j - \mu_{X_j}\right) \\ + \frac{1}{2!} \sum_{j=1}^{d} \sum_{k=1}^{d} \left.\frac{\partial^2 g}{\partial X_j \partial X_k}\right|_{\left(\mu_{X_1}, \mu_{X_2}, \dots, \mu_{X_d}\right)} \left(x_j - \mu_{X_j}\right)\left(x_k - \mu_{X_k}\right) \end{aligned} \tag{2.57}$$

The second-order Taylor approximation, using the abbreviations introduced in Section 2.2, becomes:

$$Y \approx g_\mu + \sum_{j=1}^{d} g_{,j}\left(x_j - \mu_{X_j}\right) + \frac{1}{2} \sum_{j=1}^{d} \sum_{k=1}^{d} g_{,jk}\left(x_j - \mu_{X_j}\right)\left(x_k - \mu_{X_k}\right) \tag{2.58}$$

The zeroth, first, and second-order terms are denoted as o_0, o_1, and o_2 respectively to compress the subsequent mathematical derivations:

$$\begin{aligned} o_0 &= g_\mu \\ o_1 &= \sum_{j=1}^{d} g_{,j}\left(x_j - \mu_{X_j}\right) \\ o_2 &= \frac{1}{2} \sum_{j=1}^{d} \sum_{k=1}^{d} g_{,jk}\left(x_j - \mu_{X_j}\right)\left(x_k - \mu_{X_k}\right) \end{aligned} \tag{2.59}$$

2.5.1 Expected value second-order

The mean value of a general function $Y = g(X)$ is given by:

$$\mathrm{E}[Y] = \mu_Y = \mathrm{E}[g(X)] = \int_{-\infty}^{\infty} g(X) f_X(x)\, dx \tag{2.60}$$

Being $f_X(x)$ the probability density function of the random variables and $dx = dx_1 dx_2 \dots dx_n$. Inserting the second-order Taylor approximation at the mean vector of the random variables leads to:

$$\begin{aligned}
\mathrm{E}[Y] &\approx \int_{-\infty}^{\infty} \left[\overbrace{\underbrace{g_\mu}_{I}}^{o_0} + \overbrace{\underbrace{\sum_{j=1}^{d} g_{,j} \left(x_j - \mu_{X_j}\right)}_{II}}^{o_1} + \overbrace{\underbrace{\frac{1}{2} \sum_{j=1}^{d} \sum_{k=1}^{d} g_{,jk} \left(x_j - \mu_{X_j}\right)\left(x_k - \mu_{X_k}\right)}_{III}}^{o_2} \right] f_X(x)\, dx \\
&\approx \int_{-\infty}^{\infty} g_\mu f_X(x)\, dx + \int_{-\infty}^{\infty} \sum_{j=1}^{d} g_{,j} \left(x_j - \mu_{X_j}\right) f_X(x)\, dx \\
&\quad + \int_{-\infty}^{\infty} \frac{1}{2} \sum_{j=1}^{d} \sum_{k=1}^{d} g_{,jk} \left(x_j - \mu_{X_j}\right)\left(x_k - \mu_{X_k}\right) f_X(x)\, dx \\
&\approx g_\mu \underbrace{\int_{-\infty}^{\infty} f_X(x)\, dx}_{1} + \sum_{j=1}^{d} g_{,j} \underbrace{\int_{-\infty}^{\infty} \left(x_j - \mu_{X_j}\right) f_X(x)\, dx}_{0} \\
&\quad + \frac{1}{2} \sum_{j=1}^{d} \sum_{k=1}^{d} g_{,jk} \underbrace{\int_{-\infty}^{\infty} \left(x_j - \mu_{X_j}\right)\left(x_k - \mu_{X_k}\right) f_X(x)\, dx}_{\mu_{jk}}
\end{aligned} \tag{2.61}$$

Remarks regarding the horizontal curly braces:

- In the second-order approximation for the expected value, the I, II and III summation terms that has to be integrated match with the zeroth, first, and second-order Taylor terms denoted as o_0, o_1, and o_2 respectively.
- The integral of probability density function over the entire space is equal to 1.
- The first central moment of a r.v. always equals to 0. Not to be confused with the first raw moment which is the expected value.
- The second mixed or cross central moment of two random variables X_j and X_k is the covariance denoted as μ_{jk}.

Summarizing, the second-order approximation for the expected value of an arbitrary general function is:

$$\mathrm{E}[Y] = \mu_Y \approx g_\mu + \frac{1}{2}\sum_{j=1}^{d}\sum_{k=1}^{d} g_{,jk}\mu_{jk} \tag{2.62}$$

The above equation is equivalent to the Eq. (2.48) derived from the matrix form.

The complete derivation of the expected value second-order approximation assuming independence between the input r.v.s can be found in Appendix A.

2.5.2 Expected value first-order

From the second-order approximation for the expected value derived in Eq. (2.61), the first-order approximation can be obtained omitting the non-linear terms, o_2 term, of the second-order Taylor approximation thus the first-order Taylor approximation is left. Using the o_0, o_1 and o_2 notation presented in Eq. (2.59) and skipping the terms containing o_2, the first-order expected value approximation leads to:

$$(o_0 + o_1 + \cancel{o_2}) = \underbrace{o_0}_{I} + \underbrace{o_1}_{II} + \underbrace{\cancel{o_2}}_{III} \tag{2.63}$$

The first-order expected value approximation obtained omitting the corresponding o_2 term from the Eq. (2.62) equals:

$$\mathrm{E}[Y] = \mu_Y \approx g_\mu \tag{2.64}$$

The above equation is equivalent to the Eq. (2.46) derived from the matrix form. Note that in this case the equation is valid for general or independent variables.

2.5.3 Variance second-order

To estimate the variance of the general function Y, first, working with the definition of variance:

$$\begin{aligned}
\mathrm{Var}(Y) &= \sigma_Y^2 \\
&= \mathrm{E}\left[(Y-\mu_Y)^2\right] \\
&= \mathrm{E}\left[Y^2 - 2Y\mu_Y + \mu_Y^2\right] \\
&= \mathrm{E}\left[Y^2\right] - 2\,\mathrm{E}[Y]\,\mu_Y + \mu_Y^2 \\
&= \mathrm{E}\left[Y^2\right] - \mu_Y^2
\end{aligned} \tag{2.65}$$

Note that $\mathrm{E}[Y]\,\mu_Y = \mu_Y^2$.

Then applying the expected value defined as the integral:

$$\begin{aligned} \mathrm{Var}\,(Y) &= \mathrm{E}\left[Y^2\right] - \mu_Y^2 \\ &= \int_{-\infty}^{\infty} \left[g\,(X)\right]^2 f_X(x)\,dx - \mu_Y^2 \end{aligned} \tag{2.66}$$

Introducing the second-order Taylor series approximation of $Y = g\,(X)$ yields:

$$\mathrm{Var}\,(Y) = \int_{-\infty}^{\infty} \left[g_\mu + \sum_{j=1}^{d} g_{,j}\left(x_j - \mu_{X_j}\right) + \frac{1}{2}\sum_{j=1}^{d}\sum_{k=1}^{d} g_{,jk}\left(x_j - \mu_{X_j}\right)\left(x_k - \mu_{X_k}\right) \right]^2 f_X(x)\,dx - \mu_Y^2 \tag{2.67}$$

With the notation o_0, o_1 and o_2 used in Eq. (2.59), the sum that has to be integrated reads $(o_0 + o_1 + o_2)^2$, and applying the multinomial theorem when raised to the second power, the Taylor series becomes:

$$(o_0 + o_1 + o_2)^2 = \underbrace{o_0^2}_{I} + \underbrace{o_1^2}_{II} + \underbrace{o_2^2}_{III} + 2(\underbrace{o_0 o_1}_{IV} + \underbrace{o_0 o_2}_{V} + \underbrace{o_1 o_2}_{VI}) \tag{2.68}$$

$$\begin{aligned} \mathrm{Var}\,(Y) = \int_{-\infty}^{\infty} \Bigg[& \underbrace{g_\mu^2}_{I} + \underbrace{\left[\sum_{j=1}^{d} g_{,j}\left(x_j - \mu_{X_j}\right)\right]^2}_{II} + \underbrace{\left[\frac{1}{2}\sum_{j=1}^{d}\sum_{k=1}^{d} g_{,jk}\left(x_j - \mu_{X_j}\right)\left(x_k - \mu_{X_k}\right)\right]^2}_{III} \\ & + \underbrace{2g_\mu \sum_{j=1}^{d} g_{,j}\left(x_j - \mu_{X_j}\right)}_{IV} + \underbrace{2g_\mu \frac{1}{2}\sum_{j=1}^{d}\sum_{k=1}^{d} g_{,jk}\left(x_j - \mu_{X_j}\right)\left(x_k - \mu_{X_k}\right)}_{V} \\ & + \underbrace{2\left[\sum_{j=1}^{d} g_{,j}\left(x_j - \mu_{X_j}\right)\right]\left[\frac{1}{2}\sum_{j=1}^{d}\sum_{k=1}^{d} g_{,jk}\left(x_j - \mu_{X_j}\right)\left(x_k - \mu_{X_k}\right)\right]}_{VI} \Bigg] f_X(x)\,dx - \mu_Y^2 \end{aligned} \tag{2.69}$$

The sum rule in integration states that the integral of a sum of functions is equal to the sum of their integrals, so the I to VI terms can be integrated individually.

***I*:** o_0^2

$$\int_{-\infty}^{\infty} g_\mu^2 f_X(x)\,dx = g_\mu^2 \underbrace{\int_{-\infty}^{\infty} f_X(x)\,dx}_{1} = g_\mu^2 \tag{2.70}$$

***II*:** o_1^2

$$\int_{-\infty}^{\infty} \left[\sum_{j=1}^{d} g_{,j}\left(x_j - \mu_{X_j}\right)\right]^2 f_X(x)\,dx \tag{2.71a}$$

Applying again the multinomial theorem and using summation notation:

$$\left[\sum_{j=1}^{d} g_{,j}\left(x_j - \mu_{X_j}\right)\right]^2 = \sum_{j=1}^{d}\sum_{k=1}^{d} g_{,j}g_{,k}\left(x_j - \mu_{X_j}\right)\left(x_k - \mu_{X_k}\right) \tag{2.71b}$$

$$\begin{aligned}&\int_{-\infty}^{\infty} \sum_{j\ =1}^{d}\sum_{k\ =1}^{d} g_{,j}g_{,k}\left(x_j - \mu_{X_j}\right)\left(x_k - \mu_{X_k}\right) f_X(x)\,dx \\ &\quad = \sum_{j=1}^{d}\sum_{k=1}^{d} g_{,j}g_{,k} \underbrace{\int_{-\infty}^{\infty} \left(x_j - \mu_{X_j}\right)\left(x_k - \mu_{X_k}\right) f_X(x)\,dx}_{\mu_{jk}}\end{aligned} \tag{2.71c}$$

***III*:** o_2^2

$$\int_{-\infty}^{\infty} \left[\frac{1}{2}\sum_{j=1}^{d}\sum_{k=1}^{d} g_{,jk}\left(x_j - \mu_{X_j}\right)\left(x_k - \mu_{X_k}\right)\right]^2 f_X(x)\,dx \tag{2.72a}$$

Applying the multinomial theorem and using summation notation:

$$\begin{aligned}&\left[\frac{1}{2}\sum_{j=1}^{d}\sum_{k=1}^{d} g_{,jk}\left(x_j - \mu_{X_j}\right)\left(x_k - \mu_{X_k}\right)\right]^2 \\ &= \frac{1}{4}\sum_{j=1}^{d}\sum_{k=1}^{d}\sum_{l=1}^{d}\sum_{m=1}^{d} g_{,jk}g_{,lm}\left(x_j - \mu_{X_j}\right)\left(x_k - \mu_{X_k}\right)\left(x_l - \mu_{X_l}\right)\left(x_m - \mu_{X_m}\right)\end{aligned} \tag{2.72b}$$

$$\begin{aligned}
&\int_{-\infty}^{\infty} \frac{1}{4} \sum_{j=1}^{d} \sum_{k=1}^{d} \sum_{l=1}^{d} \sum_{m=1}^{d} g_{,jk} g_{,lm} \left(x_j - \mu_{X_j}\right) \left(x_k - \mu_{X_k}\right) \left(x_l - \mu_{X_l}\right) \left(x_m - \mu_{X_m}\right) f_X(x)\, dx \\
&= \frac{1}{4} \sum_{j=1}^{d} \sum_{k=1}^{d} \sum_{l=1}^{d} \sum_{m=1}^{d} g_{,jk} g_{,lm} \underbrace{\int_{-\infty}^{\infty} \left(x_j - \mu_{X_j}\right) \left(x_k - \mu_{X_k}\right) \left(x_l - \mu_{X_l}\right) \left(x_m - \mu_{X_m}\right) f_X(x)\, dx}_{\mu_{jklm}}
\end{aligned} \tag{2.72c}$$

***IV*:** $2o_0o_1$

$$\int_{-\infty}^{\infty} 2g_\mu \sum_{j=1}^{d} g_{,j} \left(x_j - \mu_{X_j}\right) f_X(x)\, dx = 2g_\mu \sum_{j=1}^{d} g_{,j} \underbrace{\int_{-\infty}^{\infty} \left(x_j - \mu_{X_j}\right) f_X(x)\, dx}_{0} = 0 \tag{2.73}$$

Remark: The first central moment of a r.v. always equals to 0. Not to be confused with the first raw moment which is the the expected value.

***V*:** $2o_0o_2$

$$\begin{aligned}
&\int_{-\infty}^{\infty} 2g_\mu \frac{1}{2} \sum_{j=1}^{d} \sum_{k=1}^{d} g_{,jk} \left(x_j - \mu_{X_j}\right) \left(x_k - \mu_{X_k}\right) f_X(x)\, dx \\
&= g_\mu \sum_{j=1}^{d} \sum_{k=1}^{d} g_{,jk} \underbrace{\int_{-\infty}^{\infty} \left(x_j - \mu_{X_j}\right) \left(x_k - \mu_{X_k}\right) f_X(x)\, dx}_{\mu_{jk}}
\end{aligned} \tag{2.74}$$

***VI*:** $2o_1o_2$

$$\begin{aligned}
&\int_{-\infty}^{\infty} 2 \left[\sum_{j=1}^{d} g_{,j} \left(x_j - \mu_{X_j}\right)\right] \left[\frac{1}{2} \sum_{j=1}^{d} \sum_{k=1}^{d} g_{,jk} \left(x_j - \mu_{X_j}\right) \left(x_k - \mu_{X_k}\right)\right] f_X(x)\, dx \\
&= \int_{-\infty}^{\infty} \sum_{j=1}^{d} \sum_{k=1}^{d} \sum_{l=1}^{d} g_{,j} g_{,kl} \left(x_j - \mu_{X_j}\right) \left(x_k - \mu_{X_k}\right) \left(x_l - \mu_{X_l}\right) f_X(x)\, dx \\
&= \sum_{j=1}^{d} \sum_{k=1}^{d} \sum_{l=1}^{d} g_{,j} g_{,kl} \underbrace{\int_{-\infty}^{\infty} \left(x_j - \mu_{X_j}\right) \left(x_k - \mu_{X_k}\right) \left(x_l - \mu_{X_l}\right) f_X(x)\, dx}_{\mu_{jkl}}
\end{aligned} \tag{2.75}$$

Summarizing, the second-order approximation for the variance of an arbitrary general function is:

$$\begin{aligned}\mathrm{Var}\,(Y) = \sigma_Y^2 \\ \approx \underbrace{g_\mu^2}_{I} + \underbrace{\sum_{j=1}^{d}\sum_{k=1}^{d} g_{,j}g_{,k}\mu_{jk}}_{II} + \underbrace{\frac{1}{4}\sum_{j=1}^{d}\sum_{k=1}^{d}\sum_{l=1}^{d}\sum_{m=1}^{d} g_{,jk}g_{,lm}\mu_{jklm}}_{III} \\ + \underbrace{0}_{IV} + \underbrace{g_\mu \sum_{j=1}^{d}\sum_{k=1}^{d} g_{,jk}\mu_{jk}}_{V} + \underbrace{\sum_{j=1}^{d}\sum_{k=1}^{d}\sum_{l=1}^{d} g_{,j}g_{,kl}\mu_{jkl}}_{VI} - \mu_Y^2\end{aligned} \tag{2.76}$$

without the horizontal curly braces and omitting the IV term, the approximation of the variance is given by:

$$\begin{aligned}\mathrm{Var}\,(Y) = \sigma_Y^2 \\ \approx g_\mu^2 + \sum_{j=1}^{d}\sum_{k=1}^{d} g_{,j}g_{,k}\mu_{jk} + \frac{1}{4}\sum_{j=1}^{d}\sum_{k=1}^{d}\sum_{l=1}^{d}\sum_{m=1}^{d} g_{,jk}g_{,lm}\mu_{jklm} \\ + g_\mu \sum_{j=1}^{d}\sum_{k=1}^{d} g_{,jk}\mu_{jk} + \sum_{j=1}^{d}\sum_{k=1}^{d}\sum_{l=1}^{d} g_{,j}g_{,kl}\mu_{jkl} - \mu_Y^2\end{aligned} \tag{2.77}$$

The complete derivation of the variance second-order approximation assuming independence between the input r.v.s can be found in Appendix A.

2.5.4 Variance first-order

As explained in the introduction Section 2.1, if only linear terms of the Taylor expansion are considered, the highest moments that occur, when computing the variance, are of second-order, and then the method is commonly referred to as first-order second moment (FOSM) method. In this thesis, it is preferred to name the method simply as first-order variance approximation, being more general and being valid for every moment order.

From the second-order approximation for the variance Eq. (2.76), the first-order approximation can be derived omitting the non-linear terms of the second-order Taylor approximation thus the first-order Taylor approximation is retained. Using

the o_0, o_1 and o_2 notation presented in Eq. (2.59) and skipping the terms containing o_2, the first-order variance approximation leads to:

$$\begin{aligned}(o_0 + o_1 + \cancel{o_2})^2 &= \underbrace{o_0^2}_{I} + \underbrace{o_1^2}_{II} + \underbrace{\cancel{o_2^2}}_{III} + 2(\underbrace{o_0 o_1}_{IV} + \underbrace{\cancel{o_0 o_2}}_{V} + \underbrace{\cancel{o_1 o_2}}_{VI}) \\ (o_0 + o_1)^2 &= \underbrace{o_0^2}_{I} + \underbrace{o_1^2}_{II} + 2(\underbrace{o_0 o_1}_{IV})\end{aligned} \tag{2.78}$$

Then the Eq. (2.76) becomes:

$$\begin{aligned}\operatorname{Var}(Y) &= \sigma_Y^2 \\ &\approx \underbrace{g_\mu^2}_{I} + \underbrace{\sum_{j=1}^{d}\sum_{k=1}^{d} g_{,j} g_{,k} \mu_{jk}}_{II} + \underbrace{0}_{IV} - \mu_Y^2\end{aligned} \tag{2.79}$$

And knowing that the first-order expected value approximation is $\mathrm{E}[Y] = \mu_Y \approx g_\mu$, as shown in Eq. (2.64), the first-order variance approximation is:

$$\operatorname{Var}(Y) = \sigma_Y^2 \approx \underbrace{\sum_{j=1}^{d}\sum_{k=1}^{d} g_{,j} g_{,k} \mu_{jk}}_{II} \tag{2.80}$$

The above equation is equivalent to the Eq. (2.54) derived from the matrix form.

2.5.5 Third central moment *skewness* second-order

The skewness of $Y = g(X)$ can be determined from the third central moment $\mu_3(Y,Y,Y) = \mu_{Y,3}$ divided by the standard deviation raised to the third power σ_Y^3. It is also referred to as normalized or standardized third central moment. The skewness is denoted as γ_{1_Y}, $\operatorname{Skew}(Y)$, or $S(Y,Y,Y)$ as indicated below:

$$S(Y,Y,Y) = \frac{\mu_{Y,3}}{\sigma_Y^3} \tag{2.81}$$

To estimate the third central moment $\mu_3(Y,Y,Y) = \mu_{Y,3}$ of the general function Y, first, working with the definition of the third central moment:

$$\begin{aligned}\mu_3(Y,Y,Y) &= \mu_{Y,3} \\ &= \mathrm{E}\left[(Y - \mu_Y)^3\right] \\ &= \mathrm{E}\left[Y^3 - 3Y^2\mu_Y + 3Y\mu_Y^2 - \mu_Y^3\right] \\ &= \mathrm{E}\left[Y^3\right] - 3\mu_Y\left(\mathrm{E}\left[Y^2\right] - \mu_Y \mathrm{E}[Y]\right) - \mu_Y^3 \\ &= \mathrm{E}\left[Y^3\right] - 3\mu_Y\sigma_Y^2 - \mu_Y^3\end{aligned} \tag{2.82}$$

Note that $\sigma_Y^2 = \left(\mathrm{E}\left[Y^2\right] - \mu_Y \mathrm{E}\left[Y\right]\right)$ from Eq. (2.65) is replaced. Then applying the expected value defined as the integral:

$$\begin{aligned}\mu_3\left(Y,Y,Y\right) &= \mathrm{E}\left[Y^3\right] - 3\mu_Y\sigma_Y^2 - \mu_Y^3 \\ &= \int_{-\infty}^{\infty} \left[g\left(X\right)\right]^3 f_X(x)\,dx - 3\mu_Y\sigma_Y^2 - \mu_Y^3\end{aligned} \tag{2.83}$$

Introducing the second-order Taylor series approximation of $Y = g\left(X\right)$ yields:

$$\begin{aligned}&\mu_3\left(Y,Y,Y\right) \\ &= \int_{-\infty}^{\infty} \left[g_\mu + \sum_{j=1}^{d} g_{,j}\left(x_j - \mu_{X_j}\right) + \frac{1}{2}\sum_{j=1}^{d}\sum_{k=1}^{d} g_{,jk}\left(x_j - \mu_{X_j}\right)\left(x_k - \mu_{X_k}\right)\right]^3 f_X(x)\,dx \\ &\quad - 3\mu_Y\sigma_Y^2 - \mu_Y^3\end{aligned} \tag{2.84}$$

With the notation o_0, o_1 and o_2 used in Eq. (2.59), the sum that has to be integrated reads $\left(o_0 + o_1 + o_2\right)^3$, and applying the multinomial theorem when raised to the third power, the Taylor series becomes:

$$\left(o_0 + o_1 + o_2\right)^3 = \underbrace{o_0^3}_{I} + \underbrace{o_1^3}_{II} + \underbrace{o_2^3}_{III} + 3(\underbrace{o_0^2 o_1}_{IV} + \underbrace{o_0^2 o_2}_{V} + \underbrace{o_0 o_1^2}_{VI} + \underbrace{o_1^2 o_2}_{VII} + \underbrace{o_0 o_2^2}_{VIII} + \underbrace{o_1 o_2^2}_{IX}) + 6(\underbrace{o_0 o_1 o_2}_{X}) \tag{2.85}$$

The summands in the integral can be integrated individually.

I: o_0^3

$$\int_{-\infty}^{\infty} g_\mu^3 f_X(x)\,dx = g_\mu^3 \underbrace{\int_{-\infty}^{\infty} f_X(x)\,dx}_{1} = g_\mu^3 \tag{2.86}$$

II: o_1^3

$$\int_{-\infty}^{\infty} \left[\sum_{j=1}^{d} g_{,j}\left(x_j - \mu_{X_j}\right)\right]^3 f_X(x)\,dx \tag{2.87a}$$

Applying again the multinomial theorem and using summation notation:

$$\left[\sum_{j=1}^{d} g_{,j}\left(x_j - \mu_{X_j}\right)\right]^3 = \sum_{j=1}^{d}\sum_{k=1}^{d}\sum_{l=1}^{d} g_{,j}g_{,k}g_{,l}\left(x_j - \mu_{X_j}\right)\left(x_k - \mu_{X_k}\right)\left(x_l - \mu_{X_l}\right) \tag{2.87b}$$

$$\begin{aligned}&\int_{-\infty}^{\infty} \sum_{j=1}^{d}\sum_{k=1}^{d}\sum_{l=1}^{d} g_{,j}g_{,k}g_{,l}\left(x_j-\mu_{X_j}\right)\left(x_k-\mu_{X_k}\right)\left(x_l-\mu_{X_l}\right) f_X(x)\,dx \\ &\quad=\sum_{j=1}^{d}\sum_{k=1}^{d}\sum_{l=1}^{d} g_{,j}g_{,k}g_{,l}\underbrace{\int_{-\infty}^{\infty}\left(x_j-\mu_{X_j}\right)\left(x_k-\mu_{X_k}\right)\left(x_l-\mu_{X_l}\right) f_X(x)\,dx}_{\mu_{jkl}}\end{aligned} \tag{2.87c}$$

***III*:** o_2^3

$$\int_{-\infty}^{\infty}\left[\frac{1}{2}\sum_{j=1}^{d}\sum_{k=1}^{d} g_{,jk}\left(x_j-\mu_{X_j}\right)\left(x_k-\mu_{X_k}\right)\right]^3 f_X(x)\,dx \tag{2.88a}$$

Applying the multinomial theorem and using summation notation:

$$\begin{aligned}&\left[\frac{1}{2}\sum_{j=1}^{d}\sum_{k=1}^{d} g_{,jk}\left(x_j-\mu_{X_j}\right)\left(x_k-\mu_{X_k}\right)\right]^3 \\ &\quad=\frac{1}{8}\sum_{j=1}^{d}\sum_{k=1}^{d}\sum_{l=1}^{d}\sum_{m=1}^{d}\sum_{r=1}^{d}\sum_{s=1}^{d} g_{,jk}g_{,lm}g_{,rs} \\ &\qquad\cdot\left(x_j-\mu_{X_j}\right)\left(x_k-\mu_{X_k}\right)\left(x_l-\mu_{X_l}\right)\left(x_m-\mu_{X_m}\right)\left(x_r-\mu_{X_r}\right)\left(x_s-\mu_{X_s}\right)\end{aligned} \tag{2.88b}$$

$$\begin{aligned}&\int_{-\infty}^{\infty}\frac{1}{8}\sum_{j=1}^{d}\sum_{k=1}^{d}\sum_{l=1}^{d}\sum_{m=1}^{d}\sum_{r=1}^{d}\sum_{s=1}^{d} g_{,jk}g_{,lm}g_{,rs} \\ &\qquad\cdot\left(x_j-\mu_{X_j}\right)\left(x_k-\mu_{X_k}\right)\left(x_l-\mu_{X_l}\right)\left(x_m-\mu_{X_m}\right)\left(x_r-\mu_{X_r}\right)\left(x_s-\mu_{X_s}\right) f_X(x)\,dx \\ &\quad=\frac{1}{8}\sum_{j=1}^{d}\sum_{k=1}^{d}\sum_{l=1}^{d}\sum_{m=1}^{d}\sum_{r=1}^{d}\sum_{s=1}^{d} g_{,jk}g_{,lm}g_{,rs} \\ &\qquad\cdot\underbrace{\int_{-\infty}^{\infty}\left(x_j-\mu_{X_j}\right)\left(x_k-\mu_{X_k}\right)\left(x_l-\mu_{X_l}\right)\left(x_m-\mu_{X_m}\right)\left(x_r-\mu_{X_r}\right)\left(x_s-\mu_{X_s}\right) f_X(x)\,dx}_{\mu_{jklmrs}}\end{aligned} \tag{2.88c}$$

***IV*:** $3o_0^2 o_1$

$$\int_{-\infty}^{\infty} 3g_\mu^2 \sum_{j=1}^{d} g_{,j} \left(x_j - \mu_{X_j}\right) f_X(x)\, dx = 3g_\mu^2 \sum_{j=1}^{d} g_{,j} \underbrace{\int_{-\infty}^{\infty} \left(x_j - \mu_{X_j}\right) f_X(x)\, dx}_{0} = 0 \tag{2.89}$$

***V*:** $3o_0^2 o_2$

$$\begin{aligned} &\int_{-\infty}^{\infty} 3g_\mu^2 \frac{1}{2} \sum_{j\,=1}^{d} \sum_{k\,=1}^{d} g_{,jk} \left(x_j - \mu_{X_j}\right) \left(x_k - \mu_{X_k}\right) f_X(x)\, dx \\ &\quad = 3g_\mu^2 \frac{1}{2} \sum_{j=1}^{d} \sum_{k=1}^{d} g_{,jk} \underbrace{\int_{-\infty}^{\infty} \left(x_j - \mu_{X_j}\right) \left(x_k - \mu_{X_k}\right) f_X\left(x\right) dx}_{\mu_{jk}} \end{aligned} \tag{2.90}$$

***VI*:** $3o_0 o_1^2$

$$\begin{aligned} &\int_{-\infty}^{\infty} 3g_\mu \left[\sum_{j=1}^{d} g_{,j} \left(x_j - \mu_{X_j}\right)\right]^2 f_X(x)\, dx \\ &\quad = 3g_\mu \sum_{j=1}^{d} \sum_{k=1}^{d} g_{,j} g_{,k} \underbrace{\int_{-\infty}^{\infty} \left(x_j - \mu_{X_j}\right) \left(x_k - \mu_{X_k}\right) f_X\left(x\right) dx}_{\mu_{jk}} \end{aligned} \tag{2.91}$$

***VII*:** $3o_1^2 o_2$

$$\begin{aligned} &\int_{-\infty}^{\infty} 3 \left[\sum_{j=1}^{d} g_{,j} \left(x_j - \mu_{X_j}\right)\right]^2 \left[\frac{1}{2} \sum_{j=1}^{d} \sum_{k=1}^{d} g_{,jk} \left(x_j - \mu_{X_j}\right) \left(x_k - \mu_{X_k}\right)\right] f_X(x)\, dx \\ &= \int_{-\infty}^{\infty} 3 \left[\sum_{j=1}^{d} \sum_{k=1}^{d} g_{,j} g_{,k} \left(x_j - \mu_{X_j}\right) \left(x_k - \mu_{X_k}\right)\right] \left[\frac{1}{2} \sum_{j=1}^{d} \sum_{k=1}^{d} g_{,jk} \left(x_j - \mu_{X_j}\right) \left(x_k - \mu_{X_k}\right)\right] f_X(x)\, dx \\ &= 3\frac{1}{2} \sum_{j=1}^{d} \sum_{k=1}^{d} \sum_{l=1}^{d} \sum_{m=1}^{d} g_{,j} g_{,k} g_{,lm} \underbrace{\int_{-\infty}^{\infty} \left(x_j - \mu_{X_j}\right) \left(x_k - \mu_{X_k}\right) \left(x_l - \mu_{X_l}\right) \left(x_m - \mu_{X_m}\right) f_X(x)\, dx}_{\mu_{jklm}} \end{aligned} \tag{2.92}$$

***VIII*:** $3o_0o_2^2$

$$\int_{-\infty}^{\infty} 3g_\mu \left[\frac{1}{2}\sum_{j=1}^{d}\sum_{k=1}^{d} g_{,jk}\left(x_j-\mu_{X_j}\right)\left(x_k-\mu_{X_k}\right)\right]^2 f_X(x)\,dx$$

$$= \int_{-\infty}^{\infty} 3g_\mu \frac{1}{4}\sum_{j=1}^{d}\sum_{k=1}^{d}\sum_{l=1}^{d}\sum_{m=1}^{d} g_{,jk}g_{,lm}\left(x_j-\mu_{X_j}\right)\left(x_k-\mu_{X_k}\right)\left(x_l-\mu_{X_l}\right)\left(x_m-\mu_{X_m}\right)f_X(x)\,dx$$

$$= 3g_\mu \frac{1}{4}\sum_{j=1}^{d}\sum_{k=1}^{d}\sum_{l=1}^{d}\sum_{m=1}^{d} g_{,jk}g_{,lm} \underbrace{\int_{-\infty}^{\infty}\left(x_j-\mu_{X_j}\right)\left(x_k-\mu_{X_k}\right)\left(x_l-\mu_{X_l}\right)\left(x_m-\mu_{X_m}\right)f_X(x)\,dx}_{\mu_{jklm}}$$

(2.93)

***IX*:** $3o_1o_2^2$

$$\int_{-\infty}^{\infty} 3\left[\sum_{j=1}^{d} g_{,j}\left(x_j-\mu_{X_j}\right)\right]\left[\frac{1}{2}\sum_{j=1}^{d}\sum_{k=1}^{d} g_{,jk}\left(x_j-\mu_{X_j}\right)\left(x_k-\mu_{X_k}\right)\right]^2 f_X(x)\,dx$$

$$= \int_{-\infty}^{\infty} 3\left[\sum_{j=1}^{d} g_{,j}\left(x_j-\mu_{X_j}\right)\right] \cdot \left[\frac{1}{4}\sum_{j=1}^{d}\sum_{k=1}^{d}\sum_{l=1}^{d}\sum_{m=1}^{d} g_{,jk}g_{,lm}\left(x_j-\mu_{X_j}\right)\left(x_k-\mu_{X_k}\right)\left(x_l-\mu_{X_l}\right)\left(x_m-\mu_{X_m}\right)\right] f_X(x)\,dx$$

$$= 3\frac{1}{4}\sum_{j=1}^{d}\sum_{k=1}^{d}\sum_{l=1}^{d}\sum_{m=1}^{d}\sum_{r=1}^{d} g_{,j}g_{,kl}g_{,mr} \cdot \underbrace{\int_{-\infty}^{\infty}\left(x_j-\mu_{X_j}\right)\left(x_k-\mu_{X_k}\right)\left(x_l-\mu_{X_l}\right)\left(x_m-\mu_{X_m}\right)\left(x_r-\mu_{X_r}\right)f_X(x)\,dx}_{\mu_{jklmr}}$$

(2.94)

$\boldsymbol{X}:\ 6o_0o_1o_2$

$$\begin{aligned}
&\int_{-\infty}^{\infty} 6g_\mu \left[\sum_{j=1}^{d} g_{,j}\left(x_j-\mu_{X_j}\right)\right]\left[\frac{1}{2}\sum_{j=1}^{d}\sum_{k=1}^{d} g_{,jk}\left(x_j-\mu_{X_j}\right)\left(x_k-\mu_{X_k}\right)\right] f_X(x)\,dx \\
&\quad = 6g_\mu \frac{1}{2}\sum_{j=1}^{d}\sum_{k=1}^{d}\sum_{l=1}^{d} g_{,j}g_{,kl}\underbrace{\int_{-\infty}^{\infty}\left(x_j-\mu_{X_j}\right)\left(x_k-\mu_{X_k}\right)\left(x_l-\mu_{X_l}\right) f_X(x)\,dx}_{\mu_{jkl}}
\end{aligned} \tag{2.95}$$

Summarizing, the second-order approximation for the third central moment of an arbitrary general function is:

$$\begin{aligned}
\mu_3(Y,Y,Y) &= \mu_{Y,3} \\
&\approx \underbrace{g_\mu^3}_{I} + \underbrace{\sum_{j=1}^{d}\sum_{k=1}^{d}\sum_{l=1}^{d} g_{,j}g_{,k}g_{,l}\mu_{jkl}}_{II} + \underbrace{\frac{1}{8}\sum_{j=1}^{d}\sum_{k=1}^{d}\sum_{l=1}^{d}\sum_{m=1}^{d}\sum_{r=1}^{d}\sum_{s=1}^{d} g_{,jk}g_{,lm}g_{,rs}\mu_{jklmrs}}_{III} \\
&\quad + \underbrace{0}_{IV} + \underbrace{3g_\mu^2\frac{1}{2}\sum_{j=1}^{d}\sum_{k=1}^{d} g_{,jk}\mu_{jk}}_{V} + \underbrace{3g_\mu\sum_{j=1}^{d}\sum_{k=1}^{d} g_{,j}g_{,k}\mu_{jk}}_{VI} \\
&\quad + \underbrace{3\frac{1}{2}\sum_{j=1}^{d}\sum_{k=1}^{d}\sum_{l=1}^{d}\sum_{m=1}^{d} g_{,j}g_{,k}g_{,lm}\mu_{jklm}}_{VII} + \underbrace{3g_\mu\frac{1}{4}\sum_{j=1}^{d}\sum_{k=1}^{d}\sum_{l=1}^{d}\sum_{m=1}^{d} g_{,jk}g_{,lm}\mu_{jklm}}_{VIII} \\
&\quad + \underbrace{3\frac{1}{4}\sum_{j=1}^{d}\sum_{k=1}^{d}\sum_{l=1}^{d}\sum_{m=1}^{d}\sum_{r=1}^{d} g_{,j}g_{,kl}g_{,mr}\mu_{jklmr}}_{IX} \\
&\quad + \underbrace{6g_\mu\frac{1}{2}\sum_{j=1}^{d}\sum_{k=1}^{d}\sum_{l=1}^{d} g_{,j}g_{,kl}\mu_{jkl}}_{X} - 3\mu_Y\sigma_Y^2 - \mu_Y^3
\end{aligned} \tag{2.96}$$

Note that the $_{j,k,l,m,r,s,t,u}$ letters are used as summation indices where $_{n,o,p,q}$ are skipped because n, p and q are used to indicate parameters of the NASGRO equation and o is used to denote the order terms of the Taylor approximation.

The derivation of the third central moment second-order approximation assuming independence between the input r.v.s can be found in Appendix A.

2.5.6 Third central moment *skewness* first-order

From the second-order approximation for the third central moment Eq. (2.96), the first-order approximation can be derived omitting the non-linear terms of the second-order Taylor approximation thus the first-order Taylor approximation is left. Using the o_0, o_1 and o_2 notation presented in Eq. (2.59), and skipping the terms containing o_2, the first-order approximation for the third central moment leads to:

$$\begin{aligned}(o_0+o_1+\cancel{o_2})^3 &= \underbrace{o_0^3}_{I}+\underbrace{o_1^3}_{II}+\underbrace{\cancel{o_2^3}}_{III}+3(\underbrace{o_0^2o_1}_{IV}+\underbrace{\cancel{o_0^2o_2}}_{V}+\underbrace{o_0o_1^2}_{VI}+\underbrace{\cancel{o_1^2o_2}}_{VII}+\underbrace{\cancel{o_0o_2^2}}_{VIII}+\underbrace{\cancel{o_1o_2^2}}_{IX})+6(\underbrace{\cancel{o_0o_1o_2}}_{X})\\ (o_0+o_1)^3 &= \underbrace{o_0^3}_{I}+\underbrace{o_1^3}_{II}+3(\underbrace{o_0^2o_1}_{IV}+\underbrace{o_0o_1^2}_{VI})\end{aligned} \tag{2.97}$$

Then the Eq. (2.96) becomes:

$$\begin{aligned}\mu_3(Y,Y,Y) &= \mu_{Y,3}\\ &\approx \underbrace{g_\mu^3}_{I}+\underbrace{\sum_{j=1}^{d}\sum_{k=1}^{d}\sum_{l=1}^{d}g_{,j}g_{,k}g_{,l}\mu_{jkl}}_{II}+\underbrace{0}_{IV}+\underbrace{3g_\mu\sum_{j=1}^{d}\sum_{k=1}^{d}g_{,j}g_{,k}\mu_{jk}}_{VI}-3\mu_Y\sigma_Y^2-\mu_Y^3\end{aligned} \tag{2.98}$$

And knowing that the first-order expected value approximation is $\mathrm{E}[Y]=\mu_Y\approx g_\mu$ from Eq. (2.64) and the first-order variance approximation is $\mathrm{Var}(Y)=\sigma_Y^2\approx\sum_{j=1}^{d}\sum_{k=1}^{d}g_{,j}g_{,k}\mu_{jk}$ from Eq. (2.80), the third central moment approximation of first-order is:

$$\mu_3(Y,Y,Y)=\mu_{Y,3}\approx\underbrace{\sum_{j=1}^{d}\sum_{k=1}^{d}\sum_{l=1}^{d}g_{,j}g_{,k}g_{,l}\mu_{jkl}}_{II} \tag{2.99}$$

2.5.7 Fourth central moment *kurtosis* second-order

The kurtosis of $Y=g(X)$ can be determined from the fourth central moment $\mu_4(Y,Y,Y,Y)=\mu_{Y,4}$ divided by the standard deviation raised to the fourth power σ_Y^4. It is also referred to as normalized or standardized fourth central moment. The kurtosis is denoted as β_{2_Y}, $\mathrm{Kurt}(Y)$, or $K(Y,Y,Y,Y)$ as indicated below:

$$K(Y,Y,Y,Y)=\frac{\mu_{Y,4}}{\sigma_Y^4} \tag{2.100}$$

To estimate the fourth central moment $\mu_4(Y,Y,Y,Y) = \mu_{Y,4}$ of the general function Y, first, working with the definition of the fourth central moment:

$$\begin{aligned}
\mu_4(Y,Y,Y,Y) &= \mu_{Y,4} \\
&= \mathrm{E}\left[(Y-\mu_Y)^4\right] \\
&= \mathrm{E}\left[Y^4 - 4Y^3\mu_Y + 6Y^2\mu_Y^2 - 4Y\mu_Y^3 + \mu_Y^4\right] \\
&= \mathrm{E}\left[Y^4\right] - 4\mu_Y\,\mathrm{E}\left[Y^3\right] + 6\mu_Y^2\,\mathrm{E}\left[Y^2\right] - 3\mu_Y^4 \\
&= \mathrm{E}\left[Y^4\right] - 4\mu_Y\left(\mu_{Y,3} + 3\mu_Y\sigma_Y^2 + \mu_Y^3\right) + 6\mu_Y^2\left(\sigma_Y^2 + \mu_Y^2\right) - 3\mu_Y^4 \\
&= \mathrm{E}\left[Y^4\right] - 4\mu_Y\mu_{Y,3} - 12\mu_Y^2\sigma_Y^2 - 4\mu_Y^4 + 6\mu_Y^2\sigma_Y^2 + 6\mu_Y^4 - 3\mu_Y^4 \\
&= \mathrm{E}\left[Y^4\right] - 4\mu_Y\mu_{Y,3} - 6\mu_Y^2\sigma_Y^2 - \mu_Y^4
\end{aligned} \tag{2.101}$$

Note that $\sigma_Y^2 = \mathrm{E}\left[Y^2\right] - \mu_Y\,\mathrm{E}[Y] = \mathrm{E}\left[Y^2\right] - \mu_Y^2$ from Eq. (2.65) and $\mu_{Y,3} = \mathrm{E}\left[Y^3\right] - 3\mu_Y\sigma_Y^2 - \mu_Y^3$ from Eq. (2.82) are replaced isolating the raw moments $\mathrm{E}\left[Y^2\right]$ and $\mathrm{E}\left[Y^3\right]$. Then applying the expected value defined as the integral:

$$\begin{aligned}
\mu_4(Y,Y,Y,Y) &= \mathrm{E}\left[Y^4\right] - 4\mu_Y\mu_{Y,3} - 6\mu_Y^2\sigma_Y^2 - \mu_Y^4 \\
&= \int_{-\infty}^{\infty} [g(X)]^4 f_X(x)\,dx - 4\mu_Y\mu_{Y,3} - 6\mu_Y^2\sigma_Y^2 - \mu_Y^4
\end{aligned} \tag{2.102}$$

Introducing the second-order Taylor series approximation of $Y = g(X)$ yields:

$$\begin{aligned}
&\mu_4(Y,Y,Y,Y) \\
&= \int_{-\infty}^{\infty} \left[g_\mu + \sum_{j=1}^{d} g_{,j}\left(x_j - \mu_{X_j}\right) + \frac{1}{2}\sum_{j=1}^{d}\sum_{k=1}^{d} g_{,jk}\left(x_j - \mu_{X_j}\right)\left(x_k - \mu_{X_k}\right) \right]^4 f_X(x)\,dx \\
&\quad - 4\mu_Y\mu_{Y,3} - 6\mu_Y^2\sigma_Y^2 - \mu_Y^4
\end{aligned} \tag{2.103}$$

With the notation o_0, o_1 and o_2 used in Eq. (2.59), the sum that has to be integrated reads $(o_0 + o_1 + o_2)^4$, and applying the multinomial theorem when raised to the fourth power, the Taylor series becomes:

$$\begin{aligned}
(o_0+o_1+o_2)^4 = {} & \underbrace{o_0^4}_{I} + \underbrace{o_1^4}_{II} + \underbrace{o_2^4}_{III} + 4(\underbrace{o_0^3 o_1}_{IV} + \underbrace{o_0^3 o_2}_{V} + \underbrace{o_0 o_1^3}_{VI} + \underbrace{o_1^3 o_2}_{VII} + \underbrace{o_0 o_2^3}_{VIII} + \underbrace{o_1 o_2^3}_{IX}) \\
& + 6(\underbrace{o_0^2 o_1^2}_{X} + \underbrace{o_0^2 o_2^2}_{XI} + \underbrace{o_1^2 o_2^2}_{XII}) + 12(\underbrace{o_0^2 o_1 o_2}_{XIII} + \underbrace{o_0 o_1^2 o_2}_{XIV} + \underbrace{o_0 o_1 o_2^2}_{XV})
\end{aligned} \tag{2.104}$$

The summands in the integral can be integrated individually.

***I*:** o_0^4

$$\int_{-\infty}^{\infty} g_\mu^4 f_X(x)\,dx = g_\mu^4 \underbrace{\int_{-\infty}^{\infty} f_X(x)\,dx}_{1} = g_\mu^4 \tag{2.105}$$

***II*:** o_1^4

$$\int_{-\infty}^{\infty} \left[\sum_{j=1}^{d} g_{,j}\left(x_j - \mu_{X_j}\right)\right]^4 f_X(x)\,dx \tag{2.106a}$$

Applying again the multinomial theorem and using summation notation:

$$\left[\sum_{j=1}^{d} g_{,j}\left(x_j - \mu_{X_j}\right)\right]^4 = \sum_{j=1}^{d}\sum_{k=1}^{d}\sum_{l=1}^{d}\sum_{m=1}^{d} g_{,j}g_{,k}g_{,l}g_{,m}\left(x_j - \mu_{X_j}\right)\left(x_k - \mu_{X_k}\right)\left(x_l - \mu_{X_l}\right)\left(x_m - \mu_{X_m}\right) \tag{2.106b}$$

$$\int_{-\infty}^{\infty} \sum_{j=1}^{d}\sum_{k=1}^{d}\sum_{l=1}^{d}\sum_{m=1}^{d} g_{,j}g_{,k}g_{,l}g_{,m}\left(x_j - \mu_{X_j}\right)\left(x_k - \mu_{X_k}\right)\left(x_l - \mu_{X_l}\right)\left(x_m - \mu_{X_m}\right) f_X(x)\,dx$$
$$= \sum_{j=1}^{d}\sum_{k=1}^{d}\sum_{l=1}^{d}\sum_{m=1}^{d} g_{,j}g_{,k}g_{,l}g_{,m} \underbrace{\int_{-\infty}^{\infty} \left(x_j - \mu_{X_j}\right)\left(x_k - \mu_{X_k}\right)\left(x_l - \mu_{X_l}\right)\left(x_m - \mu_{X_m}\right) f_X(x)\,dx}_{\mu_{jklm}} \tag{2.106c}$$

***III*:** o_2^4

$$\int_{-\infty}^{\infty} \left[\frac{1}{2}\sum_{j=1}^{d}\sum_{k=1}^{d} g_{,jk}\left(x_j - \mu_{X_j}\right)\left(x_k - \mu_{X_k}\right)\right]^4 f_X(x)\,dx \tag{2.107a}$$

Applying the multinomial theorem and using summation notation:

$$\left[\frac{1}{2}\sum_{j=1}^{d}\sum_{k=1}^{d} g_{,jk}\left(x_j - \mu_{X_j}\right)\left(x_k - \mu_{X_k}\right)\right]^4 = \frac{1}{16}\sum_{j=1}^{d}\sum_{k=1}^{d}\sum_{l=1}^{d}\sum_{m=1}^{d}\sum_{r=1}^{d}\sum_{s=1}^{d}\sum_{t=1}^{d}\sum_{u=1}^{d} g_{,jk}g_{,lm}g_{,rs}g_{,tu}$$
$$\cdot\left(x_j - \mu_{X_j}\right)\left(x_k - \mu_{X_k}\right)\left(x_l - \mu_{X_l}\right)\left(x_m - \mu_{X_m}\right)\left(x_r - \mu_{X_r}\right)\left(x_s - \mu_{X_s}\right)\left(x_t - \mu_{X_t}\right)\left(x_u - \mu_{X_u}\right) \tag{2.107b}$$

$$\int_{-\infty}^{\infty} \frac{1}{16} \sum_{j=1}^{d}\sum_{k=1}^{d}\sum_{l=1}^{d}\sum_{m=1}^{d}\sum_{r=1}^{d}\sum_{s=1}^{d}\sum_{t=1}^{d}\sum_{u=1}^{d} g_{,jk}g_{,lm}g_{,rs}g_{,tu}\left(x_j-\mu_{X_j}\right)\cdots\left(x_u-\mu_{X_u}\right) f_X(x)\,dx$$

$$= \frac{1}{16} \sum_{j=1}^{d}\sum_{k=1}^{d}\sum_{l=1}^{d}\sum_{m=1}^{d}\sum_{r=1}^{d}\sum_{s=1}^{d}\sum_{t=1}^{d}\sum_{u=1}^{d} g_{,jk}g_{,lm}g_{,rs}g_{,tu} \underbrace{\int_{-\infty}^{\infty} \left(x_j-\mu_{X_j}\right)\cdots\left(x_u-\mu_{X_u}\right) f_X(x)\,dx}_{\mu_{jklmrstu}} \tag{2.107c}$$

***IV*:** $4o_0^3o_1$

$$\int_{-\infty}^{\infty} 4g_\mu^3 \sum_{j=1}^{d} g_{,j}\left(x_j-\mu_{X_j}\right) f_X(x)\,dx = 4g_\mu^3 \sum_{j=1}^{d} g_{,j} \underbrace{\int_{-\infty}^{\infty} \left(x_j-\mu_{X_j}\right) f_X(x)\,dx}_{0} = 0 \tag{2.108}$$

***V*:** $4o_0^3o_2$

$$\begin{aligned} &\int_{-\infty}^{\infty} 4g_\mu^3 \frac{1}{2} \sum_{j=1}^{d}\sum_{k=1}^{d} g_{,jk}\left(x_j-\mu_{X_j}\right)\left(x_k-\mu_{X_k}\right) f_X(x)\,dx \\ &\quad = 4g_\mu^3 \frac{1}{2} \sum_{j=1}^{d}\sum_{k=1}^{d} g_{,jk} \underbrace{\int_{-\infty}^{\infty} \left(x_j-\mu_{X_j}\right)\left(x_k-\mu_{X_k}\right) f_X\left(x\right)dx}_{\mu_{jk}} \end{aligned} \tag{2.109}$$

***VI*:** $4o_0o_1^3$

$$\begin{aligned} &\int_{-\infty}^{\infty} 4g_\mu \left[\sum_{j=1}^{d} g_{,j}\left(x_j-\mu_{X_j}\right)\right]^3 f_X(x)\,dx \\ &\quad = 4g_\mu \sum_{j=1}^{d}\sum_{k=1}^{d}\sum_{l=1}^{d} g_{,j}g_{,k}g_{,l} \underbrace{\int_{-\infty}^{\infty} \left(x_j-\mu_{X_j}\right)\left(x_k-\mu_{X_k}\right)\left(x_l-\mu_{X_l}\right) f_X(x)\,dx}_{\mu_{jkl}} \end{aligned} \tag{2.110}$$

***VII*:** $4o_1^3 o_2$

$$\begin{aligned}
&\int_{-\infty}^{\infty} 4\left[\sum_{j=1}^{d} g_{,j}\left(x_j-\mu_{X_j}\right)\right]^3\left[\frac{1}{2}\sum_{j=1}^{d}\sum_{k=1}^{d} g_{,jk}\left(x_j-\mu_{X_j}\right)\left(x_k-\mu_{X_k}\right)\right] f_X(x)\,dx \\
&= \int_{-\infty}^{\infty} 4\left[\sum_{j=1}^{d}\sum_{k=1}^{d}\sum_{l=1}^{d} g_{,j}g_{,k}g_{,l}\left(x_j-\mu_{X_j}\right)\left(x_k-\mu_{X_k}\right)\left(x_l-\mu_{X_l}\right)\right] \\
&\quad\cdot\left[\frac{1}{2}\sum_{j=1}^{d}\sum_{k=1}^{d} g_{,jk}\left(x_j-\mu_{X_j}\right)\left(x_k-\mu_{X_k}\right)\right] f_X(x)\,dx \\
&= 4\frac{1}{2}\sum_{j=1}^{d}\sum_{k=1}^{d}\sum_{l=1}^{d}\sum_{m=1}^{d}\sum_{r=1}^{d} g_{,j}g_{,k}g_{,l}g_{,mr}\underbrace{\int_{-\infty}^{\infty}\left(x_j-\mu_{X_j}\right)\cdots\left(x_r-\mu_{X_r}\right) f_X(x)\,dx}_{\mu_{jklmr}}
\end{aligned} \tag{2.111}$$

***VIII*:** $4o_0 o_2^3$

$$\begin{aligned}
&\int_{-\infty}^{\infty} 4g_\mu\left[\frac{1}{2}\sum_{j=1}^{d}\sum_{k=1}^{d} g_{,jk}\left(x_j-\mu_{X_j}\right)\left(x_k-\mu_{X_k}\right)\right]^3 f_X(x)\,dx \\
&= \int_{-\infty}^{\infty} 4g_\mu\frac{1}{8}\sum_{j=1}^{d}\sum_{k=1}^{d}\sum_{l=1}^{d}\sum_{m=1}^{d}\sum_{r=1}^{d}\sum_{s=1}^{d} g_{,jk}g_{,lm}g_{,rs}\left(x_j-\mu_{X_j}\right)\cdots\left(x_s-\mu_{X_s}\right) f_X(x)\,dx \\
&= 4g_\mu\frac{1}{8}\sum_{j=1}^{d}\sum_{k=1}^{d}\sum_{l=1}^{d}\sum_{m=1}^{d}\sum_{r=1}^{d}\sum_{s=1}^{d} g_{,jk}g_{,lm}g_{,rs}\underbrace{\int_{-\infty}^{\infty}\left(x_j-\mu_{X_j}\right)\cdots\left(x_s-\mu_{X_s}\right) f_X(x)\,dx}_{\mu_{jklmrs}}
\end{aligned} \tag{2.112}$$

$\boldsymbol{IX}$: $4o_1o_2^3$

$$\begin{aligned}
&\int_{-\infty}^{\infty} 4\left[\sum_{j=1}^{d} g_{,j}\left(x_j-\mu_{X_j}\right)\right]\left[\frac{1}{2}\sum_{j=1}^{d}\sum_{k=1}^{d} g_{,jk}\left(x_j-\mu_{X_j}\right)\left(x_k-\mu_{X_k}\right)\right]^3 f_X(x)\,dx \\
&\quad=\int_{-\infty}^{\infty} 4\left[\sum_{j=1}^{d} g_{,j}\left(x_j-\mu_{X_j}\right)\right]\left[\frac{1}{8}\sum_{j=1}^{d}\sum_{k=1}^{d}\sum_{l=1}^{d}\sum_{m=1}^{d}\sum_{r=1}^{d}\sum_{s=1}^{d} g_{,jk}g_{,lm}g_{,rs}\right. \\
&\qquad\left.\cdot\left(x_j-\mu_{X_j}\right)\left(x_k-\mu_{X_k}\right)\left(x_l-\mu_{X_l}\right)\left(x_m-\mu_{X_m}\right)\left(x_r-\mu_{X_r}\right)\left(x_s-\mu_{X_s}\right)\right] f_X(x)\,dx \\
&\quad=4\frac{1}{8}\sum_{j=1}^{d}\sum_{k=1}^{d}\sum_{l=1}^{d}\sum_{m=1}^{d}\sum_{r=1}^{d}\sum_{s=1}^{d}\sum_{t=1}^{d} g_{,j}g_{,kl}g_{,mr}g_{,st}\underbrace{\int_{-\infty}^{\infty}\left(x_j-\mu_{X_j}\right)\cdots\left(x_t-\mu_{X_t}\right)f_X(x)\,dx}_{\mu_{jklmrst}}
\end{aligned} \tag{2.113}$$

$\boldsymbol{X}$: $6o_0^2o_1^2$

$$\int_{-\infty}^{\infty} 6g_\mu^2\left[\sum_{j=1}^{d} g_{,j}\left(x_j-\mu_{X_j}\right)\right]^2 f_X(x)\,dx = 6g_\mu^2\sum_{j=1}^{d}\sum_{k=1}^{d} g_{,j}g_{,k}\underbrace{\int_{-\infty}^{\infty}\left(x_j-\mu_{X_j}\right)\left(x_k-\mu_{X_k}\right)f_X\left(x\right)dx}_{\mu_{jk}} \tag{2.114}$$

$\boldsymbol{XI}$: $6o_0^2o_2^2$

$$\begin{aligned}
&\int_{-\infty}^{\infty} 6g_\mu^2\left[\frac{1}{2}\sum_{j=1}^{d}\sum_{k=1}^{d} g_{,jk}\left(x_j-\mu_{X_j}\right)\left(x_k-\mu_{X_k}\right)\right]^2 f_X(x)\,dx \\
&=\int_{-\infty}^{\infty} 6g_\mu^2\frac{1}{4}\sum_{j=1}^{d}\sum_{k=1}^{d}\sum_{l=1}^{d}\sum_{m=1}^{d} g_{,jk}g_{,lm}\left(x_j-\mu_{X_j}\right)\left(x_k-\mu_{X_k}\right)\left(x_l-\mu_{X_l}\right)\left(x_m-\mu_{X_m}\right)f_X(x)\,dx \\
&=6g_\mu^2\frac{1}{4}\sum_{j=1}^{d}\sum_{k=1}^{d}\sum_{l=1}^{d}\sum_{m=1}^{d} g_{,jk}g_{,lm}\underbrace{\int_{-\infty}^{\infty}\left(x_j-\mu_{X_j}\right)\left(x_k-\mu_{X_k}\right)\left(x_l-\mu_{X_l}\right)\left(x_m-\mu_{X_m}\right)f_X(x)\,dx}_{\mu_{jklm}}
\end{aligned} \tag{2.115}$$

***XII*:** $6o_1^2o_2^2$

$$\begin{aligned}
&\int_{-\infty}^{\infty} 6\left[\sum_{j=1}^{d} g_{,j}\left(x_j-\mu_{X_j}\right)\right]^2\left[\frac{1}{2}\sum_{j=1}^{d}\sum_{k=1}^{d} g_{,jk}\left(x_j-\mu_{X_j}\right)\left(x_k-\mu_{X_k}\right)\right]^2 f_X(x)\,dx \\
&= \int_{-\infty}^{\infty} 6\left[\sum_{j=1}^{d}\sum_{k=1}^{d} g_{,j}g_{,k}\int_{-\infty}^{\infty}\left(x_j-\mu_{X_j}\right)\left(x_k-\mu_{X_k}\right)f_X\left(x\right)dx\right] \\
&\quad\cdot\left[\frac{1}{4}\sum_{j=1}^{d}\sum_{k=1}^{d}\sum_{l=1}^{d}\sum_{m=1}^{d} g_{,jk}g_{,lm}\left(x_j-\mu_{X_j}\right)\left(x_k-\mu_{X_k}\right)\left(x_l-\mu_{X_l}\right)\left(x_m-\mu_{X_m}\right)\right] f_X(x)\,dx \\
&= 6\frac{1}{4}\sum_{j=1}^{d}\sum_{k=1}^{d}\sum_{l=1}^{d}\sum_{m=1}^{d}\sum_{r=1}^{d}\sum_{s=1}^{d} g_{,j}g_{,k}g_{,lm}g_{,rs}\underbrace{\int_{-\infty}^{\infty}\left(x_j-\mu_{X_j}\right)\cdots\left(x_s-\mu_{X_s}\right)f_X(x)\,dx}_{\mu_{jklmrs}}
\end{aligned} \tag{2.116}$$

***XIII*:** $12o_0^2o_1o_2$

$$\begin{aligned}
&\int_{-\infty}^{\infty} 12g_\mu^2\left[\sum_{j=1}^{d} g_{,j}\left(x_j-\mu_{X_j}\right)\right]\left[\frac{1}{2}\sum_{j=1}^{d}\sum_{k=1}^{d} g_{,jk}\left(x_j-\mu_{X_j}\right)\left(x_k-\mu_{X_k}\right)\right] f_X(x)\,dx \\
&= \\
&= 12g_\mu^2\frac{1}{2}\sum_{j=1}^{d}\sum_{k=1}^{d}\sum_{l=1}^{d} g_{,j}g_{,kl}\underbrace{\int_{-\infty}^{\infty}\left(x_j-\mu_{X_j}\right)\left(x_k-\mu_{X_k}\right)\left(x_l-\mu_{X_l}\right)f_X(x)\,dx}_{\mu_{jkl}}
\end{aligned} \tag{2.117}$$

***XIV*:** $12o_0o_1^2o_2$

$$\begin{aligned}
&\int_{-\infty}^{\infty} 12g_\mu \left[\sum_{j=1}^{d} g_{,j}\left(x_j-\mu_{X_j}\right)\right]^2 \left[\frac{1}{2}\sum_{j=1}^{d}\sum_{k=1}^{d} g_{,jk}\left(x_j-\mu_{X_j}\right)\left(x_k-\mu_{X_k}\right)\right] f_X(x)\,dx \\
&= \int_{-\infty}^{\infty} 12g_\mu \left[\sum_{j=1}^{d}\sum_{k=1}^{d} g_{,j}g_{,k}\left(x_j-\mu_{X_j}\right)\left(x_k-\mu_{X_k}\right)\right] \\
&\quad \cdot \left[\frac{1}{2}\sum_{j=1}^{d}\sum_{k=1}^{d} g_{,jk}\left(x_j-\mu_{X_j}\right)\left(x_k-\mu_{X_k}\right)\right] f_X(x)\,dx \\
&= 12g_\mu \frac{1}{2}\sum_{j=1}^{d}\sum_{k=1}^{d}\sum_{l=1}^{d}\sum_{m=1}^{d} g_{,j}g_{,k}g_{,lm} \underbrace{\int_{-\infty}^{\infty}\left(x_j-\mu_{X_j}\right)\left(x_k-\mu_{X_k}\right)\left(x_l-\mu_{X_l}\right)\left(x_m-\mu_{X_m}\right) f_X(x)\,dx}_{\mu_{jklm}}
\end{aligned} \tag{2.118}$$

***XV*:** $12o_0o_1o_2^2$

$$\begin{aligned}
&\int_{-\infty}^{\infty} 12g_\mu \left[\sum_{j=1}^{d} g_{,j}\left(x_j-\mu_{X_j}\right)\right] \left[\frac{1}{2}\sum_{j=1}^{d}\sum_{k=1}^{d} g_{,jk}\left(x_j-\mu_{X_j}\right)\left(x_k-\mu_{X_k}\right)\right]^2 f_X(x)\,dx \\
&= \int_{-\infty}^{\infty} 12g_\mu \left[\sum_{j=1}^{d} g_{,j}\left(x_j-\mu_{X_j}\right)\right]\left[\frac{1}{4}\sum_{j=1}^{d}\sum_{k=1}^{d}\sum_{l=1}^{d}\sum_{m=1}^{d} g_{,jk}g_{,lm}\left(x_j-\mu_{X_j}\right)\cdots\left(x_m-\mu_{X_m}\right)\right] f_X(x)\,dx \\
&= 12g_\mu \frac{1}{4}\sum_{j=1}^{d}\sum_{k=1}^{d}\sum_{l=1}^{d}\sum_{m=1}^{d}\sum_{r=1}^{d} g_{,j}g_{,kl}g_{,mr} \underbrace{\int_{-\infty}^{\infty}\left(x_j-\mu_{X_j}\right)\cdots\left(x_r-\mu_{X_r}\right) f_X(x)\,dx}_{\mu_{jklmr}}
\end{aligned} \tag{2.119}$$

The complete final formula derived in this section for the second-order approximation for the fourth central moment is enclosed in the following page.

The derivation of the fourth central moment second-order approximation assuming independence between the input r.v.s can be found in Appendix A.

Summarizing, the second-order approximation for the fourth central moment of an arbitrary general function is:

$$
\begin{aligned}
\mu_4(Y,Y,Y,Y) = \mu_{Y,4} \\
&\approx \underbrace{g_\mu^4}_{I} + \underbrace{\sum_{j=1}^{d}\sum_{k=1}^{d}\sum_{l=1}^{d}\sum_{m=1}^{d} g_{,j}g_{,k}g_{,l}g_{,m}\mu_{jklm}}_{II} \\
&\quad + \underbrace{\frac{1}{16}\sum_{j=1}^{d}\sum_{k=1}^{d}\sum_{l=1}^{d}\sum_{m=1}^{d}\sum_{r=1}^{d}\sum_{s=1}^{d}\sum_{t=1}^{d}\sum_{u=1}^{d} g_{,jk}g_{,lm}g_{,rs}g_{,tu}\mu_{jklmrstu}}_{III} \\
&\quad + \underbrace{0}_{IV} + \underbrace{4g_\mu^3\frac{1}{2}\sum_{j=1}^{d}\sum_{k=1}^{d} g_{,jk}\mu_{jk}}_{V} + \underbrace{4g_\mu\sum_{j=1}^{d}\sum_{k=1}^{d}\sum_{l=1}^{d} g_{,j}g_{,k}g_{,l}\mu_{jkl}}_{VI} \\
&\quad + \underbrace{4\frac{1}{2}\sum_{j=1}^{d}\sum_{k=1}^{d}\sum_{l=1}^{d}\sum_{m=1}^{d}\sum_{r=1}^{d} g_{,j}g_{,k}g_{,l}g_{,mr}\mu_{jklmr}}_{VII} \\
&\quad + \underbrace{4g_\mu\frac{1}{8}\sum_{j=1}^{d}\sum_{k=1}^{d}\sum_{l=1}^{d}\sum_{m=1}^{d}\sum_{r=1}^{d}\sum_{s=1}^{d} g_{,jk}g_{,lm}g_{,rs}\mu_{jklmrs}}_{VIII} \\
&\quad + \underbrace{4\frac{1}{8}\sum_{j=1}^{d}\sum_{k=1}^{d}\sum_{l=1}^{d}\sum_{m=1}^{d}\sum_{r=1}^{d}\sum_{s=1}^{d}\sum_{t=1}^{d} g_{,j}g_{,kl}g_{,mr}g_{,st}\mu_{jklmrst}}_{IX} \\
&\quad + \underbrace{6g_\mu^2\sum_{j=1}^{d}\sum_{k=1}^{d} g_{,j}g_{,k}\mu_{jk}}_{X} + \underbrace{6g_\mu^2\frac{1}{4}\sum_{j=1}^{d}\sum_{k=1}^{d}\sum_{l=1}^{d}\sum_{m=1}^{d} g_{,jk}g_{,lm}\mu_{jklm}}_{XI} \\
&\quad + \underbrace{6\frac{1}{4}\sum_{j=1}^{d}\sum_{k=1}^{d}\sum_{l=1}^{d}\sum_{m=1}^{d}\sum_{r=1}^{d}\sum_{s=1}^{d} g_{,j}g_{,k}g_{,lm}g_{,rs}\mu_{jklmrs}}_{XII} \\
&\quad + \underbrace{12g_\mu^2\frac{1}{2}\sum_{j=1}^{d}\sum_{k=1}^{d}\sum_{l=1}^{d} g_{,j}g_{,kl}\mu_{jkl}}_{XIII} + \underbrace{12g_\mu\frac{1}{2}\sum_{j=1}^{d}\sum_{k=1}^{d}\sum_{l=1}^{d}\sum_{m=1}^{d} g_{,j}g_{,k}g_{,lm}\mu_{jklm}}_{XIV} \\
&\quad + \underbrace{12g_\mu\frac{1}{4}\sum_{j=1}^{d}\sum_{k=1}^{d}\sum_{l=1}^{d}\sum_{m=1}^{d}\sum_{r=1}^{d} g_{,j}g_{,kl}g_{,mr}\mu_{jklmr}}_{XV} - 4\mu_Y\mu_{Y,3} - 6\mu_Y^2\sigma_Y^2 - \mu_Y^4
\end{aligned}
\tag{2.120}
$$

2.5.8 Fourth central moment *kurtosis* first-order

From the second-order approximation for the fourth central moment Eq. (2.120), the first-order approximation can be derived omitting the non-linear terms of the second-order Taylor approximation thus the first-order Taylor approximation is left. Using the o_0, o_1 and o_2 notation presented in Eq. (2.59), and skipping the terms containing o_2, the first-order approximation for the fourth central moment leads to:

$$\begin{aligned}(o_0+o_1+\cancel{o_2})^4 = {} & \underbrace{o_0^4}_{I} + \underbrace{o_1^4}_{II} + \underbrace{\cancel{o_2^4}}_{III} + 4(\underbrace{o_0^3 o_1}_{IV} + \underbrace{\cancel{o_0^3 o_2}}_{V} + \underbrace{o_0 o_1^3}_{VI} + \underbrace{\cancel{o_1^3 o_2}}_{VII} + \underbrace{\cancel{o_0 o_2^3}}_{VIII} + \underbrace{\cancel{o_1 o_2^3}}_{IX}) \\ & + 6(\underbrace{o_0^2 o_1^2}_{X} + \underbrace{\cancel{o_0^2 o_2^2}}_{XI} + \underbrace{\cancel{o_1^2 o_2^2}}_{XII}) + 12(\underbrace{\cancel{o_0^2 o_1 o_2}}_{XIII} + \underbrace{\cancel{o_0 o_1^2 o_2}}_{XIV} + \underbrace{\cancel{o_0 o_1 o_2^2}}_{XV}) \\ (o_0+o_1)^4 = {} & \underbrace{o_0^4}_{I} + \underbrace{o_1^4}_{II} + 4(\underbrace{o_0^3 o_1}_{IV} + \underbrace{o_0 o_1^3}_{VI}) + 6(\underbrace{o_0^2 o_1^2}_{X})\end{aligned} \tag{2.121}$$

Then the Eq. (2.120) becomes:

$$\begin{aligned}\mu_4(Y,Y,Y,Y) = {} & \mu_{Y,4} \\ \approx {} & \underbrace{g_\mu^4}_{I} + \underbrace{\sum_{j=1}^{d}\sum_{k=1}^{d}\sum_{l=1}^{d}\sum_{m=1}^{d} g_{,j}g_{,k}g_{,l}g_{,m}\mu_{jklm}}_{II} + \underbrace{0}_{IV} + \underbrace{4g_\mu \sum_{j=1}^{d}\sum_{k=1}^{d}\sum_{l=1}^{d} g_{,j}g_{,k}g_{,l}\mu_{jkl}}_{VI} \\ & + \underbrace{6g_\mu^2 \sum_{j=1}^{d}\sum_{k=1}^{d} g_{,j}g_{,k}\mu_{jk}}_{X} - 4\mu_Y\mu_{Y,3} - 6\mu_Y^2\sigma_Y^2 - \mu_Y^4\end{aligned} \tag{2.122}$$

And knowing that the first-order expected value approximation is $\mathrm{E}[Y] = \mu_Y \approx g_\mu$ from Eq. (2.64), the first-order variance approximation is $\mathrm{Var}(Y) = \sigma_Y^2 \approx \sum_{j=1}^{d}\sum_{k=1}^{d} g_{,j}g_{,k}\mu_{jk}$ from Eq. (2.80), and the first-order approximation for the third central moment is $\mu_3(Y,Y,Y) = \mu_{Y,3} \approx \sum_{j=1}^{d}\sum_{k=1}^{d}\sum_{l=1}^{d} g_{,j}g_{,k}g_{,l}\mu_{jkl}$ from Eq. (2.99), the fourth central moment approximation of first-order is:

$$\mu_4(Y,Y,Y,Y) = \mu_{Y,4} \approx \underbrace{\sum_{j=1}^{d}\sum_{k=1}^{d}\sum_{l=1}^{d}\sum_{m=1}^{d} g_{,j}g_{,k}g_{,l}g_{,m}\mu_{jklm}}_{II} \tag{2.123}$$

3

Probabilistic fatigue crack growth (FCG) methodology in the damage tolerance assessment (DTA) of railway axles

3.1 Introduction

Currently, the design and operation of railway axles is based on a two-stage safety concept comprising *safe life* and *damage tolerance* approaches. These safety levels are illustrated in Fig. 3.1. It also includes an additional stage *in-service damage indication systems* with further options that offer potential for establishing a third stage safety concept. For completeness, the Fig. 3.1 also indicates the maturity of the technologies in the three stages, by using a three-level scale as follows: (*) state of the art, (**) present and future development, and (***) original contribution within this thesis. The figure is adapted from an extended review on safe life and damage tolerance aspects of railway axles in [22], therefore the reader is referred to this paper for full details. It is important to note that the developments in this thesis aim at enriching the secondary safety level DTA, by improving the periodic inspection definition currently based on operating experience or based on a limited use of deterministic approaches through the use of a more comprehensive probabilistic approach that provides a higher level of safety assurance. In consequence, they constitute an extension of the nowadays and under development practices by proposing the use of probabilistic fracture mechanics together with non-destructive testing methods.

Primary safety level: "Safe Life"	
*	Design for fatigue strength (EN 13103)
**	Design for fatigue strength (damage accumulation)
**	Design for finite life (one million miles axle)
Secondary safety level: "Damage Tolerance"	
*	Periodic inspection based on operating experience
**	Periodic inspection based on fracture mechanics & NDI (POD)
***	Periodic inspection based on Probabilistic fracture mechanics & NDI (POD)
Tertiary safety level: In-service damage indication systems	
**	Based on vibration characteristics, laser pulse ultrasonic, etc.

*	**State of the art**
**	**Present and future development**
***	**Original contribution within this thesis**

Figure 3.1. Components of a safety assessment system for railway axles.

A summary on existing and potential innovative safe life and damage tolerance methods for the design and operation of railway axles is given above. In the following, a number of selected issues are investigated, promising potential for the further increase of the safety of railway axles. This chapter is devoted to presenting the different parts and principles of the probabilistic fatigue methodology developed for the damage tolerance assessment of railway axles. The devised methodology intends to plan periodic inspections based on probabilistic fracture mechanics and non-destructive methods. The need to optimize inspection intervals of railway axles involves, among other aspects, a reliable estimation of fatigue crack growth life in the axles. With this in mind, the core of the developments in the present thesis revolves around the redefinition of the fatigue crack growth process from a deterministic to a probabilistic point of view. The ultimate target is to provide a method for reliability design and inspection optimization in the operation of railway axles.

An overview of the damage tolerance analysis (DTA) of railway axles is presented in Fig. 3.2. It remarks the original contributions that are result of the present thesis. In the DTA of railway axles there are three main steps that are organized in the blocs: (i) input parameters; (ii) fatigue crack growth analysis: Deterministic / Probabilistic; and (iii) results evaluation. Firstly, in block (i), the input parameters row is at the same time divided in three columns regarding geometry, loading conditions and

material properties. The three of them include uncertainties if a probabilistic approach is desired, otherwise they are simply deterministic parameters. Secondly, in block (ii), the fatigue crack growth analysis has two twin paths, the deterministic and the probabilistic one. The first one, follows the deterministic approach as indicated with arrows in black. It covers the deterministic fatigue crack growth (FCG) NASGRO model that uses the weight functions for efficient stress intensity factors evaluation and the subsequent deterministic fatigue life estimation. The second one, in blue, follows the probabilistic FCG methodology in the damage tolerance assessment of railway axles developed within this thesis. It includes the full second-order approach (FSOA) for the approximation of the first to four stochastic moments of the fatigue life N, being its accuracy correlated with Monte Carlo (MC) results during developing stages. Then, it uses these four moments to fit a probability distribution using the versatile Pearson family. Subsequently, the probability distribution is evaluated for certain reliability in order to obtain a conservative reliability-based estimation of the fatigue life. In the end, a probabilistic fatigue life estimation is available. Finally, in block (iii), the evaluation of results includes the definition of the inspection intervals based on the previous deterministic or probabilistic fatigue life calculation. It encompasses the forward, the backward and the last chance detection schemes. Then the inspection intervals are further evaluated attending to the performance of the non-destructive testing (NDT) techniques such as the magnetic testing or the ultrasonic testing in the near-endor far-end configuration. Ultimately, the probability of failure or its complementary probability of crack detection is calculated according to the combination of inspection alternative and NDT method selected in the two previous steps. Note that the NDT has a probabilistic background and this is why when following the probabilistic path in blue, the result of the probability of failure can be though in essence as doubly probabilistic.

This chapter is organized as follows. Firstly, an overview of the deterministic NASGRO model is provided. In addition, the probabilistic expressions regarding its integration with the full second-order approach are derived. Additionally, an outline of the weight functions method for efficient stress intensity factors calculation is included. Secondly, a summary of the Pearson distribution family and the estimation of the distribution parameters from prescribed moments is given. In the third place, the use of probabilistic fatigue life estimation in defining inspection intervals for railway axles is developed. The steps of damage tolerance analysis are briefly reviewed and the results of the probabilistic fatigue crack growth life are adapted for the final definition of the reliability-based inspection intervals. Finally, the performance of the non-destructive inspection techniques and the different alternatives for evaluating the probability of detection of cracks in railway axles are described in detail.

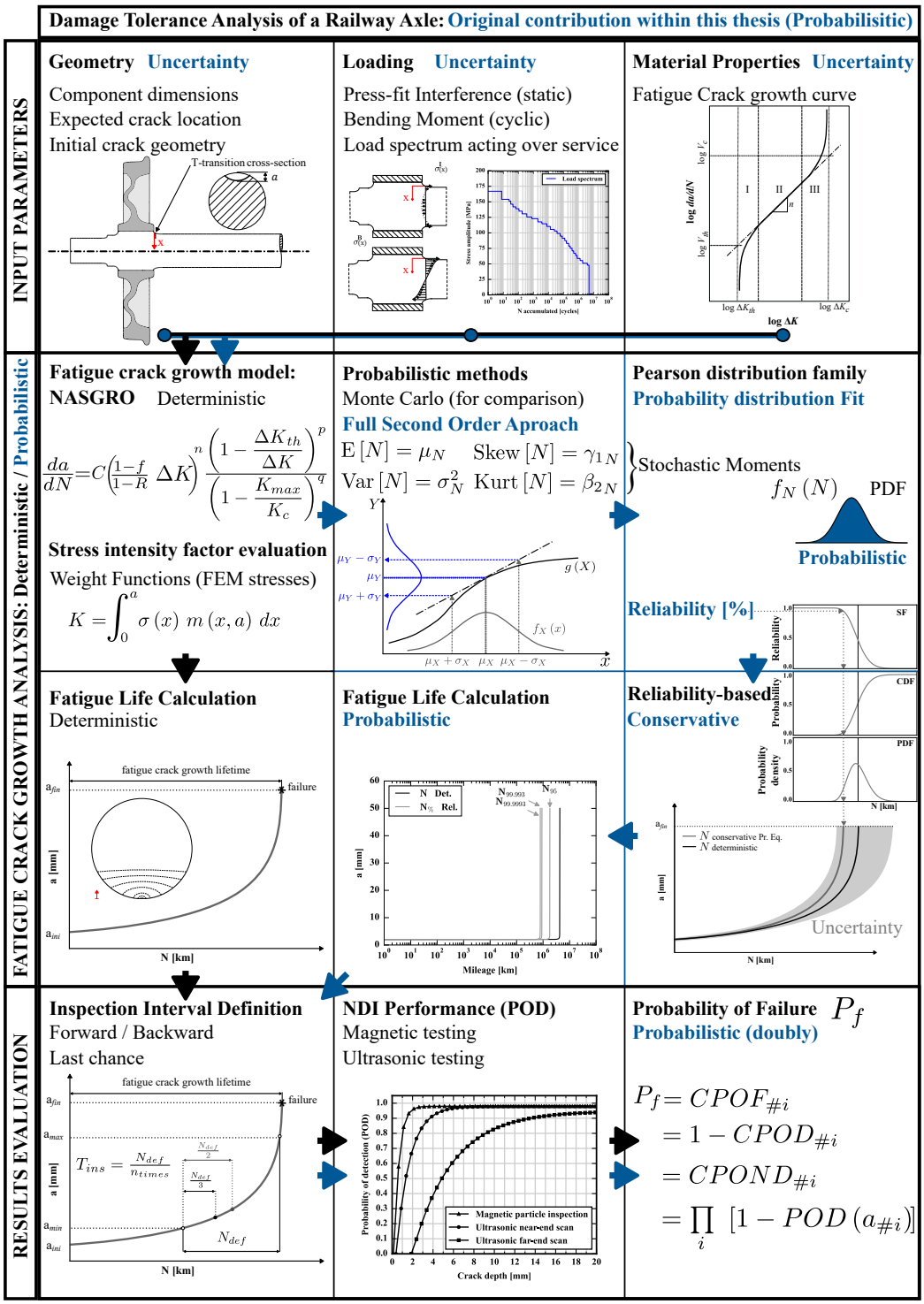

Figure 3.2. Overview of the damage tolerance assessment of railway axles.

3.2 Fatigue crack growth model

It is well-known that the choice of the fatigue crack growth model plays a crucial role in life prediction. Among the various models that are available in the literature, summarized in Subsection 1.2.5, for the present purpose, the NASGRO crack growth model is presented from two viewpoints: the deterministic and the probabilistic one.

3.2.1 Deterministic NASGRO equation

NASGRO expressions are enclosed in Eqs. (3.1) to (3.9).

$$\frac{da}{dN} = C(\Delta K_{eff})^n \frac{\left(1 - \frac{\Delta K_{th}}{\Delta K}\right)^p}{\left(1 - \frac{K_{max}}{K_c}\right)^q} \tag{3.1}$$

$$\Delta K_{eff} = \frac{1-f}{1-R}(\Delta K) \tag{3.2}$$

$$\Delta K_{th} = \Delta K_{th0} \frac{\sqrt{\frac{a}{a+a_0}}}{\left(\frac{1-f}{(1-A_0)(1-R)}\right)^{1+C_{th}R}} \tag{3.3}$$

$$C_{th} = \begin{cases} C_{th}^p & if\ R \geq 0 \\ C_{th}^m & if\ R < 0 \end{cases} \tag{3.4}$$

$$f = \begin{cases} max\left(R, A_0 + A_1 R + A_2 R^2 + A_3 R^3\right) & if\ R > 0 \\ A_0 + A_1 R & if\ R \leq 0 \end{cases} \tag{3.5}$$

$$A_0 = \left(0.825 - 0.34\alpha + 0.05\alpha^2\right)\left[\cos\left(\frac{\pi}{2}\frac{S_{max}}{\sigma_0}\right)\right]^{\frac{1}{\alpha}} \tag{3.6}$$

$$A_1 = (0.415 - 0.071\alpha)\frac{S_{max}}{\sigma_0} \tag{3.7}$$

$$A_2 = 1 - A_0 - A_1 - A_3 \tag{3.8}$$

$$A_3 = 2A_0 + A_1 - 1 \tag{3.9}$$

where da/dN is the crack propagation rate, N is the number of applied cycles, a is the crack depth, R is the stress ratio, ΔK is the stress intensity factor (SIF) range from the maximum and minimum K, i.e. K_{max} and K_{min}, f is the crack opening function, ΔK_{th} is the threshold stress intensity factor range, K_c is the critical stress intensity factor, ΔK_{eff} is the effective stress intensity factor range, and C, n, p, and q are material empirically derived constants. The Eq. (3.1) consists of three different terms according to the three different propagation regimes: (i) Region I

at low growth rates, $\left(1-\frac{\Delta K_{th}}{\Delta K}\right)^{p}$, is used to describe the regime close to the fatigue threshold; (ii) Region II at mid-range of growth rates, $C(\Delta K_{eff})^{n}$, represents the linear or so-called Paris regime; and (iii) Region III at high growth rates, $\left(1-\frac{K_{max}}{K_c}\right)^{q}$, describes the regime up to the critical SIF. The term ΔK_{eff} is the effective stress intensity factor range and it is described by the Eq. (3.2) where f describes the plasticity-induced crack closure effect as mentioned, and R is the stress ratio such as above. The crack size and stress ratio dependency of the threshold is expressed as in Eq. (3.3) with ΔK_{th0} being the threshold SIF range at $R=0$, a the crack depth aforementioned and a_0 the El-Haddad parameter. C_{th} is an empirical constant which distinguishes positive, C_{th}^{p}, from negative, C_{th}^{m}, stress ratio R values as defined in Eq. (3.4). A_0 is a parameter used in the crack opening function f in Eq. (3.5) and defined according to Eq. (3.6). The crack opening function f also depends on the A_1, A_2, and A_3 values calculated as expressed in Eqs. (3.7), (3.8), and (3.9). These four parameters are function of the stress state defined by the plane stress/strain constraint factor α, and by the ratio of the maximum applied stress, S_{max} to the flow stress σ_0, typically assumed to be constant. The use of this ratio as a constant has been shown to produce acceptable results for positive stress ratios, where the effect of S_{max}/σ_0 on the crack opening function is relatively small. For most of the materials, a value $S_{max}/\sigma_0 = 0.3$ is adopted, chosen as an average value obtained from fatigue crack growth experiments, adopting different geometries for the specimens. For a more detailed description of the previous equations refer to [64].

For a sufficiently small step increment, the crack propagation rate in Eq. (3.1) can be approximated for the ratio between finite increments Eq. (3.10), enabling the use of an iterative scheme suitable for computing Eq. (3.11), where i is the step increment up to the ns steps number.

$$\frac{da}{dN} \approx \frac{\Delta a}{\Delta N} \tag{3.10}$$

$$\frac{\Delta a^{i}}{\Delta N^{i}} \approx \frac{a^{i+1}-a^{i}}{N^{i+1}-N^{i}} \tag{3.11}$$

3.2.2 Probabilistic NASGRO equations

In stochastic fatigue crack growth analyses, the following probability distributions are achievable: the distribution of the crack size at any given number of load cycles and the distribution of the number of load cycles to reach any given crack size. In damage tolerance analyses of railway axles, the number of load cycles distribution is preferred as it enables the definition of interval inspections verifying crack sizes.

The FSOA for the moments of functions of random variables presented in Chapter 2, enables the prediction of the first raw and the second, third, and fourth central moments of a general function. At this point, to bridge the gap between the FSOA and

the fatigue crack growth life prediction, the probabilistic formulations for propagating the first to fourth moments through the fatigue crack growth NASGRO model are deduced. This section, starts with the introduction of the discretised version of the NASGRO equation focusing on the lifespan of interest. Then, it derives the probabilistic formulations for propagating the first raw, and the second, third and fourth central moments through the fatigue crack growth NASGRO model. And finally, it describes the manner in which the first to fourth moments of the fatigue lifespan of interest N are calculated recalling that the first to fourth moments are related, by definition, to the expected value, first raw moment; the variance, second central moment; the skewness, third central standardized moment; and the kurtosis, fourth central standardized moment, of the random output variable.

To begin with, the NASGRO model is adapted to obtain the distribution of the number of load cycles N to reach a given crack depth a. Introducing Eq. (3.2) into Eq. (3.1), the original NASGRO crack propagation rate da/dN is built, then isolating dN and using the discretised version for every i^{th} crack growth increment gives Eq. (3.12).

$$dN^i = \frac{da^i}{C\left(\frac{1-f^i}{1-R^i}\Delta K^i\right)^n} \frac{\left(1-\frac{K^i_{max}}{K_c}\right)^q}{\left(1-\frac{\Delta K^i_{th}}{\Delta K^i}\right)^p} \tag{3.12}$$

To continue with, the expected value of the fatigue life, $\mathrm{E}[N]$, is obtained by applying the expectation operator to the total number of cycles N which is the summation of the ns life increments dN^i up to a final crack depth a_{fin}. Applying the linearity property of the expectation operator, leads to Eq. (3.13).

$$\mathrm{E}[N] = \mathrm{E}\left[\sum_{i=1}^{ns} dN^i\right] = \sum_{i=1}^{ns} \mathrm{E}\left[dN^i\right] \tag{3.13}$$

The variance of the fatigue life, $\mathrm{Var}(N)$, is obtained by applying the variance definition to N. Using the formula for the variance of the sum of random variables gives Eq. (3.14). To promote understanding, the derivation of the formula for variance of the sum of random variables is given in Appendix B by means of the Eq. (B.1).

$$\mathrm{Var}(N) = \mathrm{Var}\left(\sum_{i=1}^{ns} dN^i\right) = \sum_{i_1=1}^{ns} \mathrm{Var}\left(dN^{i_1}\right) + 2\sum_{i_1=1}^{ns-1}\sum_{i_2=i_1+1}^{ns} \mathrm{Cov}\left(dN^{i_1}, dN^{i_2}\right) \tag{3.14}$$

Similarly, the third central moment of the fatigue life $\mu_3(N,N,N)$ is obtained by applying the third central moment definition to the total number of cycles N. Using the formula for the third central moment of the sum of random variables leads to Eq. (3.15).

$$\begin{aligned}\mu_3(N,N,N) &= \mu_3\left(\sum_{i=1}^{ns} dN^i, \sum_{i=1}^{ns} dN^i, \sum_{i=1}^{ns} dN^i\right) \\ &= \sum_{i_1=1}^{ns} \mu_3\left(dN^{i_1}, dN^{i_1}, dN^{i_1}\right) + 3\sum_{i=i_1}^{ns} \sum_{\substack{i_2=1 \\ i_2\neq i_1}}^{ns} \mu_3\left(dN^{i_1}, dN^{i_1}, dN^{i_2}\right) \\ &\quad + 6\sum_{i_1=1}^{ns-2} \sum_{i_2=i_1+1}^{ns-1} \sum_{i_3=i_2+1}^{ns} \mu_3\left(dN^{i_1}, dN^{i_2}, dN^{i_3}\right)\end{aligned} \tag{3.15}$$

In the same manner as above, the fourth central moment of the fatigue life $\mu_4(N,N,N,N)$ is obtained by using the formula for the fourth central moment of the sum of random variables giving Eq. (3.16).

$$\begin{aligned}\mu_4(N,N,N,N) &= \mu_4\left(\sum_{i=1}^{ns} dN^i, \sum_{i=1}^{ns} dN^i, \sum_{i=1}^{ns} dN^i, \sum_{i=1}^{ns} dN^i\right) \\ &= \sum_{i_1=1}^{ns} \mu_4\left(dN^{i_1}, dN^{i_1}, dN^{i_1}, dN^{i_1}\right) + 4\sum_{i_1=1}^{ns} \sum_{\substack{i_2=1 \\ i_2\neq i_1}}^{ns} \mu_4\left(dN^{i_1}, dN^{i_1}, dN^{i_1}, dN^{i_2}\right) \\ &\quad + 6\sum_{i_1=1}^{ns-1} \sum_{i_2=i_1+1}^{ns} \mu_4\left(dN^{i_1}, dN^{i_1}, dN^{i_2}, dN^{i_2}\right) \\ &\quad + 12\sum_{i_1=1}^{ns} \sum_{\substack{i_2=1 \\ i_2\neq i_1}}^{ns} \sum_{\substack{i_3=1 \\ i_3\neq i_1 \\ i_3\neq i_2}}^{ns} \mu_4\left(dN^{i_1}, dN^{i_1}, dN^{i_2}, dN^{i_3}\right) \\ &\quad + 24\sum_{i_1=1}^{ns-3} \sum_{i_2=i_1+1}^{ns-2} \sum_{i_3=i_2+1}^{ns-1} \sum_{i_4=i_3+1}^{ns} \mu_4\left(dN^{i_1}, dN^{i_2}, dN^{i_3}, dN^{i_4}\right)\end{aligned} \tag{3.16}$$

To conclude, in Eq. (3.13), $\mathrm{E}\left[dN^i\right]$ is obtained by applying the FSOA derived to obtain the stochastic first moment Eq. (2.62), on the dN^i function Eq. (3.12). Similarly, the moments of dN^i in Eq. (3.14), are obtained by applying the FSOA developed to obtain the stochastic second central moment Eq. (2.77). In Eqs. (3.15) and (3.16) the moments μ_3 and μ_4 of dN^i are obtained by applying the FSOA devoted to obtaining the stochastic central moments of third and fourth order Eqs. (2.96) and (2.120) respectively, on the dN^i function Eq. (3.12). Note that, Eqs. (3.13) and (3.14) are referred to as the probabilistic NASGRO equations for the expected value and variance calculation respectively and Eqs. (3.15) and (3.16) are referred to as the probabilistic NASGRO equations for the third and fourth central moments respectively.

In summary, for every i^{th} crack growth increment, the first to fourth moments of the fatigue lifetime increment dN^i, i.e. the first raw, the second central moment, the third and fourth central moments, are calculated by applying the full second-order approach (FSOA) method on the discretised version of the NASGRO equation. It requires the first and second partial derivatives of the NASGRO equation with respect to the random input variables, and the first to eighth order moments of the random input variables. Then, the first to fourth moments of the fatigue lifetime N are obtained by applying the NASGRO probabilistic equations (Pr. Eqs.), namely Eqs. (3.13), (3.14), (3.15), and (3.16), providing a continuous result along the crack depth a. Finally, the expected value of N, its variance, the skewness and the kurtosis are calculated based on the first to fourth predicted moments.

3.2.3 Stress intensity factor evaluation: weight functions

The crack propagation is calculated at two different points, the deepest point named A and the crack surface point named B as depicted in Fig. 3.3.

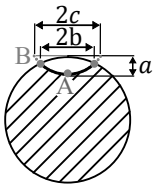

Figure 3.3. Axle cross-section with a postulated crack.

It is important to note that the crack geometry is described by two parameters that represent the two axes of a semiellipse. Therefore, the crack growth rate that also depends on the boundary conditions, is calculated at the two different points, the deepest point A, and the crack surface point B. Accordingly, to determine the crack evolution, the SIFs are evaluated in the two points, which determine the crack shape in the next step of the calculation. The NASGRO Eq. (3.1) is therefore separately applied to the crack deepest point and its surface point, for the latter case replacing a by b.

To use the NASGRO equation efficiently, fast SIFs calculations, which are dependent on the instant crack shape, is therefore fundamental. To do that, the weight functions method is used. The weight function method is based on the principle of superposition as presented in the schematic of Fig. 3.4. The stress intensity factor for a cracked body subjected to external loads shown in Fig. 3.4a can be obtained by calculating the stress intensity factor in a geometrically identical body with the local stress field $\sigma(x)$ applied to the crack faces as it is shown in Fig. 3.4c. The local stress field $\sigma(x)$ induced by the external load in the crack plane is determined by neglecting the presence of the crack as illustrated in Fig. 3.4b.

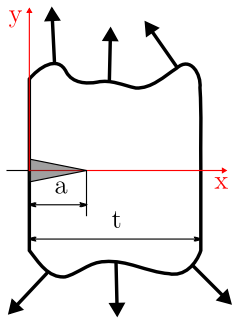

(a) Cracked body with externally applied stress.

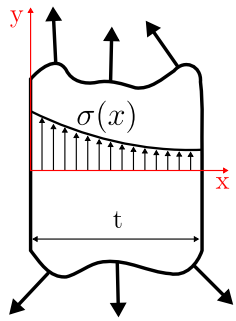

(b) Uncracked geometrically identical body.

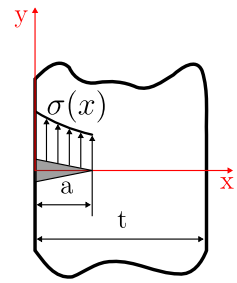

(c) Geometrically identical body with local stress applied to the crack faces.

Figure 3.4. Schematic of the weight function method.

According to the method, for a one-dimensional variation of stresses acting across the crack plane, the relation between the stress intensity factor and the stress distribution is given by the definite integral in the Eq. (3.17), where $\sigma(x)$ is the stress distribution in the uncracked component and $m(x,a)$ are the weight functions, which are dependent on the instant crack shape and on the position along the crack front in which the SIFs are calculated.

$$K = \int_0^a \sigma(x)\; m(x,a)\; dx \tag{3.17}$$

The main advantage of the weight functions method is its universality. It is possible to obtain the weight function for a given cracked body and it can be used afterwards to estimate the SIF induced by any other externally applied load. The weight functions used at the calculation points come from [44].

3.3 Pearson distribution family fit from prescribed moments

Many statistical analyses consider the normal distribution when no more information about the underlying probability distribution is available, however, this assumption does not always reflect the reality. Among the different distributions that can be chosen, the Pearson distribution family is used in the methodology as it is a versatile family that covers a broad range of distribution shapes, and therefore it is able to model a wide range of data accurately. Moreover, it enables the expression of the distribution parameters as a function of the first four moments of the distribution without a priori hypotheses, and thus it is an efficient and objective procedure. This is why this procedure is often referred to as Pearson distribution family fit using the method of moments.

The Pearson distribution is a family of continuous probability distributions [141]. A Pearson probability density function $p(x)$ is defined to be any valid solution to the first order linear differential equation presented in Eq. (3.18), where λ is a location parameter, β_1 is the square of the skewness, β_2 is the kurtosis, and μ_2 is the second central moment of the distribution.

$$\frac{p'(x)}{p(x)} + \frac{(x-\lambda)+a}{b_0 + b_1(x-\lambda) + b_2(x-\lambda)^2} = 0 \quad \text{with:} \tag{3.18}$$

$$b_0 = \frac{4\beta_2 - 3\beta_1}{10\beta_2 - 12\beta_1 - 18}\mu_2, \quad a \equiv b_1 = \sqrt{\mu_2}\sqrt{\beta_1}\frac{\beta_2 + 3}{10\beta_2 - 12\beta_1 - 18}, \quad b_2 = \frac{2\beta_2 - 3\beta_1 - 6}{10\beta_2 - 12\beta_1 - 18}$$

The solution to the above differential equation is shown in Eq. (3.19).

$$p(x) \propto \exp\left(-\int \frac{x+a}{b_2x^2 + b_1x + b_0}dx\right) \tag{3.19}$$

The variety of solutions differs in the values of the coefficients a, b_0, b_1 and b_2. Furthermore, the integral in this solution simplifies when certain cases of the integrand are considered. These cases are distinguished by the number of real roots of the quadratic function in the denominator. The two cases are: (i) negative discriminant $b_1^2 - 4b_2b_0 < 0$, and (ii) non-negative discriminant $b_1^2 - 4b_2b_0 \geq 0$. Additionally, further subdivisions, referred to as Pearson distribution types, are derived depending on the quantities β_1 and β_2. Recall that the first quantity is the square of the skewness shown in Eq. (2.12) and the second one is the kurtosis defined in Eq. (2.13). In other words, the type of distribution to which the data belong is entirely determined by the skewness and the kurtosis. The Pearson distribution types correspond to common probability distributions. The following types and their common distribution associated arise: type I (beta), type II (symmetrical beta), type III (gamma), type IV (Cauchy), type V (inverse-gamma), type VI (beta prime), type VII (Student's t) and the limit of type I, III, IV, V (normal).

Once the Pearson distribution type is determined, the two, three or four parameters of the particular distribution type can be calculated as a function of the expected value, variance, skewness and kurtosis, i.e. from the first four moments. The formulas to calculate the parameters for each type of Pearson distribution are given in [149]. As an example, the following formulas can be used for the Pearson distribution type I that arises from the case (ii) when the real roots of the quadratic equation a_1 and a_2 are of opposite sign. The real roots $a_1 < 0 < a_2$ are enclosed in Eq. (3.20).

$$a_1 = \frac{-b_1 - \sqrt{b_1^2 - 4b_2b_0}}{2b_2}, \quad a_2 = \frac{-b_1 + \sqrt{b_1^2 - 4b_2b_0}}{2b_2} \tag{3.20}$$

In this case, the solution of the differential equation in Eq. (3.19) becomes Eq. (3.21).

$$p(x) \propto \left(1 - \frac{x}{a_1}\right)^{-\frac{a+a_1}{b_2(a_1-a_2)}} \left(1 - \frac{x}{a_2}\right)^{\frac{a+a_2}{b_2(a_1-a_2)}} \tag{3.21}$$

The previous solution $p(x)$ is supported on the interval (a_1, a_2), then applying the substitution $x = a_1 + y(a_2 - a_1)$ yields a solution in terms of y that is supported on the interval $(0, 1)$ as it is shown in Eq. (3.22).

$$p(y) \propto \left(\frac{a_1 - a_2}{a_1} y\right)^{-\frac{a+a_1}{b_2(a_1-a_2)}} \left(\frac{a_2 - a_1}{a_2}(1 - y)\right)^{\frac{a+a_2}{b_2(a_1-a_2)}} \tag{3.22}$$

The exponents are named as m_1 and m_2 as it is designated in Eq. (3.23).

$$m_1 = -\frac{a + a_1}{b_2\,(a_1 - a_2)}, \quad m_2 = \frac{a + a_2}{b_2\,(a_1 - a_2)} \tag{3.23}$$

After substituting and regrouping, the solution in Eq. (3.22) simplifies to Eq. (3.24).

$$p(y) \propto y^{m_1}(1 - y)^{m_2} \tag{3.24}$$

Note that Eq. (3.24) corresponds to the probability density function of the beta distribution for $0 < y < 1$, and shape parameters $\alpha = m_1 + 1$ and $\beta = m_2 + 1$. Thus, $(x - \lambda)/(a_2 - a_1)$ follows a beta distribution with the same shape parameters α and β, scale parameter $(a_2 - a_1)$ and with a location parameter λ as it is shown in Eq. (3.25).

$$\frac{x - \lambda}{a_2 - a_1} \text{ follows a } \mathrm{Beta}(\alpha, \beta) \text{ with:} \tag{3.25}$$
$$\lambda = \mu_1' - (a_2 - a_1)\,\frac{m_1 + 1}{m_1 + m_2 + 2} \equiv \mu_1' - (a_2 - a_1)\,\frac{\alpha}{\alpha + \beta}$$

Note that μ_1' is the expected value of the distribution of the original x variable to model, i.e. its first raw moment.

3.4 Use of probabilistic fatigue life estimation in defining inspection intervals for railway axles

The essence of damage tolerance analysis of railway axles is to detect cracks before they become critical, providing certain level of safety for the axles in a fleet of trains by performing periodical inspections in-service. Thus, damage tolerance analyses are based on fracture mechanics to simulate crack propagation. Within the frame of the damage tolerance concept, the possibility of using probabilistic fatigue lifespan estimation is developed here. For that purpose, this section gives an overview of the steps of the damage tolerance of railway axles. Then, the propagation of uncertainty in fatigue crack growth using the FSOA and the probability distribution fit using the Pearson distribution family are outlined. Finally, the two previous elements are combined providing a reliability-based inspection interval definition.

3.4.1 Steps of the damage tolerance analysis

Damage tolerance is the classical concept of fracture mechanics application. It is illustrated in Fig. 3.5. A typical application field is the railway sector. The steps of a damage tolerance analysis of a railway axle comprise [21, 56, 66]:

Step 1. establishment of the initial crack location, orientation, shape and size,
Step 2. simulation of sub-critical crack extension, i.e. the FCG process,
Step 3. determination of critical crack size for component failure,
Step 4. determination of residual lifetime of the component, and
Step 5. establishment of inspection intervals and computation of the overall probability of crack detection.

The aim of the damage tolerance analysis in this thesis is to determine inspection intervals with an associated CPOD, what is also function of the performance of the NDT method. The different steps of the analysis are explained in detail for a particular example dealing with the fatigue crack growth in a railway axle.

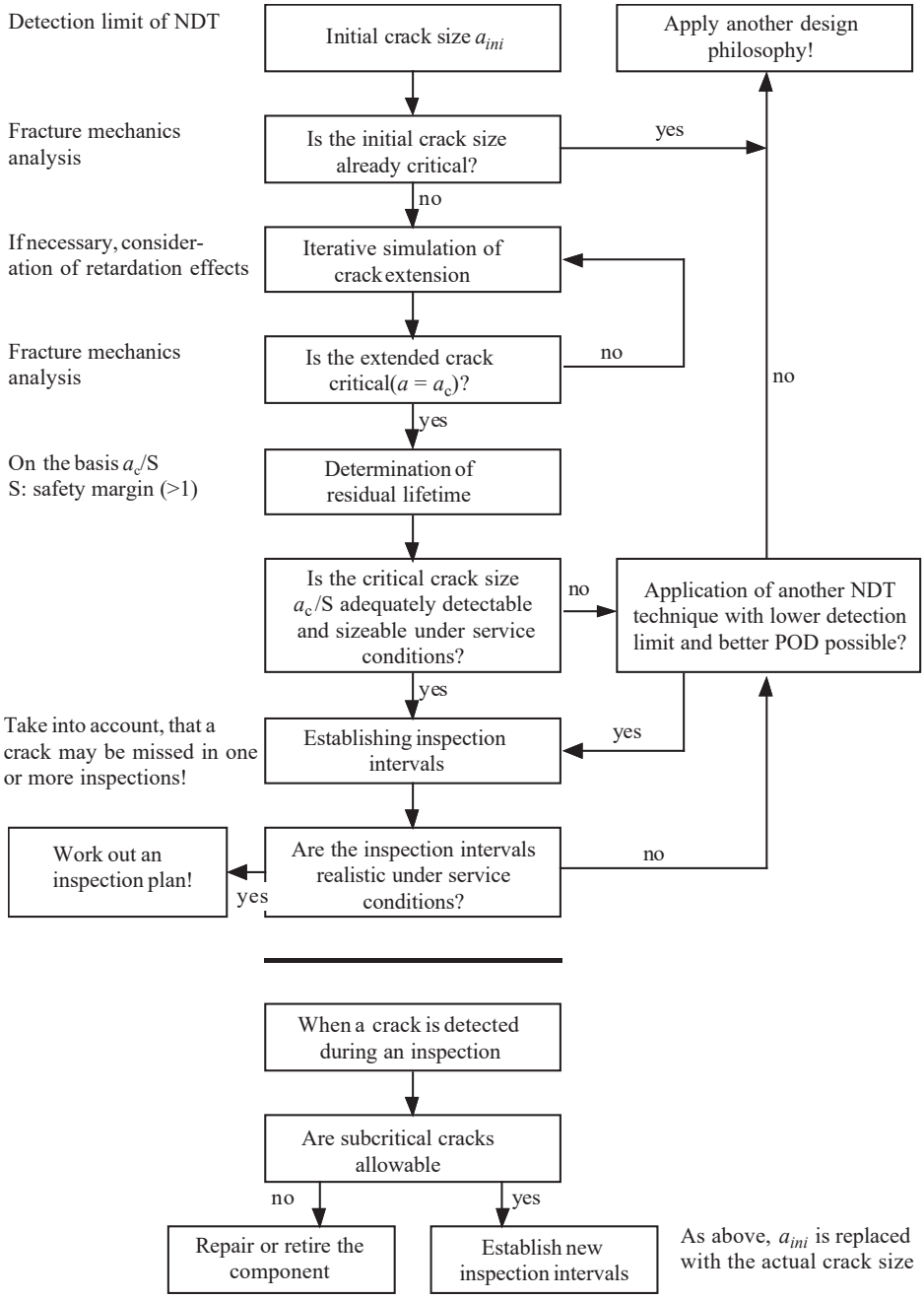

Figure 3.5. Fracture mechanics analysis within the framework of Damage Tolerant Design [21].

3.4.2 Probabilistic fatigue crack growth life

Starting from the assumption of an initial crack-like defect (step 1), the crack growth simulation (step 2) considers: (i) the component geometry and dimensions; (ii) the loading conditions including the bending moment, cyclic, the load spectra, in-service load sequences, and the press-fit, static; (iii) the material properties, primary the da/dN–ΔK curve; and (iv) the considered crack growth equation, commonly the NASGRO model. After that, different definitions of the critical crack size (step 3) are in use, but since the growth rate of long cracks is usually high due to its exponential nature, the failure is imminent whatever the relatively long crack depth. Next, the residual lifetime is calculated (step 4), that is, the number of loading cycles or the distance in kilometres, which the assumed initial crack, (step 1), would need to grow up to the final crack size, (step 3). Among all the different aspects which affect the residual lifetime (step 4), it strongly depends on the FCG process (step 2), and, as it is stochastic in nature, the residual lifetime also depends on the uncertainties inherent to the factors listed in (i) to (iv). Addressing the FCG problem from a probabilistic point of view is, therefore, a crucial point for the final (step 5), establishing inspection intervals with a probability of crack detection associated.

In order to obtain a probabilistic fatigue crack growth life estimation, this thesis applies a procedure that uses the first four moments of the fatigue crack growth life predicted by the FSOA to fit the parameters of a probability distribution based on the Pearson distribution family.

The FSOA for the moments of functions of random variables enables the prediction of the expected value, the variance, the skewness and the kurtosis of the probabilistic fatigue crack growth life. On this basis, the complete mathematical derivation of the FSOA for the first to fourth moments of functions of random variables is presented in Chapter 2. It presents the expressions involving tensors of different orders in a simple and comprehensible way. Notice that, the first to fourth moments are related, by definition, to the expected value, first raw moment; the variance, second central moment; the skewness, third central standardized moment; and the kurtosis, fourth central standardized moment, of the random output variable. For a detailed description, the manner in which the FSOA is applied to the fatigue crack growth NASGRO model for propagating the first to fourth moments of the fatigue life N through the use of the NASGRO Pr. Eqs. is explained in Subsection 3.2.2. Finally, the expected value of N, its variance, the skewness and the kurtosis are calculated based on the first to fourth predicted moments.

At this point, the problem of fitting a probability distribution from prescribed moments arises. Commonly, the normal distribution is assumed when there is not much information available about the underlying probability distribution, notwithstanding

that this assumption might not reflect the reality in some scenarios. Among the different distributions that can be considered, the Pearson distribution family, presented in Section 3.3, is used in the methodology as it is a versatile family that covers a broad range of distribution shapes. Additionally, it enables the expression of the parameters of the distribution as a function of the first four moments of the distribution without a priori hypotheses. Depending on these quantities, different common probability distributions arise, for instance, the beta, symmetrical beta, gamma, Cauchy, inverse-gamma distribution, beta prime, Student's t and the normal distribution.

Summarizing, once the FSOA method and the Pearson family fit are applied, there is available a probabilistic description of the fatigue crack growth life, that provides relevant information about the statistical distribution of the output random variable fatigue life.

3.4.3 Reliability-based inspection interval definition

The damage tolerance methodology overviewed in Subsection 3.4.1 is commonly based on the deterministic calculation of the fatigue crack growth (step 2), but, as mentioned, given the uncertainties inherent to geometric parameters, the variability of loads and the scatter of the material properties, the calculation of an axle lifespan should not be done with a simple deterministic calculation, and instead, a probabilistic approach is preferred. As shown in Fig. 3.6, the random nature of the fatigue crack growth in the railway axle needs a probabilistic description taking into account of the variabilities given by the geometric accuracy, the material properties and the actual in-service loads. With such an uncertainty, applying the probabilistic approach outlined in Subsection 3.4.2, the probability distribution of the fatigue crack growth life is available. That is, the distribution of the fatigue life predictions with allowance for these sources of uncertainty is obtained, thus leading to an enhanced and more robust control over the safety required by these critical components.

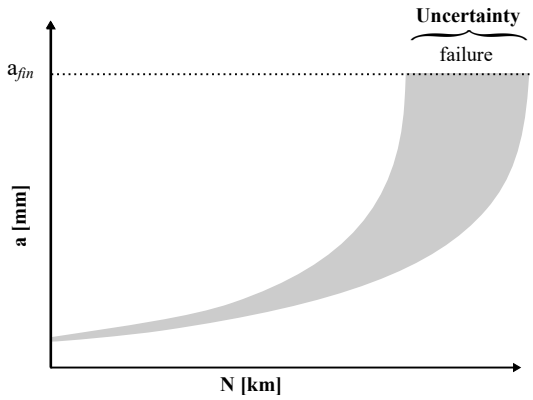

Figure 3.6. Probabilistic fatigue life.

The probability distribution can be described in various forms, such as by the survival function (SF), by the cumulative distribution function (CDF) or by the probability density function (PDF). In the context of probabilistic FCG life in railway axles, the SF is the function that gives the probability that an axle will survive beyond any specified time, cycles or kilometres. Often, in engineering, the survival function is also known as the reliability function. Alternatively, the reliability function can also be evaluated for a given reliability percent obtaining the corresponding number of kilometres. In other words, in this way it provides the minimum mileage travelled for a given surviving proportion of axles. Another name for the SF is the complementary of the cumulative distribution function (CCDF). Moreover, it is well-known that the CDF and the PDF are related. Given these basic premises, the working approach selects a reliability level in such a way that a conservative lifespan balancing safety and economic issues is achieved. Notice that, the input uncertainties and scatter are implicitly collected in the output probability distribution provided by the Pr. Eqs. and represented by its survival, cumulative distribution and probability density functions of fatigue life. The stated procedure is illustrated in Fig. 3.7.

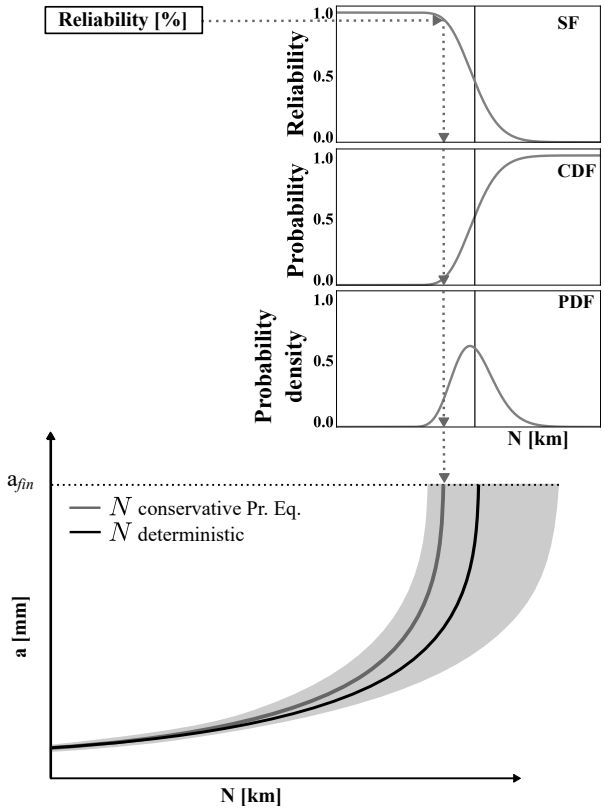

Figure 3.7. Conservative reliability-based life estimation from probabilistic fatigue life (survival, cumulative distribution and probability density functions of fatigue life).

As a result of the procedure, a conservative estimation of the lifespan is obtained, taking advantage of the knowledge available at the lower tail of the distribution of lives. Finally, instead of the deterministic lifespan calculation, the conservative lifespan estimation is considered as the FCG process (step 2) outcome, which is the basis for the subsequent steps oriented to the interval inspection definition. The idea for determining the periodicity of the NDI is depicted simply in Fig. 3.8.

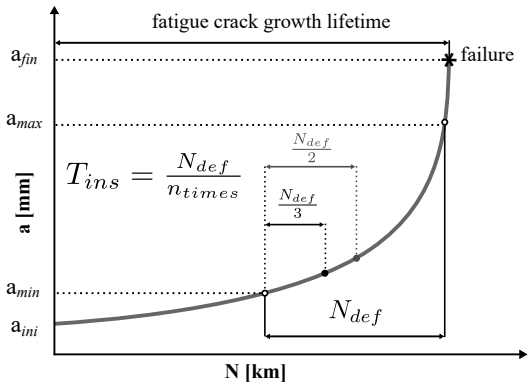

Figure 3.8. Definition of the periodicity of NDT inspections, i.e. inspection intervals of maintenance.

First, based on the conservative lifespan estimation, the residual lifetime (step 4) is delimited. This portion of lifetime is denoted as N_{def} in Fig. 3.8 in reference to the lifetime for the definition of inspection intervals. The N_{def} covers the propagation from a_{min} to a_{max} (steps 1 and 3), being the minimum and the maximum crack sizes considered for the lower and the higher lifetime bounds respectively, and it is calculated through the Eq. (3.26).

$$N_{def} = N\left(a_{max}\right) - N\left(a_{min}\right) \tag{3.26}$$

The usual assumption made is that a_{min} corresponds to crack size $a_{POD\%}$ that has certain probability of being detected by NDT, for instance the crack size $a_{95\%}$ which has a $POD = 95\%$. Finally, the inspection interval T_{ins} is determined by dividing N_{def} by a number of times n_{times} that takes account of the number of times that the crack can be detected before a failure could occur, as formulated in Eq. (3.27).

$$T_{ins} = \frac{N_{def}}{n_{times}} \tag{3.27}$$

For instance, the usual assumption considering n_{times} equal to 2 or 3 [142], allows the crack to be potentially observed at least twice or three times before it leads to catastrophic failure. This assumption is based on the fact that a crack could be missed at an inspection. It is, however, evident that even two or more inspections cannot ensure the crack detection. As already mentioned this approach is called *damage tolerance* and is applied to ensure *safe service* of the railway axle. The possible outcomes of the crack sizes with planned inspections is illustrated in Fig. 3.9.

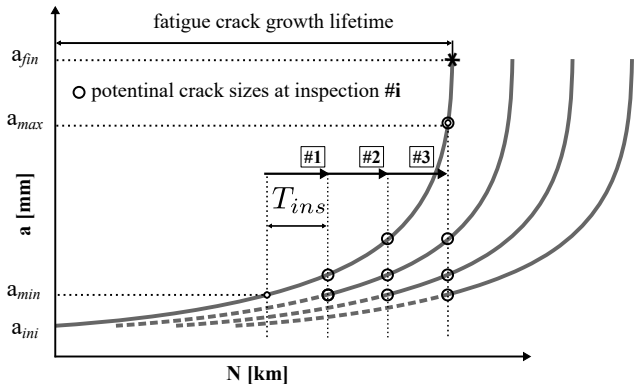

Figure 3.9. Inspections considering that a crack can be detected at least three times before failure.

It does not matter either at which lifetime the crack initiates. Inspections scheduled at e.g. $N_{def}/2$ interval will always give two chances for detection regardless of when crack growth process begins, provided that inspections are scheduled at $N_{def}/2$ interval starting from time zero, even though the possibility of having a crack is initially small. Similarly, if $N_{def}/3$ interval is chosen, there will always be three opportunities between a_{min} and a_{max} whether the crack occurs early or late, as shown in Fig. 3.9.

It is worth to remark that there is no standard regarding the inspections of railway axles, but only guidelines about freight wagons, thus, the responsibility is entirely demanded to the constructor and the maintenance operators. The guidelines in EN 15313:2016 standard [20], summarized in Table 1.3, recommend, as general indication, that an inspection has to be carried out every 400 000 km, inspecting the axle by ultrasonic testing. Additionally, the maintenance plan of railway axles for freight wagons, includes a full inspection of the axle by MPI that is carried out when the wheels are re-profiled or substituted at the major overhaul (out-off-service), typically every 1.2 million km. Intermediate inspections are carried out adopting visual and ultrasonic inspections. These inspections are usually scheduled based on progressed experience, but, recently operators of the rail sector are starting to apply engineering approaches. An approach to inspection interval design that is complementary to the empirical approach is required to establish the highest level of safety.

In summary, the approach presented here extends the current damage tolerance principles in railway axles by means of improving the crack growth simulation (step 2), replacing the deterministic crack growth estimation by a probabilistic one. The damage tolerance assessment benefits from a better knowledge of the distribution of fatigue lifespan. As a result, it would give a more conservative recommendation for the definition of inspection intervals as it is based on a probabilistic fatigue propagation instead of on a deterministic one. The specific in-service inspection procedures shall be improved continuously in order to benefit the continuous advance in the state-of-the-art technology.

3.5 Performance of the non-destructive inspection methods

During service, the railway axles are subjected to deterioration, due to: contact fatigue, friction fatigue, thermal fatigue, fatigue caused by rotating bending and/or torsional oscillations, abrasion wear and tear, corrosion from exposure to atmospheric agents and/or corrosive environments, and loss of paint or damage from ballast impact during operation or impacts with other bodies during maintenance. For this reason, in order to detect damages and prevent catastrophic failures of the safety-critical axles, the need of establishing a plan of periodic NDI during the service of the vehicle emerges. Nowadays, the most common methods for inspecting railway axles are VT, UT and MT. It should be emphasised that the VT are performed during standard inspections in the depot. Aside from visual inspection, in the other two cases, UT and MT, it is necessary to carry out more in-depth instrumental investigations and non-destructive testing.

The definition of an inspection plan is the final goal of a damage tolerance analysis of railway axles. In order to constitute an appropriate plan of the periodic inspections, it is essential to know the performances of the NDT methods used. In fact, NDT performance is a statistical matter [56], and the characteristic usually adopted for evaluating its performance is the POD vs. crack size curve, commonly referred to as POD curve. The POD vs. crack size relationships for various NDT methods are illustrated in Fig. 3.10, digitalized from [56]. These POD curves were obtained by Benyon and Watson [106], and nowadays are widely adopted in the railway axle field. They consider the case of MT also known as MPI and UT in near-end and far-end scan application conditions, defined for a solid axle in Fig. 3.11, where the axle is inspected from the end of the axle to mid-span or further in far-end, and where the axle is inspected from the end of the axle to an adjacent seat in near-end condition.

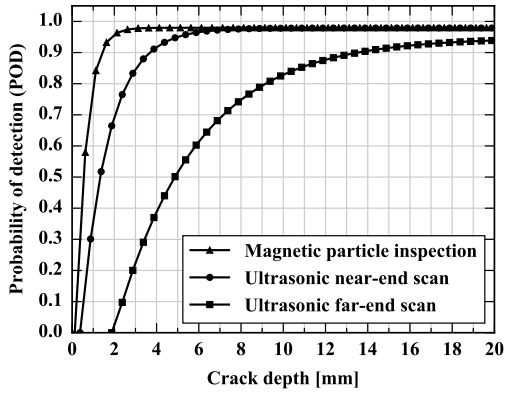

Figure 3.10. Probability of crack detection (POD) as a function of crack size for several non-destructive testing (NDT) methods [56].

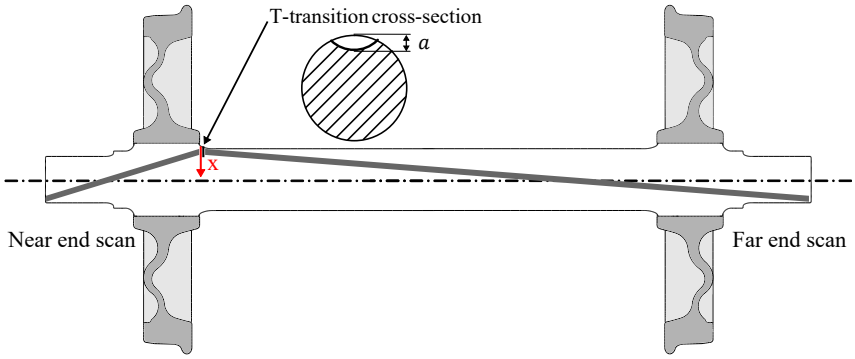

Figure 3.11. General view of a non-powered wheelset with a postulated crack in the T-transition inspected using near-end scan and far-end scan techniques.

It can be observed from Fig. 3.10 that the POD of a crack depends not only on the NDT technique but also on the actual crack size. Note that the MPI is the most powerful detecting method under consideration, providing very good results even when dealing with comparatively short crack depths. On the other side, ultrasonic techniques have notable different POD curves. The second-best method is near-end scan followed by far-end scan. Usually for the shorter interval, the inspections are performed by UT and for the larger interval by MT. It seems likely, according to Fig. 3.10, that MPI is the most cost-effective NDT technique for a bare axle (where the wheels, bearings, brake discs are removed) during its overhaul. All unfortunately rather common, fatigue cracks may be initiated and grow to failure in less time than needed to wear out the wheels, and so to re-profile or substitute them in an overhaul. Consequently, costly and because of their intrusive nature, disruptive, axle inspections in between overhauls have to be carried out. As mentioned above, they are frequently based on UT as a compromise between a limited intrusiveness, which disrupts train service, and a lower POD compared with MPI.

The POD vs. crack size curves can be used to establish inspection intervals relying on a statistical basis. It involves an additional level in the probabilistic approach, in order to guarantee the structural integrity during the life of the railway axles. Establishing inspection intervals is essentially a statistical task acting as a link between fracture mechanics analysis, non-destructive testing and the constraints of industrial practice.

Each NDT inspection method is characterized by a POD vs. crack size curve whose CDF is fitted by an exponential curve as is expressed in Eq. (3.28).

$$\begin{aligned} POD_{MPI} &= \max\left\{0.0, 0.9796\left(1.0 - 1.0236e^{-2.1360(a-0.1950)}\right)\right\} \\ POD_{near\text{-}end} &= \max\left\{0.0, 0.9787\left(1.0 - 0.9889e^{-0.7691(a-0.4114)}\right)\right\} \\ POD_{far\text{-}end} &= \max\left\{0.0, 0.9480\left(1.0 - 0.9887e^{-0.2576(a-1.9979)}\right)\right\} \end{aligned} \tag{3.28}$$

Starting from POD vs. crack size curves, the total probability of observing cracks and defects in railway axles can be quantified by two different alternatives [109] shown in the Fig. 3.12 and described below: (a) cumulative POD represented in Fig. 3.12a, and (b) last chance POD depicted in Fig. 3.12b.

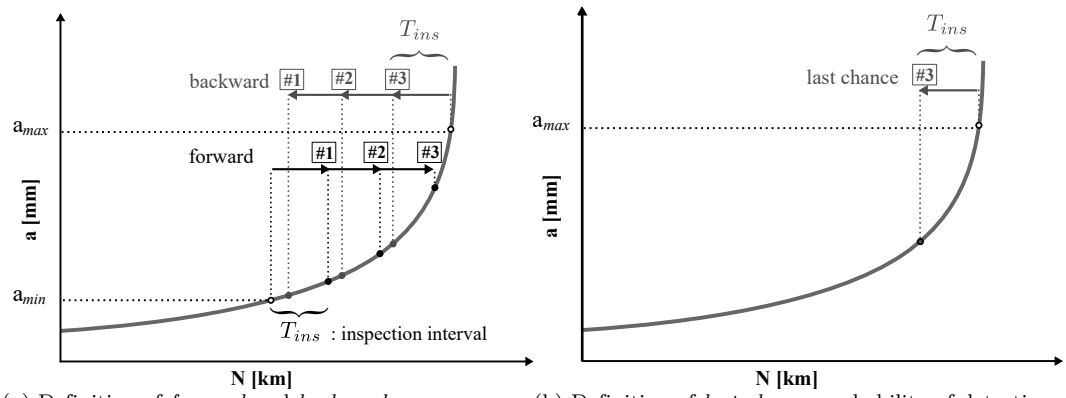

(a) Definition of *forward* and *backward* cumulative probability of detection.

(b) Definition of *last chance* probability of detection.

Figure 3.12. Options for probability of detection calculation.

The alternative (a), cumulative probability of detection in successive inspections (CPOD), arises from the consideration in Subsection 3.4.3 that the definition of an inspection schedule is done to have the possibility to inspect the axle several times prior to failure. In consequence, the probability of detection of the eventual crack is not the POD during one single NDT control, but instead, it has to be evaluated, once fixed the interval between inspections, as a function of the crack growth evolution, a-N curve, together with the NDT performance of the adopted method, POD-a curve. The CPOD increases from inspection to inspection since the crack becomes larger during the time in between. It is determined easily when the crack size vs. time dependency (step 2) in Subsection 3.4.1 and the POD vs. crack size curve for the NDT method are known. Notice that the crack size vs. time dependency is equivalent to the a-N curve, being N the number of cycles or mileage travelled in km. Note that the CPOD is sometimes replaced by its complementary cumulative probability of failure in successive inspections (CPOF) or simply referred to as P_f. Furthermore, alternative (a) offers to two additional ways to calculate the CPOD, denoted as *forward* and *backward* detection schemes as shown in Fig. 3.12a. The two approaches, based on forward detection, starting from a_{min} usually selected as the limit of detectability of the crack, and *backward* detection, going back from a_{max} commonly the final failure, are shown. The forward inspection seems to be the natural approach, while the backward approach is sometimes applied during trials after serious accidents to assign responsibilities. It should be noted that the latter should always be taken into consideration in the design of the inspection intervals, because it is systematically more conservative, giving smaller values of CPOD.

In this regard, given the length of the inspection interval in Fig. 3.12a, three inspections along the life of the railway axle are obtained as illustrated in Fig. 3.13. The CPOD of a crack growing according to the a-N curve, can be calculated based on the given number of inspections $\#i$ and the POD-a curve of the NDT method used. The easiest way to calculate the CPOD is to convert the POD of the individual inspections, $\#1, \#2, \#3$, designated with the sub-index $\#i$, to probability of non-detection (POND) by the relationship $POND\,(a_{\#i}) = 1 - POD\,(a_{\#i})$ where $a_{\#i}$ is the corresponding crack depth at the $\#i$ inspection. These PONDs, when multiplied give a cumulative probability of non-detection in successive inspections (CPOND). Notice, that the individual POND decreases with increasing crack length. Finally, the CPOND is converted back to its complementary CPOD.

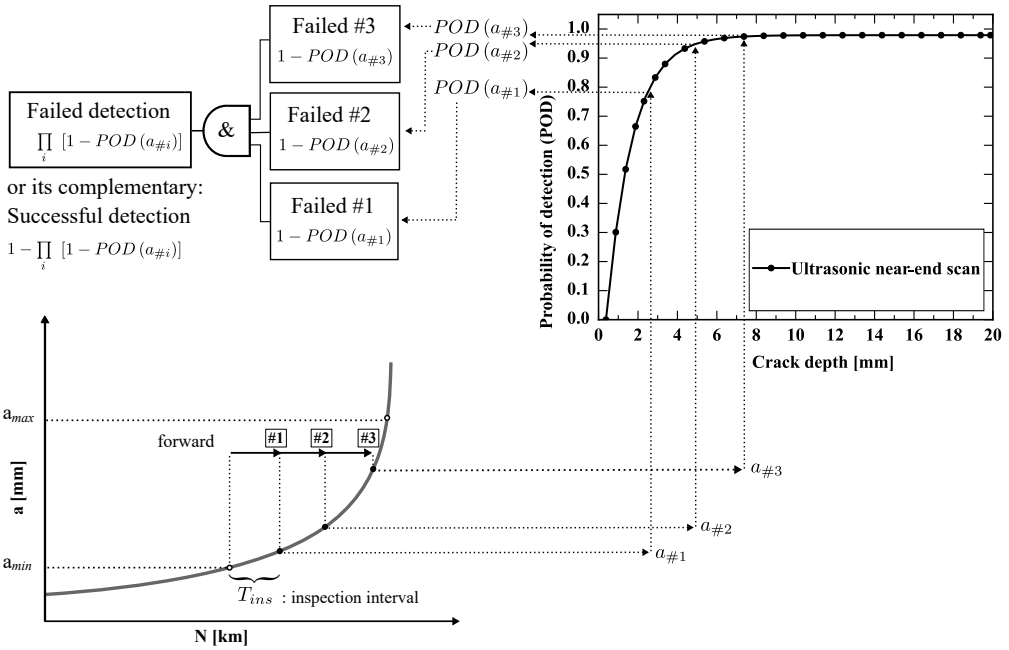

Figure 3.13. Probability of detection of $a_{\#i}$ in the $\#i$ individual inspection and fault tree of the cumulative probability of non-detection in successive inspections or its complementary cumulative probability of detection, considering the forward scheme and the ultrasonic near-end scan NDT.

In summary, the CPOD of a crack can be evaluated as in Eq. (3.29).

$$CPOD_{\#i} = 1 - CPOND_{\#i} = 1 - \prod_i POND\,(a_{\#i}) = 1 - \prod_i [1 - POD\,(a_{\#i})] \qquad (3.29)$$

The P_f, also denoted as CPOF, given that all the inspections failed to detect an actual crack, can be considered as the CPOND as expressed in Eq. (3.30).

$$P_f = CPOF_{\#i} = 1 - CPOD_{\#i} = CPOND_{\#i} = \prod_i [1 - POD\,(a_{\#i})] \qquad (3.30)$$

The alternative (b) for the evaluation of the probability of failure, was originally proposed for application in the railway axle field in [66], and so called *last chance* detection, as represented in Fig. 3.12b. This alternative is intended to avoid the error amplification of the first (a) alternative, due to the fact that in the initial stages of propagation, i.e. small cracks, the POD is really low. By the last chance alternative, only the POD of the last useful inspection in the backward direction is considered. Therefore, the last chance POD can be simply evaluated as in Eq. (3.31), and the probability of failure as in Eq. (3.32):

$$POD = POD\left(a_{\#\max(i)}\right) \tag{3.31}$$

$$P_f = 1 - POD = 1 - POD\left(a_{\#\max(i)}\right) \tag{3.32}$$

The last chance approach has the advantage of establishing a simple relationship between the POD and the inspection interval. Furthermore, with this approach it is possible to focus attention on the dimension of the crack that must be observed to have a high POD.

In particular, as it is not known exactly when crack growth is triggered by an accidental event, the component will always be subjected to inspection every T_{ins} km, and depending on the detection scheme and inspection method used, the CPOD, its complementary CPOF or the last chance POD can be computed. It is important to recall the hypothesis made here, that is, the presence of a crack (step 1) in Subsection 3.4.1 and so the probability of failure equals the probability of not detecting the crack in due time throughout the axle lifetime. This must be distinguished from the probability of failure of an arbitrary axle in a fleet of trains since an existing defect an its nucleation to a crack of that size is very unlikely. To calculate the real probability of failure, the P_f obtained in the damage tolerance analysis should be multiplied by the probability of having a defect on the axle and by the probability that a crack will nucleate from that defect and further grow during the service life. Therefore, the real probability of failure of an axle is, by orders of magnitude, smaller than the one obtained in a damage tolerance analysis. The calculation of the real probability of failure is beyond the scope of this thesis.

Preventive maintenance is a prevailing principle in the railway industry. Note that, in this context, damage tolerance does not mean that a crack detected during an inspection is considered acceptable even when its size is far from being critical. In some other applications, this is a possible option, but it should be handled with care especially for safety relevant applications, as it is the case of a railway axle. Regarding the damage tolerance methodology developed for railway axles, the approach is still under present and future development. A comparison of this relatively new approach with what is prescribed by the current standards, i.e. infinite life, and against the safe life approach, that is, damage accumulation, are still under discussion.

4

Application examples

4.1 Introduction

This chapter illustrates the devised probabilistic damage tolerance-based maintenance planning for railway axles, thorough an application example. It provides a random variables approach to the fracture mechanics based fatigue crack growth model. The case study herein tackled deals with the fatigue crack growth analysis of a railway axle. The full second-order approach in Chapter 2 takes into account the stochastic character of the fatigue crack growth, randomizing the input random variables considered in the FCG phenomenon. As explained, this method is implemented in order avoid the large computational effort required by the Monte Carlo simulation method. The probabilistic FCG methodology in the DTA of railway axles, described in the previous Chapter 3, is hereinafter applied to the chosen case study. The outcomes allow investigating the influence of probabilistic approaches on the reliability evaluation, assessing the most important factors in the definition of inspection intervals. One of the most essential aspects is the time taken for a detected crack to extend to its critical size. If this time is sufficiently large and the probability of detection meets an admissible level, the design concept based on inspection intervals could be suitable. Since the goal of DTA is to inform the maintenance decision makers about the impacts of a particular inspection interval, it is indispensable to integrate into the overall methodology the uncertainties involved in the fatigue process regarding the random input variables.

When dealing with reliability of components with a damage tolerance design concept subjected to variable amplitude fatigue loading, the following inputs, methods and results are considered in this thesis:

- the geometry of the component;
- an expected crack location, initial size and shape;
- the static and cyclic loading conditions;
- the load spectrum in service conditions;
- the elastic material properties;
- the fatigue crack growth curve;
- a fatigue crack growth equation, NASGRO;
- weight functions to evaluate the stress intensity factor at the crack tip;
- knowledge regarding the input uncertainties, i.e. the random input variables;
- a FSOA method for probabilistic fatigue crack growth and PDF reconstruction;
- a reliability-based inspection interval definition;
- the performance curves of the NDT techniques; and
- overall probability of successful detection or the complementary P_f assessment.

This chapter is organized as follows. Firstly, the case study under analysis considering a metal railway axle is described. It details the geometry, the postulated crack location, size and shape, the material parameters of the NASGRO FCG, the press-fit and bending loading conditions including the load spectrum, the mesh built together with the loads and boundary conditions for the FEM analysis, the stress fields from the FEM analysis and the results of the deterministic (Det.) simulation performed according to the NASGRO equations. Secondly the input random variables considered in the probabilistic analysis for the FCG in the railway axle are reported. The assumptions taken regarding their variability, the distributions type, and the relationships of correlation or dependence considered are thoroughly described. Finally, all the ideas presented in the chapters of this thesis are put together, illustrating the course of the reasoning for building a link between the full second-order approach applied on the FCG phenomenon and the DTA of railway axles to define inspection intervals. It considers, the most comprehensive set of random variables as the backbone when exemplifying the work-flow of the calculation, promoting a deep understanding of the r.v.s influence. In short, this brings to an end and is a celebration of my cumulative work in this field.

4.2 Case study definition: railway axle

In this section, the case study dealing with the fatigue crack growth analysis of railway axle is presented. The geometry of the wheelset is shown in Fig. 4.1. The non-powered railway axle considered in the present numerical example is 173 mm in diameter and it is made of EA1N steel defined in the EN 13261:2020 standard [19].

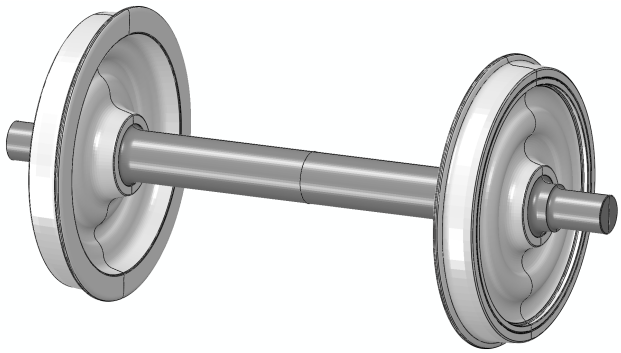

Figure 4.1. Geometry of the wheelset with external journals.

The POD of a crack depends not only on the NDI method but also on the actual crack size as shown in Fig. 3.10. For instance, MPI can detect relatively long cracks larger than 2 mm in approximately 95 % cases. That is, a crack of 2 mm in length is not detected in 5 % cases. Therefore, there is a risk that an existing crack is not detected, and so the existence of a crack should be considered. The initial crack size is often taken more or less arbitrarily, but it might be selected as a crack with a certain probability of detection. For example, it could be defined as a crack with POD of 95 %, $a_{95\%}$. Such a criterion certainly has appeal, because it seems consistent, yet it still leads to inconsistencies. In the case of study, a semicircular initial crack a_{ini} of 2 mm was postulated at the T-transition, as indicated with a red line in Fig. 4.2, in which is also defined the radial coordinate system x at the axle surface.

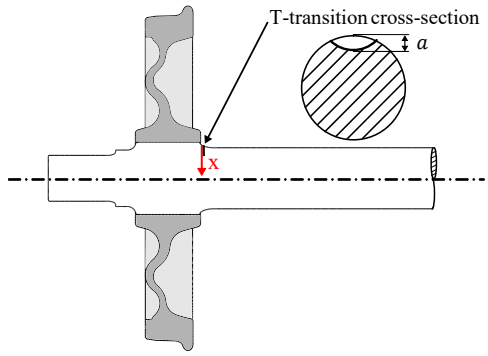

Figure 4.2. General axle view of a non-powered wheelset with a postulated crack in the T-transition.

As shown in the figure, the so-called T-notch or T-transition is defined as the transition between the wheel seat and the axle body. As it is described later, the previous crack location is assumed at the highest stressed region, what is relevant for establishing inspection intervals. This is the case even if real cracks are initiated at other locations, for instance, beneath press seats or at corrosion pits, since crack initiation process does not play a role for residual lifetime determination which assumes a pre-existing crack of a depth of some millimetres. In addition, the POD at the T-notch position is usually the poorest one along the whole railway axle.

The fatigue crack growth material parameters required for the NASGRO model evaluation are obtained from the bibliography and given in Table 4.1.

Table 4.1. NASGRO fatigue crack growth material parameters.

Parameter	Value		Reference
n	2.09	[-]	[49]
$C^{\dagger}$	3.3197×10^{-10}	[MPa^{-n} mm$^{1-n/2}$]	[49]
p	1.3	[-]	[49]
q	0.001	[-]	[49]
K_c	2434.9	[MPa $\sqrt{\text{mm}}$]	[49]
ΔK_{th0}	233.70	[MPa $\sqrt{\text{mm}}$]	[49]
C_{th}^{p}	1.442	[-]	[49]
C_{th}^{m}	−0.02	[-]	[49]
α	2.5	[-]	[7, 65]
S_{max}/σ_0	0.3	[-]	[65]
a_0	0.0381	mm	[65, 150]

† Exponents in the C parameter units make reference to n.

The loads considered in the present study are the press-fit loading produced by the wheel mounting with interference and the bending moment loading in the railway axle due to the vehicle weight and cargo. The wheel was press-fitted with 0.286 mm interference in diameter. In addition, the bending moment level selected M, equal to 70.35 MN mm, corresponded to the highest load amplitude in the spectrum of a 22.5 t per axle, plus additional forces, generated when the train goes through curved track, over crossovers, switches, rail joints, braking efforts, etc. This assumption implied the worst case scenario since such stress level corresponded to the maximum one for axle bodies according to the EN 13103-1:2017 standard [15]. Moreover, the present example considered the load spectrum acting on a railway axle over its service. The load spectrum was derived from the one available in the UIC B 169/RP 36 report [84]. The resulting service loading spectrum is shown in Fig. 4.3.

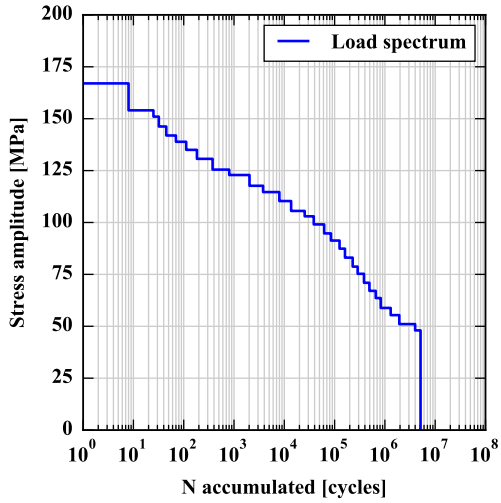

Figure 4.3. Stress spectrum, mileage 15 000 km, considered in the probabilistic analysis.

The interference stress distribution normal to the crack surface and the reference bending stress amplitude for the 70.35 MN mm bending moment needed for the stress intensity factor K_{max} and K_{min} evaluation were calculated via the finite element method (FEM).

The modelling procedure adopted was applied on the geometry of the wheelset presented in Fig. 4.1. The three-dimensional finite element model used in the simulation consists of the wheel and the railway axle, considered as deformable solids discretized by means of linear 8-node hexahedron elements with full integration (C3D8 in the ABAQUS library [151]), as shown in Fig. 4.4. The full wheelset assembly considered in the analysis is shown in Fig. 4.4a. The corresponding railway wheel was assembled together with the axle, whereas the bearings and the rail-track were modelled only as boundary conditions as explained hereafter. The mesh generated for the railway axle is presented in Fig. 4.4b and the high mesh refinement in the region of interest, i.e. the T-transition, is shown in the detail in Fig. 4.4c. Special attention was paid while meshing the T-transition in order to provide the best compromise between accuracy and running time. It is important to note here that it is not necessary to model the postulated crack since the SIFs are subsequently obtained based on the axial stresses acting across the crack plane in the uncracked component by means of the weight functions as described in Subsection 3.2.3.

The press-fit between wheel and axle was modelled. In order to emulate the press-fit loads, the `CLEARANCE` option in ABAQUS was used, and the radial interference value was chosen equal to 143.125 µm according to current EN 13260:2020 standard [18]. The contact between the wheel and axle was modelled with a `SMALL SLIDING` contact

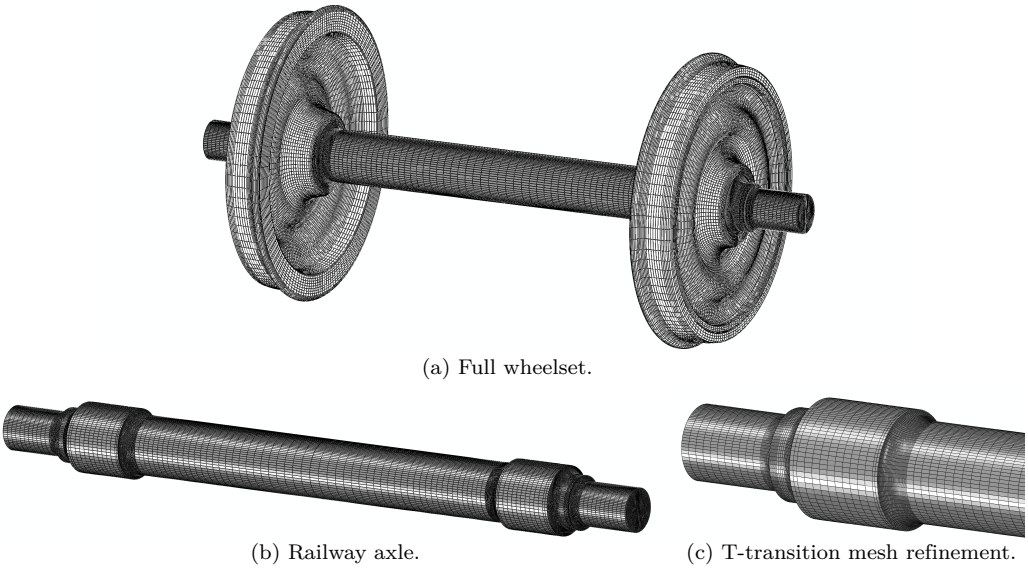

(a) Full wheelset.

(b) Railway axle.

(c) T-transition mesh refinement.

Figure 4.4. Mesh of the finite element model (FEM).

(friction coefficient $\mu = 0.6$). To obtain the bending stresses, a vertical force, F, was applied to the middle section of the bearing journal as shown in Fig. 4.5. By means of this force, the bending moment corresponding to the 22.5 t per axle is represented in the axle cross-section of interest. It also avoids the need of modelling the bearings. Additionally, the vertical translations were constrained at the bottom of the wheel ($u_3 = 0$) to simulate the track conditions. Finally, two symmetry conditions were applied. The first one, to the middle section of the axle body ($u_2 = 0$, plane 1-3). The second one, taking advantage of the longitudinal symmetry ($u_1 = 0$, plane 2-3). By doing so, only one quarter of the wheelset was actually modelled. The magnitude of the applied force is modified in accordance with the symmetries. Note that Fig. 4.5 presents the full wheelset despite the two aforementioned symmetries.

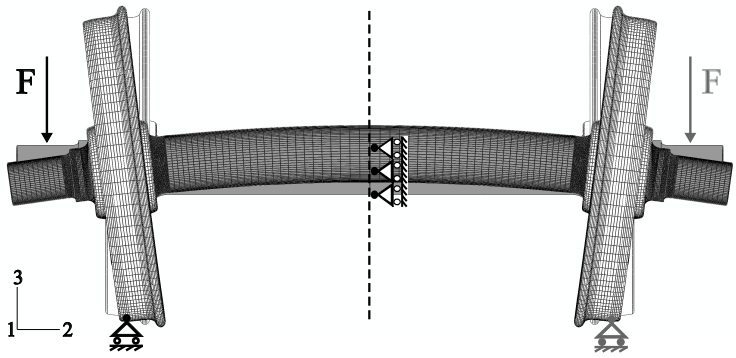

Figure 4.5. Load and boundary conditions in the symmetry model.

The analysis of results is aimed to obtain the stress distribution in the T-transition in axial direction. It should be recalled here that the crack plane is defined perpendicular to the rotation axis of the railway axle, so the results are focused on the stress distribution acting through the crack plane. The stress field in axial direction according to the press-fit with interference load case is shown in Fig. 4.6 using undeformed shape. Moreover, the stress field according to the bending moment load case is shown in Fig. 4.7 using deformed shape.

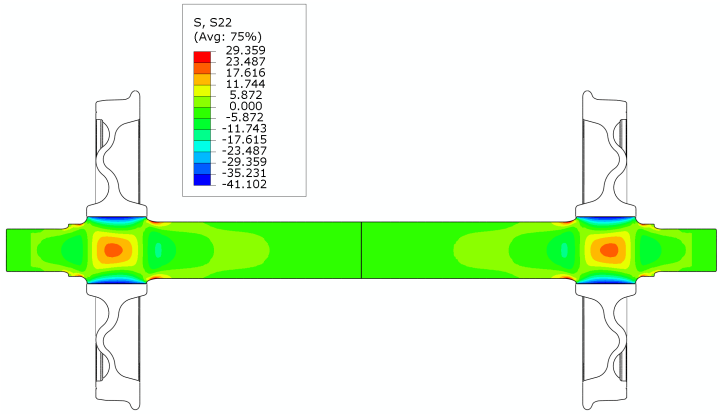

Figure 4.6. Stress distributions [MPa] in axial direction at the press-fit load case. Undeformed.

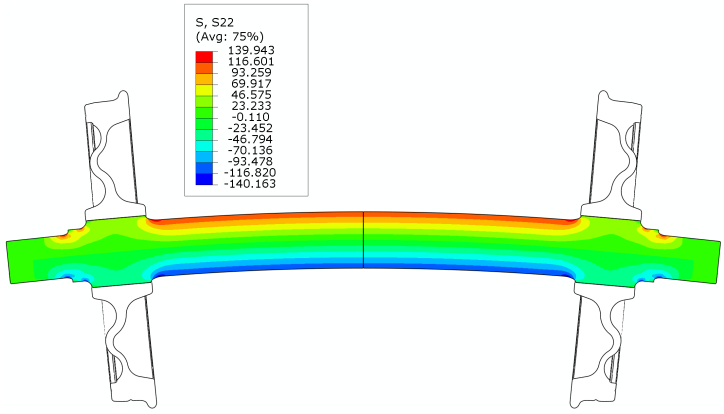

Figure 4.7. Stress distributions [MPa] in axial direction at the bending load case. Deformed x20.

The weight function procedure presented in Subsection 3.2.3 is able to provide the SIF as function of the instant crack shape and of the position along the crack front in which are calculated. To this aim, the two-dimensional stress field in the T-transition cross-section can be further simplified to the one-dimensional stress path $\sigma(x)$ in the uncracked component according to the radial coordinate system x defined at the axle surface in Fig. 4.2. The typical shape of these simpler stress paths for the press-fit with interference and for the bending moment load cases are reproduced in Fig. 4.8.

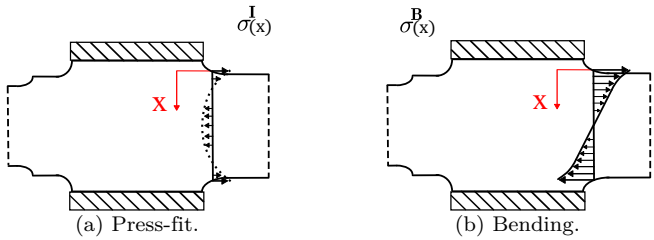

(a) Press-fit. (b) Bending.

Figure 4.8. Stress distributions in axial direction at the press-fit and at the bending load cases.

The total stress field in the axle has to be considered then as the superposition of the two different fields, the first one due to the press-fit and the second one given by the applied bending moment load. The stresses at the interference σ^I, at the reference bending moment σ^B and at the combination of both σ^{B+I} are shown in Fig. 4.9.

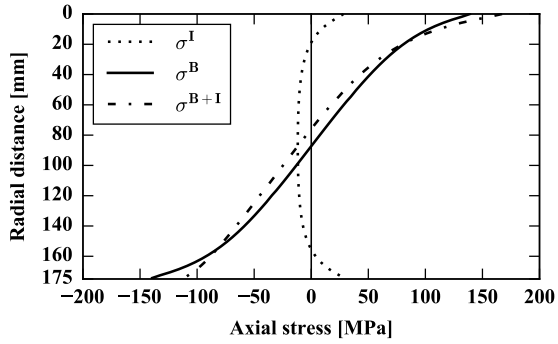

Figure 4.9. Stress distributions at the T-transition in axial direction at the press-fit with interference, at the bending and at the superposition of both load cases.

The axle rotates and the bending load always acts in the vertical plane. As a result, every revolution the crack goes through all possible positions with respect to the applied moment, and thus the resulting load type is rotary bending. In consequence, the total stress distribution on the crack depends on its angle location with respect to the axle rotation as shown in Fig. 4.10. Accordingly, the press-fit is considered as a static load inducing a stress in the axle, while the vertical load produces an alternating stress condition. It may be inferred that the maximum and minimum stresses are obtained at $\theta = 0$ and $\theta = \pi$ and are related due to the stresses symmetry.

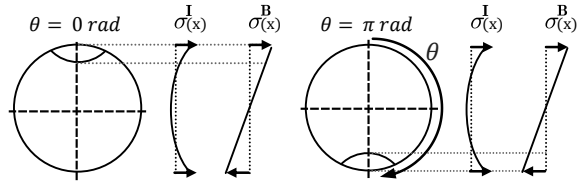

Figure 4.10. Interference and bending stress at the axle cross-section in two different angle rotations θ.

To calculate the deterministic FCG in the railway axle, the NASGRO equations in Subsection 3.2.1 are used. The combination of the loading conditions is applied repeatedly according to the iterative scheme described in Eq. (3.11), increasing the crack depth from the semicircular initial crack a_{ini} of 2 mm at the T-transition and keeping a semi-elliptical shape while growing up to a final crack depth a_{fin} of 50 mm. The final length considered was shorter than the critical length determined from fracture toughness. In addition, as a result of the spectrum in Fig. 4.3, different number of blocks are eventually damaging, i.e. contribute to the crack growth. This is because each block of the spectrum contributes or not to crack growth depending on the level of load amplitude and on the pertinent crack shape. Therefore, not damaging load levels in the stage of a short crack could become damaging in its stage of a long crack. An illustration of the crack front growing in the axle cross-section for different crack depths a according to the Det. calculation is presented in Fig. 4.11.

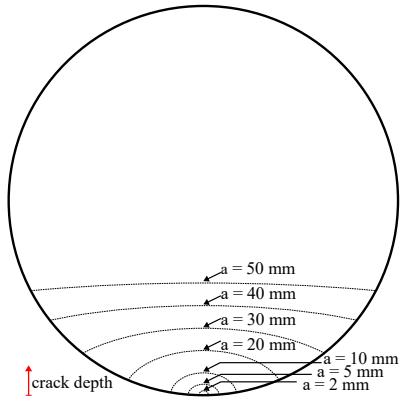

Figure 4.11. Axle cross-section with a growing crack.

The Det. simulation performed, gives the evolution of the crack depth vs. the number of km shown in Fig. 4.12.

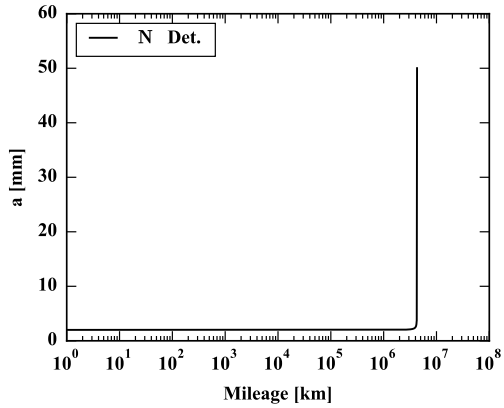

Figure 4.12. Crack depth vs. the number of km N provided by the Det. NASGRO.

4.3 Random variables

The input random variables considered in the probabilistic analysis for fatigue crack growth in the railway axle are: (i) the exponent n and the parameter C of the crack growth equation in the Paris region; (ii) the bending moment M in the railway axle; and (iii) the threshold stress intensity factor range at $R = 0$, ΔK_{th0}. For clarity, these random variables are referred to throughout this section as enumerated below:

(i) $\{n, C\}$
(ii) $\{M\}$
(iii) $\{\Delta K_{th0}\}$

The assumptions taken regarding their variability, the distributions type, and the relationships of correlation or dependence are thoroughly detailed in the following. In the application examples, all the r.v.s were assumed as having a standard deviation equal to the 1.5 % of their mean value. The mean value and the variance of the r.v.s considered are enclosed in Table 4.2. Notice that the mean values of the material parameters used in the probabilistic analysis correspond to the material parameters presented in Table 4.1. Additionally, the material parameters that are not considered probabilistic, i.e. the deterministic ones, are those included in Table 4.1.

Table 4.2. Random variables mean and variance.

r.v.	μ		σ^2	
n	2.09	[-]	9.8300×10^{-4}	[-]
$C^{\dagger}$	3.3197×10^{-10}	$[\mathrm{MPa}^{-n}\,\mathrm{mm}^{1-n/2}]$	2.4796×10^{-23}	$[\mathrm{MPa}^{-n}\,\mathrm{mm}^{1-n/2}]^2$
$M^{\ddagger}$	70.35	[MN mm]	1.11	$[\mathrm{MN\,mm}]^2$
ΔK_{th0}	233.70	$[\mathrm{MPa}\sqrt{\mathrm{mm}}]$	12.29	$[\mathrm{MPa}\sqrt{\mathrm{mm}}]^2$

† Exponents in the C parameter units make reference to n.
‡ M corresponds to the highest load amplitude in the spectrum.

The random variables n and C in (i), are assumed as a bivariate Normal–Log-normal distribution as it turns out that they are highly correlated [89]. The Pearson's correlation coefficient is obtained from [89] as $\mathrm{PCC}_{n,\ln(C)} = -0.968$. The bivariate Normal–Log-normal distribution appears at first glance to be difficult to manoeuvre, but by taking the natural log of the second variable C, the bivariate Normal distribution emerges, and this distribution is easier to handle [152]. The bivariate Normal–Log-normal distribution assumed and its projections in three orthogonal planes are shown in Fig. 4.13.

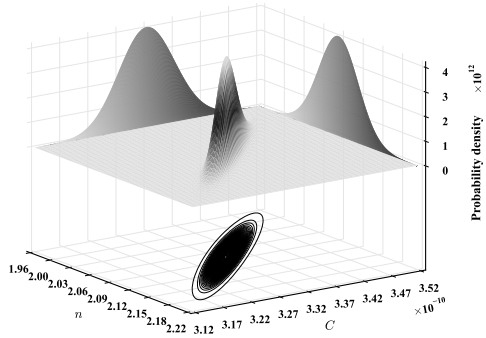

Figure 4.13. Surface of the bivariate Normal–Log-normal joint density function (n, C).

The marginal PDF of the normally distributed n and the log-normally C modelled and the histograms of the drawns sampled in the MC are presented in Fig. 4.14.

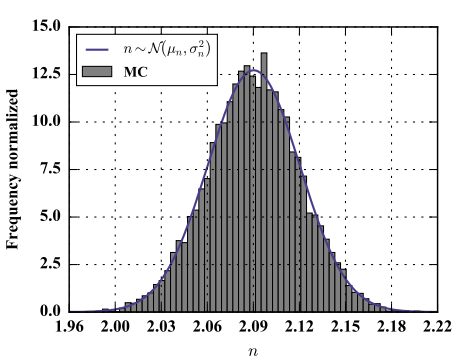

(a) $n \sim \mathcal{N}\left(\mu_n, \sigma_n^2\right)$.

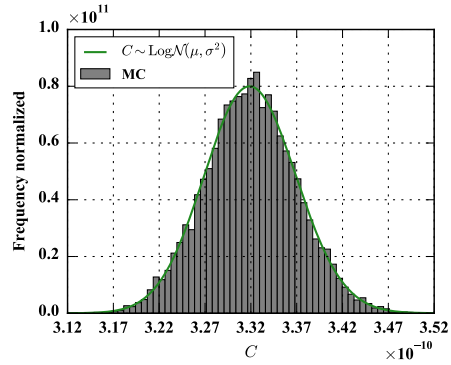

(b) $C \sim \text{Log}\mathcal{N}\left(\mu, \sigma^2\right)$.

Figure 4.14. Marginal PDFs and histograms of MC drawns of n and C r.v.s.

The random variable bending moment in a railway axle M (ii), is assumed as a random input variable normally distributed as shown in Fig. 4.15.

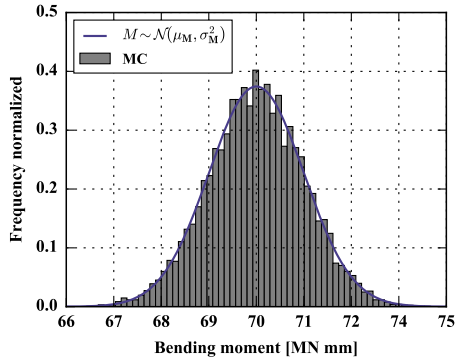

Figure 4.15. PDF of the normal distribution of M, $M \sim \mathcal{N}\left(\mu_M, \sigma_M^2\right)$.

The single source of variability from M induces variability on the bending stress, and therefore there is variability when combined with the interference stress. The bending stress distribution normal to the crack surface shown in Fig. 4.9 was considered as the reference bending stress amplitude for the mean value of bending moment. Both the bending and the interference stresses needed for the SIF evaluation, were calculated via the FEM. Accordingly, the SIFs were also stochastic, and given the axle cyclic rotary character, they were described as two r.v.s K_{max} and K_{min} that are correlated with an inverse relation, when one of them increases, the other decreases in the same proportion. It can be seen that the Pearson's correlation coefficient is $\text{PCC}_{K_{max},K_{min}} = -1$. The two r.v.s are correlated variables, so they are not independent. For illustrative purposes, the bivariate Normal distribution that emerges and its projections in three orthogonal planes are shown in Fig. 4.16. In this case, all realizations of (K_{max}, K_{min}) lie on the straight line that has zero area and thus, they actually do not have a Normal joint density function. They are still, however, said to have a bivariate Normal distribution.

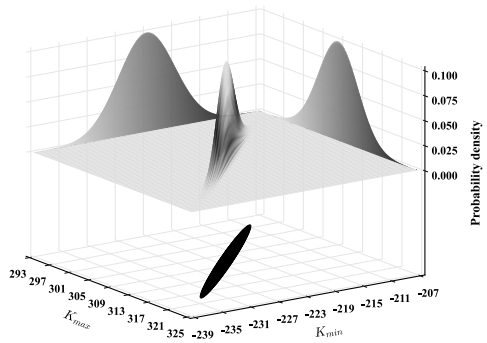

Figure 4.16. Surface of the bivariate Normal–Normal joint density function (K_{max}, K_{min}).

The marginal PDFs of the normally distributed K_{max} and K_{min} modelled and the histograms of the drawns sampled in the MC are presented in Fig. 4.17.

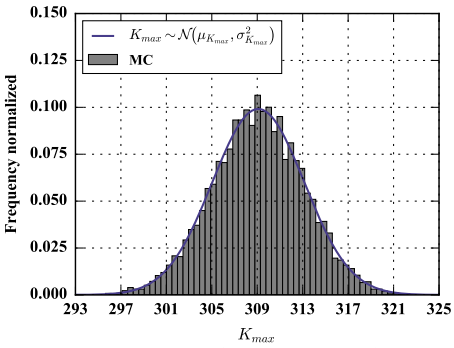

(a) $K_{max} \sim \mathcal{N}\left(\mu_{K_{max}}, \sigma^2_{K_{max}}\right)$.

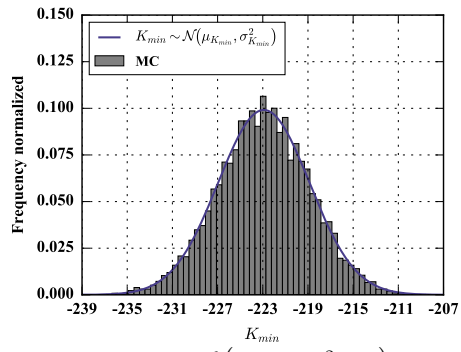

(b) $K_{min} \sim \mathcal{N}\left(\mu_{K_{min}}, \sigma^2_{K_{min}}\right)$.

Figure 4.17. Marginal PDFs and histograms of MC drawns of K_{max} and K_{min} r.v.s.

The mean value and the variance of the r.v. bending moment M assumed, and of the SIFs K_{max} and K_{min}, that are consequently random, are enclosed in Table 4.3.

Table 4.3. Bending moment M, K_{max} and K_{min} mean and variance.

r.v.	μ		σ^2	
M	70.35	[MN mm]	1.11	$[\text{MN mm}]^2$
K_{max}	308.62	$[\text{MPa}\sqrt{\text{mm}}]$	15.87	$[\text{MPa}\sqrt{\text{mm}}]^2$
K_{min}	−222.61	$[\text{MPa}\sqrt{\text{mm}}]$	15.87	$[\text{MPa}\sqrt{\text{mm}}]^2$

Regarding the random variable threshold stress intensity factor range at $R = 0$, ΔK_{th0} (iii), there is not a clear consensus about what probability distribution is most suitable. For instance, its distribution is considered normal in [90], log-normal in [92] and both normal and log-normal in [55]. In consequence, following the latter consideration, both scenarios are considered here. The ΔK_{th0} is assumed as a random input variable normally distributed and also as a random input variable log-normally distributed. In order to differentiate when the normal or the log-normal distribution is used, the enumerated as (iii) refers by default to the normal and with an asterisk (iii*) refers to the log-normal case. The normal distribution (iii) and the log-normal distribution (iii*) assumed are shown in Fig. 4.18.

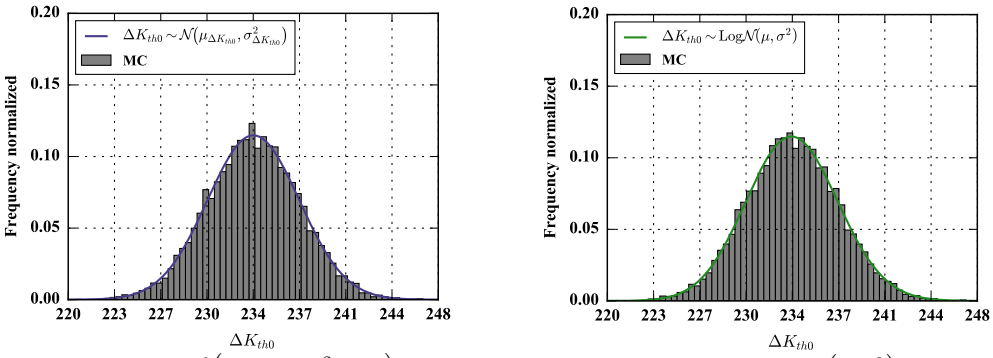

(a) $\Delta K_{th0} \sim \mathcal{N}\left(\mu_{\Delta K_{th0}}, \sigma^2_{\Delta K_{th0}}\right)$. (b) $\Delta K_{th0} \sim \text{Log}\mathcal{N}\left(\mu, \sigma^2\right)$.

Figure 4.18. PDFs and histograms of MC drawns of ΔK_{th0} r.v. assuming normal and log-normal.

The above assumptions are not the only ones possible, as the proposed FSOA method is open to any choice of input variability, distributions type, and relationships of correlation or dependence among r.v.s. Alternative statistical assumptions can be adopted and their effects directly assessed.

To recapitulate, the resulting parameters for the normal and for the log-normal PDFs are collected in Table 4.4.

Table 4.4. Random variables probability distribution parameters: shape, location, scale, and PCC.

r.v.	Prob. distr.	Shape	Location	Scale	PCC
n	Normal	-	2.09 $(=\mu_n)$	3.1400×10^{-2} $(=\sigma_n)$	$\}-0.9679$
C	Log-normal	1.4999×10^{-2} $(=\sigma)$	0.00 $(=\lambda)$	3.3193×10^{-10} $(=e^{\mu})$	
K_{max}	Normal	-	308.62 $(=\mu_{K_{max}})$	3.98 $(=\sigma_{K_{max}})$	$\}-1.0$
K_{min}	Normal	-	-222.61 $(=\mu_{K_{min}})$	3.98 $(=\sigma_{K_{min}})$	
ΔK_{th0}	Normal	-	233.70 $\left(=\mu_{\Delta K_{th0}}\right)$	3.51 $\left(=\sigma_{\Delta K_{th0}}\right)$	-
ΔK_{th0}	Log-normal	1.4999×10^{-2} $(=\sigma)$	0.00 $(=\lambda)$	233.67 $(=e^{\mu})$	-

Note that the Pearson's correlation coefficient obtained from [89] is computed using the natural logarithm $\ln(C)$, $\text{PCC}_{n,\ln(C)} = -0.968$, and here the $\text{PCC}_{n,C} = -0.9679$ makes reference to C. Note further that in the two log-normal distributions, μ and σ are the expected value (or mean) and standard deviation of the natural logarithm of the variable, not the expectation and standard deviation of the variable itself.

Based on the previous r.v.s grouped in (i) $\{n, C\}$, (ii) $\{K_{max}, K_{min}\}$, and (iii) $\{\Delta K_{th0}\}$, there are eight distinct combinations of r.v.s, subsets, including the empty set. The empty case would be the deterministic case as there is not any random variable. Additionally, the special case of ΔK_{th0} considered as log-normal is included (iii*). As a result, the eight case scenarios that arise considering different combinations of r.v.s are the following:

- (i) $\{n, C\}$
- (ii) $\{K_{max}, K_{min}\}$
- (iii) $\{\Delta K_{th0} \sim \mathcal{N}\}$
- (iii*) $\{\Delta K_{th0} \sim \text{Log}\mathcal{N}\}$
- (i) & (ii) $\{n, C, K_{max}, K_{min}\}$
- (i) & (iii) $\{n, C, \Delta K_{th0}\}$
- (ii) & (iii) $\{K_{max}, K_{min}, \Delta K_{th0}\}$
- (i) & (ii) & (iii) $\{n, C, K_{max}, K_{min}, \Delta K_{th0}\}$

The strategy presented carefully models the physical relationships among the random variables. Note that it considers the randomness of n and the randomness of C jointly. It also applies to the r.v.s K_{max} and K_{min}. These are not arbitrary options as they are jointly distributed in pairs, so a realistic probabilistic calculation or MC simulation must consider or sample from their bivariate distributions.

4.4 Putting It All Together (PIAT)

The title of this section, "Putting It All Together (PIAT)", intends to have several meanings. First, it is especially devoted to giving a deeper understanding of all the ideas presented previously, illustrating the course of the reasoning for building a link between the FSOA applied on the FCG phenomenon and the DTA of railway axles to define inspection intervals. Second, this title refers to the eighth case scenario, that is, the combination of (i) & (ii) & (iii) that builds the set $\{n, C, K_{max}, K_{min}, \Delta K_{th0}\}$. The putting it all together (PIAT) acronym, clearly refers to the consideration of all the r.v.s together in the study. This case is the most comprehensive set, and therefore it is used as the backbone when exemplifying the work-flow of the calculation, and again, promoting a deep understanding of the r.v.s influence. Since the goal of DTA is to inform the maintenance decision makers about the impacts of a particular inspection interval, it is important to integrate into the overall methodology the uncertainties involved in the fatigue process regarding the random input variables. Third, the title could refer to putting the chapters of this thesis all together. After all, I am a doctoral student so I do what I am intended to do. Thus, this is a suitable title for the section that celebrates and concludes my cumulative work. Despite these three separate meanings, they all support the same point, namely, that our field, probabilistic fatigue, is moving towards putting it all together. We have to be thoughtful now that we use this probabilistic approach wisely seeing the richness of some of the scenarios that we are presenting.

This section is organized as follows. Subsection 4.4.1 presents the MC results for the probabilistic analysis in the PIAT case. They are used as the framework for comparison in the subsequent subsections. In Subsection 4.4.2, the accuracy of the probabilistic NASGRO equations (Pr. Eqs.) obtained using the FSOA method for the PIAT combination of r.v.s is checked. The history values of the first four moments of the fatigue crack growth life N obtained using the FSOA are compared with those obtained by the MC. The purpose of presenting this case is to elucidate the strategy proposed and make clear that it can well predict the expected value μ_N, standard deviation σ_N, skewness γ_{1_N} and kurtosis β_{2_N}, of the fatigue lifetime N based on NASGRO model. Furthermore, Subsection 4.4.3 checks the precision of the developed methodology not only for the PIAT case but also, for all the eight case scenarios that arise considering the different combinations of r.v.s. For the sake of simplicity, the comparison is done in terms of the first four moments of N for a crack depth a equal to 50 mm. Subsection 4.4.4 illustrates the estimation of the distribution parameters from the prescribed moments of the lifespan provided by the FSOA, in order to fit probability distributions considering the PIAT case. In addition, the quality of PDF constructed with the Pearson distribution in comparison with the histogram from the MC method is discussed. Subsection 4.4.5 defines the inspection intervals

based on the conservative lifespan estimation obtained from the Pearson distribution of the fatigue life N fitted using the FSOA moments for the PIAT case. Finally, Subsection 4.4.6 concludes with the computation and discussion of the probabilities of successful inspections according to the suggested inspection intervals for the PIAT case, by means of quantifying the probability of crack detection calculated according to the performance of the NDT techniques frequently used in the railway industry.

4.4.1 Monte Carlo (MC) results

The example presented here deals with the fatigue crack growth in a railway axle defined in Section 4.2. The geometry is defined in Fig. 4.1 and the initial crack assumed was of 2 mm in the T-transition. The MC method was applied to obtain the probability distribution of the NASGRO model, Eq. (3.1), with the set of five input random variables $\{n, C, K_{max}, K_{min}, \Delta K_{th0}\}$, that is, for the PIAT case in Section 4.3.

There are several sources of variability from all the r.v.s in the PIAT case, constituting the set $\{n, C, K_{max}, K_{min}, \Delta K_{th0}\}$. The n and C r.v.s for each of the MC simulations were repeatedly randomly sampled from the bivariate Normal–Log-normal distribution shown in Fig. 4.13. Using the same approach, the ΔK_{th0} r.v. was repeatedly randomly sampled from the normal distribution shown in Fig. 4.18a. The remaining deterministic material properties were those enclosed in Table 4.1.

On the other hand, there was an additional source of variability from the bending moment M. It induced variability on the bending stress, and therefore there was variability in the combination of the bending with the interference stress in Fig. 4.9. As explained, the SIFs were also stochastic, and given the axle cyclic rotary character, they were described as two random variables K_{max} and K_{min} that are correlated. Then, the K_{max} and K_{min} r.v.s, which are explicitly involved in the NASGRO equation, were repeatedly randomly sampled from the bivariate Normal distribution shown in Fig. 4.16. Additionally, under realistic service conditions, the axles of rail vehicles do not experience long periods of uniform amplitude loading, they are instead subjected to a stress spectrum. Therefore, the sampled K_{max} and K_{min} r.v.s were further modulated taking into account the loading spectrum acting on a railway axle over its service shown in Fig. 4.3. As a result of the spectrum combined with the randomness of the load, different number of blocks are eventually damaging, i.e. contribute to the crack growth.

With the aim of founding the appropriate framework for comparison of the developments within this thesis regarding the FSOA, 10 000 MC simulations were performed providing the results shown in Fig. 4.19. The plot in Fig. 4.19-bottom, shows the different evolutions of the crack depth vs. the number of km for each realization, and it also represents by a red line the computed mean value. The graph in Fig. 4.19-top, shows the histogram, frequency normalized, of the random output variable fatigue

life N for a crack depth equal to 50 mm. Notice that each MC simulation is equally likely, referred to as a realization, as described in Subsection 1.4.1.

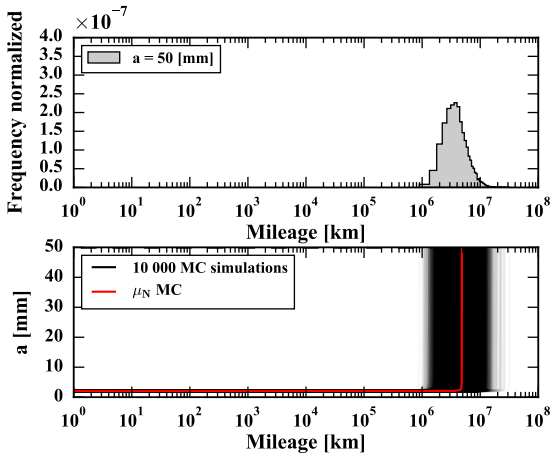

Figure 4.19. Crack depth evolution vs. the number of km (bottom) and histogram, frequency normalized, for crack depth equal to 50 mm (top).

The underlying probability distribution of N differs from a normal distribution according to a normality test based on [153]. It tests the null hypothesis that a sample comes from a normal distribution combining skew and kurtosis to produce an omnibus test of normality. To give insight into the non-normally distributed fatigue life N, a normal probability plot is shown in Fig. 4.20. The deviations from the straight line indicate departures from normality and they evidence the typical inverted C shape of a right-skewed distribution.

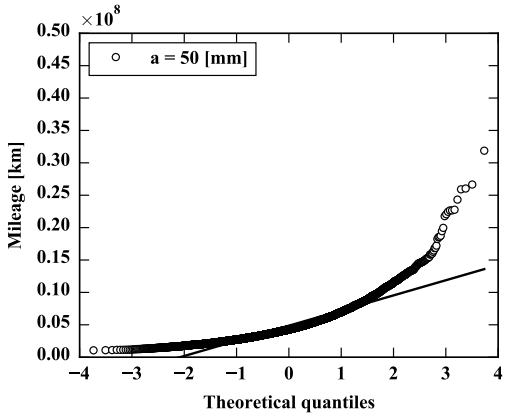

Figure 4.20. Normal probability plot of the number of km N provided by the MC for crack depth of 50 mm and the least squares fit line of the data.

Further analysis regarding the nature of the underlying distribution of N will be done in the subsections below when reconstructing the probability density function from prescribed moments.

The probability distribution of the fatigue life N can be analysed for every crack depth a into the 2–50 mm interval. The expected value μ_N, standard deviation σ_N, skewness γ_{1_N} and kurtosis β_{2_N} are computed. The history values of these moments of N are collected over the entire interval for subsequent comparison.

4.4.2 Full Second Order Approach (FSOA) results

The FSOA was applied to calculate the first moment, the second central moment, the third central moment and the fourth central moment of dN^i at every crack depth, Eq. (3.12), with the set of five input random variables $\{n, C, K_{max}, K_{min}, \Delta K_{th0}\}$, that is, for the PIAT case in Section 4.3. Then, the expected value μ_N, the variance σ_N^2, the skewness γ_{1_N}, and the kurtosis β_{2_N} of the fatigue life N were obtained from the i^{th} moments, providing a continuous result along the crack depth a. To gain further insight into the FSOA, see the Appendix C for the derived mathematical formulation of the expected value, the variance, the third central moment, and the fourth central moment, of the discretised NASGRO equation, for the consideration of only the two random variables K_{max} and K_{min} for the sake of simplicity. The results provided by the proposed methodology were compared with the results of 10 000 MC simulations. The MC results in Subsection 4.4.1 are considered here for checking the statistical moments computed via the FSOA.

To check the accuracy of the method in terms expected value μ_N, standard deviation σ_N, skewness γ_{1_N}, and kurtosis β_{2_N}, the history values of these moments of N, provided by the Monte Carlo (MC) and by the probabilistic NASGRO equations (Pr. Eqs.) obtained using the FSOA method for the PIAT combination of r.v.s are compared in Fig. 4.21. Note that Fig. 4.21a also includes the deterministic Det. number of km for the mean values of the r.v.s. Note further that the standard deviation is reported instead of the variance in Fig. 4.21b even though the variance is more convenient when developing the probabilistic formulations, since the standard deviation has the convenience of being expressed in units of the original variable, so it is more meaningful to interpret. Similarly, the use of the skewness and the kurtosis in Fig 4.21c and Fig 4.21d is more suitable for interpreting that the third and fourth central moments respectively.

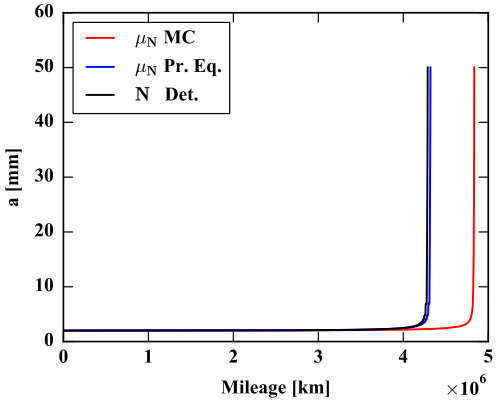

(a) Expected value of N and the Det. N.

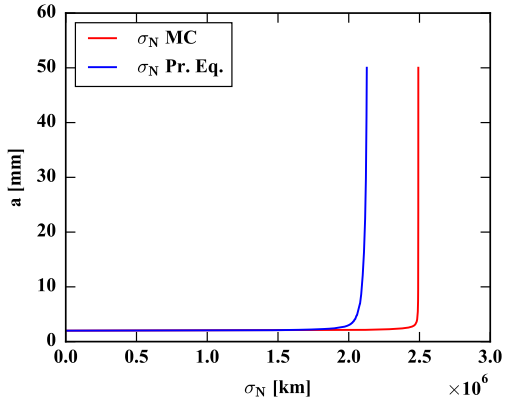

(b) Standard deviation of N.

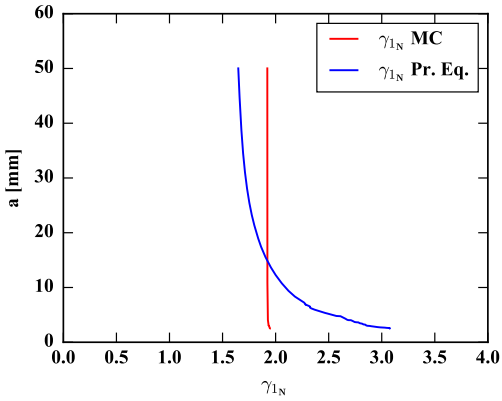

(c) Skewness of N.

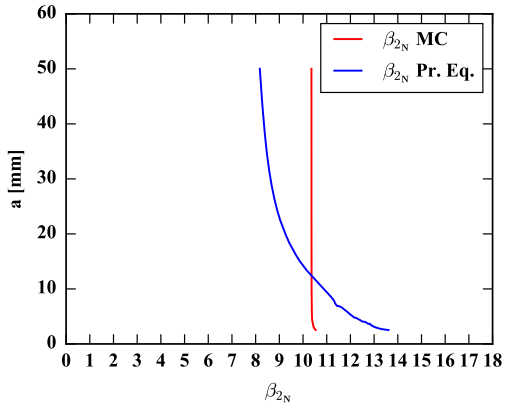

(d) Kurtosis of N.

Figure 4.21. History values of the moments of N for the PIAT combination of r.v.s, provided by the MC and by the PrEqs.

The values of the first to fourth moments in Fig. 4.21 provided by MC and by the corresponding probabilistic equation (Pr. Eq.) for 10–50 mm crack depths are listed below. The results of expected value and the Det. fatigue life in in Fig. 4.21a are listed in Table 4.5. Moreover, the results of standard deviation in Fig. 4.21b are listed in Table 4.6. Furthermore, the values of skewness in Fig. 4.21c are listed in Table 4.7. Lastly, the kurtosis results in Fig. 4.21d are listed in Table 4.8.

Table 4.5. Expected value of N for PIAT case provided by MC and by the Pr. Eq. and fatigue life according to the Det.

a [mm]	MC μ_N [km]	Pr. Eq. μ_N [km]	Det. N [km]	Pr. Eq.-MC Error [%]	Det.-MC Diff. [%]
10	4 823 669	4 278 083	4 275 831	−11.31 %	−11.36 %
20	4 830 083	4 282 748	4 280 403	−11.33 %	−11.38 %
30	4 832 836	4 286 441	4 284 032	−11.31 %	−11.36 %
40	4 834 329	4 288 400	4 285 964	−11.29 %	−11.34 %
50	4 835 142	4 289 469	4 287 044	−11.29 %	−11.34 %

Table 4.6. Standard deviation of N for PIAT case provided by the MC and by the Pr. Eq. for the variance calculation.

a [mm]	MC σ_N [km]	Pr. Eq. σ_N [km]	Pr. Eq.-MC Error [%]
10	2 490 623	2 092 753	−15.97 %
20	2 491 300	2 113 007	−15.18 %
30	2 491 499	2 121 396	−14.85 %
40	2 491 606	2 125 215	−14.71 %
50	2 491 670	2 127 529	−14.61 %

Table 4.7. Skewness of N for PIAT case provided by the MC and by the Pr. Eq.

a [mm]	MC γ_{1_N} [-]	Pr. Eq. γ_{1_N} [-]	Pr. Eq.-MC Error [%]
10	1.9226	2.0906	8.74 %
20	1.9221	1.8194	−5.34 %
30	1.9219	1.7169	−10.67 %
40	1.9218	1.6733	−12.93 %
50	1.9218	1.6481	−14.24 %

Table 4.8. Kurtosis of N for PIAT case provided by the MC and by the Pr. Eq.

a [mm]	MC β_{2_N} [-]	Pr. Eq. β_{2_N} [-]	Pr. Eq.-MC Error [%]
10	10.3608	10.8652	4.87 %
20	10.3569	9.2545	−10.64 %
30	10.3557	8.6227	−16.73 %
40	10.3553	8.3473	−19.39 %
50	10.3552	8.1754	−21.05 %

The following observations in terms of central tendency are made on the basis of the expected value curves shown in Fig. 4.21a and listed in Table 4.5. The expected value computed from the MC is considered as the framework of reference for comparison. The error in the Pr. Eq. is about $-11.31\,\%$, staying constant as the crack depth increases. The maximum difference of the Pr. Eq. leads to an expected value about $547\,000\,\mathrm{km}$ lower. The percentage difference of the Det. number of km is about the $-11.35\,\%$ and the maximum difference is less than $550\,000\,\mathrm{km}$, being the Det. value lower. In both cases, the Pr. Eq. and the Det. N are lower than the MC expected value for every crack depth. It can be explained due to the existing right-skewed distribution of N observed previously.

The next outcomes in terms of dispersion are achieved based on the standard deviation curves in Fig. 4.21b and listed in Table 4.6. Again, the standard deviation provided by the MC is considered as reference. It is trivial that the deterministic calculation does not account the variability of the response, and then it does not provide standard deviation results. It can be observed from the MC results that the larger the crack, the more the variability in km. The Pr. Eq. also reproduces this tendency. The error in the Pr. Eq. ranges from -15.97 to -14.61 %, decreasing in magnitude as the crack depth increases. The maximum difference of the Pr. Eq. calculates a standard deviation about $397\,800\,\mathrm{km}$ lower. The results in terms of standard deviation provided by the Pr. Eq. are lower than the MC for every crack depth, that is, in this case, the method underestimates the dispersion.

The following observations are made based on the skewness results in Fig. 4.21c and in Table 4.7. Once again, the skewness computed from the MC is considered as the framework of reference for comparison. It is observed that the skewness values are always positive, indicating that the right tail, in a sense, is longer and or heavier than the left one. Additionally, it can be seen that as the crack depth increases the skewness decreases reaching a value greater than 1.6 in both calculations. The range of results is wider in the case of the Pr. Eq. than in the case of the MC and also the two curves intercept before reaching their stabilization in magnitude. The error in the Pr. Eq. ranges from 8.74 to -14.24 % as the crack depth increases. The Pr. Eq. provides a slightly lower magnitude than the MC for crack depths approximately larger than $15\,\mathrm{mm}$. The maximum difference of the Pr. Eq. calculates a skewness about 0.27 lower.

The next outcomes are related to the kurtosis results in Fig. 4.21d and in Table 4.8. Once more, the kurtosis provided by the MC is considered as reference. It is observed that the larger the crack the lower kurtosis and, in both calculations, a stabilization in magnitude is reached. The error in the Pr. Eq. ranges from 4.87 to -21.05 % as the crack depth increases. The Pr. Eq. provides a slightly lower magnitude than the MC for crack depths approximately larger than $15\,\mathrm{mm}$. The maximum difference of the Pr. Eq. calculates a kurtosis about 2.18 lower.

Gathering the observations from the results together, the next outcomes are obtained:

- The expected value, the standard deviation or variance, the skewness, and the kurtosis of the fatigue life N, provided by the MC and by the Pr. Eqs. are really close, even considering the load spectrum acting on a train axle over its service. The errors between the two methods are small enough to consider the accuracy of the proposed FSOA method fully acceptable, from an engineering perspective.

- The key advantage of the proposed FSOA is the lower computational time, similar to that required for a deterministic calculation. Therefore, due to the acceptable accuracy and the computational efficiency, the FSOA method outperforms the conventional MC method. So, this method is considered to be advantageous compared to the conventional MC method.

- The output distribution of N shown in the example is not normally distributed, despite the fact that it considers several normal r.v.s as inputs.

- The probabilistic formulations provide a better description of the full complexity of fatigue crack propagation processes when compared with the partial information given by the deterministic one. The probabilistic approach presented aims to reflect the railway axle lifetimes under service conditions.

At this point, the full second-order approach (FSOA) application for the first to fourth moments of the NASGRO equation considering the PIAT random variables $\{n, C, K_{max}, K_{min}, \Delta K_{th0}\}$ is completed. As a result, the history values of these moments of N, i.e. the expected value μ_N, standard deviation σ_N, skewness γ_{1_N}, and kurtosis β_{2_N}, of the underlying lifespan probability distribution are available.

4.4.3 Summary and comparison of the eight case scenarios

This subsection broadens the accuracy check of the FSOA method described in Subsection 4.4.2. There, the history values of the first four moments of fatigue life N provided by the FSOA and by the MC for the PIAT combination of r.v.s were compared. Here, the precision of the results is further checked for all the eight case scenarios that arise considering the different combinations of r.v.s in Section 4.3. Each case is calculated using respective MC simulations and, once again, the results are considered for checking the statistical moments computed via the FSOA for the corresponding case. In addition to the accuracy check, the results provided here further illustrate the effects of the different random variables individually and their interactions when combined, on the output random variable, fatigue life N.

To check the accuracy of the FSOA, the expected value μ_N, standard deviation σ_N, skewness γ_{1_N} and kurtosis β_{2_N}, provided by the MC and by the Pr. Eqs. for all the combinations of r.v.s are compared in Fig. 4.22. This time, for the sake of simplicity, the comparison is done in terms of the first four moments of N for a crack depth a equal to 50 mm. Note that the errors between the Pr. Eq. and the MC are annotated for each of the result points. In addition, the coefficient of variation c_{v_N} is also calculated as the ratio of the σ_N to the μ_N. The c_{v_N} is shown in Fig. 4.23.

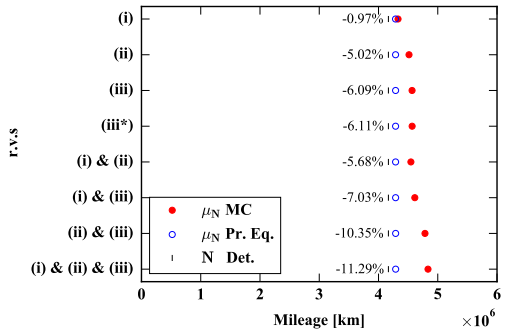

(a) Expected value of N and the Det. N.

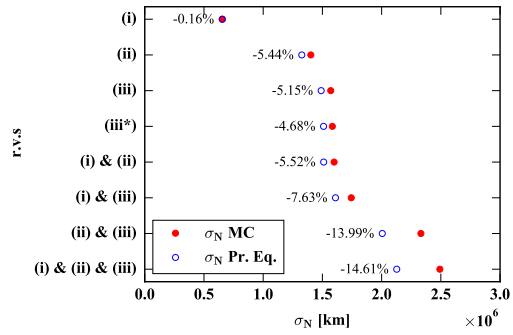

(b) Standard deviation of N.

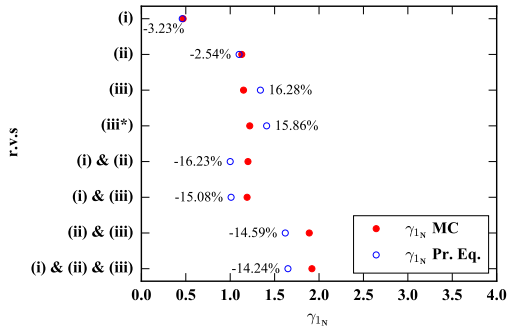

(c) Skewness of N.

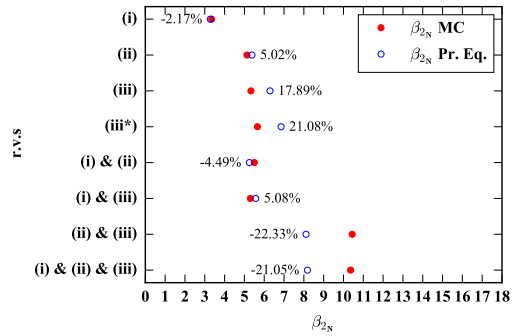

(d) Kurtosis of N.

Figure 4.22. Summary of the moments of N for a crack depth equal to 50 mm for all combinations of r.v.s considered, using the MC and the Pr. Eqs.

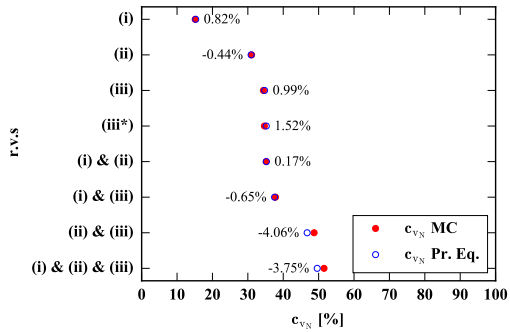

Figure 4.23. Summary of the coefficient of variation of N for a crack depth equal to 50 mm.

The values of the first to fourth moments in Fig. 4.22 provided by MC and by the Pr. Eqs. for all the combinations of r.v.s considered, can be found below. The results of expected value in Fig. 4.22a and standard deviation in Fig. 4.22b are listed in Tables 4.9 and 4.10.

Table 4.9. Expected value of N provided by MC and by the Pr. Eq. and the Det. fatigue life.

r.v.s† [combination]	a [mm]	MC μ_N [km]	Pr. Eq. μ_N [km]	Det. N [km]	Pr. Eq.-MC Error [%]	Det.-MC Diff. [%]
(i)	50	4 329 546	4 287 392	4 287 044	−0.97 %	−0.98 %
(ii)	50	4 514 673	4 287 909	4 287 044	−5.02 %	−5.04 %
(iii)	50	4 566 256	4 288 257	4 287 044	−6.09 %	−6.11 %
(iii*)	50	4 567 336	4 288 257	4 287 044	−6.11 %	−6.14 %
(i) & (ii)	50	4 546 623	4 288 257	4 287 044	−5.68 %	−5.71 %
(i) & (iii)	50	4 612 654	4 288 605	4 287 044	−7.03 %	−7.06 %
(ii) & (iii)	50	4 784 383	4 289 121	4 287 044	−10.35 %	−10.40 %
(i) & (ii) & (iii)	50	4 835 142	4 289 469	4 287 044	−11.29 %	−11.34 %

† (i)= $\{n, C\}$, (ii)= $\{K_{max}, K_{min}\}$, and (iii)= $\{\Delta K_{th0}\}$ or (iii*) for log-normal case.

Table 4.10. Standard deviation of N provided by MC and by the Pr. Eq. for the variance calculation.

r.v.s† [combination]	a [mm]	MC σ_N [km]	Pr. Eq. σ_N [km]	Pr. Eq.-MC Error [%]
(i)	50	655 124	654 066	−0.16 %
(ii)	50	1 402 147	1 325 913	−5.44 %
(iii)	50	1 570 315	1 489 379	−5.15 %
(iii*)	50	1 583 846	1 509 717	−4.68 %
(i) & (ii)	50	1 598 880	1 510 616	−5.52 %
(i) & (iii)	50	1 743 547	1 610 533	−7.63 %
(ii) & (iii)	50	2 331 541	2 005 390	−13.99 %
(i) & (ii) & (iii)	50	2 491 670	2 127 529	−14.61 %

† (i)= $\{n, C\}$, (ii)= $\{K_{max}, K_{min}\}$, and (iii)= $\{\Delta K_{th0}\}$.

Moreover, the values of skewness in Fig. 4.22c and kurtosis in Fig. 4.22d are listed in Tables 4.11 and 4.12. Furthermore, the results of coefficient of variation in Fig. 4.23 are listed in Table 4.13.

Table 4.11. Skewness of N provided by the MC and by the Pr. Eq.

r.v.s† [combination]	a [mm]	MC γ_{1_N} [-]	Pr. Eq. γ_{1_N} [-]	Pr. Eq.-MC Error [%]
(i)	50	0.47	0.46	−3.23 %
(ii)	50	1.13	1.10	−2.54 %
(iii)	50	1.15	1.34	16.28 %
(iii*)	50	1.22	1.41	15.86 %
(i) & (ii)	50	1.20	1.00	−16.23 %
(i) & (iii)	50	1.19	1.01	−15.08 %
(ii) & (iii)	50	1.89	1.62	−14.59 %
(i) & (ii) & (iii)	50	1.92	1.65	−14.24 %

† (i)= $\{n, C\}$, (ii)= $\{K_{max}, K_{min}\}$, and (iii)= $\{\Delta K_{th0}\}$.

Table 4.12. Kurtosis of N provided by the MC and by the Pr. Eq.

r.v.s† [combination]	a [mm]	MC β_{2_N} [-]	Pr. Eq. β_{2_N} [-]	Pr. Eq.-MC Error [%]
(i)	50	3.35	3.28	−2.17 %
(ii)	50	5.13	5.38	5.02 %
(iii)	50	5.33	6.29	17.89 %
(iii*)	50	5.66	6.85	21.08 %
(i) & (ii)	50	5.50	5.25	−4.49 %
(i) & (iii)	50	5.30	5.57	5.08 %
(ii) & (iii)	50	10.44	8.11	−22.33 %
(i) & (ii) & (iii)	50	10.36	8.18	−21.05 %

† (i)= $\{n, C\}$, (ii)= $\{K_{max}, K_{min}\}$, and (iii)= $\{\Delta K_{th0}\}$.

Table 4.13. Coefficient of variation of N computed using the MC and the Pr. Eq. results.

r.v.s† [combination]	a [mm]	MC c_{v_N} [%]	Pr. Eq. c_{v_N} [%]	Pr. Eq.-MC Error [%]
(i)	50	15.13 %	15.26 %	0.82 %
(ii)	50	31.06 %	30.92 %	−0.44 %
(iii)	50	34.39 %	34.73 %	0.99 %
(iii*)	50	34.68 %	35.21 %	1.52 %
(i) & (ii)	50	35.17 %	35.23 %	0.17 %
(i) & (iii)	50	37.80 %	37.55 %	−0.65 %
(ii) & (iii)	50	48.73 %	46.76 %	−4.06 %
(i) & (ii) & (iii)	50	51.53 %	49.60 %	−3.75 %

† (i)= $\{n, C\}$, (ii)= $\{K_{max}, K_{min}\}$, and (iii)= $\{\Delta K_{th0}\}$.

The next observations in terms of expected value, standard deviation, skewness, kurtosis and coefficient of variation for a crack depth a equal to 50 mm for all the combinations of r.v.s considered, are obtained. Recall that the computed results from the MC are considered as reference for comparison. The analysis describes the general tendency of the results depending on the different r.v.s considered in each case, the global trend and the magnitudes of the moments obtained, and finally, the comparison of errors between the MC and the Pr. Eq. results using the FSOA.

Regarding the expected values in Fig. 4.22a listed in Table 4.9, the MC and the Pr. Eq. method show the same behaviour. The expected value increases from the (i) to (iii*) cases, (i) & (ii), (i) & (iii) and (ii) & (iii) provide higher values than the cases of their basic r.v.s separately, and, the PIAT combination (i) & (ii) & (iii) provides the highest values of all the previous separate cases and combinations. This fact indicates that every time a combination of two or three basic random variables, (i), (ii) and (iii) or (iii*) is considered, the central tendency is higher than when considered separately. On the other hand, the Det. always calculates the same number of km for a given starting condition. It is obvious that the deterministic NASGRO equation does not deal with randomness, and therefore no matter what combination of r.v.s is involved, the Det. value is the same. Focusing on the results, the Det. number of km is always lower that the MC and the Pr. Eq. expected values. Coming back to the MC and the Pr. Eq., the expected values steadily increase from the (i) to the PIAT case, providing a moderate increment of 500 000 km in the MC results while the increment trend in the Pr. Eq. results it is not so pronounced. The magnitudes obtained in terms of km are coherent for the railway axle under study. Lastly, the expected value in the Pr. Eq. gives lower values than in the MC results in all the cases. The error in the Pr. Eq. ranges from -0.9 to -11 % what is considered very good in terms of accuracy.

Concerning the standard deviations in Fig. 4.22b listed in Table 4.10, the MC and the Pr. Eq. method show the same general tendency. The standard deviations always increase from (i) to (iii*) and also when combined from (i) & (ii) to (i) & (ii) & (iii) being the PIAT case the one with the highest standard deviation. This indicates that the (i), (ii) and (iii) or (iii*) turn out to be sorted according to increasing variability of lifespan, and also, that every time a combination of two or three basic random variables is taken into account, the dispersion obtained is higher than when the r.v.s are considered individually. Moreover, the standard deviation steeply increases both in the MC and in the Pr. Eq. from the (i) to the PIAT case, providing a high increment of 1 800 000 km in the MC results and an also high increment approximately of 1 400 000 km in the Pr. Eq. results. The magnitudes of the dispersion obtained are considered quite significant. Ultimately, the standard deviation provided by the Pr. Eq. is lower than the one provided by the MC. The error in the probabilistic equation ranges from -0.1 to -14 % what is considered good in terms of accuracy.

Regarding the skewness values in Fig. 4.22c listed in Table 4.11, both the MC and the FSOA increase form (i) to (iii*). In the MC, the combinations (i) & (ii), (i) & (iii) and (ii) & (iii), provide higher values than the corresponding cases individually. On the other hand, the FSOA for the (i) & (ii) case gives lower skewness than the individual case (ii) as a result of its interaction with (i). The same effect occurs in the combination of (i) with (iii). Then, the combination (ii) & (iii) gives higher values than (ii) and (iii) separately as well as in the MC. In both the MC and the FSOA, the values of the PIAT case, (i) & (ii) & (iii), are the highest of all the previous individual and combinations of r.v.s. Besides, the skewness values slightly alternate both in the MC and in the Pr. Eq. results, all the same, the general trend is to increase from the (i) to the (i) & (ii) & (iii) providing a high increment of 1.4 in the MC results and an also high increment of 1.2 in the Pr. Eq. values. The magnitudes of the measure of the asymmetry obtained are thought to be moderate. Eventually, the skewness provided by the Pr. Eq. mostly estimates a lower value than the MC but occasionally gives a higher value, (iii) and (iii*) cases. The error in the probabilistic equation ranges from −16 to 16 % what is considered acceptable in terms of accuracy. Note that due to the low magnitude of the skewness the errors vary sharply.

Concerning the kurtosis values in Fig. 4.22d listed in Table 4.12, both the MC and the FSOA increase form (i) to (iii*). In the MC, the combination (i) & (ii) provides a bit higher kurtosis than (i) and (ii) separately, the (i) & (iii) a bit lower than (i) and (iii) separately, and again, the (ii) & (iii) results are higher than (ii) and (iii) separately, and last of all, the (i) & (ii) & (iii) case provides higher kurtosis than all cases except for the (ii) & (iii), as a result of its interaction with (i). On the other hand, the FSOA for the combinations (i) & (ii) and (i) & (iii) give a bit lower kurtosis than the corresponding r.v.s separately, and again, the (ii) & (iii) results are higher than (ii) and (iii) separately, and finally, the PIAT combination, (i) & (ii) & (iii), provides the highest kurtosis. Furthermore, the kurtosis values slightly fluctuate both in the MC and in the Pr. Eq., but the general trend is to increase from the (i) to the PIAT case, providing a high increment of 7.0 in the MC results and an also high increment of 4.8 in the Pr. Eq. results. The magnitudes of the measure of the tailedness obtained are thought to be fairly significant. At last, the kurtosis calculated by the Pr. Eq. approach, half of the times gives lower values, (i), (i) & (ii), (ii) & (iii), and (i) & (ii) & (iii), and half of the times gives higher values, (ii), (iii), (iii*) and (i) & (iii) cases. The error in the probabilistic equation ranges from −22 to 21 % what is considered acceptable in terms of accuracy. Note that due to the low magnitude of the kurtosis the errors vary steeply.

Regarding coefficients of variation in Fig. 4.23 listed in Table 4.13, as explained, they are calculated as the ratio of the standard deviation σ_N to the expected value μ_N, and due to the observations regarding the expected value and standard deviation, they always increase from (i) to the PIAT case, (i) & (ii) & (iii), resulting the highest value in the PIAT case scenario, for both the MC and the Pr. Eq. method. In

addition, it markedly increases from the (i) to the PIAT case in the 15–50 % range for both the MC and the Pr. Eq. approaches. The magnitudes obtained, showing the extent of the variabilities in relation to the expected values, are reasonable. Lastly, the coefficient of variation Pr. Eq. results, half of the times gives lower values, (ii), (i) & (iii), (ii) & (iii), and (i) & (ii) & (iii), and half of the times gives higher values, (i), (iii), (iii*), (i) & (ii) cases. The error in the probabilistic equation ranges from −4.0 to 1.5 % what is considered fully acceptable in terms of accuracy.

In short, the effect of the different r.v.s in the fatigue lifespan N and their interactions when combined have been interpreted. The results demonstrated that:

- Definitely, there is a general agreement between the results provided by the MC and the ones obtained through the FSOA method.
- The accuracy of the fatigue lifetime moments obtained via the FSOA presented, and its efficiency when compared to an equivalent MC method analysis, prove the good performance of the proposed approach.
- The selection of the most comprehensive set of r.v.s, the PIAT case, as backbone to exemplify the work-flow of the calculation is further justified. This is because in this case, high values of expected value, standard deviation, skewness and kurtosis emerge, and therefore the PIAT case is suitable for checking and proving the validity of the FCG methodology in the DTA of railway axles.

4.4.4 Probability distribution reconstruction

At this point, the FSOA part of the methodology presented in Chapter 2 is completed. As a result, the first to fourth moments of the underlying lifespan probability distribution are available for the set of five input random variables $\{n, C, K_{max}, K_{min}, \Delta K_{th0}\}$, that is, for the PIAT case in Section 4.3. Recapitulating, the moments of fatigue life N provided by the probabilistic NASGRO equations for a crack depth a equal to 50 mm are enclosed in Table 4.14.

Table 4.14. Expected value, standard deviation, skewness and kurtosis of N provided by the Pr. Eqs.

	Pr. Eq.	Pr. Eq.	Pr. Eq.	Pr. Eq.
a	μ_N	σ_N	γ_{1_N}	β_{2_N}
[mm]	[km]	[km]	[-]	[-]
50	4 289 469	2 127 529	1.6481	8.1754

Note that the square root of the variance, i.e. the standard deviation σ_N, is reported instead of the variance σ_N^2 even though the variance is more convenient when developing the probabilistic formulations. This is because the standard deviation is more meaningful to interpret since it is expressed in units of the original variable.

The next part of the methodology addresses the problem of fitting a probability distribution from prescribed moments of the lifespan provided by the FSOA for the PIAT r.v.s. In this case, it is possible to construct probability distributions with more than two parameters given that the first four moments are available. To check the benefits of the uncertainty propagation methodology presented in terms of life distributions, three scenarios were considered: (i) the lifespan was assumed to be normally distributed; (ii) the lifespan was assumed to be log-normally distributed; and (iii) the Pearson distribution family was used to model the lifespan, thus avoiding the need of assuming a distribution in advance. The Pearson family is compared with the other two scenarios to verify that the proposed improvements contribute to a better knowledge of the distribution of fatigue life. For that purpose, the three probability functions were constructed as described below from the moments in Table 4.14.

In the normal case (i), the PDF for the lifespan N is assumed to be normally distributed, and therefore it is derived from the well-known PDF for the standard normal distribution $\phi(x)$. Specifically, the PDF is parametrized in terms of a location parameter which is directly the expected value of the fatigue life N, and a scale parameter which is directly the square root of the variance, i.e. the standard deviation of the random output variable fatigue life N. As a result, the lifespan N distributed normally is characterised by the PDF $f_N(N;\mu_N,\sigma_N)$, where μ_N and σ_N are fixed parameters. Notice that to fit the normal distribution only the first raw moment and the second central moment are needed.

In the log-normal case (ii), the PDF for the lifespan N is assumed to be log-normally distributed, and therefore it is derived from the standardized form for the log-normal PDF $f(x;\sigma)$ with σ as a shape parameter. Commonly, the PDF is further parametrized in terms of a location parameter λ and a scale parameter e^{μ}. The location parameter λ was set equal to zero, hence only two parameters remain to be estimated. The physical meaning of the location parameter is realistic since it indicates that crack growth occurs after any given cycle and so the support of the distribution is non-negative. The shape σ and the scale e^{μ} parameters of the log-normal are functions of the expected value and the variance of the fatigue life N. As a consequence, the lifespan N distributed log-normally is described by the PDF $f_N(N;\sigma,\lambda,e^{\mu})$ where σ, λ and e^{μ} are fixed parameters. Note that in consequence to fit the log-normal distribution only the first raw moment and the second central moment are needed.

In case (iii), the Pearson distribution type was automatically determined based on the skewness and kurtosis, more specifically, the quantities $\beta_{1_N} = \gamma_{1_N}^2$ and β_{2_N} as it is described in Section 3.3. In the PIAT example, the procedure leads to the Pearson type VI that corresponds to the beta prime distribution. Afterwards, the parameters of the beta prime distribution were estimated making the statistical moments of the constructed lifespan distribution match the first four prescribed moments predicted by the Pr. Eq. provided by the FSOA. In this case, the PDF for

the lifespan N beta prime-distributed is derived from the standardized form for the beta prime PDF $f(x;\alpha,\beta)$ in Eq. (4.1) with α, β as shape parameters and where Γ is the gamma function $\Gamma(x) = (x-1)!$. Once again, the PDF is further parametrized by introducing two parameters representing the location and the scale. The shape parameters α and β, the scale and the location parameter λ were calculated by using the closed form expressions described in Section 3.3 that express the parameters as function of the first four moments of the fatigue life N distribution. Recall that in these expressions the expected value μ_N or first raw moment is denoted as μ_1'. As a result, the lifespan N following a beta prime distribution is characterized by the PDF $f_N(N;\alpha,\beta,\lambda,a_2-a_1)$ given in Eq. (4.2).

$$f(x;\alpha,\beta) = \frac{\Gamma(\alpha+\beta)x^{\alpha-1}(1+x)^{-\alpha-\beta}}{\Gamma(\alpha)\Gamma(\beta)} \tag{4.1}$$

$$f_N(N;\alpha,\beta,\lambda,a_2-a_1) = \frac{f\left(\frac{N-\lambda}{a_2-a_1};\alpha,\beta\right)}{a_2-a_1} \tag{4.2}$$

Note that in the $f_N(N;\alpha,\beta,\lambda,a_2-a_1)$ PDF the α, β, λ and a_2-a_1 are fixed parameters.

The resulting parameters for the three probability density functions constructed for the PIAT combinations of r.v.s, are collected in Table 4.15.

Table 4.15. Shape, location, and scale parameters computed from the first four moments of the lifespan N for a crack depth equal to 50 mm.

Prob. Distr.	Shape		Location		Scale	
Normal	-		4 289 469	$(=\mu_N)$	2 127 529	$(=\sigma_N)$
Log-normal	0.47	$(=\sigma)$	0	$(=\lambda)$	3 842 763	$(=e^{\mu})$
Pearson type VI (Beta prime)	4.02, 13.15	$(=\alpha,\beta)$	748 774	$(=\lambda)$	10 713 037	$(=a_2-a_1)$

The PDFs of the three aforementioned distributions, and the MC histogram of the fatigue life N for a crack depth equal to 50 mm for the PIAT combinations of r.v.s are compared in Fig. 4.24.

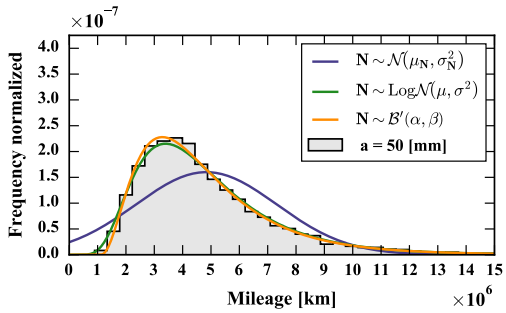

Figure 4.24. Histogram of fatigue life N provided by the MC and PDF of the normal, the log-normal and the beta prime distributions fitted from moments provided by the Pr. Eqs. for 50 mm crack depth.

The histogram of fatigue life N provided by the MC simulations is taken for the comparison of the three PDFs constructed. The differences between the normal distribution and the MC histogram highlight the degree of non-normality and non-symmetry of the underlying lifespan distribution. The log-normal distribution includes a certain degree of asymmetry, and therefore it is a more convenient choice over the symmetrical normal distribution. It can be observed that the log-normal is advantageous to the normal distribution in describing the lower and higher tails of the lifespan, although the degree of asymmetry in the log-normal is not directly defined. On the other hand the beta prime distribution was determined from the Pearson distribution family according to the quantities related to shape β_1 and β_2. It can be observed that the beta prime distribution agrees well with the MC histogram for all the lifespan range, including the tails and also the peak. The superiority of the beta prime and the log-normal distributions over the normal to represent the MC results is clear. Furthermore, the differences between the beta prime and the log-normal distributions are evident especially when describing the lower tail of the distribution of lives, which is of great importance in reliability and in DTA. The behaviour of the normal and the log-normal distributions in the lower tail region slightly underestimate the lifespan. The better tail performance of the beta prime distribution is due to the fact that the first four moments of the lifespan N are matched when estimating the parameters of the Pearson distribution. That is, the PDF using the Pearson distribution family is sensitive to variations in skewness and kurtosis. Besides, the Pearson distribution type is selected depending on the moments that are related to the shape of the underlying distribution, and afterwards the corresponding probability distribution parameters are calculated. On the contrary, the construction of the normal and log-normal distributions does not consider the skewness or kurtosis changes given that their third and fourth moments are not matched to the calculated lifespan N moments. In fact, the normal distribution has 0 skewness and a kurtosis equal to 3 inherently, and the skewness and the kurtosis of the log-normal distribution are determined indirectly once the distribution is defined in terms of the expected value and variance of the lifespan N. Consequently, the quality of the normal and log-normal PDFs is influenced by the similarity between them and the actual lifespan distribution, which is not always known. In other words, the quality can only be good if the lifespan is close to the selected distribution. It must be emphasized that in some applications the normal or the log-normal assumption may be enough, however, the Pearson distribution family still offers a perceptible improvement as the goodness and quality of the PDF constructed is not compromised by an a priori selection or assumption of a probability distribution.

Additionally, a Kolmogorov-Smirnov test [154] was used to measure quantitatively the goodness of fit between the constructed probability distributions and the MC results. The test statistic quantifies the distance between the cumulative distribution functions of the constructed distribution and the cumulative MC histogram of

reference, and therefore the lowest value indicates the best representation of the underlying distribution. On the other hand, the null-hypothesis for the Kolmogorov-Smirnov test is that the distributions are the same, in consequence, the lower the p-value the greater the statistical evidence to reject the null hypothesis and to conclude that the distributions are different. The test statistics and the p-values obtained for the three probability distributions constructed are enclosed in Table 4.16.

Table 4.16. Kolmogorov-Smirnov test statistics and p-values for goodness of fit of the distributions.

Prob. Distr.	Test statistic	p-value
Normal	1.12×10^{-1}	7.81×10^{-109}
Log-normal	1.56×10^{-2}	1.48×10^{-2}
Pearson	8.68×10^{-3}	4.40×10^{-1}

The test statistics obtained for the normal, log-normal, and the beta prime distributions, show that the best representation of the underlying distribution is achieved with the beta prime distribution that arises from the Pearson family, as it gives the smaller magnitude for the test statistic. Additionally, the highest p-value is obtained for the beta prime distribution what supports the statistical evidence that this is the best fit distribution. These values confirm the advantage of the beta prime distribution over the log-normal and the normal distributions to represent the MC results in the case of the PIAT r.v.s combinations.

The following outcomes are drawn from the analysis of the probability distributions obtained by applying the uncertainty propagation methodology:

- The expected value, the variance, the skewness and kurtosis provided by the Pr. Eqs. enable the construction of PDFs with more than two parameters as it is the case of the versatile Pearson distribution family.
- The automatic selection of the Pearson distribution type that is based on the moments of the underlying distribution is a more general procedure than the selection of an arbitrary probability distribution to fit.
- The parameters of the particular Pearson distribution type are directly computed from the moments, using the called method of moments. It makes calculating the parameters of the Pearson distribution type quite simple and fast. At the same time it does not use minimization or maximization algorithms as in the case of optimization procedures used in other existing methods for estimating probability distribution parameters.
- The overall similarity between the Pearson type VI, i.e. the beta prime distribution, and the MC histogram confirms that the Pearson distribution family accurately captures and provides a good description of the underlying lifespan distribution under stochastic conditions.

As mentioned above, the beta prime distribution of the fatigue life N fitted using the FSOA, can be represented by the SF, by the CDF and by the PDF as shown in Fig. 4.25 for the PIAT combinations of r.v.s and for a crack depth equal to 50 mm. The normal and the log-normal distributions are also plotted for comparative purposes. These three functions consider the input variabilities involved in the fatigue problem.

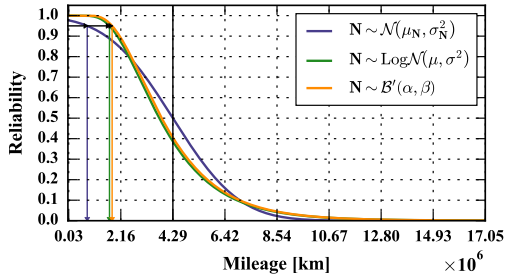

(a) Survival function (SF).

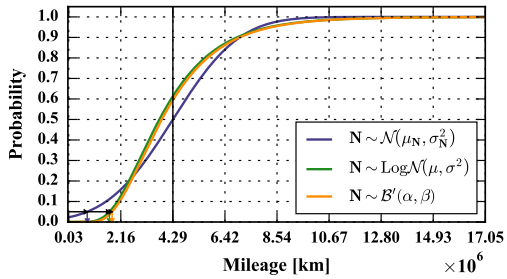

(b) Cumulative distribution function (CDF).

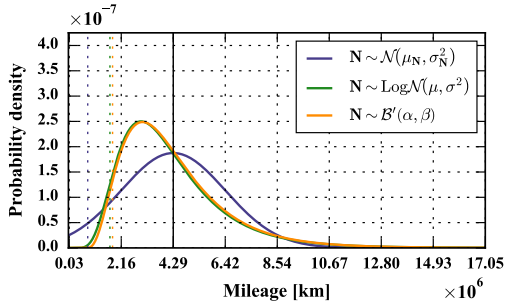

(c) Probability density function (PDF).

Figure 4.25. SF, CDF and PDF of the normal, the log-normal and the beta prime distributions fitted from moments provided by the Pr. Eqs. for 50 mm crack depth for the PIAT r.v.s.

The reliability-based inspection interval definition in Subsection 3.4.3 takes advantage of the probabilistic information contained in Fig. 4.25. The application of the complete procedure is detailed in the following.

4.4.5 Definition of inspection intervals

This subsection defines the inspection intervals based on a conservative estimation of the lifespan obtained from the probability distribution of the fatigue life N for the PIAT case. The probability distribution is fitted as illustrated in Subsection 4.4.4, using the Pearson distribution family together with the FSOA moments. Therefore, the use of probabilistic fracture mechanics and thus probabilistic fatigue life estimation to define inspection intervals for railway axles is introduced in the framework of a damage tolerance concept. At the same time, it enables the analysis of more detailed scenarios that can only be explored with a complete probabilistic approach. In addition, for comparative purposes, the deterministic lifespan calculation is also used as basis for the interval inspection definition. As a result, it is possible to evaluate the inspection intervals obtained according to the traditional, deterministic, and proposed, probabilistic, fatigue life calculation procedures.

First of all, in order to apply the reliability-based inspection interval definition described in Subsection 3.4.3, it is necessary to briefly review the principles and requirements for the safety, serviceability and durability of structures concerning the probability of failure and reliability. The Eurocode EN 1990:2002 standard [155] describes the basis for the design and verification of structures and gives guidelines for related aspects of structural reliability. It provides recommendation for the probability of failure, P_f, and its corresponding reliability index, β, for structural design. It should be emphasized that these values are only notional, and therefore do not necessarily represent the actual failure rates but, they can be used as operational values and for comparison of reliability levels of structures. According to the standard, the equation that relates the probability of failure and the reliability index is as in Eq. (4.3), where Φ represents the cumulative distribution function for the standard normal distribution.

$$P_f = \Phi\left(-\beta\right) \tag{4.3}$$

As for the failure probability of a railway axle, EN 1990:2002 standard [155] defines a reliability index, β, of 3.8 for a construction during the entire life. By using Eq. (4.3), the probability of failure, $P_{f,\ EN\ 1990}$, is $7{\times}10^{-5}$.

The reliability function in this context is theoretically defined as the probability of not failing, i.e. the probability that the crack does not grow up to a final crack depth a_{fin} of 50 mm. Alternatively it can be defined as the probability of survival beyond any specified time, number of cycles or kilometres travelled. To this end, in [25], the reliability is expressed by using an exponential survival distribution, where the probability of failure is the same in every time interval, no matter the age of the axle. The exponential survival distribution is shown in Eq. (4.4), where λ is the failure rate in failures/year.

$$R\left(t\right) = e^{-\lambda t} \tag{4.4}$$

Then, for 30 years of operation that would roughly correspond to a mileage of 10^7 km in a railway axle, the failure rate, $\lambda_{\ EN\ 1990}$, is $2.33{\times}10^{-6}$ failures/year. Hence, on a fleet of a million axles, this would correspond to approximately two axle failures per year. This figure is very close to the present situation in Europe [3]. In order to improve this figure, the failure probability might be reduced one order of magnitude by setting $\lambda = 2.33{\times}10^{-7}$ failures/year, what, doing the calculations in reverse, results in a probability of failure, P_f, equal to $7{\times}10^{-6}$.

In addition to the previous values of P_f, the CEN/TR 17469:2020 technical report [156], states: 'In reliable approaches, the aim is to have a *just necessary* design associated to a probability of failure. For safety critical components, the probability of failure during the lifetime generally vary from 10^{-5} to 10^{-8}. In the example given in [157] on an automotive engine part, the probability is 10^{-6}. For railway safety applications, if one considers that the number of accidents due to mechanical failures is rather small, a probability of failure between 10^{-6} and 10^{-7} sounds reasonable.' Note that the preceding paragraph is taken from the article [158]. Additionally, the observations of the technical committee CEN/TC 256/SC 2/WG 11, also included in the CEN/TR 17469:2020 technical report [156], add: 'The probability of failure value quoted (10^{-6} to 10^{-7}) is a failure rate per axle during its whole life. It is approximately in line with the 10^{-9} failure rate per operational hour defined in the common safety method for risk evaluation and assessment in the EU regulation No 402/2013 [159], for technical systems for which a functional failure with immediate disastrous consequences is assumed.' The EU regulation No 402/2013 [159] declares: 'For technical systems where a functional failure has a credible direct potential for a catastrophic consequence, the associated risk does not have to be reduced further if the rate of that failure is less than or equal to 10^{-9} per operating hour.' All the same, all these statements and considerations are consistent with the reliability values previously presented taken from the notions in EN 1990:2002 standard [155].

The recommendations given above shall consider the probability of having a defect on the axle and the probability that a crack will nucleate from that defect and further grow during the service life. In practice, disregarding that in a real axle the existence of a defect and its nucleation to a crack of a sufficient size that is very unlikely, the hypothesis made here is that according to the probabilistic fracture mechanics analysis, there is a potential that the actual fatigue life of a proportion of railway axles could be shorter than deterministically expected, therefore the DTA should consider a conservative minimum mileage related to a desired reliability.

Taking all these guidance and hypotheses, the probability of failure was chosen to be $7{\times}10^{-5}$ in the present case study, which is consistent with the EN 1990:2002 standard [155] for non-redundant primary components whose failure consequences are extremely severe. In addition, an improved probability of failure was also selected to be $7{\times}10^{-6}$ as in [25]. Moreover, for the sake of comparison, a third probability

of failure is assumed to be 5×10^{-2} which is three and four orders of magnitude larger respectively. Therefore, three levels of probability of failure are considered, 5×10^{-2}, 7×10^{-5} and 7×10^{-6}. Accordingly, the complementary reliability levels are 95 %, 99.993 % and 99.9993 % respectively.

The SF, CDF and PDF of the fatiuge life probability distribution determined in Subsection 4.4.4, consider the input variabilities involved in the fatigue problem. In other words, they stand for the probabilistic fatigue life propagation of interest. This information is exploited during the reliability-based inspection interval definition included next. The SF of the beta prime distribution fitted based on the FSOA moments, shown in Fig. 4.25a, was evaluated for a 95 %, 99.993 % and 99.9993 % reliability percent, following the procedure described in Subsection 3.4.3. The conservative estimations of the fatigue life based on the Pearson probability distribution for 95 %, 99.993 % and 99.9993 % reliabilities are shown in Fig. 4.26.

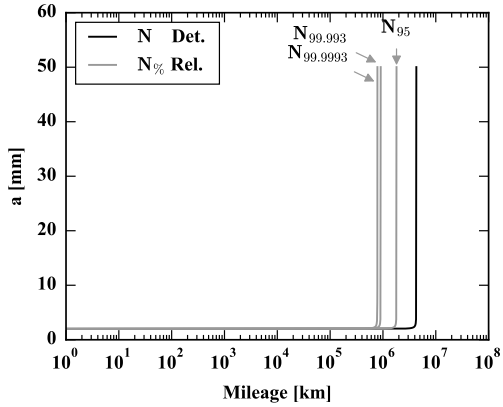

Figure 4.26. Estimation of a conservative number of km for 95 %, 99.993 % and 99.9993 % reliability.

The selected proportion of axles surviving led to a minimum mileage travelled of 1.806×10^6 km, 9.06×10^5 km and 8.35×10^5 km each, that is, according to the probabilistic FCG simulation, 95 %, 99.993 % and 99.9993 % of axles respectively survive beyond these conservative mileages. The calculations in Fig. 4.26 are conservative when compared to the Det. estimation since there is the additional prescription of a reliability percent during the SF evaluation. Note that apart from a reliability percent, the shape of the distribution significantly influences the conservative life estimates. Therefore, the ability of the methodology in describing the lower tail of the lifespan is a key aspect. Note further that because of the conservatism introduced in the adoption of the 95 %, 99.993 % and 99.9993 % reliability, the FCG lifetimes obtained from a probabilistic basis were shorter than the one obtained by simply using the Det. calculation. This is somehow comparable to the use of safety factors but, rather than being arbitrarily chosen, this procedure uses the available knowledge of the lifespan response as a result of the randomness of the input sources,

and therefore its application has a probabilistic foundation. In this example, the three conservative lifespans calculated in this manner are obtained according to the randomness of the combination of all the input r.v.s in the PIAT case, that is, the set $\{n, C, K_{max}, K_{min}, \Delta K_{th0}\}$, due to their randomness is considered in the lifespan N moments estimation and in the subsequent probability distribution fit.

The assumptions adopted to calculate the lifetime N_{def}, (step 4) in Subsection 3.4.1, from a_{min} to a_{max} and the number of times that the crack can be detected before a failure could occur, considered for the inspection interval definition (step 5) are given in Table 4.17.

Table 4.17. Assumptions on the inspection period definition.

a_{min} [mm]	a_{max} [mm]	n_{times} [-]
2	50	3

The impact of the reliability values on the calculated conservative lifespan according to the beta prime distribution fitted from FSOA moments, was assessed by using the Det. number of km and the 95 %, 99.993 % and 99.9993 % lifetimes as basis for the interval inspection definition.

Based on the Det. number of km, the suggested inspection interval (step 5) is calculated according to the algorithm for establishing railway axle maintenance inspection intervals described in Subsection 3.4.3 using Fig. 3.8, providing the inspection periodicity T_{ins}, shown in Table 4.18.

Table 4.18. Det. number of km N and corresponding inspection period definition.

	N [km]	T_{ins} [km]
Det.	4 287 044	1 429 015

Based on the conservative number of km in Fig. 4.26 obtained from the beta prime distribution fitted using the FSOA moments, the suggested inspection interval (step 5) according to the idea depicted in Fig. 3.8, led to the three T_{ins} shown in Table 4.19.

Table 4.19. Conservative number of km N from the beta prime distribution fitted using the FSOA moments and inspection period definition for the 95 %, 99.993 % and 99.9993 % reliability levels.

Reliability [%]	Conservative N [km]	T_{ins} [km]
95 %	1 806 819	602 273
99.993 %	906 666	302 222
99.9993 %	835 800	278 600

At this point of the methodology, several inspection periodicities are available for the planning of periodic non-destructive tests during service in order to ensure structural integrity throughout the useful life of the railway axles. Given these proposals for inspection intervals, the application of different NDT techniques, i.e. different POD curves, is further investigated in the next subsection, in order to evaluate the probabilities of observing cracks and defects in railway axles.

The observations of the results lead to the following general outcomes:

- The stochastic approach provides viable means for evaluating the effect of r.v.s upon the definition of interval inspections within the damage tolerance concept.
- A probabilistic lifespan prediction can be integrated in the design and inspection planning of railway axles.
- The methodology devised can handle conservative FCG estimations that are related to the input variabilities involved in the FCG phenomenon.

4.4.6 Probabilities of successful inspections

This subsection closes with the calculation and discussion of the probabilities of successful inspections in accordance with the suggested inspection intervals obtained in Subsection 4.4.5 for the PIAT case scenario. For this purpose, the probability of crack detection is quantified considering the performance of the NDT techniques. Notice that, not only the deterministic lifespan calculation, but also the conservative lifespan estimations are used as basis for the interval inspection definition and the subsequent calculation of probabilities associated with the selected NDT techniques. Inspection intervals must be defined so that the CPOD or POD of potential cracks, ensure the safety of the axle under service conditions. Therefore, the NDT techniques affect directly to the selection of the best interval periodicity.

As introduced, the suggested inspection intervals are assessed by means of quantifying the probability of crack detection. Given the length of the inspection intervals, the CPOD in successive inspections considering the forward and backward detection schemes in Fig. 3.12a and the POD considering the last chance detection scheme in Fig. 3.12b, are calculated according to the performance of the NDT methods. The NDT techniques that are frequently used in the railway industry are: the ultrasonic testing (UT) in the far-end and near-end scan application conditions, and the magnetic particle testing (MT) also referred to as magnetic particle inspection (MPI). The POD curves of these methods are presented in Fig. 3.10.

The damage tolerance inspection plan must be designed as a function of the crack evolution expected during the service lifetime and of the inspection technique employed to detect such defect. The four inspection periodicities, T_{ins}, suggested in

Subsection 4.4.5 are assessed. In order to check which T_{ins} is more suitable, the actual crack growth evolution in a given freight axle is considered to be equal, for example, to the computed Det. results. In other words, the assumed history values, a [mm] vs. N [km] to be analysed as the pertinent crack growth, correspond with the the Det. case shown in Fig. 4.26. Consequently, the four T_{ins}, one of them obtained based on the Det. number of km, and the other three obtained based on the 95 %, 99.993 % and 99.9993 % reliability levels, are evaluated in the same FCG life situation, obtaining the corresponding values of probabilities of successful inspections. The four different T_{ins} are 1 429 000 km, 602 000 km, 302 000 km, and 278 000 km as shown in Tables 4.18 and 4.19.

To begin with, the results of probability of detection are discussed from a visual perspective in order to illustrate the general trends and make comparisons. Afterwards, an in-depth analysis of the specific values of probabilities of detection and failure is provided. The analyses consider all the different alternatives to understand the effects of: (i) the various T_{ins} studied, (ii) the three crack detection schemes, and (iii) the three characteristic NDT techniques. For the ease of understanding, the appearance of all figures uses the same stiles and color pattern which is as follows: (i) the sizes of the markers vary from small to large according to the length of T_{ins}; (ii) the colors of the lines and the colors of the fillings and edges of the markers match the colors of the different alternatives for the detection schemes shown in Fig. 3.12, i.e. all black for the cumulative forward detection scheme, all grey for the cumulative backward detection scheme, and a marker filled in grey with black edge for the last chance detection scheme, in which the use of lines is not necessary; and (iii) the shapes of the markers agree with the ones used in the NDT performance in Fig. 3.10, that is, a square for UT far-end scan, a circle for UT near-end, and a triangle for MPI.

The history values of CPOD in successive inspections using the forward and backward detection schemes and the values of POD considering the last chance detection scheme, are shown for the UT near-end scan in Fig. 4.27.

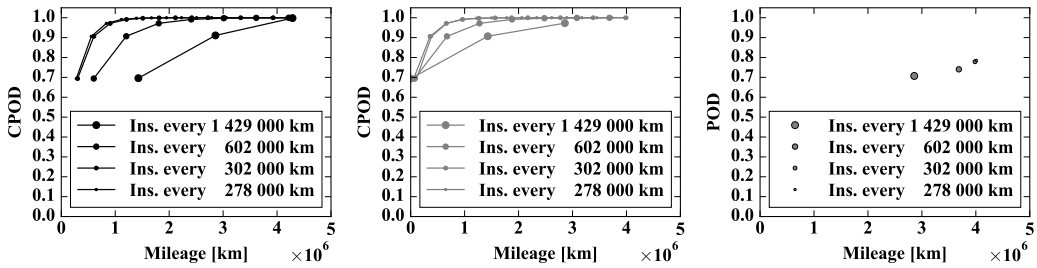

(a) Forward. (b) Backward. (c) Last chance.

Figure 4.27. History of $CPOD_i/POD$ vs. mileage [km] for near-end scan.

It can be observed an increase in instantaneous CPOD value due to the repetition inspections. Note that, the individual POD increases with increasing crack length, and thus the CPOD in successive inspections becomes also higher. Note further that the final CPOD value corresponds to the overall accumulated CPOD, and thus it is the maximum one. From the previous curves, it is also evident that the shorter the T_{ins} is, the earlier a high CPOD is reached, what was obviously expected. The POD last chance values show the shorter the inspection interval the longest the distance travelled at the last inspection based on the backward configuration and thus the larger the crack, and therefore the higher its probability of detection.

There are clear differences in the history evolution of CPOD and also in the PODs when comparing the 1 429 000 km and the 602 000 km inspection intervals, providing higher values in the 602 000 km schedule. These differences are even more pronounced when comparing the two aforementioned T_{ins} with the shorter 302 000 km and 278 000 km periodicities, which outperform in detectability. The CPOD histories in successive inspections corresponding to 302 000 km and 278 000 km T_{ins} are almost superimposed, for all the situations considered. The same happens in their PODs.

The FCG curve assumed as reference, and the PODs according to the last chance detection scheme obtained for the three NDT techniques and using the four T_{ins} proposed are shown in Fig. 4.28. Note that the PODs appear in annotations whose markers are located in the corresponding (mileage [km], a [mm]) coordinates.

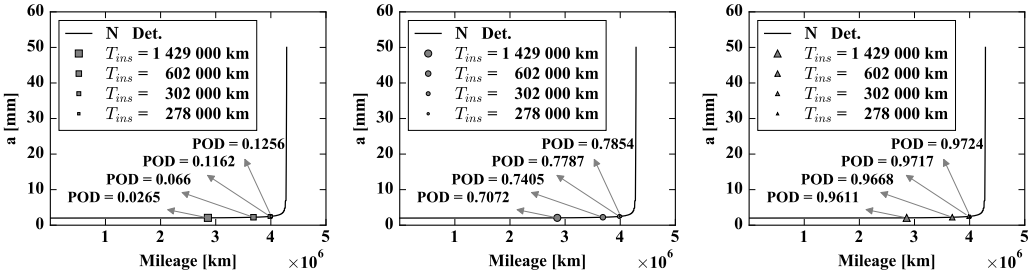

(a) Far-end scan. (b) Near-end scan. (c) MPI.

Figure 4.28. Fatigue crack growth a [mm] vs. mileage [km] and *POD* last chance.

Given the four inspection intervals, the last chance detection scheme provides the POD of a crack that corresponds only to the last useful inspection before failure according to the backward detection scheme. In consequence, the POD last chance values show that the shorter the inspection interval the longest the distance travelled at the last inspection before failure and thus the larger the crack, and therefore the larger its probability of detection with whatever NDT method used. As general outcome, the UT far-end scan provides poor POD according to the last chance detection scheme, the UT near-end scan configuration gives POD values that range in the 70–79 % range increasing as the T_{ins} reduces, and the POD when using

MPI is approximately 97 % not showing a significant variation with the different T_{ins} considered. It is important to note that the drawback of a shorter inspection periodicity is that it involves a more expensive maintenance schedule. The above representation is intended to increase understanding of the POD values as they establish a simple relationship between the inspection intervals and the POD. It also gives further insight regarding the importance of the NDT method used, as they provide really different probabilities at the same mileage points. Once again, it can be seen here that the POD in the last chance configuration that correspond to the 302 000 km and 278 000 km are almost equivalent.

The history values of CPOD in successive inspections for the four inspection periodicities are shown in Fig. 4.29, for the three NDT methods combined with the backward detection scheme.

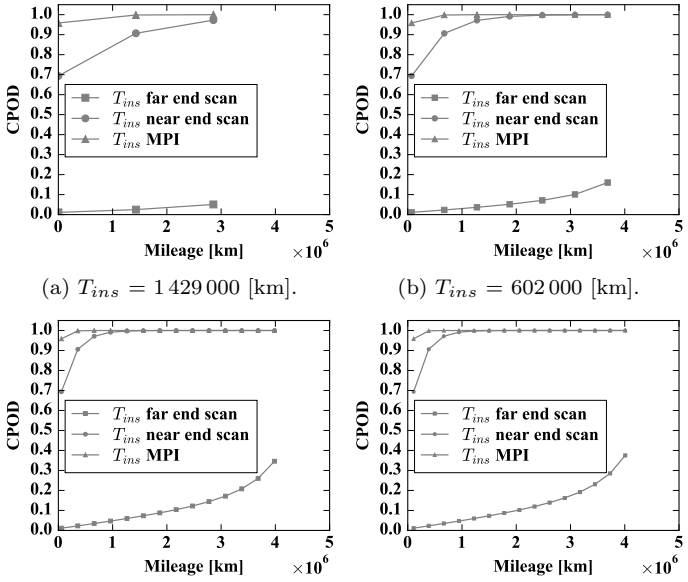

(a) T_{ins} = 1 429 000 [km]. (b) T_{ins} = 602 000 [km].

(c) T_{ins} = 302 000 [km]. (d) T_{ins} = 278 000 [km].

Figure 4.29. $CPOD_i$ vs. mileage [km] for the three NDT and backward scheme.

It can be seen an increase in the successive CPOD values due to the repetition inspections and accumulation of POD. The first inspection falls into early stages of the crack growth, and therefore the crack is still short and thus the POD no matter what NDT, is in its lower range. Then, the successive inspections take into account increasing crack lengths, and so the individual PODs increase and thus the CPOD becomes also higher. For the specific lengths of T_{ins}, the application of different NDT techniques with different POD curves leads to significantly different values for the total CPOD. In this representation, the different pace until reaching a high CPOD for each T_{ins}, depends on the NDT method used. This is due to the fact that the mileage

is the same for a given a T_{ins} but the POD to accumulate changes. Furthermore, it can be observed that the shorter the inspection interval, the fastest the pace for reaching a high CPOD. This is because the shorter the inspection periodicity the more number of inspections, and therefore the earlier a high CPOD arises. For the periodicities of 302 000 km and 278 000 km, the highest values for CPOD are obtained.

The history values of CPOD or the value of POD, for the four inspection periodicities is shown in Fig. 4.30, considering the three detection schemes combined with the near-end scan NDT method. Note that the y-axis label stands for CPOD for the forward and backward detection schemes, and stands for POD in the last chance.

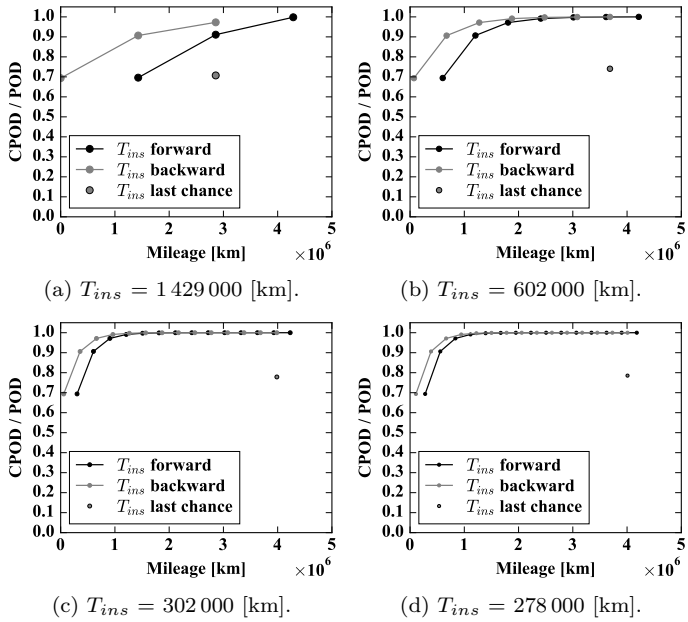

(a) $T_{ins} = 1\,429\,000$ [km]. (b) $T_{ins} = 602\,000$ [km].

(c) $T_{ins} = 302\,000$ [km]. (d) $T_{ins} = 278\,000$ [km].

Figure 4.30. $CPOD_i/POD$ vs. mileage [km] for the three schemes and Near-end.

The impact of the detection scheme considered for the calculation of the CPOD or the POD is signified here. First, it is explicit the offset between the different mileages that come from the different consideration of the starting and final inspection controls as explained in Section 3.5. In the forward detection, it starts from the initial crack, while, in the backward detection, it goes back from the final failure. On the other hand, the last chance scheme considers only the last inspection based on the backward configuration.

For a T_{ins} short enough, the curves from the forward and the backward detection scheme intersect. It is important to highlight that they intersect in a different inspection number. For instance, for a T_{ins} of 302 000 km, approximately at the fourth inspection in the forward detection scheme and at the third inspection for the backward. It means that in this case both schemes provides approximately the same

CPOD but with different number of inspections, what would involve a different cost. Focusing on the CPOD values, for both the forward and backward schemes, from the fourth inspection onwards, the tendency of the CPOD values seems to be flat but in fact the cumulative probability always increases. This behaviour is significant and makes a difference when evaluating these values in detail, as it is done in the later comprehensive analysis based on the specific probability values.

Additional calculations of CPODs and PODs are performed to construct trend curves. The T_{ins} used for the trends calculation sweep the lifespan space in the 100 000–2 500 000 km range with 25 different levels. The range limits are approximately 60 % below and above of the lowest and the highest of the four T_{ins} proposed. The trends of the overall CPOD for the backward detection scheme and POD for the last chance, for the different inspection periodicities are plotted in Fig. 4.31, for each of the three NDT methods. Note that the lines that join the different markers are only intended to be a guide to the eye, as their individual data are calculated separately from point to point depending on each particular T_{ins}.

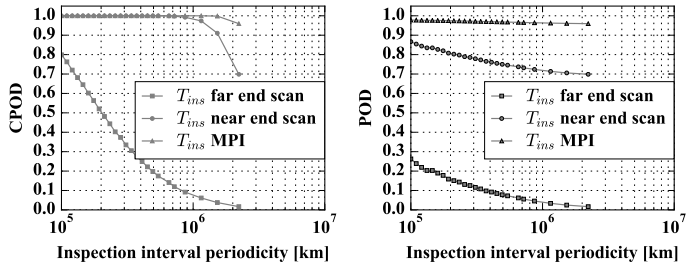

(a) Backward. (b) Last chance.

Figure 4.31. $CPOD/POD$ trend varying the T_{ins}. The lines are a guide to the eye.

It can be observed that the final CPOD value for each T_{ins}, that corresponds to the overall accumulated CPOD and thus it is the maximum for each T_{ins}, always decreases as the length of the inspections increase, whatever NDT method used.

To conclude, an in-depth analysis of the specific probability values is provided here. Given the length of the inspection intervals suggested, the CPOD in successive inspections considering the forward and backward detection schemes and the POD considering the last chance detection scheme are evaluated. The comparison of all the probability of detection results for the UT far-end scan technique, are shown in Table 4.20, for the UT near-end scan technique in Table 4.21, and for the MPI technique in Table 4.22. Note that, as mentioned, in the case of forward and backward detection schemes, the results are cumulative so CPOD values are used. On the other hand, in the case of the last chance detection scheme, the probability result is computed in a single inspection and, thus, the results are expressed in terms of POD.

Table 4.20. CPOD and POD probabilities in the case of UT far-end scan technique.

		Far-end scan		
T_{ins} [km]	No. of ins. [-]	CPOD Forward	CPOD Backward	POD Last chance
1 429 000	3	0.950 095 921 7	0.050 799 868 1	0.026 462 930 4
602 000	7	0.428 784 473 0	0.160 298 702 3	0.066 043 630 3
302 000	14	0.586 526 771 6	0.346 257 964 4	0.116 161 407 3
278 000	15	0.489 225 612 9	0.375 073 290 7	0.125 574 192 1

Table 4.21. CPOD and POD probabilities in the case of UT near-end scan technique.

		Near-end scan		
T_{ins} [km]	No. of ins. [-]	CPOD Forward	CPOD Backward	POD Last chance
1 429 000	3	0.998 110 076 4	0.972 719 048 4	0.707 172 570 5
602 000	7	0.999 934 199 2	0.999 808 081 5	0.740 534 011 0
302 000	14	0.999 999 991 5	0.999 999 970 4	0.778 712 395 1
278 000	15	0.999 999 995 4	0.999 999 991 8	0.785 394 962 0

Table 4.22. CPOD and POD probabilities in the case of MPI magnetic particle inspection.

		MPI		
T_{ins} [km]	No. of ins. [-]	CPOD Forward	CPOD Backward	POD Last chance
1 429 000	3	0.999 967 520 8	0.999 933 661 5	0.961 131 885 6
602 000	7	0.999 999 999 9	0.999 999 999 9	0.966 780 739 6
302 000	14	1	1	0.971 725 640 2
278 000	15	1	1	0.972 438 831 5

Furthermore, the P_f can be considered as the probability of non-detection of a crack throughout the axle lifetime. Therefore, the P_f can be calculated as $P_f = 1 - CPOD$ in the forward or backward schemes, or $P_f = 1 - POD$ in the last chance. This hypothesis is valid since the existence of a crack is considered as premise, and thus the P_f equals the probability of not-detecting the crack that would certainly grow during service life. This P_f should then be multiplied by the probability of having a surface defect on the axle, e.g. a corrosion pit or an impact, and by the probability of nucleation from the initial defect to a small fatigue crack during service life. When these probabilities are considered, the actual probability of failure of railway axles commonly moves towards the 10^{-9}–10^{-10} range. Considering these probabilities is out of the scope of this thesis. Then, the comparison of all the P_f computed as described for the UT far-end scan technique, are shown in Table 4.23, for the UT near-end scan technique in Table 4.24, and for the MPI technique in Table 4.25.

Table 4.23. Probability of failure, P_f, in the case of UT far-end scan technique.

		Far-end scan		
T_{ins} [km]	No. of ins. [-]	P_f Forward	P_f Backward	P_f Last chance
1 429 000	3	4.9904×10^{-2}	9.4920×10^{-1}	9.7354×10^{-1}
602 000	7	5.7122×10^{-1}	8.3970×10^{-1}	9.3396×10^{-1}
302 000	14	4.1347×10^{-1}	6.5374×10^{-1}	8.8384×10^{-1}
278 000	15	5.1077×10^{-1}	6.2493×10^{-1}	8.7443×10^{-1}

Table 4.24. Probability of failure, P_f, in the case of UT near-end scan technique.

		Near-end scan		
T_{ins} [km]	No. of ins. [-]	P_f Forward	P_f Backward	P_f Last chance
1 429 000	3	1.8899×10^{-3}	2.7281×10^{-2}	2.9283×10^{-1}
602 000	7	6.5801×10^{-5}	1.9192×10^{-4}	2.5947×10^{-1}
302 000	14	8.5292×10^{-9}	2.9589×10^{-8}	2.2129×10^{-1}
278 000	15	4.6405×10^{-9}	8.2208×10^{-9}	2.1461×10^{-1}

Table 4.25. Probability of failure, P_f, in the case of MPI magnetic particle inspection.

		MPI		
T_{ins} [km]	No. of ins. [-]	P_f Forward	P_f Backward	P_f Last chance
1 429 000	3	3.2479×10^{-5}	6.6339×10^{-5}	3.8868×10^{-2}
602 000	7	7.6251×10^{-11}	1.4492×10^{-10}	3.3219×10^{-2}
302 000	14	0	0	2.8274×10^{-2}
278 000	15	0	0	2.7561×10^{-2}

Notice that the maintenance plan of railway axles prescribes additional off-service inspection during main wheelset overhauling, typically every $\approx 1\times10^6$ km for freight application. This inspection of axles is performed by using MPI. Performing such an inspection is not considered in the previous calculations, what would further increase the CPOD values and it would decrease the P_f values.

Since the four suggested T_{ins} were evaluated considering the same FCG life situation, i.e. assuming that the actual scenario would follow an identical a [mm] vs. N [km] evolution, and since the four T_{ins} are of different km in length, the number of possible inspections that would be performed within the studied span would be different for each one. Three inspections were possible for the span of the T_{ins} defined from the Det. calculation. Seven, fourteen and fifteen inspections were possible for the span of the T_{ins} defined from the conservative FCG estimations for the 95 %, 99.993 % and 99.9993 % reliability levels. It can be observed in Tables 4.20 to 4.22, that the

CPOD and the POD always increase when reducing the T_{ins} except for the case that combines the far-end scan and the forward scheme. This is due to the fact that the forward scheme is highly dependent on when the last inspection falls within the a vs. N curve. This can be inferred since the growth rate of long cracks is usually high due to its exponential nature, in consequence the crack size and its associated POD change extremely depending on the given number of km set for calculation. Therefore, in some circumstances, the CPOD calculated using the forward scheme may not be trustworthy. This is more evident when considering the far-end scan, which provides relatively low PODs for small cracks, and therefore the overall CPOD is highly influenced on the POD of larger cracks as it is the case of the last inspection.

The previous issue does not emerge when using the backward scheme due to the fact that the effect of the last inspection in the CPOD is not so pronounced because the computation scheme goes back from the final failure. Additionally, it can be seen that the backward provides more conservative results when compared with the forward, as it always provides smaller probabilities under the same conditions. Furthermore, it must be highlighted that the last chance scheme gives even more conservative results. This is clearly because the last chance scheme only considers the POD of the last inspection according to the backward scheme, and therefore it does not accumulate the previous PODs of smaller cracks. For these reasons, the results combining far-end NDT and forward scheme will not be considered for further analysis from now on. It should be noted that the same conclusions are reached from the P_f analysis since it is the complementary of the CPOD or POD values.

First, analysing the results obtained for each of the T_{ins}, the differences between CPOD values and POD for the three NDT techniques are remarkable. Notice that if only one inspection were performed, both the backward and the last chance values would be coincident. Focussing on the CPOD, high differences are obtained between UT far-end scan and the other two NDT methods due to the better performance of the UT near-end and the even better MPI. This fact is more significant when a longer T_{ins} is considered because of the lower number of inspections possible. Regarding the POD, the significant differences between the three NDT techniques are directly related to the NDT performance as a result of the last chance calculation procedure.

Secondly, comparing the results between the four T_{ins}, it can be observed that UT near-end scan and MPI reach higher CPOD or POD values even with lower number of inspections than the UT far-end scan. This fact exposes the worse performance of the far-end condition even when many inspections are done. As mentioned, the CPOD in the backward scheme, and the POD in the last chance scheme, always increase when reducing the T_{ins}. The reason is clear when analysing the POD last chance values, as they show that the shorter the inspection interval, the longest the distance travelled at the last inspection based on the backward configuration, and therefore the larger the crack and thus the larger its probability of detection with

whatever NDT method used. The same reasoning can be extended to the backward scheme, where, the intermediate successive inspections also accumulate probability of detection and, the shorter the T_{ins} the more number of inspections are performed.

Now, it is time to analyse which is the best and *just necessary* T_{ins} with a permissible level of P_f. A crucial question is what permissible P_f is really justifiable in practice. For safety critical components, the P_f during the lifetime generally ranges from 10^{-5} to 10^{-8}. Recall that the P_f considered in EN 1990:2002 standard [155] is $7{\times}10^{-5}$. Note further that the technical report CEN/TR 17469:2020 [156] states that a P_f between 10^{-6} and 10^{-7} seems reasonable in railway applications, since the number of mechanical failures is rather small. Given these notions, the permissible level for P_f is selected as the threshold of $P_f \leq 7{\times}10^{-6}$, reducing the probability of $P_{f,\ EN\ 1990}$ by one order of magnitude. This can be considered as part of the actions for improving the reliability of axles. As a result, the analysis is performed in terms of P_f as it is meaningful to interpret and also has a sound basis from the standards. The objective in the design of the maintenance inspection plan is to achieve a P_f lower than the previous specific threshold by selecting an appropriate T_{ins}. Two additional postulates have to be considered here. The first one is to consider the backward scheme since it is more trustworthy than the forward scheme and also it is more realistic than the last chance due to the fact that several inspections are performed, so the backward P_f is the most representative. The second is to consider as NDT technique the UT near-end scan as its conditions take place frequently, has a better performance than the UT far-end and, additionally, the MPI is reserved for the overhauling inspections. It should also be added that the MPI is more expensive as it is necessary to disassemble the axle or, in the case of a mounted axle, it does not allow inspecting the axle transitions. In summary, the three assumptions are: (i) $P_f \leq 7{\times}10^{-6}$, (ii) backward detection scheme, and (iii) UT near-end scan NDT.

Finally, given these premises, a detailed analysis of the P_f in Table 4.24, that encloses the results for the UT near-end scan, is provided. Focusing on the backward scheme, it can be observed that the P_f for an T_{ins} of 1 429 000 km is $2.7281{\times}10^{-2}$ what is not compliant with the acceptable P_f selected as the threshold $P_f \leq 7{\times}10^{-6}$. It can also be observed that the P_f for an inspection interval of 602 000 km is $1.9192{\times}10^{-4}$, again not complying with the threshold defined. Lastly, the two T_{ins} that comply with the $P_f \leq 7{\times}10^{-6}$ when using the backward scheme are 302 000 km and 278 000 km, providing $P_f = 2.9589{\times}10^{-8}$ and $P_f = 8.2208{\times}10^{-9}$ respectively. Moreover, it should be highlighted here that the latter two T_{ins}, which meet all assumptions established, are really close in terms of distance, and consequently in terms of P_f, providing values close enough to consider the differences between them negligible. Since the purpose of DTA is to inform the maintenance managers about the impacts of a particular inspection interval, from the results analysed, it is advisable to perform NDT using the UT in the near-end application condition every $\approx$ 300 000 km.

The present analysis of the PIAT case scenario, though based on assumptions that are fairly important such as severe service conditions, shows how a probabilistic damage tolerance approach can be assumed as a complement to the classic fatigue design for railway axles. From the results analysed, the most important outcome is that it is possible to safely assume inspection intervals every $\approx 300\,000\,\text{km}$ using the UT in the near-end application condition. It is demonstrated that the selected inspection interval was adequate to ensure a high CPOD prior to the potential failure.

The observations of the results lead to the following general outcomes:

- For a specific length of inspection interval, the application of different NDT techniques with different POD curves leads to significantly different values for the overall probability of detecting cracks and defects in railway axles.
- According to the assumptions of: (i) $P_f \leq 7{\times}10^{-6}$, (ii) backward detection scheme, and (iii) UT near-end scan NDT, it is recommended to perform NDT using the UT in the near-end application condition every $\approx 300\,000\,\text{km}$.
- The analysis shows that the probability of successful detection is high, having few inspections with high CPOD provided by the near-end scan NDT technique.
- If the probability of having a defect, and the probability of nucleation from the initial defect to a small crack were considered, the inspection intervals would be longer than those considered here since the actual probabilities of failure would be smaller by several orders of magnitude. The calculated probabilities of failure shall not be taken for their absolute values, but the approach enables comparison between different scenarios.
- The CPOD values would further increase, and, accordingly, the P_f values would decrease, provided that the previous calculations considered the prescribed additional off-service MPI inspection during the main wheelset overhauling, commonly every $\approx 1{\times}10^{6}\,\text{km}$.
- A damage tolerance assessment based on a probabilistic fatigue crack growth life estimation, can optimize the definition of inspection intervals of railway axles that could reduce the total life cycle cost of wheelsets.
- The procedure presented establishes a reliability-based inspection planning, and thus enables the optimization of maintenance expenses selecting an appropriate inspection periodicity.

5

Conclusions and Outlook

5.1 Conclusions

This thesis is intended to take the readers on a journey that starts with the evolution of railway axles safety assessment, probabilistic aspects of damage tolerance and the principles of probabilistic analysis methods for fatigue crack growth in metal components and ends with a thorough illustration of the probabilistic methodology devised to be applied to the damage tolerance assessment of railway axles, progressively developed over the past few years and brings this thesis to an end.

This thesis has presented new probabilistic analyses for the maintenance planning for railway axles within the damage tolerance concept. The most relevant conclusions are:

- It presents a procedure devised for the determination of inspection intervals within the damage tolerance analysis of railway axles that is based on a probabilistic description of fatigue lifespan. It considers the input uncertainties through a conservative fatigue crack growth life estimation based on the lifespan probability distribution, benefiting from the knowledge available at the lower tail of the distribution. The most important advantage of this approach is that it is based on a probabilistic fatigue crack growth life that is more conservative than the deterministic one. The benefit consists in a simple relationship between the adopted reliability in the probabilistic lifespan and the conservative prediction of the residual fatigue lifetime for practical use. Moreover, this methodology allows focusing on establishing an optimum inspection interval combining probabilistic approaches into the damage tolerance assessment phase. However, it must also balance a number of safety, economic and vehicle availability issues.

- This work presents a novel uncertainty propagation methodology, also known as stochastic moment approximation, for efficiently estimating the probability distribution of the fatigue crack growth lifetime. It implements the Pearson distribution family and takes advantage of the statistical moments of the lifetime predicted via innovative approaches based on NASGRO model. The main advantages that are worth mentioning include: (i) the ability to automatically determine the pertinent distribution shape using a simple and uniform criterion for choosing the corresponding Pearson distribution type and thus avoiding the need to assume a probability distribution in advance; (ii) the versatility for constructing probability distributions with more than two parameters if required, given that in the current methodology the skewness and the kurtosis are calculated in addition to the expected value and variance; (iii) the significant improvement in the accuracy of the probability density function constructed in fatigue crack growth life analysis, especially in the lower tail of the distribution of life which is of notable interest in reliability assessment. It demonstrates that in practical engineering it is relevant to determine the third and fourth central moments for a precise description of the probabilistic fatigue crack growth life.

- This research offers a full second-order probabilistic formulation to predict the statistical moments, expected value, variance, skewness, and kurtosis, of the fatigue crack growth lifetime based on NASGRO model, using information about the input random variables distribution. These four moments are used to estimate the parameters of the Pearson distribution to represent the underlying lifespan distribution. The probability distribution constructed from the first four prescribed is helpful to describe the crack growth phenomenon and infer its probability distribution, under stochastic conditions such as a real service load spectrum acting on a component combined with a random bending moment loading and also considering the scatter of material properties.

- The accuracy of the fatigue lifetime moments obtained via the full second-order approach presented, and its efficiency when compared to an equivalent Monte Carlo method analysis, prove the good performance of the proposed approach. Its performance, or balance of accuracy and efficiency, is the most important advantage of this method. The present uncertainty propagation methodology is found to be advantageous compared with the Monte Carlo method analysis. It is remarkable that the provided method can be used for predicting stochastic effects on fatigue life history in applications that require a low computation time, for example, in reliability studies implemented in design stages.

- The damage tolerance assessment of components such as railway axles can benefit from the results provided to define interval inspections with a certain level of safety, optimizing maintenance costs. The present approach offers potential application in practice, and it could have a remarkable effect on

the definition of inspection intervals. This analysis proposal can be used as a complementary support to current standards and practices and also to get a more accurate assessment in complex geometrical sections of the railway axle that are of special interest to the designer.

- It is worth emphasizing that the probabilistic approach proposed is significantly relevant in the definition of inspection intervals of components, as in the railway axle investigated, where the low resolution of commonly used non-destructive testing techniques provides a short crack detection range from detectable cracks to failure, and thus narrows the analysis of fatigue cycles to a short fraction of the entire fatigue life.
- The advances in this thesis contribute to the competitiveness of the railway sector and its environmental sustainability through the integration of probabilistic simulation techniques and damage tolerance analysis concepts, that allow predicting the functional behaviour and the service life of railway axles to improve the final performance of the products and to extend their service life by making efficient use of materials and energy. The methods provided are expected to have an impact on the optimization of maintenance intervals, thus promoting efficient use of rail transport to carry people and freight. In this sense, its implementation would also decrease the environmental impact of the mankind due to air pollution caused by transport, as it helps rail transport to become a more environmentally friendly alternative.
- All in all, this thesis results in a probabilistic analysis method for fatigue crack growth in metal components which has a positive and comprehensive effect in engineering applications such as in the probabilistic life prediction. The lifespan probability distribution provided has the potential to be used in probabilistic damage tolerance design and integrity assessment of components and structures. Therefore, the novel operational framework for uncertainty analysis in this thesis is expected to be a promising asset in a broad range of engineering problems dealing with random variables.

5.2 Conclusiones

Esta tesis pretende llevar a los lectores en un viaje que comienza con los primeros desarrollos en la evaluación de la seguridad de ejes ferroviarios y su evolución, aspectos probabilistas de tolerancia al daño y los principios de los métodos de análisis probabilista para el crecimiento de grieta por fatiga en componentes metálicos, y termina con una ilustración exhaustiva de la metodología probabilista concebida para ser aplicada en la evaluación de tolerancia al daño de ejes ferroviarios, desarrollada progresivamente en los últimos años y que pone fin a esta tesis.

En esta tesis se han presentado nuevos tratamientos probabilistas para la planificación del mantenimiento de ejes ferroviarios dentro del concepto de tolerancia al daño. Las conclusiones más relevantes son las siguientes:

- Esta tesis presenta un procedimiento desarrollado para la determinación de intervalos de inspección dentro del análisis de tolerancia al daño de ejes ferroviarios que se basa en una descripción probabilista de la vida a fatiga. El procedimiento considera las incertidumbres de entrada a través de una estimación conservadora de la vida en crecimiento de grieta por fatiga basada en la distribución de probabilidad de la vida, beneficiándose del conocimiento disponible en la cola inferior de la distribución. La ventaja más importante de este enfoque es que se basa en una vida en crecimiento de grieta por fatiga probabilista que es más conservadora que la determinista. La ventaja consiste en una relación sencilla entre la fiabilidad adoptada en la vida probabilista y la predicción conservadora de la vida residual a fatiga para su uso práctico. Además, esta metodología permite centrarse en establecer un intervalo de inspección óptimo combinando enfoques probabilistas en la fase de análisis de tolerancia al daño. Sin embargo, hay que tener en cuenta que también debe equilibrar una serie de cuestiones en cuanto a seguridad, economía y de disponibilidad de vehículos.

- Este trabajo presenta una novedosa metodología de propagación de incertidumbre, también conocida como aproximación estocástica de momentos, para estimar eficazmente la distribución de probabilidad de la vida en crecimiento de grieta por fatiga. La metodología implementa la familia de distribuciones de Pearson y aprovecha los momentos estadísticos de la vida estimados mediante enfoques innovadores basados en el modelo NASGRO. Las principales ventajas que cabe mencionar son: (i) la capacidad para determinar automáticamente la forma de la distribución pertinente utilizando un criterio simple y uniforme para elegir el tipo de distribución de Pearson correspondiente y evitando así la necesidad de asumir de antemano una distribución de probabilidad; (ii) gran

versatilidad para construir distribuciones de probabilidad con más de dos parámetros si es necesario, dado que en la metodología actual se calculan la asimetría y la curtosis además del valor esperado y la varianza; (iii) una mejora significativa de la precisión de la función de densidad de probabilidad construida en el análisis de la vida en crecimiento de grieta por fatiga, especialmente en la cola inferior de la distribución de vida que es de notable interés en la evaluación de la fiabilidad. La metodología demuestra que en la práctica ingenieril es relevante determinar el tercer y cuarto momento central para obtener una descripción precisa de la vida probabilista en crecimiento de grieta por fatiga.

- Esta investigación ofrece una formulación probabilista de segundo orden completo para predecir los momentos estadísticos, valor esperado, varianza, asimetría, y curtosis, de la vida en crecimiento de grieta por fatiga basada en el modelo NASGRO, utilizando información sobre la distribución de las variables aleatorias de entrada. Estos cuatro momentos se usan para estimar los parámetros de la distribución de Pearson que representa la distribución de vida subyacente. La distribución de probabilidad construida a partir de los cuatro primeros momentos prescritos es útil para describir el fenómeno de crecimiento de grieta e inferir su distribución de probabilidad, bajo condiciones estocásticas como un espectro de carga de servicio real actuando sobre un componente combinado con una carga de momento de flexión aleatoria y considerando también la dispersión de las propiedades del material.

- La precisión de los momentos de la vida a fatiga obtenidos mediante el enfoque de segundo orden completo presentado, y su eficiencia cuando se comparan con un análisis equivalente mediante el método de Monte Carlo, demuestran el buen rendimiento del enfoque propuesto. Su rendimiento, o equilibrio entre precisión y eficiencia, es la ventaja más importante de este método. La presente metodología de propagación de incertidumbre resulta ventajosa en comparación con el método Monte Carlo. Cabe señalar que el método proporcionado puede ser utilizado para predecir efectos estocásticos en la historia de la vida a fatiga en aplicaciones que requieren un bajo tiempo computacional, por ejemplo, en estudios de fiabilidad implementados en etapas de diseño.

- El análisis de tolerancia al daño de componentes como ejes ferroviarios puede beneficiarse de los resultados proporcionados para definir intervalos de inspección con un cierto nivel de seguridad, optimizando los costes de mantenimiento. El presente enfoque ofrece una potencial aplicación práctica, y podría tener un efecto notable en la definición de intervalos de inspección. El análisis propuesto puede servir de complemento a las normas y prácticas actuales y también para obtener una evaluación más precisa en secciones geométricas complejas del eje ferroviario que son de especial interés para el diseñador.

- Cabe destacar que el enfoque probabilista propuesto es significativamente relevante en la definición de intervalos de inspección de componentes, como el eje ferroviario investigado, en el que la baja resolución de las técnicas de ensayo no destructivas comúnmente usadas proporciona un corto rango de detección de grieta desde grietas detectables hasta el fallo, y por lo tanto reduce el análisis de los ciclos de fatiga a una fracción corta de toda la vida a fatiga.
- Los avances en esta tesis contribuyen a la competitividad del sector ferroviario y a su sostenibilidad medioambiental mediante la integración de técnicas de simulación probabilista y conceptos de análisis de tolerancia al daño, que permiten predecir el comportamiento funcional y la vida de ejes ferroviarios para mejorar el comportamiento final de los productos y alargar su vida útil haciendo un uso eficiente de los materiales y la energía. Se espera que los métodos aportados tengan repercusión en la optimización de los intervalos de mantenimiento, promoviendo así un uso eficiente del transporte ferroviario para desplazar personas y mercancías. En este sentido, su implementación también disminuiría el impacto medioambiental de la humanidad debido a la contaminación atmosférica causada por el transporte, ya que ayuda a que el transporte ferroviario se convierta en una alternativa más respetuosa con el medio ambiente.
- En definitiva, esta tesis constituye un método de análisis probabilista para el crecimiento de grieta por fatiga en componentes metálicos que tiene un efecto positivo y global en aplicaciones de ingeniería como es la predicción probabilista de la vida a fatiga. La distribución de probabilidad de vida a fatiga proporcionada tiene el potencial de ser utilizada en el diseño probabilista de tolerancia al daño y en la evaluación de la integridad de componentes y estructuras. Por lo tanto, se espera que el novedoso marco operativo para el análisis de incertidumbres en esta tesis sea un recurso prometedor para una amplia gama de problemas de ingeniería que tratan con variables aleatorias.

5.3 Original contributions

This section includes the main novelties in the state of the art introduced by this thesis. The original contributions are the following:

- Proposal and development of a novel computational methodology for the probabilistic analysis of fatigue crack growth life in metal components.
- Derivation of the full second-order approach for the first to fourth moments of functions of random variables using matrix and summation notation.
- Original expressions of the probabilistic NASGRO equations for the calculation of the expected value, first raw moment; the variance, second central moment; the skewness, third central standardized moment; and the kurtosis, fourth central standardized moment, of the fatigue life, based on the Taylor series approximation.
- Efficient and accurate estimation of the statistical moments of the variable of interest, fatigue life.
- Incorporation of the Pearson distribution family in the reconstruction of the underlying fatigue lifespan probability distribution.
- Combination of probabilistic fatigue life estimation results with reliability principles and damage tolerance concepts.
- Establishment of a reliability-based inspection planning that enables the optimization of maintenance costs selecting an appropriate inspection periodicity.
- Objectively assessment and quantification of the reliability of a railway axle, according to damage tolerance criteria through the use of probabilities of crack detection.
- A tool for its integration in design stages, which represents a leap forward in the use of probabilistic approaches in the decision-making process of selecting inspection intervals of maintenance that affect the life cycle of a product. That is, the methodology developed helps to reduce the maintenance works and costs, which reduces the environmental footprint of the rail system, and therefore contributes to the protection of the environment to reach climate neutrality.

5.4 Aportaciones originales

Esta sección recoge las principales novedades en el estado del arte introducidas por esta tesis. Las aportaciones originales son las siguientes:

- Propuesta y desarrollo de una metodología computacional novedosa para el análisis probabilista de la vida en el crecimiento de grieta por fatiga en componentes metálicos.
- Derivación de la aproximación de segundo orden completo para los momentos primero a cuarto de funciones de variables aleatorias utilizando notación matricial y sumatoria.
- Expresiones originales de las ecuaciones probabilistas de NASGRO para el cálculo del valor esperado, primer momento; la varianza, segundo momento central; la asimetría, tercer momento central estandarizado; y la curtosis, cuarto momento central estandarizado, de la vida a fatiga, basadas en una aproximación en serie de Taylor.
- Estimación eficiente y precisa de los momentos estadísticos de la variable de interés, la vida a fatiga.
- Incorporación de la familia de distribuciones de Pearson en la reconstrucción de la distribución de probabilidad subyacente de la vida a fatiga.
- Combinación de los resultados de la estimación probabilista de la vida a fatiga con principios de fiabilidad y conceptos de tolerancia al daño.
- Establecimiento de una planificación de inspecciones basada en la fiabilidad que permite optimizar los costes de mantenimiento seleccionando una periodicidad de inspección adecuada.
- Evaluación y cuantificación objetiva de la fiabilidad de un eje ferroviario, de acuerdo con criterios de tolerancia al daño mediante el uso de probabilidades de detección de grieta.
- Una herramienta para su integración en las fases de diseño, que supone todo un salto en el uso de enfoques probabilistas en el proceso de toma de decisiones de selección de intervalos de inspección de mantenimiento que inciden en el ciclo de vida de un producto. Es decir, la metodología desarrollada ayuda a reducir los trabajos y costes asociados a su mantenimiento, lo que reduce la huella ambiental del sistema ferroviario y, por tanto, contribuye a la protección del medio ambiente con el fin alcanzar la neutralidad climática.

5.5 Future work

The work presented opens interesting new possibilities for future research in probabilistic fatigue. In the following, a number of selected issues and proposals that promise potential for further increasing the safety level of axles are discussed. Some possible future works are:

- Consideration of more input variables of interest as random due to the inherent randomness of the variables involved in the fatigue process. The approach presented provides a stochastic model of fatigue crack growth, with respect to whatever random variables that are selected. Therefore, the applicability of the full second-order approach goes beyond the illustrated example that considers the variability in the loading conditions and in some material properties, that is, $\{n, C, K_{max}, K_{min}, \Delta K_{th0}\}$. As an example, the scatter of the fatigue crack growth curve can be additionally represented by means of considering the remaining material parameters involved in the NASGRO equation, i.e. $\{K_c, p, q\}$ as random variables. It is important to remark that the method proposed takes into account the relationships among the random variables in terms of probability in addition to the statistical moments of the random variables individually. Notice that disregarding the inherent correlations between random variables could lead to incorrect results. The strategy to include the variability and correlations between the aforementioned parameters into the method architecture is straightforward. This suggested work would allow the results presented to be extended, contributing to a better knowledge of the distribution of fatigue life.

- Further investigations should focus on more accurately characterizing the statistical variability of the NASGRO model material parameters for typical EA4T and EA1N steels for railway axles. In this respect, it would be useful to dedicate further effort to obtain a comprehensible characterization of the variability of the parameters from specimen to specimen, via their statistical moments as the empirical mean value, the empirical variance, as well as correlation coefficients for the model parameters, especially the latter as they are indispensable for proper probabilistic fatigue crack growth assessment. This input variability investigation should also be broadened to cover the randomness of relevant geometrical input variables such as initial crack geometry and size, component dimensional tolerances and expected crack location and orientation.

- Extension of the experimental campaigns on full-scale railway axles to obtain the fatigue crack growth rate versus the stress intensity range, that is, the da/dN–ΔK curve. The fatigue crack growth curve can be obtained by using traditional measurement methods such as crack opening displacement

extensometers or using novel alternatives such as the use of experimental full-field non-contact measurement techniques like the digital image correlation in combination with numerical post-processing methods.

- The cumulative probability of detection in successive inspections, the probability of detection and the probability of failure calculated are very sensitive to the input random variables used in the probabilistic approximation, particularly the input of loading conditions. Thus, it is necessary to have a complete database, representative of all situations that may be encountered in service. The way the data are extrapolated to relevant mileage needs to be improved to make it more statistically relevant. In addition, the assumptions taken to simplify the measurements and translate them to an equivalent spectrum of bending loads can have an important impact on the final result. Future research is required including additional measurements in order to cover a wider range of vehicles, especially freight wagons for which very little data are available, and routes, in order to take into account all circumstances that may occur.

- The damage tolerance methodology considers as premise the existence of a crack due to the most commonly reasons for fatigue crack initiation which are corrosion pits, damage due to flying ballast impacts, non-metallic inclusions in the material, damages during maintenance, etc. However, for the calculation of the probabilities of failure, it does not take into account the probability of having a defect or the probability of fatigue crack nucleation from the initial defect to a small crack. More sophisticated approaches could be to consider these sources of uncertainty in order to calculate more realistic probabilities of failure that would be smaller by several orders of magnitude, and therefore the inspection intervals would be longer than those considered in this work.

- Regarding non-destructive testing reliability, the probability of detection using different methods has been evaluated. Besides the probabilistic fracture mechanics based residual lifetime estimation, the probability of detection performance of the non-destructive testing technique is the second essential parameter for establishing inspection intervals. Therefore, any improvement of the probability of detection vs. crack size curve is of great importance for reliable damage tolerance design.

- In the present approach, the probability of failure is calculated by considering that the state of the component remains the same during its life. It means that it is assumed that thanks to the maintenance, the strength of the axle remains the same during its whole life and that the calculation can be performed the way described. Further investigations regarding time-variant and time-invariant component assumptions, limit state functions, intersection probabilities, conditional probability events linked to fatigue failure, crack detection and reliability updating by actual observations events are suggested.

- Combination of the methodology developed with a digital twin, fed by experimental measurements obtained by sensors, such as those used in structural health monitoring, for updating the prediction on-line so that predictive maintenance can be performed during operation based on the condition of the component.
- Integration of extensive probabilistic analyses when dealing with random variables in fatigue design and damage tolerance assessment of railway axles. For that, continued efforts are needed to make reliability-based procedures and probabilistic analyses more integrated into the maintenance planning of damage tolerant railway axles. Moreover, further efforts are needed to gradually improve and adapt the current methods for the design and assessment of railway axles that are mainly based on conventional analytical calculations, towards the new design concept and assessment process that relies on larger statistical input data, specific probabilistic formulations embedded in innovative software and enhanced engineering capabilities. Probabilistic fatigue life estimations, rather than being used only for establishing inspection intervals, should also be adopted as a complementary approach to traditional fatigue strength design. It would give wheelset designers the chance to gain experience for further improvement. These differences in approach should be identified when choosing the methodology for design, as they have an impact on the costs throughout the life cycle of the component, from design to final operation.

5.6 Trabajo futuro

El trabajo presentado abre nuevas e interesantes posibilidades para futuras investigaciones en fatiga probabilista. A continuación, se abordan una serie de cuestiones y propuestas de trabajo futuro que prometen tener potencial para seguir aumentando el nivel de seguridad de los ejes. Algunos posibles trabajos futuros son:

- Consideración de más variables de entrada de interés como aleatorias debido a la aleatoriedad inherente de las variables que intervienen en el proceso de fatiga. El enfoque presentado proporciona un modelo estocástico de crecimiento de grieta por fatiga, con respecto a cualquier parámetro que se seleccione. Por lo tanto, la aplicabilidad del enfoque de segundo orden completo va más allá del ejemplo ilustrado que considera la variabilidad en las condiciones de carga y en algunas propiedades del material, es decir, $\{n, C, K_{max}, K_{min}, \Delta K_{th0}\}$. Como ejemplo, la dispersión de la curva de crecimiento de grieta por fatiga puede representarse adicionalmente mediante la consideración del resto de parámetros del material que intervienen en la ecuación NASGRO, es decir, $\{K_c, p, q\}$ como variables aleatorias. Es importante señalar que el método propuesto tiene en cuenta las relaciones entre parámetros aleatorios en términos de probabilidad, además de los momentos estadísticos de los parámetros individualmente. Cabe señalar que no tener en cuenta las inherentes correlaciones entre parámetros aleatorios podría conducir a resultados incorrectos. La estrategia para incluir la variabilidad y correlaciones entre los parámetros mencionados en la arquitectura del método es directa. Este trabajo propuesto permitiría ampliar los resultados presentados, contribuyendo a un mejor conocimiento de la distribución de la vida a la fatiga.

- Investigaciones posteriores deberían centrarse en caracterizar con mayor precisión la variabilidad estadística de los parámetros del material del modelo NASGRO para los aceros EA4T y EA1N típicos en ejes ferroviarios. En este sentido, sería útil dedicar más esfuerzos a obtener una caracterización exhaustiva de la variabilidad estadística de los parámetros de una muestra a otra, a través de sus momentos estadísticos como el valor medio empírico, la varianza empírica, así como los coeficientes de correlación para los parámetros del modelo, especialmente estos últimos, ya que son indispensables para una evaluación probabilista rigurosa del crecimiento de grieta por fatiga. Esta investigación de la variabilidad de los datos de entrada también debería ampliarse para abarcar la aleatoriedad de las variables geométricas de entrada pertinentes, como la geometría y el tamaño inicial de la grieta, las tolerancias dimensionales de los componentes y la ubicación y orientación probables de la grieta.

- Ampliación de las campañas experimentales en ejes ferroviarios a escala real para obtener la tasa de crecimiento de grieta por fatiga frente al rango de intensidad de tensiones, es decir, la curva da/dN–ΔK. La curva de crecimiento de grieta por fatiga puede obtenerse utilizando métodos de medición tradicionales como los extensómetros de desplazamiento de apertura de grieta o utilizando novedosas alternativas como el uso de técnicas experimentales de medición de campo completo y sin contacto como la correlación digital de imágenes en combinación con métodos numéricos de postproceso.

- La probabilidad acumulada de detección en inspecciones sucesivas, la probabilidad de detección y la probabilidad de fallo calculadas son muy sensibles a los parámetros aleatorios de entrada utilizados en la aproximación probabilista, en particular las condiciones de carga. Por ello, es necesario disponer de una base de datos completa, representativa de todas las situaciones que pueden darse en servicio. Es necesario mejorar la forma de extrapolar los datos al kilometraje pertinente para que sea más relevante desde el punto de vista estadístico. Además, las hipótesis adoptadas para simplificar las mediciones y traducirlas a un espectro equivalente de cargas de flexión pueden tener un impacto importante en el resultado final. Es necesario realizar futuras investigaciones que incluyan mediciones adicionales para abarcar una gama más amplia de vehículos, especialmente los vagones de mercancías de los que se dispone de muy pocos datos, y de rutas, con el fin de tener en cuenta todas las circunstancias que pueden darse.

- La metodología de tolerancia al daño considera como premisa la existencia de una grieta debida a las causas más comunes de iniciación de grietas por fatiga, que son las picaduras de corrosión, los daños debidos a impactos de balasto volante, las inclusiones no metálicas en el material, los daños durante el mantenimiento, etc. Sin embargo, para el cálculo de las probabilidades de fallo, no se tiene en cuenta la probabilidad de tener un defecto o la probabilidad de nucleación de la grieta por fatiga desde el defecto inicial hasta una pequeña grieta. Enfoques más sofisticados podrían considerar estas fuentes de incertidumbre para calcular probabilidades de fallo más realistas que serían más reducidas en varios órdenes de magnitud y, por tanto, los intervalos de inspección serían más largos que los considerados en este trabajo.

- En cuanto a la fiabilidad de los ensayos no destructivos, se ha evaluado la probabilidad de detección utilizando diferentes métodos. Además de la estimación probabilista de la vida a fatiga basada en la mecánica de la fractura, la probabilidad de detección de la técnica de ensayo no destructivo es el segundo parámetro esencial para establecer los intervalos de inspección. Por lo tanto, cualquier mejora de la curva de probabilidad de detección vs. tamaño de la grieta es de gran importancia para un diseño seguro en la tolerancia al daño.

- En el presente enfoque, la probabilidad de fallo se calcula considerando que el estado del componente es el mismo durante su vida útil. Esto significa que se supone que, gracias al mantenimiento, la resistencia del eje sigue siendo la misma durante toda su vida y que el cálculo puede realizarse de la forma descrita. Se plantea realizar investigaciones adicionales en relación con suposiciones de componentes variables e invariables en el tiempo, funciones de estado límite, probabilidad de la intersección de sucesos, eventos de probabilidad condicional relacionados con el fallo por fatiga, la detección de grieta y la actualización de la fiabilidad mediante eventos de observaciones reales.
- Combinación de la metodología desarrollada con un gemelo digital, alimentado por medidas experimentales obtenidas por sensores, como los utilizados en la monitorización de la salud estructural, para actualizar la predicción de forma on-line de modo que se pueda realizar un mantenimiento predictivo durante la operación basado en la condición del componente.
- Integración de amplios análisis probabilistas al tratar con variables aleatorias en el diseño a fatiga y la evaluación de la tolerancia al daño de los ejes ferroviarios. Por ello, es necesario seguir trabajando para que los procedimientos basados en fiabilidad y análisis probabilistas estén más integrados en la planificación del mantenimiento de ejes ferroviarios tolerantes al daño. Además, hay que seguir trabajando para mejorar y adaptar gradualmente los métodos actuales estándar de diseño y evaluación de ejes ferroviarios, que se basan principalmente en cálculos analíticos convencionales, hacia el nuevo concepto de diseño y proceso de evaluación basado en datos estadísticos de entrada más completos, en formulaciones probabilistas específicas integradas en software innovador y en capacidades de ingeniería mejoradas. Las estimaciones probabilistas de la vida a la fatiga, en lugar de utilizarse únicamente para establecer los intervalos de inspección, deben adoptarse también como un enfoque complementario al diseño tradicional para la resistencia a la fatiga. Esto daría a los diseñadores de ejes montados la posibilidad de ganar experiencia para seguir mejorando. Estas diferencias de enfoque deben identificarse a la hora de elegir la metodología para diseñar, ya que tienen un impacto en el coste a lo largo del ciclo de vida del componente, desde el diseño hasta el funcionamiento final.

A

Full second-order approach assuming independence

This appendix presents the complete derivation of the expected value, variance, skewness and kurtosis second-order approximations assuming independence between the input random variables. The first-order approximation is also given for completeness.

A.1 Abbreviations and conventions: moments of the joint distribution.

This section enlarges the abbreviations and conventions in Section 2.2 for the 5^{th} to 8^{th} higher-order moments of the joint distribution.

- The moments of the joint distribution of $X = \{X_1, X_2, \ldots, X_d\}$ random variables are defined similar to the n^{th} central moments. For d random variables, the number of non-trivial n^{th} order mixed or often called cross central moments are:

$$\frac{(n+d-1)!}{n!\,(d-1)!} - d \tag{A.1}$$

  Non-trivial means that the cross central moments that involve only one variable are excluded.

  The n^{th} central multivariate moments of continuous random variables are denoted with consecutive indexes, two for the 2^{nd} central moment μ_{jk}, three indexes for the 3^{rd} central moment μ_{jkl}, four indexes for the 4^{th} central moment μ_{jklm}, five

for the 5^{th} central moment μ_{jklmr}, six indexes for the 6^{th} central moment μ_{jklmrs}, seven indexes for the 7^{th} central moment $\mu_{jklmrst}$ and eight indexes for the 8^{th} central moment $\mu_{jklmrstu}$. Note that the presence of up to eight indices does not imply that more than two random variables are involved. Each index runs from 1 to d random variables.

– 5^{th} central moment: *Hyperskewness*

The fifth central moment indicates the relative importance of tails vs. center in causing skewness, in other words, measures the asymmetric sensitivity of the kurtosis. Any symmetric distribution will have a fifth central moment of 0.

The number of random variables d must be at least two for the concept of hyperskewness to be non-trivial. For two continuous random variables X_j and X_k, where $j \neq k$, the four non-trivial fifth mixed central moments are:

$$\begin{aligned}
\mu_{jjjjk} &= \mu_5\left(X_j, X_j, X_j, X_j, X_k\right) = \int_{-\infty}^{\infty}\int_{-\infty}^{\infty}\left(x_j - \mu_{X_j}\right)^4\left(x_k - \mu_{X_k}\right) f_X\left(x_j, x_k\right) dx_j dx_k \\
\mu_{jjjkk} &= \mu_5\left(X_j, X_j, X_j, X_k, X_k\right) = \int_{-\infty}^{\infty}\int_{-\infty}^{\infty}\left(x_j - \mu_{X_j}\right)^3\left(x_k - \mu_{X_k}\right)^2 f_X\left(x_j, x_k\right) dx_j dx_k \\
\mu_{jjkkk} &= \mu_5\left(X_j, X_j, X_k, X_k, X_k\right) = \int_{-\infty}^{\infty}\int_{-\infty}^{\infty}\left(x_j - \mu_{X_j}\right)^2\left(x_k - \mu_{X_k}\right)^3 f_X\left(x_j, x_k\right) dx_j dx_k \\
\mu_{jkkkk} &= \mu_5\left(X_j, X_k, X_k, X_k, X_k\right) = \int_{-\infty}^{\infty}\int_{-\infty}^{\infty}\left(x_j - \mu_{X_j}\right)\left(x_k - \mu_{X_k}\right)^4 f_X\left(x_j, x_k\right) dx_j dx_k
\end{aligned} \tag{A.2}$$

The special case in which the same variable is considered five times leads:

$$\mu_{jjjjj} = \mu_5\left(X_j, X_j, X_j, X_j, X_j\right) = \int_{-\infty}^{\infty}\left(x_j - \mu_{X_j}\right)^5 f_X\left(x_j\right) dx_j \tag{A.3}$$

The normalized or standardized μ_{jjjjj} dividing by the standard deviation raised to the fifth power σ_j^5 is known as hyperskewness, denoted as $\tilde{S}$.

$$\tilde{S}\left(X_j, X_j, X_j, X_j, X_j\right) = \frac{\mu_{jjjjj}}{\sigma_j^5} \tag{A.4}$$

– 6^{th} central moment: *Hyperflatness*

The sixth central moment measures the combined weight, heaviness, of the tails relative to the rest of the distribution but with an even heavier focus on outliers than the fourth central moment.

The number of random variables d must be at least two for the concept of hyperflatness to be non-trivial. For two continuous random variables X_j and X_k, where $j \neq k$, the five non-trivial sixth mixed central moments are:

$$\begin{aligned}
\mu_{jjjjjk} &= \mu_6\left(X_j, X_j, X_j, X_j, X_j, X_k\right) = \int_{-\infty}^{\infty}\int_{-\infty}^{\infty}\left(x_j - \mu_{X_j}\right)^5\left(x_k - \mu_{X_k}\right) f_X\left(x_j, x_k\right) dx_j dx_k \\
\mu_{jjjjkk} &= \mu_6\left(X_j, X_j, X_j, X_j, X_k, X_k\right) = \int_{-\infty}^{\infty}\int_{-\infty}^{\infty}\left(x_j - \mu_{X_j}\right)^4\left(x_k - \mu_{X_k}\right)^2 f_X\left(x_j, x_k\right) dx_j dx_k \\
\mu_{jjjkkk} &= \mu_6\left(X_j, X_j, X_j, X_k, X_k, X_k\right) = \int_{-\infty}^{\infty}\int_{-\infty}^{\infty}\left(x_j - \mu_{X_j}\right)^3\left(x_k - \mu_{X_k}\right)^3 f_X\left(x_j, x_k\right) dx_j dx_k \\
\mu_{jjkkkk} &= \mu_6\left(X_j, X_j, X_k, X_k, X_k, X_k\right) = \int_{-\infty}^{\infty}\int_{-\infty}^{\infty}\left(x_j - \mu_{X_j}\right)^2\left(x_k - \mu_{X_k}\right)^4 f_X\left(x_j, x_k\right) dx_j dx_k \\
\mu_{jkkkkk} &= \mu_6\left(X_j, X_k, X_k, X_k, X_k, X_k\right) = \int_{-\infty}^{\infty}\int_{-\infty}^{\infty}\left(x_j - \mu_{X_j}\right)\left(x_k - \mu_{X_k}\right)^5 f_X\left(x_j, x_k\right) dx_j dx_k
\end{aligned} \tag{A.5}$$

The special case in which the same variable is considered six times leads:

$$\mu_{jjjjjj} = \mu_6\left(X_j, X_j, X_j, X_j, X_j, X_j\right) = \int_{-\infty}^{\infty}\left(x_j - \mu_{X_j}\right)^6 f_X\left(x_j\right) dx_j \tag{A.6}$$

The normalized or standardized μ_{jjjjjj} dividing by the standard deviation raised to the sixth power σ_j^6 is known as hyperflatness or hyperkurtosis, denoted as $\tilde{K}$.

$$\tilde{K}\left(X_j, X_j, X_j, X_j, X_j, X_j\right) = \frac{\mu_{jjjjjj}}{\sigma_j^6} \tag{A.7}$$

– 7^{th} central moment:

The seventh moment measures similarly to the third central moment *skewness* but with an even heavier focus on outliers than the fifth moment.

The number of random variables d must be at least two for the concept of 7^{th} central moment to be non-trivial. For two continuous random variables X_j and X_k, where $j \neq k$, the six non-trivial seventh mixed central moments are:

$$\begin{aligned}
\mu_{jjjjjjk} &= \mu_7\left(X_j, X_j, X_j, X_j, X_j, X_j, X_k\right) = \int_{-\infty}^{\infty}\int_{-\infty}^{\infty}\left(x_j - \mu_{X_j}\right)^6\left(x_k - \mu_{X_k}\right) f_X\left(x_j, x_k\right) dx_j dx_k \\
\mu_{jjjjjkk} &= \mu_7\left(X_j, X_j, X_j, X_j, X_j, X_k, X_k\right) = \int_{-\infty}^{\infty}\int_{-\infty}^{\infty}\left(x_j - \mu_{X_j}\right)^5\left(x_k - \mu_{X_k}\right)^2 f_X\left(x_j, x_k\right) dx_j dx_k \\
\mu_{jjjjkkk} &= \mu_7\left(X_j, X_j, X_j, X_j, X_k, X_k, X_k\right) = \int_{-\infty}^{\infty}\int_{-\infty}^{\infty}\left(x_j - \mu_{X_j}\right)^4\left(x_k - \mu_{X_k}\right)^3 f_X\left(x_j, x_k\right) dx_j dx_k \\
\mu_{jjjkkkk} &= \mu_7\left(X_j, X_j, X_j, X_k, X_k, X_k, X_k\right) = \int_{-\infty}^{\infty}\int_{-\infty}^{\infty}\left(x_j - \mu_{X_j}\right)^3\left(x_k - \mu_{X_k}\right)^4 f_X\left(x_j, x_k\right) dx_j dx_k \\
\mu_{jjkkkkk} &= \mu_7\left(X_j, X_j, X_k, X_k, X_k, X_k, X_k\right) = \int_{-\infty}^{\infty}\int_{-\infty}^{\infty}\left(x_j - \mu_{X_j}\right)^2\left(x_k - \mu_{X_k}\right)^5 f_X\left(x_j, x_k\right) dx_j dx_k \\
\mu_{jkkkkkk} &= \mu_7\left(X_j, X_k, X_k, X_k, X_k, X_k, X_k\right) = \int_{-\infty}^{\infty}\int_{-\infty}^{\infty}\left(x_j - \mu_{X_j}\right)\left(x_k - \mu_{X_k}\right)^6 f_X\left(x_j, x_k\right) dx_j dx_k
\end{aligned} \tag{A.8}$$

The special case in which the same variable is considered seven times leads:

$$\mu_{jjjjjjj} = \mu_7\left(X_j, X_j, X_j, X_j, X_j, X_j, X_j\right) = \int_{-\infty}^{\infty}\left(x_j - \mu_{X_j}\right)^7 f_X\left(x_j\right) dx_j \tag{A.9}$$

The seventh central moment $\mu_{jjjjjjj}$ can be also normalized or standardized dividing by the standard deviation raised to the seventh power σ_j^7:

$$\frac{\mu_{jjjjjjj}}{\sigma_j^7} \tag{A.10}$$

– 8^{th} central moment:

The eighth moment measures similarly to the fourth central moment *kurtosis* but with an even heavier focus on outliers than the sixth moment.

The number of random variables d must be at least two for the concept of 8^{th} central moment to be non-trivial. For two continuous random variables X_j and X_k, where $j \neq k$, the seven non-trivial eighth mixed central moments are:

$$\begin{aligned}
\mu_{jjjjjjjk} &= \mu_8\left(X_j, X_j, X_j, X_j, X_j, X_j, X_j, X_k\right) = \int_{-\infty}^{\infty}\int_{-\infty}^{\infty}\left(x_j - \mu_{X_j}\right)^7\left(x_k - \mu_{X_k}\right) f_X\left(x_j, x_k\right) dx_j dx_k \\
\mu_{jjjjjjkk} &= \mu_8\left(X_j, X_j, X_j, X_j, X_j, X_j, X_k, X_k\right) = \int_{-\infty}^{\infty}\int_{-\infty}^{\infty}\left(x_j - \mu_{X_j}\right)^6\left(x_k - \mu_{X_k}\right)^2 f_X\left(x_j, x_k\right) dx_j dx_k \\
\mu_{jjjjjkkk} &= \mu_8\left(X_j, X_j, X_j, X_j, X_j, X_k, X_k, X_k\right) = \int_{-\infty}^{\infty}\int_{-\infty}^{\infty}\left(x_j - \mu_{X_j}\right)^5\left(x_k - \mu_{X_k}\right)^3 f_X\left(x_j, x_k\right) dx_j dx_k \\
\mu_{jjjjkkkk} &= \mu_8\left(X_j, X_j, X_j, X_j, X_k, X_k, X_k, X_k\right) = \int_{-\infty}^{\infty}\int_{-\infty}^{\infty}\left(x_j - \mu_{X_j}\right)^4\left(x_k - \mu_{X_k}\right)^4 f_X\left(x_j, x_k\right) dx_j dx_k \\
\mu_{jjjkkkkk} &= \mu_8\left(X_j, X_j, X_j, X_k, X_k, X_k, X_k, X_k\right) = \int_{-\infty}^{\infty}\int_{-\infty}^{\infty}\left(x_j - \mu_{X_j}\right)^3\left(x_k - \mu_{X_k}\right)^5 f_X\left(x_j, x_k\right) dx_j dx_k \\
\mu_{jjkkkkkk} &= \mu_8\left(X_j, X_j, X_k, X_k, X_k, X_k, X_k, X_k\right) = \int_{-\infty}^{\infty}\int_{-\infty}^{\infty}\left(x_j - \mu_{X_j}\right)^2\left(x_k - \mu_{X_k}\right)^6 f_X\left(x_j, x_k\right) dx_j dx_k \\
\mu_{jkkkkkkk} &= \mu_8\left(X_j, X_k, X_k, X_k, X_k, X_k, X_k, X_k\right) = \int_{-\infty}^{\infty}\int_{-\infty}^{\infty}\left(x_j - \mu_{X_j}\right)\left(x_k - \mu_{X_k}\right)^7 f_X\left(x_j, x_k\right) dx_j dx_k
\end{aligned} \tag{A.11}$$

The special case in which the same variable is considered eight times leads:

$$\mu_{jjjjjjjj} = \mu_8\left(X_j, X_j, X_j, X_j, X_j, X_j, X_j, X_j\right) = \int_{-\infty}^{\infty}\left(x_j - \mu_{X_j}\right)^8 f_X\left(x_j\right) dx_j \tag{A.12}$$

The eighth central moment $\mu_{jjjjjjjj}$ can be also normalized or standardized dividing by the standard deviation raised to the eighth power σ_j^8:

$$\frac{\mu_{jjjjjjjj}}{\sigma_j^8} \tag{A.13}$$

A.2 Non-linear combinations: summation notation assuming independence

A.2.1 Expected value second-order

Assuming independence between the random variables, the covariances between the variables μ_{jk} that $_{j\neq k}$ are equal to 0 and the covariances μ_{jk} that $_{j=k}$ lead to the variance $\mu_{j,2} = \mathrm{Var}(X_j)$. As a result, the Eq. (2.62) is compacted as:

$$\mathrm{E}[Y] \approx g_\mu + \frac{1}{2}\sum_{j=1}^{d} g_{,jj}\mu_{j,2} \tag{A.14}$$

A.2.2 Expected value first-order

The first order expected value approximation (for general or independent variables) obtained omitting the corresponding o_2 term from the Eq. (2.62) equals:

$$\mathrm{E}[Y] = \mu_Y \approx g_\mu \tag{A.15}$$

A.2.3 Variance second-order

Assuming independence between the random variables, the Eq. (2.76) is compacted further:

II:

The covariances between the variables μ_{jk} that $_{j\neq k}$ are equal to 0 and the covariances μ_{jk} that $_{j=k}$ lead to the variance $\mu_{j,2} = \mathrm{Var}(X_j)$.

$$\sum_{j=1}^{d}\sum_{k=1}^{d} g_{,j}g_{,k}\mu_{jk} = \sum_{j=1}^{d} g_{,j}^2\mu_{j,2} \tag{A.16}$$

III:

The fourth mixed or cross central moments between the variables μ_{jklm} that $_{j=k\neq l=m}$:

$$\frac{1}{4}\sum_{j=1}^{d}\sum_{l=1}^{d} g_{,jj}g_{,ll}\mu_{j,2}\mu_{l,2} \tag{A.17a}$$

The fourth mixed or cross central moments between the variables μ_{jklm} that $_{j=l\neq k=m}$:

$$\frac{1}{4}\sum_{j=1}^{d}\sum_{k=1}^{d} g_{,jk}^2\mu_{j,2}\mu_{k,2} \tag{A.17b}$$

The fourth cross central moments between the variables μ_{jklm} that $_{j=m\neq k=l}$ (equivalent to previous case):

$$\frac{1}{4}\sum_{j=1}^{d}\sum_{k=1}^{d} g_{,jk}^{2}\mu_{j,2}\mu_{k,2} \tag{A.17c}$$

The fourth mixed or cross central moments between the variables μ_{jklm} that $_{j=k=l=m}$ lead to the fourth moment $\mu_{j,4}$.

$$\frac{1}{4}\sum_{j=1}^{d} g_{,jj}^{2}\mu_{j,4} \tag{A.17d}$$

Summarizing and reassigning indexes to compact further (indexes $_j$ and $_k$ are preferred for clarity purposes, because it does not matter how they are named):

$$\begin{aligned}\frac{1}{4}\sum_{j=1}^{d}\sum_{k=1}^{d}\sum_{l=1}^{d}\sum_{m=1}^{d} g_{,jk}g_{,lm}\mu_{jklm} &= \frac{1}{4}\sum_{j=1}^{d}\sum_{\substack{k=1\\k\neq j}}^{d} g_{,jj}g_{,kk}\mu_{j,2}\mu_{k,2} \\ &+ \frac{1}{4}2\sum_{j=1}^{d}\sum_{\substack{k=1\\k\neq j}}^{d} g_{,jk}^{2}\mu_{j,2}\mu_{k,2} + \frac{1}{4}\sum_{j=1}^{d} g_{,jj}^{2}\mu_{j,4}\end{aligned} \tag{A.17e}$$

Changing in the symmetric terms, the first upper limit $_d$ for $_{d-1}$, the second lower limit $\frac{k=1}{k\neq j}$ for $_{k=j+1}$ and multiplying by 2 to compensate the symmetry lost with the limits change:

$$\begin{aligned}\frac{1}{4}\sum_{j=1}^{d}\sum_{k=1}^{d}\sum_{l=1}^{d}\sum_{m=1}^{d} g_{,jk}g_{,lm}\mu_{jklm} &= \frac{1}{4}\cdot 2\sum_{j=1}^{d-1}\sum_{k=j+1}^{d} g_{,jj}g_{,kk}\mu_{j,2}\mu_{k,2} \\ &+ \frac{1}{4}2\cdot 2\sum_{j=1}^{d-1}\sum_{k=j+1}^{d} g_{,jk}^{2}\mu_{j,2}\mu_{k,2} + \frac{1}{4}\sum_{j=1}^{d} g_{,jj}^{2}\mu_{j,4}\end{aligned} \tag{A.17f}$$

V:

This term follows the same strategy as in II.

$$g_\mu \sum_{j=1}^{d}\sum_{k=1}^{d} g_{,jk}\mu_{jk} = g_\mu \sum_{j=1}^{d} g_{,jj}\mu_{j,2} \tag{A.18}$$

VI:

The third mixed or cross central moments between the variables μ_{jkl} that $_{j\neq k\neq l}$ are equal to 0 and the third cross central moments μ_{jkl} that $_{j=k=l}$ lead to the third central moment $\mu_{j,3}$.

$$\sum_{j=1}^{d}\sum_{k=1}^{d}\sum_{l=1}^{d} g_{,j}g_{,kl}\mu_{jkl} = \sum_{j=1}^{d} g_{,j}g_{,jj}\mu_{j,3} \tag{A.19}$$

As a result, the second order approximation for the variance assuming independence is given by:

$$\begin{aligned}
\mathrm{Var}\,(Y) = \sigma_Y^2 \\
&\approx \underbrace{g_\mu^2}_{I} + \underbrace{\sum_{j=1}^{d} g_{,j}^2\mu_{j,2}}_{II} \\
&\quad + \underbrace{\frac{1}{2}\sum_{j=1}^{d-1}\sum_{k=j+1}^{d} g_{,jj}g_{,kk}\mu_{j,2}\mu_{k,2} + \sum_{j=1}^{d-1}\sum_{k=j+1}^{d} g_{,jk}^2\mu_{j,2}\mu_{k,2} + \frac{1}{4}\sum_{j=1}^{d} g_{,jj}^2\mu_{j,4}}_{III} \\
&\quad + \underbrace{0}_{IV} + \underbrace{g_\mu \sum_{j=1}^{d} g_{,jj}\mu_{j,2}}_{V} + \underbrace{\sum_{j=1}^{d} g_{,j}g_{,jj}\mu_{j,3}}_{VI} - \mu_Y^2
\end{aligned} \tag{A.20}$$

A.2.4 Variance first-order

The variance first-order approximation for independent random variables is derived from Eq. (2.80) and Eq. (A.20) leading to:

$$\mathrm{Var}\,(Y) = \sigma_Y^2 \approx \underbrace{\sum_{j=1}^{d} g_{,j}^2\mu_{j,2}}_{II} \tag{A.21}$$

A.2.5 Third central moment *skewness* second-order

Assuming independence between the random variables, the Eq. (2.96) becomes:

II:

The third mixed or cross central moments between the variables μ_{jkl} that $_{j\neq k\neq l}$ are equal to 0 and the third cross central moments μ_{jkl} that $_{j=k=l}$ lead to the third central moment $\mu_{j,3}$.

$$\sum_{j=1}^{d}\sum_{k=1}^{d}\sum_{l=1}^{d} g_{,j}g_{,k}g_{,l}\mu_{jkl} = \sum_{j=1}^{d} g_{,j}^{3}\mu_{j,3} \tag{A.22}$$

III:

Note that in the following mathematical derivation, several equivalent cases are grouped together for brevity.

The sixth mixed or cross central moments between the variables μ_{jklmrs} that $_{j=k\neq l=m\neq r=s}$:

$$\frac{1}{8}\sum_{j=1}^{d}\sum_{\substack{k=1\\k\neq j}}^{d}\sum_{\substack{l=1\\l\neq k\\l\neq j}}^{d} g_{,jj}g_{,kk}g_{,ll}\mu_{j,2}\mu_{k,2}\mu_{l,2} \tag{A.23a}$$

The sixth mixed or cross central moments between the variables μ_{jklmrs} that:

$$\begin{array}{lll} j=k\ \neq l=r\neq m=s & j=k\neq l=s\neq r=m & l=m\neq j=r\ \neq k=s \\ l=m\neq j=s\neq k\ =r & r=s\neq j=l\ \neq k=m & r=s\ \neq j=m\neq k=l \end{array}$$

All together reassigning indexes lead to:

$$\frac{1}{8}6\sum_{j=1}^{d}\sum_{\substack{k=1\\k\neq j}}^{d}\sum_{\substack{l=1\\l\neq k\\l\neq j}}^{d} g_{,jj}g_{,kl}^{2}\mu_{j,2}\mu_{k,2}\mu_{l,2} \tag{A.23b}$$

The sixth mixed or cross central moments between the variables μ_{jklmrs} that:

$$\begin{array}{llll} j=l\neq k=r\neq m=s & j=l\neq k=s\ \neq m=r & j=m\neq k=r\neq l\ =s & j=m\neq k=s\ \neq l=r \\ j=r\neq k=l\neq m=s & j=r\neq k=m\neq l\ =s & j=s\ \neq k=l\neq m=r & j=s\ \neq k=m\neq l=r \end{array}$$

All together reassigning indexes lead to:

$$\frac{1}{8}8\sum_{j=1}^{d}\sum_{\substack{k=1\\k\neq j}}^{d}\sum_{\substack{l=1\\l\neq k\\l\neq j}}^{d} g_{,jk}g_{,jl}g_{,kl}\mu_{j,2}\mu_{k,2}\mu_{l,2} \tag{A.23c}$$

The sixth mixed or cross central moments between the variables μ_{jklmrs} that:

$$\begin{array}{lll} j=k\ =l\neq m=r=s & j=k=r\neq l\ =m=s & l=m=j\neq k=r=s \\ l=m=r\neq j\ =k=s & r=s=j\neq k=l\ \ =m & r=s\ \ =l\neq j=k=m \end{array}$$

$$\frac{1}{8}6\sum_{j=1}^{d}\sum_{\substack{k=1\\k\neq j}}^{d} g_{,jj}g_{,jk}g_{,kk}\mu_{j,3}\mu_{k,3} \tag{A.23d}$$

The sixth mixed or cross central moments between the variables μ_{jklmrs} that:

$$j=l=r\neq k=m=s \qquad j=l=s\neq k=m=r \qquad j=m=r\neq k=l=s \qquad j=m=s\neq k=l=r$$

All together reassigning indexes lead to:

$$\frac{1}{8}4\sum_{j=1}^{d}\sum_{\substack{k=1\\k\neq j}}^{d} g_{,jk}^{3}\mu_{j,3}\mu_{k,3} \tag{A.23e}$$

The sixth mixed or cross central moments between the variables μ_{jklmrs} that:

$$j=k\neq l=m=r=s \qquad l=m\neq j=k=r=s \qquad r=s\neq j=k=l=m$$

All together reassigning indexes lead to:

$$\frac{1}{8}3\sum_{j=1}^{d}\sum_{\substack{k=1\\k\neq j}}^{d} g_{,jj}g_{,kk}^{2}\mu_{j,2}\mu_{k,4} \tag{A.23f}$$

The sixth mixed or cross central moments between the variables μ_{jklmrs} that:

$$\begin{array}{llll} j=l\neq k=m=r\ =s & j=m\neq k=l\ =r\ =s & j\ =r\neq k=l\ =m=s & j\ =s\neq k=l\ =m=r \\ k=l\neq j=m=r\ =s & k=m\neq j=l\ =r\ =s & k\ =r\neq j=l\ =m=s & k\ =s\neq j=l\ =m=r \\ l=r\neq j=k\ =m=s & l=s\ \neq j=k=m=r & m=r\neq j=k=l\ \ =s & m=s\neq j=k=l\ \ =r \end{array}$$

All together reassigning indexes lead to:

$$\frac{1}{8}12\sum_{j=1}^{d}\sum_{\substack{k=1\\k\neq j}}^{d} g_{,jk}^{2}g_{,kk}\mu_{j,2}\mu_{k,4} \tag{A.23g}$$

The sixth mixed or cross central moments between the variables μ_{jklmrs} that $_{j=k=l=m=r=s}$ lead to the sixth moment $\mu_{j,6}$.

$$\frac{1}{8}\sum_{j=1}^{d} g_{,jj}^{3}\mu_{j,6} \tag{A.23h}$$

Summarizing:

$$\begin{aligned}
&\frac{1}{8}\sum_{j=1}^{d}\sum_{k=1}^{d}\sum_{l=1}^{d}\sum_{m=1}^{d}\sum_{r=1}^{d}\sum_{s=1}^{d} g_{,jk}g_{,lm}g_{,rs}\mu_{jklmrs} \\
&\quad=\frac{1}{8}\sum_{j=1}^{d}\sum_{\substack{k=1\\k\neq j}}^{d}\sum_{\substack{l=1\\l\neq k\\l\neq j}}^{d} g_{,jj}g_{,kk}g_{,ll}\mu_{j,2}\mu_{k,2}\mu_{l,2}+\frac{1}{8}6\sum_{j=1}^{d}\sum_{\substack{k=1\\k\neq j}}^{d}\sum_{\substack{l=1\\l\neq k\\l\neq j}}^{d} g_{,jj}g_{,kl}^{2}\mu_{j,2}\mu_{k,2}\mu_{l,2} \\
&\qquad+\frac{1}{8}8\sum_{j=1}^{d}\sum_{\substack{k=1\\k\neq j}}^{d}\sum_{\substack{l=1\\l\neq k\\l\neq j}}^{d} g_{,jk}g_{,jl}g_{,kl}\mu_{j,2}\mu_{k,2}\mu_{l,2}+\frac{1}{8}6\sum_{j=1}^{d}\sum_{\substack{k=1\\k\neq j}}^{d} g_{,jj}g_{,jk}g_{,kk}\mu_{j,3}\mu_{k,3} \\
&\qquad+\frac{1}{8}4\sum_{j=1}^{d}\sum_{\substack{k=1\\k\neq j}}^{d} g_{,jk}^{3}\mu_{j,3}\mu_{k,3}+\frac{1}{8}3\sum_{j=1}^{d}\sum_{\substack{k=1\\k\neq j}}^{d} g_{,jj}g_{,kk}^{2}\mu_{j,2}\mu_{k,4} \\
&\qquad+\frac{1}{8}12\sum_{j=1}^{d}\sum_{\substack{k=1\\k\neq j}}^{d} g_{,jk}^{2}g_{,kk}\mu_{j,2}\mu_{k,4}+\frac{1}{8}\sum_{j=1}^{d} g_{,jj}^{3}\mu_{j,6}
\end{aligned} \tag{A.23i}$$

Changing in the symmetric terms (with respect to two indexes), the first upper limit d for $d-1$, the second lower limit $\substack{k=1\\k\neq j}$ for $k=j+1$ and multiplying by 2 to compensate the symmetry lost. And changing in the symmetric terms (with respect to three indexes), the first upper limit d for $d-2$, the second upper limit d for $d-1$, the second lower limit $\substack{k=1\\k\neq j}$ for $k=j+1$, the third lower limit $\substack{l=1\\l\neq k\\l\neq j}$ for $l=k+1$ and multiplying by $3\cdot 2$ to compensate the symmetry lost with the limits change:

$$\begin{aligned}
&\frac{1}{8}\sum_{j=1}^{d}\sum_{k=1}^{d}\sum_{l=1}^{d}\sum_{m=1}^{d}\sum_{r=1}^{d}\sum_{s=1}^{d} g_{,jk}g_{,lm}g_{,rs}\mu_{jklmrs} \\
&\quad=\frac{1}{8}\cdot 3\cdot 2\sum_{j=1}^{d-2}\sum_{k=j+1}^{d-1}\sum_{l=k+1}^{d} g_{,jj}g_{,kk}g_{,ll}\mu_{j,2}\mu_{k,2}\mu_{l,2}+\frac{1}{8}6\cdot 2\sum_{j=1}^{d}\sum_{\substack{k=1\\k\neq j}}^{d-1}\sum_{\substack{l=k+1\\l\neq j}}^{d} g_{,jj}g_{,kl}^{2}\mu_{j,2}\mu_{k,2}\mu_{l,2} \\
&\qquad+\frac{1}{8}8\cdot 3\cdot 2\sum_{j=1}^{d-2}\sum_{k=j+1}^{d-1}\sum_{l=k+1}^{d} g_{,jk}g_{,jl}g_{,kl}\mu_{j,2}\mu_{k,2}\mu_{l,2} \\
&\qquad+\frac{1}{8}6\cdot 2\sum_{j=1}^{d-1}\sum_{k=j+1}^{d} g_{,jj}g_{,jk}g_{,kk}\mu_{j,3}\mu_{k,3}+\frac{1}{8}4\cdot 2\sum_{j=1}^{d-1}\sum_{k=j+1}^{d} g_{,jk}^{3}\mu_{j,3}\mu_{k,3} \\
&\qquad+\frac{1}{8}3\sum_{j=1}^{d}\sum_{\substack{k=1\\k\neq j}}^{d} g_{,jj}g_{,kk}^{2}\mu_{j,2}\mu_{k,4}+\frac{1}{8}12\sum_{j=1}^{d}\sum_{\substack{k=1\\k\neq j}}^{d} g_{,jk}^{2}g_{,kk}\mu_{j,2}\mu_{k,4}+\frac{1}{8}\sum_{j=1}^{d} g_{,jj}^{3}\mu_{j,6}
\end{aligned} \tag{A.23j}$$

V:

The covariances between the variables μ_{jk} that $_{j\neq k}$ are equal to 0 and the covariances μ_{jk} that $_{j=k}$ lead to the variance $\mu_{j,2} = \mathrm{Var}\,(X_j)$.

$$3g_\mu^2 \frac{1}{2} \sum_{j=1}^{d} \sum_{k=1}^{d} g_{,jk}\mu_{jk} = 3g_\mu^2 \frac{1}{2} \sum_{j=1}^{d} g_{,jj}\mu_{j,2} \tag{A.24}$$

VI:

This term follows the same strategy as in V.

$$3g_\mu \sum_{j=1}^{d} \sum_{k=1}^{d} g_{,j}g_{,k}\mu_{jk} = 3g_\mu \sum_{j=1}^{d} g_{,j}^2\mu_{j,2} \tag{A.25}$$

VII:

The fourth mixed or cross central moments between the variables μ_{jklm} that $_{j=k\neq l=m}$:

$$3\frac{1}{2} \sum_{j=1}^{d} \sum_{l=1}^{d} g_{,j}^2 g_{,ll}\mu_{j,2}\mu_{l,2} \tag{A.26a}$$

The fourth mixed or cross central moments between the variables μ_{jklm} that $_{j=l\neq k=m}$:

$$3\frac{1}{2} \sum_{j=1}^{d} \sum_{k=1}^{d} g_{,j}g_{,k}g_{,jk}\mu_{j,2}\mu_{k,2} \tag{A.26b}$$

The fourth cross moments between the variables μ_{jklm} that $_{j=m\neq k=l}$ (equivalent to previous case):

$$3\frac{1}{2} \sum_{j=1}^{d} \sum_{k=1}^{d} g_{,j}g_{,k}g_{,jk}\mu_{j,2}\mu_{k,2} \tag{A.26c}$$

The fourth mixed or cross central moments between the variables μ_{jklm} that $_{j=k=l=m}$ lead to the fourth moment $\mu_{j,4}$.

$$3\frac{1}{2} \sum_{j=1}^{d} g_{,j}^2 g_{,jj}\mu_{j,4} \tag{A.26d}$$

Summarizing and reassigning indexes to compact further:

$$\begin{aligned} 3\frac{1}{2} \sum_{j=1}^{d} \sum_{k=1}^{d} \sum_{l=1}^{d} \sum_{m=1}^{d} g_{,j}g_{,k}g_{,lm}\mu_{jklm} = {} & 3\frac{1}{2} \sum_{j=1}^{d} \sum_{\substack{k=1 \\ k\neq j}}^{d} g_{,j}^2 g_{,kk}\mu_{j,2}\mu_{k,2} \\ & + 3\frac{1}{2}2 \sum_{j=1}^{d} \sum_{\substack{k=1 \\ k\neq j}}^{d} g_{,j}g_{,k}g_{,jk}\mu_{j,2}\mu_{k,2} + 3\frac{1}{2} \sum_{j=1}^{d} g_{,j}^2 g_{,jj}\mu_{j,4} \end{aligned} \tag{A.26e}$$

Changing in the symmetric terms, the first upper limit d for $d-1$, the second lower limit $\overset{k=1}{k\neq j}$ for $k=j+1$ and multiplying by 2 to compensate the symmetry lost with the limits change:

$$\begin{aligned} 3\frac{1}{2}\sum_{j=1}^{d}\sum_{k=1}^{d}\sum_{l=1}^{d}\sum_{m=1}^{d} g_{,j}g_{,k}g_{,lm}\mu_{jklm} = {} & 3\frac{1}{2}\sum_{j=1}^{d}\sum_{\substack{k=1\\k\neq j}}^{d} g_{,j}^{2}g_{,kk}\mu_{j,2}\mu_{k,2} \\ & + 3\frac{1}{2}2\cdot 2\sum_{j=1}^{d-1}\sum_{k=j+1}^{d} g_{,j}g_{,k}g_{,jk}\mu_{j,2}\mu_{k,2} \\ & + 3\frac{1}{2}\sum_{j=1}^{d} g_{,j}^{2}g_{,jj}\mu_{j,4} \end{aligned} \tag{A.26f}$$

VIII:

The fourth mixed or cross central moments between the variables μ_{jklm} that $j=k\neq l=m$:

$$3g_{\mu}\frac{1}{4}\sum_{j=1}^{d}\sum_{l=1}^{d} g_{,jj}g_{,ll}\mu_{j,2}\mu_{l,2} \tag{A.27a}$$

The fourth mixed or cross central moments between the variables μ_{jklm} that $j=l\neq k=m$:

$$3g_{\mu}\frac{1}{4}\sum_{j=1}^{d}\sum_{k=1}^{d} g_{,jk}^{2}\mu_{j,2}\mu_{k,2} \tag{A.27b}$$

The fourth cross moments between the variables μ_{jklm} that $j=m\neq k=l$ (equivalent to previous case):

$$3g_{\mu}\frac{1}{4}\sum_{j=1}^{d}\sum_{k=1}^{d} g_{,jk}^{2}\mu_{j,2}\mu_{k,2} \tag{A.27c}$$

The fourth mixed or cross central moments between the variables μ_{jklm} that $j=k=l=m$ lead to the fourth moment $\mu_{j,4}$.

$$3g_{\mu}\frac{1}{4}\sum_{j=1}^{d} g_{,jj}^{2}\mu_{j,4} \tag{A.27d}$$

Summarizing and reassigning indexes to compact further:

$$3g_\mu \frac{1}{4}\sum_{j=1}^{d}\sum_{k=1}^{d}\sum_{l=1}^{d}\sum_{m=1}^{d} g_{,jk}g_{,lm}\mu_{jklm} = 3g_\mu \frac{1}{4}\sum_{j=1}^{d}\sum_{\substack{k=1\\k\neq j}}^{d} g_{,jj}g_{,kk}\mu_{j,2}\mu_{k,2} + 3g_\mu \frac{1}{4}2\sum_{j=1}^{d}\sum_{\substack{k=1\\k\neq j}}^{d} g_{,jk}^2\mu_{j,2}\mu_{k,2} + 3g_\mu \frac{1}{4}\sum_{j=1}^{d} g_{,jj}^2\mu_{j,4} \tag{A.27e}$$

Changing in the symmetric terms, the first upper limit d for $d-1$, the second lower limit $\substack{k=1\\k\neq j}$ for $k=j+1$ and multiplying by 2 to compensate the symmetry lost with the limits change:

$$3g_\mu \frac{1}{4}\sum_{j=1}^{d}\sum_{k=1}^{d}\sum_{l=1}^{d}\sum_{m=1}^{d} g_{,jk}g_{,lm}\mu_{jklm} = 3g_\mu \frac{1}{4}\cdot 2\sum_{j=1}^{d-1}\sum_{k=j+1}^{d} g_{,jj}g_{,kk}\mu_{j,2}\mu_{k,2} + 3g_\mu \frac{1}{4}2\cdot 2\sum_{j=1}^{d-1}\sum_{k=j+1}^{d} g_{,jk}^2\mu_{j,2}\mu_{k,2} + 3g_\mu \frac{1}{4}\sum_{j=1}^{d} g_{,jj}^2\mu_{j,4} \tag{A.27f}$$

IX:

Note that in the following mathematical derivation, several equivalent cases are grouped together for brevity. The fifth mixed or cross central moments between the variables μ_{jklmr} that $j=k\neq l=m=r$, $j=l\neq k=m=r$, $j=m\neq k=l=r$ and $j=r\neq k=l=m$ are equivalent. All together reassigning indexes lead to:

$$3\frac{1}{4}4\sum_{j=1}^{d}\sum_{\substack{k=1\\k\neq j}}^{d} g_{,j}g_{,jk}g_{,kk}\mu_{j,2}\mu_{k,3} \tag{A.28a}$$

The fifth mixed or cross central moments between the variables μ_{jklmr} that $j=k=l\neq m=r$ and $j=m=r\neq k=l$ are equivalent. All together reassigning indexes lead to:

$$3\frac{1}{4}2\sum_{j=1}^{d}\sum_{\substack{k=1\\k\neq j}}^{d} g_{,j}g_{,jj}g_{,kk}\mu_{j,3}\mu_{k,2} \tag{A.28b}$$

The fifth mixed or cross central moments between the variables μ_{jklmr} that $_{j=k=m\neq l=r}$, $_{j=k=r\neq l=m}$, $_{j=l=m\neq k=r}$ and $_{j=l=r\neq k=m}$ are equivalent. All together reassigning indexes lead to:

$$3\frac{1}{4}4\sum_{j=1}^{d}\sum_{\substack{k=1\\k\neq j}}^{d} g_{,j}g_{,jk}^{2}\mu_{j,3}\mu_{k,2} \tag{A.28c}$$

The fifth mixed or cross central moments between the variables μ_{jklmr} that $_{j=k=l=m=r}$ lead to the fifth moment $\mu_{j,5}$.

$$3\frac{1}{4}\sum_{j=1}^{d} g_{,j}g_{,jj}^{2}\mu_{j,5} \tag{A.28d}$$

Summarizing:

$$\begin{aligned}3\frac{1}{4}\sum_{j=1}^{d}\sum_{k=1}^{d}\sum_{l=1}^{d}\sum_{m=1}^{d}\sum_{r=1}^{d} g_{,j}g_{,kl}g_{,mr}\mu_{jklmr} &= 3\frac{1}{4}4\sum_{j=1}^{d}\sum_{\substack{k=1\\k\neq j}}^{d} g_{,j}g_{,jk}g_{,kk}\mu_{j,2}\mu_{k,3}\\ &+ 3\frac{1}{4}2\sum_{j=1}^{d}\sum_{\substack{k=1\\k\neq j}}^{d} g_{,j}g_{,jj}g_{,kk}\mu_{j,3}\mu_{k,2}\\ &+ 3\frac{1}{4}4\sum_{j=1}^{d}\sum_{\substack{k=1\\k\neq j}}^{d} g_{,j}g_{,jk}^{2}\mu_{j,3}\mu_{k,2} + 3\frac{1}{4}\sum_{j=1}^{d} g_{,j}g_{,jj}^{2}\mu_{j,5}\end{aligned} \tag{A.28e}$$

$\boldsymbol{X}$:

This term follows the same strategy as in II.

$$6g_{\mu}\frac{1}{2}\sum_{j=1}^{d}\sum_{k=1}^{d}\sum_{l=1}^{d} g_{,j}g_{,kl}\mu_{jkl} = 6g_{\mu}\frac{1}{2}\sum_{j=1}^{d} g_{,j}g_{,jj}\mu_{j,3} \tag{A.29}$$

As a result, the second order approximation for the third central moment assuming independence leads to:

$$
\begin{aligned}
&\mu_3(Y,Y,Y) = \mu_{Y,3} \\
&\approx \underbrace{g_\mu^3}_{I} + \underbrace{\sum_{j=1}^{d} g_{,j}^3 \mu_{j,3}}_{II} \\
&\quad \underbrace{+\frac{3}{4}\sum_{j=1}^{d-2}\sum_{k=j+1}^{d-1}\sum_{l=k+1}^{d} g_{,jj}g_{,kk}g_{,ll}\mu_{j,2}\mu_{k,2}\mu_{l,2} + \frac{3}{2}\sum_{j=1}^{d}\sum_{\substack{k=1\\k\neq j}}^{d-1}\sum_{\substack{l=k+1\\l\neq j}}^{d} g_{,jj}g_{,kl}^2\mu_{j,2}\mu_{k,2}\mu_{l,2}}_{III} \\
&\quad \underbrace{+6\sum_{j=1}^{d-2}\sum_{k=j+1}^{d-1}\sum_{l=k+1}^{d} g_{,jk}g_{,jl}g_{,kl}\mu_{j,2}\mu_{k,2}\mu_{l,2} + \frac{3}{2}\sum_{j=1}^{d-1}\sum_{k=j+1}^{d} g_{,jj}g_{,jk}g_{,kk}\mu_{j,3}\mu_{k,3}}_{III} \\
&\quad \underbrace{+\sum_{j=1}^{d-1}\sum_{k=j+1}^{d} g_{,jk}^3\mu_{j,3}\mu_{k,3} + \frac{3}{8}\sum_{j=1}^{d}\sum_{\substack{k=1\\k\neq j}}^{d} g_{,jj}g_{,kk}^2\mu_{j,2}\mu_{k,4} + \frac{3}{2}\sum_{j=1}^{d}\sum_{\substack{k=1\\k\neq j}}^{d} g_{,jk}^2 g_{,kk}\mu_{j,2}\mu_{k,4}}_{III} \\
&\quad \underbrace{+\frac{1}{8}\sum_{j=1}^{d} g_{,jj}^3\mu_{j,6}}_{III} + \underbrace{0}_{IV} + \underbrace{\frac{3}{2}g_\mu^2\sum_{j=1}^{d} g_{,jj}\mu_{j,2}}_{V} + \underbrace{3g_\mu\sum_{j=1}^{d} g_{,j}^2\mu_{j,2}}_{VI} \\
&\quad \underbrace{+\frac{3}{2}\sum_{j=1}^{d}\sum_{\substack{k=1\\k\neq j}}^{d} g_{,j}^2 g_{,kk}\mu_{j,2}\mu_{k,2} + 6\sum_{j=1}^{d-1}\sum_{k=j+1}^{d} g_{,j}g_{,k}g_{,jk}\mu_{j,2}\mu_{k,2} + \frac{3}{2}\sum_{j=1}^{d} g_{,j}^2 g_{,jj}\mu_{j,4}}_{VII} \\
&\quad \underbrace{+\frac{3}{2}g_\mu\sum_{j=1}^{d-1}\sum_{k=j+1}^{d} g_{,jj}g_{,kk}\mu_{j,2}\mu_{k,2} + 3g_\mu\sum_{j=1}^{d-1}\sum_{k=j+1}^{d} g_{,jk}^2\mu_{j,2}\mu_{k,2} + \frac{3}{4}g_\mu\sum_{j=1}^{d} g_{,jj}^2\mu_{j,4}}_{VIII} \\
&\quad \underbrace{+3\sum_{j=1}^{d}\sum_{\substack{k=1\\k\neq j}}^{d} g_{,j}g_{,jk}g_{,kk}\mu_{j,2}\mu_{k,3} + \frac{3}{2}\sum_{j=1}^{d}\sum_{\substack{k=1\\k\neq j}}^{d} g_{,j}g_{,jj}g_{,kk}\mu_{j,3}\mu_{k,2} + 3\sum_{j=1}^{d}\sum_{\substack{k=1\\k\neq j}}^{d} g_{,j}g_{,jk}^2\mu_{j,3}\mu_{k,2}}_{IX} \\
&\quad \underbrace{+\frac{3}{4}\sum_{j=1}^{d} g_{,j}g_{,jj}^2\mu_{j,5}}_{IX} + \underbrace{3g_\mu\sum_{j=1}^{d} g_{,j}g_{,jj}\mu_{j,3}}_{X} - 3\mu_Y\sigma_Y^2 - \mu_Y^3
\end{aligned}
\tag{A.30}
$$

Note that the III and IX terms are divided into multiple lines.

A.2.6 Third central moment *skewness* first-order

The third central moment *skewness* first-order approximation for independent random variables is derived from Eq. (2.99) and Eq. (A.30) leading to:

$$\mu_3(Y,Y,Y) = \mu_{Y,3} \approx \underbrace{\sum_{j=1}^{d} g_{,j}^3 \mu_{j,3}}_{II} \tag{A.31}$$

A.2.7 Fourth central moment *kurtosis* second-order

Assuming independence between the random variables, the Eq. (2.120) becomes:

II:

The fourth mixed or cross central moments between the variables μ_{jklm} that $_{j\neq k\neq l\neq m}$ are equal to 0 and the fourth cross central moments μ_{jklm} that $_{j=k=l=m}$ lead to the fourth central moment $\mu_{j,4}$.

$$\sum_{j=1}^{d}\sum_{k=1}^{d}\sum_{l=1}^{d}\sum_{m=1}^{d} g_{,j}g_{,k}g_{,l}g_{,m}\mu_{jklm} = \sum_{j=1}^{d} g_{,j}^4 \mu_{j,4} \tag{A.32}$$

III:

Note that in the following mathematical derivation, several equivalent cases are grouped together for brevity. Moreover, the equivalent combinations of indexes in this term have been omitted for conciseness.

The eighth mixed or cross central moments between the variables $\mu_{jklmrstu}$ that $_{j=k\neq l=m\neq r=s\neq t=u}$:

$$\frac{1}{16}\sum_{j=1}^{d}\sum_{\substack{k=1\\k\neq j}}^{d}\sum_{\substack{l=1\\l\neq k\\l\neq j}}^{d}\sum_{\substack{m=1\\m\neq l\\m\neq k\\m\neq j}}^{d} g_{,jj}g_{,kk}g_{,ll}g_{,mm}\mu_{j,2}\mu_{k,2}\mu_{l,2}\mu_{m,2} \tag{A.33a}$$

The eighth mixed or cross central moments between the variables $\mu_{jklmrstu}$ that $_{j=k\neq l=m\neq r=t\neq s=u}$, and considering up to twelve equivalent combinations lead to:

$$\frac{1}{16}12\sum_{j=1}^{d}\sum_{\substack{k=1\\k\neq j}}^{d}\sum_{\substack{l=1\\l\neq k\\l\neq j}}^{d}\sum_{\substack{m=1\\m\neq l\\m\neq k\\m\neq j}}^{d} g_{,jj}g_{,kk}g_{,lm}^2\mu_{j,2}\mu_{k,2}\mu_{l,2}\mu_{m,2} \tag{A.33b}$$

The eighth mixed or cross central moments between the variables $\mu_{jklmrstu}$ that $_{j=l\neq k=m\neq r=t\neq s=u}$, and considering up to twelve equivalent combinations lead to:

$$\frac{1}{16}12\sum_{j=1}^{d}\sum_{\substack{k=1\\k\neq j}}^{d}\sum_{\substack{l=1\\l\neq k\\l\neq j}}^{d}\sum_{\substack{m=1\\m\neq l\\m\neq k\\m\neq j}}^{d} g_{,jk}^{2}g_{,lm}^{2}\mu_{j,2}\mu_{k,2}\mu_{l,2}\mu_{m,2} \tag{A.33c}$$

The eighth mixed or cross central moments between the variables $\mu_{jklmrstu}$ that $_{j=k\neq l=r\neq m=t\neq s=u}$, and considering up to thirty-two equivalent combinations lead to:

$$\frac{1}{16}32\sum_{j=1}^{d}\sum_{\substack{k=1\\k\neq j}}^{d}\sum_{\substack{l=1\\l\neq k\\l\neq j}}^{d}\sum_{\substack{m=1\\m\neq l\\m\neq k\\m\neq j}}^{d} g_{,jj}g_{,kl}g_{,km}g_{,lm}\mu_{j,2}\mu_{k,2}\mu_{l,2}\mu_{m,2} \tag{A.33d}$$

The eighth mixed or cross central moments between the variables $\mu_{jklmrstu}$ that $_{j=l\neq k=r\neq m=t\neq s=u}$, and considering up to forty-eight equivalent combinations lead to:

$$\frac{1}{16}48\sum_{j=1}^{d}\sum_{\substack{k=1\\k\neq j}}^{d}\sum_{\substack{l=1\\l\neq k\\l\neq j}}^{d}\sum_{\substack{m=1\\m\neq l\\m\neq k\\m\neq j}}^{d} g_{,jk}g_{,jl}g_{,km}g_{,lm}\mu_{j,2}\mu_{k,2}\mu_{l,2}\mu_{m,2} \tag{A.33e}$$

The eighth mixed or cross central moments between the variables $\mu_{jklmrstu}$ that $_{j=k\neq l=r=t\neq m=s=u}$, and considering up to sixteen equivalent combinations lead to:

$$\frac{1}{16}16\sum_{j=1}^{d}\sum_{\substack{k=1\\k\neq j}}^{d}\sum_{\substack{l=1\\l\neq k\\l\neq j}}^{d} g_{,jj}g_{,kl}^{3}\mu_{j,2}\mu_{k,3}\mu_{l,3} \tag{A.33f}$$

The eighth mixed or cross central moments between the variables $\mu_{jklmrstu}$ that $_{j=k=l\neq m=r=s\neq t=u}$, and considering up to twenty-four equivalent combinations lead to:

$$\frac{1}{16}24\sum_{j=1}^{d}\sum_{\substack{k=1\\k\neq j}}^{d}\sum_{\substack{l=1\\l\neq k\\l\neq j}}^{d} g_{,jj}g_{,jk}g_{,kk}g_{,ll}\mu_{j,3}\mu_{k,3}\mu_{l,2} \tag{A.33g}$$

The eighth mixed or cross central moments between the variables $\mu_{jklmrstu}$ that $_{j=k=l\neq r=s=t\neq m=u}$, and considering up to forty-eight equivalent combinations lead to:

$$\frac{1}{16}48\sum_{j=1}^{d}\sum_{\substack{k=1\\k\neq j}}^{d}\sum_{\substack{l=1\\l\neq k\\l\neq j}}^{d} g_{,jj}g_{,kk}g_{,jl}g_{,kl}\mu_{j,3}\mu_{k,3}\mu_{l,2} \tag{A.33h}$$

The eighth mixed or cross central moments between the variables $\mu_{jklmrstu}$ that $_{j=k=l\neq m=r=t\neq s=u}$, and considering up to ninety-six equivalent combinations lead to:

$$\frac{1}{16}96\sum_{j=1}^{d}\sum_{\substack{k=1\\k\neq j}}^{d}\sum_{\substack{l=1\\l\neq k\\l\neq j}}^{d} g_{,jj}g_{,kl}^{2}g_{,jk}\mu_{j,3}\mu_{k,3}\mu_{l,2} \tag{A.33i}$$

The eighth mixed or cross central moments between the variables $\mu_{jklmrstu}$ that $_{j=l\neq k=r=t\neq m=s=u}$, and considering up to ninety-six equivalent combinations lead to:

$$\frac{1}{16}96\sum_{j=1}^{d}\sum_{\substack{k=1\\k\neq j}}^{d}\sum_{\substack{l=1\\l\neq k\\l\neq j}}^{d} g_{,jk}g_{,jl}g_{,kl}^{2}\mu_{j,2}\mu_{k,3}\mu_{l,3} \tag{A.33j}$$

The eighth mixed or cross central moments between the variables $\mu_{jklmrstu}$ that $_{j=k=l=m\neq r=s\neq t=u}$, and considering up to six equivalent combinations lead to:

$$\frac{1}{16}6\sum_{j=1}^{d}\sum_{\substack{k=1\\k\neq j}}^{d}\sum_{\substack{l=1\\l\neq k\\l\neq j}}^{d} g_{,jj}^{2}g_{,kk}g_{,ll}\mu_{j,4}\mu_{k,2}\mu_{l,2} \tag{A.33k}$$

The eighth mixed or cross central moments between the variables $\mu_{jklmrstu}$ that $_{j=k=l=m\neq r=t\neq s=u}$, and considering up to twelve equivalent combinations lead to:

$$\frac{1}{16}12\sum_{j=1}^{d}\sum_{\substack{k=1\\k\neq j}}^{d}\sum_{\substack{l=1\\l\neq k\\l\neq j}}^{d} g_{,jj}^{2}g_{,kl}^{2}\mu_{j,4}\mu_{k,2}\mu_{l,2} \tag{A.33l}$$

The eighth mixed or cross central moments between the variables $\mu_{jklmrstu}$ that $_{j=k\neq l=m=r=t\neq s=u}$, and considering up to forty-eight equivalent combinations lead to:

$$\frac{1}{16}48\sum_{j=1}^{d}\sum_{\substack{k=1\\k\neq j}}^{d}\sum_{\substack{l=1\\l\neq k\\l\neq j}}^{d} g_{,jj}g_{,kk}g_{,kl}^{2}\mu_{j,2}\mu_{k,4}\mu_{l,2} \tag{A.33m}$$

The eighth mixed or cross central moments between the variables $\mu_{jklmrstu}$ that $_{j=l=r=t\neq k=m\neq s=u}$, and considering up to forty-eight equivalent combinations lead to:

$$\frac{1}{16}48\sum_{j=1}^{d}\sum_{\substack{k=1\\k\neq j}}^{d}\sum_{\substack{l=1\\l\neq k\\l\neq j}}^{d} g_{,jk}^{2}g_{,jl}^{2}\mu_{j,4}\mu_{k,2}\mu_{l,2} \tag{A.33n}$$

The eighth mixed or cross central moments between the variables $\mu_{jklmrstu}$ that $_{j=k=l=r\neq m=t\neq s=u}$, and considering up to ninety-six equivalent combinations lead to:

$$\frac{1}{16}96\sum_{j=1}^{d}\sum_{\substack{k=1\\k\neq j}}^{d}\sum_{\substack{l=1\\l\neq k\\l\neq j}}^{d} g_{,jj}g_{,jk}g_{,kl}g_{,jl}\mu_{j,4}\mu_{k,2}\mu_{l,2} \tag{A.33o}$$

The eighth mixed or cross central moments between the variables $\mu_{jklmrstu}$ that $_{j=k=l=m\neq r=s=t=u}$, and considering up to three equivalent combinations lead to:

$$\frac{1}{16}3\sum_{j=1}^{d}\sum_{\substack{k=1\\k\neq j}}^{d} g_{,jj}^{2}g_{,kk}^{2}\mu_{j,4}\mu_{k,4} \tag{A.33p}$$

The eighth mixed or cross central moments between the variables $\mu_{jklmrstu}$ that $_{j=l=r=t\neq k=m=s=u}$, and considering up to eight equivalent combinations lead to:

$$\frac{1}{16}8\sum_{j=1}^{d}\sum_{\substack{k=1\\k\neq j}}^{d} g_{,jk}^{4}\mu_{j,4}\mu_{k,4} \tag{A.33q}$$

The eighth mixed or cross central moments between the variables $\mu_{jklmrstu}$ that $_{j=k=l=r\neq m=s=t=u}$, and considering up to twenty-four equivalent combinations lead to:

$$\frac{1}{16}24\sum_{j=1}^{d}\sum_{\substack{k=1\\k\neq j}}^{d} g_{,jj}g_{,kk}g_{,jk}^{2}\mu_{j,4}\mu_{k,4} \tag{A.33r}$$

The eighth mixed or cross central moments between the variables $\mu_{jklmrstu}$ that $_{j=k=l=m=r=s=t=u}$ lead to the eighth moment $\mu_{j,8}$.

$$\frac{1}{16}\sum_{j=1}^{d} g_{,jj}^{4}\mu_{j,8} \tag{A.33s}$$

Summarizing:

$$\frac{1}{16}\sum_{j=1}^{d}\sum_{k=1}^{d}\sum_{l=1}^{d}\sum_{m=1}^{d}\sum_{r=1}^{d}\sum_{s=1}^{d}\sum_{t=1}^{d}\sum_{u=1}^{d} g_{,jk}g_{,lm}g_{,rs}g_{,tu}\mu_{jklmrstu}$$

$$= \frac{1}{16}\sum_{j=1}^{d}\sum_{\substack{k=1\\k\neq j}}^{d}\sum_{\substack{l=1\\l\neq k\\l\neq j}}^{d}\sum_{\substack{m=1\\m\neq l\\m\neq k\\m\neq j}}^{d} g_{,jj}g_{,kk}g_{,ll}g_{,mm}\mu_{j,2}\mu_{k,2}\mu_{l,2}\mu_{m,2}$$

$$+ \frac{1}{16}12\sum_{j=1}^{d}\sum_{\substack{k=1\\k\neq j}}^{d}\sum_{\substack{l=1\\l\neq k\\l\neq j}}^{d}\sum_{\substack{m=1\\m\neq l\\m\neq k\\m\neq j}}^{d} g_{,jj}g_{,kk}g_{,lm}^2\mu_{j,2}\mu_{k,2}\mu_{l,2}\mu_{m,2}$$

$$+ \frac{1}{16}12\sum_{j=1}^{d}\sum_{\substack{k=1\\k\neq j}}^{d}\sum_{\substack{l=1\\l\neq k\\l\neq j}}^{d}\sum_{\substack{m=1\\m\neq l\\m\neq k\\m\neq j}}^{d} g_{,jk}^2g_{,lm}^2\mu_{j,2}\mu_{k,2}\mu_{l,2}\mu_{m,2}$$

$$+ \frac{1}{16}32\sum_{j=1}^{d}\sum_{\substack{k=1\\k\neq j}}^{d}\sum_{\substack{l=1\\l\neq k\\l\neq j}}^{d}\sum_{\substack{m=1\\m\neq l\\m\neq k\\m\neq j}}^{d} g_{,jj}g_{,kl}g_{,km}g_{,lm}\mu_{j,2}\mu_{k,2}\mu_{l,2}\mu_{m,2}$$

$$+ \frac{1}{16}48\sum_{j=1}^{d}\sum_{\substack{k=1\\k\neq j}}^{d}\sum_{\substack{l=1\\l\neq k\\l\neq j}}^{d}\sum_{\substack{m=1\\m\neq l\\m\neq k\\m\neq j}}^{d} g_{,jk}g_{,jl}g_{,km}g_{,lm}\mu_{j,2}\mu_{k,2}\mu_{l,2}\mu_{m,2} + \frac{1}{16}16\sum_{j=1}^{d}\sum_{\substack{k=1\\k\neq j}}^{d}\sum_{\substack{l=1\\l\neq k\\l\neq j}}^{d} g_{,jj}g_{,kl}^3\mu_{j,2}\mu_{k,3}\mu_{l,3}$$

$$+ \frac{1}{16}24\sum_{j=1}^{d}\sum_{\substack{k=1\\k\neq j}}^{d}\sum_{\substack{l=1\\l\neq k\\l\neq j}}^{d} g_{,jj}g_{,jk}g_{,kk}g_{,ll}\mu_{j,3}\mu_{k,3}\mu_{l,2} + \frac{1}{16}48\sum_{j=1}^{d}\sum_{\substack{k=1\\k\neq j}}^{d}\sum_{\substack{l=1\\l\neq k\\l\neq j}}^{d} g_{,jj}g_{,kk}g_{,jl}g_{,kl}\mu_{j,3}\mu_{k,3}\mu_{l,2}$$

$$+ \frac{1}{16}96\sum_{j=1}^{d}\sum_{\substack{k=1\\k\neq j}}^{d}\sum_{\substack{l=1\\l\neq k\\l\neq j}}^{d} g_{,jj}g_{,kl}^2g_{,jk}\mu_{j,3}\mu_{k,3}\mu_{l,2} + \frac{1}{16}96\sum_{j=1}^{d}\sum_{\substack{k=1\\k\neq j}}^{d}\sum_{\substack{l=1\\l\neq k\\l\neq j}}^{d} g_{,jk}g_{,jl}g_{,kl}^2\mu_{j,2}\mu_{k,3}\mu_{l,3}$$

$$+ \frac{1}{16}6\sum_{j=1}^{d}\sum_{\substack{k=1\\k\neq j}}^{d}\sum_{\substack{l=1\\l\neq k\\l\neq j}}^{d} g_{,jj}^2g_{,kk}g_{,ll}\mu_{j,4}\mu_{k,2}\mu_{l,2} + \frac{1}{16}12\sum_{j=1}^{d}\sum_{\substack{k=1\\k\neq j}}^{d}\sum_{\substack{l=1\\l\neq k\\l\neq j}}^{d} g_{,jj}^2g_{,kl}^2\mu_{j,4}\mu_{k,2}\mu_{l,2}$$

$$+ \frac{1}{16}48\sum_{j=1}^{d}\sum_{\substack{k=1\\k\neq j}}^{d}\sum_{\substack{l=1\\l\neq k\\l\neq j}}^{d} g_{,jj}g_{,kk}g_{,kl}^2\mu_{j,2}\mu_{k,4}\mu_{l,2} + \frac{1}{16}48\sum_{j=1}^{d}\sum_{\substack{k=1\\k\neq j}}^{d}\sum_{\substack{l=1\\l\neq k\\l\neq j}}^{d} g_{,jk}^2g_{,jl}^2\mu_{j,4}\mu_{k,2}\mu_{l,2}$$

$$+ \frac{1}{16}96\sum_{j=1}^{d}\sum_{\substack{k=1\\k\neq j}}^{d}\sum_{\substack{l=1\\l\neq k\\l\neq j}}^{d} g_{,jj}g_{,jk}g_{,kl}g_{,jl}\mu_{j,4}\mu_{k,2}\mu_{l,2} + \frac{1}{16}3\sum_{j=1}^{d}\sum_{\substack{k=1\\k\neq j}}^{d} g_{,jj}^2g_{,kk}^2\mu_{j,4}\mu_{k,4}$$

$$+ \frac{1}{16}8\sum_{j=1}^{d}\sum_{\substack{k=1\\k\neq j}}^{d} g_{,jk}^4\mu_{j,4}\mu_{k,4} + \frac{1}{16}24\sum_{j=1}^{d}\sum_{\substack{k=1\\k\neq j}}^{d} g_{,jj}g_{,kk}g_{,jk}^2\mu_{j,4}\mu_{k,4} + \frac{1}{16}\sum_{j=1}^{d} g_{,jj}^4\mu_{j,8} \tag{A.33t}$$

Changing in the symmetric terms (with respect to two indexes), the first upper limit d for $d-1$, the second lower limit $\substack{k=1\\k\neq j}$ for $k=j+1$ and multiplying by 2 to compensate the symmetry lost. Changing in the symmetric terms (with respect to three indexes), the first upper limit d for $d-2$, the second upper limit d for $d-1$, the second lower limit $\substack{k=1\\k\neq j}$ for $k=j+1$, the third lower limit $\substack{l=1\\l\neq k\\l\neq j}$ for $l=k+1$ and multiplying by $3\cdot 2$ to compensate the symmetry lost. And changing in the symmetric terms (with respect to four indexes), the first upper limit d for $d-3$, the second upper limit d for $d-2$, the third upper limit d for $d-1$, the second lower limit $\substack{k=1\\k\neq j}$ for $k=j+1$, the third lower limit $\substack{l=1\\l\neq k\\l\neq j}$ for $l=k+1$, the fourth lower limit $\substack{m=1\\m\neq l\\m\neq k\\m\neq j}$ for $m=l+1$, and multiplying by $4\cdot 3\cdot 2$ to compensate the symmetry lost with the limits change:

$$
\begin{aligned}
&\frac{1}{16}\sum_{j=1}^{d}\sum_{k=1}^{d}\sum_{l=1}^{d}\sum_{m=1}^{d}\sum_{r=1}^{d}\sum_{s=1}^{d}\sum_{t=1}^{d}\sum_{u=1}^{d} g_{,jk}g_{,lm}g_{,rs}g_{,tu}\mu_{jklmrstu} \\
&= \frac{1}{16}\cdot 4\cdot 3\cdot 2\sum_{j=1}^{d-3}\sum_{k=j+1}^{d-2}\sum_{l=k+1}^{d-1}\sum_{m=l+1}^{d} g_{,jj}g_{,kk}g_{,ll}g_{,mm}\mu_{j,2}\mu_{k,2}\mu_{l,2}\mu_{m,2} \\
&\quad + \frac{1}{16}12\cdot 2\cdot 2\sum_{j=1}^{d-1}\sum_{k=j+1}^{d}\sum_{\substack{l=1\\ l\neq k\\ l\neq j}}^{d-1}\sum_{\substack{m=l+1\\ m\neq k\\ m\neq j}}^{d} g_{,jj}g_{,kk}g_{,lm}^2\mu_{j,2}\mu_{k,2}\mu_{l,2}\mu_{m,2} \\
&\quad + \frac{1}{16}12\cdot 4\cdot 3\cdot 2\sum_{j=1}^{d-3}\sum_{k=j+1}^{d-2}\sum_{l=k+1}^{d-1}\sum_{m=l+1}^{d} g_{,jk}^2g_{,lm}^2\mu_{j,2}\mu_{k,2}\mu_{l,2}\mu_{m,2} \\
&\quad + \frac{1}{16}32\cdot 2\sum_{j=1}^{d}\sum_{\substack{k=1\\ k\neq j}}^{d}\sum_{\substack{l=1\\ l\neq k\\ l\neq j}}^{d-1}\sum_{\substack{m=l+1\\ m\neq k\\ m\neq j}}^{d} g_{,jj}g_{,kl}g_{,km}g_{,lm}\mu_{j,2}\mu_{k,2}\mu_{l,2}\mu_{m,2} \\
&\quad + \frac{1}{16}48\cdot 4\cdot 3\cdot 2\sum_{j=1}^{d-3}\sum_{k=j+1}^{d-2}\sum_{l=k+1}^{d-1}\sum_{m=l+1}^{d} g_{,jk}g_{,jl}g_{,km}g_{,lm}\mu_{j,2}\mu_{k,2}\mu_{l,2}\mu_{m,2} \\
&\quad + \frac{1}{16}16\cdot 2\sum_{j=1}^{d}\sum_{\substack{k=1\\ k\neq j}}^{d-1}\sum_{\substack{l=k+1\\ l\neq j}}^{d} g_{,jj}g_{,kl}^3\mu_{j,2}\mu_{k,3}\mu_{l,3} + \frac{1}{16}24\cdot 2\sum_{j=1}^{d-1}\sum_{k=j+1}^{d}\sum_{\substack{l=1\\ l\neq k\\ l\neq j}}^{d} g_{,jj}g_{,jk}g_{,kk}g_{,ll}\mu_{j,3}\mu_{k,3}\mu_{l,2} \\
&\quad + \frac{1}{16}48\cdot 2\sum_{j=1}^{d-1}\sum_{k=j+1}^{d}\sum_{\substack{l=1\\ l\neq k\\ l\neq j}}^{d} g_{,jj}g_{,kk}g_{,jl}g_{,kl}\mu_{j,3}\mu_{k,3}\mu_{l,2} + \frac{1}{16}96\sum_{j=1}^{d}\sum_{\substack{k=1\\ k\neq j}}^{d}\sum_{\substack{l=1\\ l\neq k\\ l\neq j}}^{d} g_{,jj}g_{,jk}^2g_{,kl}\mu_{j,3}\mu_{k,3}\mu_{l,2} \\
&\quad + \frac{1}{16}96\cdot 2\sum_{j=1}^{d}\sum_{\substack{k=1\\ k\neq j}}^{d-1}\sum_{\substack{l=k+1\\ l\neq j}}^{d} g_{,jk}g_{,jl}g_{,kl}^2\mu_{j,2}\mu_{k,3}\mu_{l,3} + \frac{1}{16}6\cdot 2\sum_{j=1}^{d}\sum_{\substack{k=1\\ k\neq j}}^{d-1}\sum_{\substack{l=k+1\\ l\neq j}}^{d} g_{,jj}^2g_{,kk}g_{,ll}\mu_{j,4}\mu_{k,2}\mu_{l,2} \\
&\quad + \frac{1}{16}12\cdot 2\sum_{j=1}^{d}\sum_{\substack{k=1\\ k\neq j}}^{d-1}\sum_{\substack{l=k+1\\ l\neq j}}^{d} g_{,jj}^2g_{,kl}^2\mu_{j,4}\mu_{k,2}\mu_{l,2} + \frac{1}{16}48\sum_{j=1}^{d}\sum_{\substack{k=1\\ k\neq j}}^{d}\sum_{\substack{l=1\\ l\neq k\\ l\neq j}}^{d} g_{,jj}g_{,kk}g_{,kl}^2\mu_{j,2}\mu_{k,4}\mu_{l,2} \\
&\quad + \frac{1}{16}48\cdot 2\sum_{j=1}^{d}\sum_{\substack{k=1\\ k\neq j}}^{d-1}\sum_{\substack{l=k+1\\ l\neq j}}^{d} g_{,jk}^2g_{,jl}^2\mu_{j,4}\mu_{k,2}\mu_{l,2} + \frac{1}{16}96\cdot 2\sum_{j=1}^{d}\sum_{\substack{k=1\\ k\neq j}}^{d-1}\sum_{l=k+1}^{d}\sum_{\substack{l\neq j}} g_{,jj}g_{,jk}g_{,kl}g_{,jl}\mu_{j,4}\mu_{k,2}\mu_{l,2} \\
&\quad + \frac{1}{16}3\cdot 2\sum_{j=1}^{d-1}\sum_{k=j+1}^{d} g_{,jj}^2g_{,kk}^2\mu_{j,4}\mu_{k,4} + \frac{1}{16}8\cdot 2\sum_{j=1}^{d-1}\sum_{k=j+1}^{d} g_{,jk}^4\mu_{j,4}\mu_{k,4} \\
&\quad + \frac{1}{16}24\cdot 2\sum_{j=1}^{d-1}\sum_{k=j+1}^{d} g_{,jj}g_{,kk}g_{,jk}^2\mu_{j,4}\mu_{k,4} + \frac{1}{16}\sum_{j=1}^{d} g_{,jj}^4\mu_{j,8}
\end{aligned}
\tag{A.33u}
$$

V:

The covariances between the variables μ_{jk} that $_{j\neq k}$ are equal to 0 and the covariances μ_{jk} that $_{j=k}$ lead to the variance $\mu_{j,2} = \mathrm{Var}\,(X_j)$.

$$4g_\mu^3 \frac{1}{2} \sum_{j=1}^{d} \sum_{k=1}^{d} g_{,jk} \mu_{jk} = 4g_\mu^3 \frac{1}{2} \sum_{j=1}^{d} g_{,jj} \mu_{j,2} \tag{A.34}$$

VI:

The third mixed or cross central moments between the variables μ_{jkl} that $_{j\neq k\neq l}$ are equal to 0 and the third cross central moments μ_{jkl} that $_{j=k=l}$ lead to the third central moment $\mu_{j,3}$.

$$4g_\mu \sum_{j=1}^{d} \sum_{k=1}^{d} \sum_{l=1}^{d} g_{,j} g_{,k} g_{,l} \mu_{jkl} = 4g_\mu \sum_{j=1}^{d} g_{,j}^3 \mu_{j,3} \tag{A.35}$$

VII:

Note that in the following mathematical derivation, several equivalent cases are grouped together for brevity.

The fifth mixed or cross central moments between the variables μ_{jklmr} that $_{j=k=l\neq m=r}$:

$$4\frac{1}{2} \sum_{j=1}^{d} \sum_{\substack{k=1 \\ k\neq j}}^{d} g_{,j}^3 g_{,kk} \mu_{j,3} \mu_{k,2} \tag{A.36a}$$

The fifth mixed or cross central moments between the variables μ_{jklmr} that:

$$j = k \neq l = m = r \qquad j = l \neq k = m = r \qquad k = l \neq j = m = r$$

All together reassigning indexes lead to:

$$4\frac{1}{2} 3 \sum_{j=1}^{d} \sum_{\substack{k=1 \\ k\neq j}}^{d} g_{,j}^2 g_{,k} g_{,kk} \mu_{j,2} \mu_{k,3} \tag{A.36b}$$

The fifth mixed or cross central moments between the variables μ_{jklmr} that:

$$\begin{array}{lll} j = k = m \neq l = r & j = k = r \neq l = m & j = l = m \neq k = r \\ j = l = r \neq k = m & k = l = m \neq j = r & k = l = r \neq j = m \end{array}$$

All together reassigning indexes lead to:

$$4\frac{1}{2} 6 \sum_{j=1}^{d} \sum_{\substack{k=1 \\ k\neq j}}^{d} g_{,j}^2 g_{,k} g_{,jk} \mu_{j,3} \mu_{k,2} \tag{A.36c}$$

The fifth mixed or cross central moments between the variables μ_{jklmr} that $_{j=k=l=m=r}$ lead to the fifth moment $\mu_{j,5}$.

$$4\frac{1}{2}\sum_{j=1}^{d} g_{,j}^{3} g_{,jj} \mu_{j,5} \tag{A.36d}$$

Summarizing:

$$\begin{aligned}
4\frac{1}{2}\sum_{j=1}^{d}\sum_{k=1}^{d}\sum_{l=1}^{d}\sum_{m=1}^{d}\sum_{r=1}^{d} g_{,j} g_{,k} g_{,l} g_{,mr} \mu_{jklmr} = {} & 4\frac{1}{2}\sum_{j=1}^{d}\sum_{\substack{k=1\\k\neq j}}^{d} g_{,j}^{3} g_{,kk} \mu_{j,3}\mu_{k,2} \\
& + 4\frac{1}{2}3\sum_{j=1}^{d}\sum_{\substack{k=1\\k\neq j}}^{d} g_{,j}^{2} g_{,k} g_{,kk} \mu_{j,2}\mu_{k,3} \\
& + 4\frac{1}{2}6\sum_{j=1}^{d}\sum_{\substack{k=1\\k\neq j}}^{d} g_{,j}^{2} g_{,k} g_{,jk} \mu_{j,3}\mu_{k,2} \\
& + 4\frac{1}{2}\sum_{j=1}^{d} g_{,j}^{3} g_{,jj} \mu_{j,5}
\end{aligned} \tag{A.36e}$$

VIII:

This term follows the same strategy as in third central moment *skewness* in Subsection A.2.5, independence consideration of the III term.

$$\begin{aligned}
& 4g_{\mu}\frac{1}{8}\sum_{j=1}^{d}\sum_{k=1}^{d}\sum_{l=1}^{d}\sum_{m=1}^{d}\sum_{r=1}^{d}\sum_{s=1}^{d} g_{,jk} g_{,lm} g_{,rs} \mu_{jklmrs} \\
& = 4g_{\mu}\frac{1}{8}\cdot 2\cdot 3\sum_{j=1}^{d-2}\sum_{k=j+1}^{d-1}\sum_{l=k+1}^{d} g_{,jj} g_{,kk} g_{,ll} \mu_{j,2}\mu_{k,2}\mu_{l,2} \\
& \quad + 4g_{\mu}\frac{1}{8}6\cdot 2\sum_{j=1}^{d}\sum_{\substack{k=1\\k\neq j}}^{d-1}\sum_{\substack{l=k+1\\l\neq j}}^{d} g_{,jj} g_{,kl}^{2} \mu_{j,2}\mu_{k,2}\mu_{l,2} \\
& \quad + 4g_{\mu}\frac{1}{8}8\cdot 2\cdot 3\sum_{j=1}^{d-2}\sum_{k=j+1}^{d-1}\sum_{l=k+1}^{d} g_{,jk} g_{,jl} g_{,kl} \mu_{j,2}\mu_{k,2}\mu_{l,2} \\
& \quad + 4g_{\mu}\frac{1}{8}6\cdot 2\sum_{j=1}^{d-1}\sum_{k=j+1}^{d} g_{,jj} g_{,jk} g_{,kk} \mu_{j,3}\mu_{k,3} + 4g_{\mu}\frac{1}{8}4\cdot 2\sum_{j=1}^{d-1}\sum_{k=j+1}^{d} g_{,jk}^{3} \mu_{j,3}\mu_{k,3} \\
& \quad + 4g_{\mu}\frac{1}{8}3\sum_{j=1}^{d}\sum_{\substack{k=1\\k\neq j}}^{d} g_{,jj} g_{,kk}^{2} \mu_{j,2}\mu_{k,4} + 4g_{\mu}\frac{1}{8}12\sum_{j=1}^{d}\sum_{\substack{k=1\\k\neq j}}^{d} g_{,jk}^{2} g_{,kk} \mu_{j,2}\mu_{k,4} + 4g_{\mu}\frac{1}{8}\sum_{j=1}^{d} g_{,jj}^{3} \mu_{j,6}
\end{aligned} \tag{A.37}$$

IX:

The seventh mixed or cross central moments between the variables $\mu_{jklmrst}$ that $j{=}k{=}l{\neq}m{=}r{\neq}s{=}t$, $j{=}m{=}r{\neq}k{=}l{\neq}s{=}t$ and $j{=}s{=}t{\neq}k{=}l{\neq}m{=}r$ are equivalent. All together reassigning indexes lead to:

$$4\frac{1}{8}3\sum_{j=1}^{d}\sum_{\substack{k=1\\k\neq j}}^{d}\sum_{\substack{l=1\\l\neq k\\l\neq j}}^{d} g_{,j}g_{,jj}g_{,kk}g_{,ll}\mu_{j,3}\mu_{k,2}\mu_{l,2} \tag{A.38a}$$

The seventh mixed or cross central moments between the variables $\mu_{jklmrst}$ that:

$$\begin{array}{llll} j=k\ =l\neq m=s\neq r=t & j=k=l\neq m=t\ \neq r=s & j=m=r\neq k=s\neq l=t \\ j=m=r\neq k\ =t\neq l=s & j=s=t\neq k\ =m\neq l=r & j=s\ =t\neq k=r\neq l=m \end{array}$$

$$4\frac{1}{8}6\sum_{j=1}^{d}\sum_{\substack{k=1\\k\neq j}}^{d}\sum_{\substack{l=1\\l\neq k\\l\neq j}}^{d} g_{,j}g_{,jj}g_{,kl}^{2}\mu_{j,3}\mu_{k,2}\mu_{l,2} \tag{A.38b}$$

The seventh mixed or cross central moments between the variables $\mu_{jklmrst}$ that:

$$\begin{array}{llllll} j=r=t\neq k=l\ \neq m=s & j=r=s\ \neq k=l\neq m=t & j=m=t\neq k=l\ \neq r\ =s & j=m=s\ \neq k=l\neq r\ =t \\ j=l=t\neq k=s\ \neq m=r & j=l=s\ \neq k=t\neq m=r & j=k\ =t\neq l=s\ \neq m=r & j=k\ =s\ \neq l=t\neq m=r \\ j=l=r\neq k=m\neq s\ =t & j=l=m\neq k=r\neq s\ =t & j=k\ =r\neq l=m\neq s\ =t & j=k\ =m\neq l=r\neq s\ =t \end{array}$$

$$4\frac{1}{8}12\sum_{j=1}^{d}\sum_{\substack{k=1\\k\neq j}}^{d}\sum_{\substack{l=1\\l\neq k\\l\neq j}}^{d} g_{,j}g_{,jk}^{2}g_{,ll}\mu_{j,3}\mu_{k,2}\mu_{l,2} \tag{A.38c}$$

The seventh mixed or cross central moments between the variables $\mu_{jklmrst}$ that:

$$\begin{array}{llllll} j=k\ \neq l=m=r\neq s\ =t & j=k\ \neq l\ =s=t\neq m=r & j=l\neq k=m=r\ \neq s\ =t & j=l\neq k\ =s=t\neq m=r \\ j=m\neq k=l\ =r\neq s\ =t & j=m\neq r\ =s=t\neq k\ =l & j=r\neq k=l\ =m\neq s\ =t & j=r\neq m=s=t\neq k\ =l \\ j=s\ \neq k=l\ =t\neq m=r & j=s\ \neq m=r=t\neq k\ =l & j=t\neq k=l\ =s\ \neq m=r & j=t\neq m=r=s\neq k\ =l \end{array}$$

$$4\frac{1}{8}12\sum_{j=1}^{d}\sum_{\substack{k=1\\k\neq j}}^{d}\sum_{\substack{l=1\\l\neq k\\l\neq j}}^{d} g_{,j}g_{,jk}g_{,kk}g_{,ll}\mu_{j,2}\mu_{k,3}\mu_{l,2} \tag{A.38d}$$

The seventh mixed or cross central moments between the variables $\mu_{jklmrst}$ that:

$$\begin{array}{llllll} j=k\ \neq l=m\neq r=s\ =t & j=k\ \neq l=r\ \neq m=s\ =t & j=k\ \neq l\ =s\neq m=r=t & j=k\ \neq l\ =t\neq m=r=s \\ j=l\ \neq k=m\neq r=s\ =t & j=l\ \neq k=r\ \neq m=s\ =t & j=l\ \neq k\ =s\neq m=r=t & j=l\ \neq k\ =t\neq m=r=s \\ j=m\neq k=r\ \neq l=s\ =t & j=m\neq l=r\ \neq k\ =s\ =t & j=m\neq r\ =s\neq k\ =l=t & j=m\neq r\ =t\neq k\ =l=s \\ j=r\ \neq k=m\neq l=s\ =t & j=r\ \neq l=m\neq k\ =s\ =t & j=r\ \neq m=s\neq k\ =l=t & j=r\ \neq m=t\neq k\ =l=s \\ j=s\ \neq k=t\ \neq l=m=r & j=s\ \neq l=t\ \neq k\ =m=r & j=s\ \neq m=t\neq k\ =l=r & j=s\ \neq r\ =t\neq k\ =l=m \\ j=t\ \neq k=s\ \neq l=m=r & j=t\ \neq l=s\ \neq k\ =m=r & j=t\ \neq m=s\neq k\ =l=r & j=t\ \neq r\ =s\neq k\ =l=m \end{array}$$

$$4\frac{1}{8}24\sum_{j=1}^{d}\sum_{\substack{k=1\\k\neq j}}^{d}\sum_{\substack{l=1\\l\neq k\\l\neq j}}^{d} g_{,j}g_{,jk}g_{,kl}g_{,ll}\mu_{j,2}\mu_{k,2}\mu_{l,3} \tag{A.38e}$$

The seventh mixed or cross central moments between the variables $\mu_{jklmrst}$ that:

$$\begin{array}{llll}
j=r=t\neq k=m\neq l=s & j=r=s\neq k=m\neq l=t & j=l=t\neq k=m\neq r=s & j=l=s\neq k=m\neq r=t\\
j=m=t\neq k=r\neq l=s & j=m=s\neq k=r\neq l=t & j=l=t\neq k=r\neq m=s & j=l=s\neq k=r\neq m=t\\
j=r=t\neq k=s\neq l=m & j=m=t\neq k=s\neq l=r & j=l=r\neq k=s\neq m=t & j=l=m\neq k=s\neq r=t\\
j=r=s\neq k=t\neq l=m & j=m=s\neq k=t\neq l=r & j=l=r\neq k=t\neq m=s & j=l=m\neq k=t\neq r=s\\
j=k=t\neq l=m\neq r=s & j=k=s\neq l=m\neq r=t & j=k=t\neq l=r\neq m=s & j=k=s\neq l=r\neq m=t\\
j=k=r\neq l=s\neq m=t & j=k=m\neq l=s\neq r=t & j=k=r\neq l=t\neq m=s & j=k=m\neq l=t\neq r=s
\end{array}$$

$$4\frac{1}{8}24\sum_{j=1}^{d}\sum_{\substack{k=1\\k\neq j}}^{d}\sum_{\substack{l=1\\l\neq k\\l\neq j}}^{d} g_{,j}g_{,jk}g_{,kl}g_{,jl}\mu_{j,3}\mu_{k,2}\mu_{l,2} \tag{A.38f}$$

The seventh mixed or cross central moments between the variables $\mu_{jklmrst}$ that:

$$\begin{array}{llll}
j=k\neq m=s\neq l=r=t & j=k\neq m=t\neq l=r=s & j=k\neq r=s\neq l=m=t & j=k\neq r=t\neq l=m=s\\
j=l\neq m=s\neq k=r=t & j=l\neq m=t\neq k=r=s & j=l\neq r=s\neq k=m=t & j=l\neq r=t\neq k=m=s\\
j=m\neq k=s\neq l=r=t & j=m\neq k=t\neq l=r=s & j=m\neq l=s\neq k=r=t & j=m\neq l=t\neq k=r=s\\
j=r\neq k=s\neq l=m=t & j=r\neq k=t\neq l=m=s & j=r\neq l=s\neq k=m=t & j=r\neq l=t\neq k=m=s\\
j=s\neq k=m\neq l=r=t & j=s\neq k=r\neq l=m=t & j=s\neq l=m\neq k=r=t & j=s\neq l=r\neq k=m=t\\
j=t\neq k=m\neq l=r=s & j=t\neq k=r\neq l=m=s & j=t\neq l=m\neq k=r=s & j=t\neq l=r\neq k=m=s
\end{array}$$

$$4\frac{1}{8}24\sum_{j=1}^{d}\sum_{\substack{k=1\\k\neq j}}^{d}\sum_{\substack{l=1\\l\neq k\\l\neq j}}^{d} g_{,j}g_{,jl}g_{,kl}^{2}\mu_{j,2}\mu_{k,2}\mu_{l,3} \tag{A.38g}$$

The seventh mixed or cross central moments between the variables $\mu_{jklmrst}$ that:

$$j=k=l=m=r\neq s=t \qquad j=k=l=s=t\neq m=r \qquad j=m=r=s=t\neq k=l$$

$$4\frac{1}{8}3\sum_{j=1}^{d}\sum_{\substack{k=1\\k\neq j}}^{d} g_{,j}g_{,jj}^{2}g_{,kk}\mu_{j,5}\mu_{k,2} \tag{A.38h}$$

The seventh mixed or cross central moments between the variables $\mu_{jklmrst}$ that:

$$\begin{array}{lll}
j=k\neq l=m=r=s=t & j=l\neq k=m=r=s=t & j=m\neq k=l=r=s=t\\
j=r\neq k=l=m=s=t & j=s\neq k=l=m=r=t & j=t\neq k=l=m=r=s
\end{array}$$

$$4\frac{1}{8}6\sum_{j=1}^{d}\sum_{\substack{k=1\\k\neq j}}^{d} g_{,j}g_{,jk}g_{,kk}^{2}\mu_{j,2}\mu_{k,5} \tag{A.38i}$$

The seventh mixed or cross central moments between the variables $\mu_{jklmrst}$ that:

$$\begin{array}{llll}
j=k=l=m=s\neq r=t & j=k=l=m=t\neq r=s & j=k=l=r=s\neq m=t & j=k=l=r=t\neq m=s\\
j=k=m=r=s\neq l=t & j=k=m=r=t\neq l=s & j=k=m=s=t\neq l=r & j=k=r=s=t\neq l=m\\
j=l=m=r=s\neq k=t & j=l=m=r=t\neq k=s & j=l=m=s=t\neq k=r & j=l=r=s=t\neq k=m
\end{array}$$

$$4\frac{1}{8}12\sum_{j=1}^{d}\sum_{\substack{k=1\\k\neq j}}^{d} g_{,j}g_{,jj}g_{,jk}^{2}\mu_{j,5}\mu_{k,2} \tag{A.38j}$$

The seventh mixed or cross central moments between the variables $\mu_{jklmrst}$ that:

$$j=k=l\neq m=r=s=t \qquad j=m=r\neq k=l=s=t \qquad j=s=t\neq k=l=m=r$$

$$4\frac{1}{8}3\sum_{j=1}^{d}\sum_{\substack{k=1\\k\neq j}}^{d} g_{,j}g_{,jj}g_{,kk}^{2}\mu_{j,3}\mu_{k,4} \tag{A.38k}$$

The seventh mixed or cross central moments between the variables $\mu_{jklmrst}$ that:

$$\begin{array}{llll} j=k=l=m\neq r=s=t & j=k=l=r\neq m=s=t & j=k=l=s\neq m=r=t & j=k=l=t\neq m=r=s \\ j=k=m=r\neq l=s=t & j=k=s=t\neq l=m=r & j=l=m=r\neq k=s=t & j=l=s=t\neq k=m=r \\ j=m=r=s\neq k=l=t & j=m=r=t\neq k=l=s & j=m=s=t\neq k=l=r & j=r=s=t\neq k=l=m \end{array}$$

$$4\frac{1}{8}12\sum_{j=1}^{d}\sum_{\substack{k=1\\k\neq j}}^{d} g_{,j}g_{,jj}g_{,kk}g_{,jk}\mu_{j,4}\mu_{k,3} \tag{A.38l}$$

The seventh mixed or cross central moments between the variables $\mu_{jklmrst}$ that:

$$\begin{array}{llll} j=k=m\neq l=r=s=t & j=k=r\neq l=m=s=t & j=k=s\neq l=m=r=t & j=k=t\neq l=m=r=s \\ j=l=m\neq k=r=s=t & j=l=r\neq k=m=s=t & j=l=s\neq k=m=r=t & j=l=t\neq k=m=r=s \\ j=m=s\neq k=l=r=t & j=m=t\neq k=l=r=s & j=r=s\neq k=l=m=t & j=r=t\neq k=l=m=s \end{array}$$

$$4\frac{1}{8}12\sum_{j=1}^{d}\sum_{\substack{k=1\\k\neq j}}^{d} g_{,j}g_{,kk}g_{,jk}^{2}\mu_{j,3}\mu_{k,4} \tag{A.38m}$$

The seventh mixed or cross central moments between the variables $\mu_{jklmrst}$ that:

$$\begin{array}{llll} j=k=m=s\neq l=r=t & j=k=m=t\neq l=r=s & j=k=r=s\neq l=m=t & j=k=r=t\neq l=m=s \\ j=l=m=s\neq k=r=t & j=l=m=t\neq k=r=s & j=l=r=s\neq k=m=t & j=l=r=t\neq k=m=s \end{array}$$

$$4\frac{1}{8}8\sum_{j=1}^{d}\sum_{\substack{k=1\\k\neq j}}^{d} g_{,j}g_{,jk}^{3}\mu_{j,4}\mu_{k,3} \tag{A.38n}$$

The seventh mixed or cross central moments between the variables $\mu_{jklmrst}$ that $_{j=k=l=m=r=s=t}$ lead to the seventh moment $\mu_{j,7}$.

$$4\frac{1}{8}\sum_{j=1}^{d} g_{,j}g_{,jj}^{3}\mu_{j,7} \tag{A.38o}$$

Summarizing:

$$
\begin{aligned}
&4\frac{1}{8}\sum_{j=1}^{d}\sum_{k=1}^{d}\sum_{l=1}^{d}\sum_{m=1}^{d}\sum_{r=1}^{d}\sum_{s=1}^{d}\sum_{t=1}^{d} g_{,j}g_{,kl}g_{,mr}g_{,st}\mu_{jklmrst}\\
&\quad= 4\frac{1}{8}3\sum_{j=1}^{d}\sum_{\substack{k=1\\k\neq j}}^{d}\sum_{\substack{l=1\\l\neq k\\l\neq j}}^{d} g_{,j}g_{,jj}g_{,kk}g_{,ll}\mu_{j,3}\mu_{k,2}\mu_{l,2} + 4\frac{1}{8}6\sum_{j=1}^{d}\sum_{\substack{k=1\\k\neq j}}^{d}\sum_{\substack{l=1\\l\neq k\\l\neq j}}^{d} g_{,j}g_{,jj}g_{,kl}^{2}\mu_{j,3}\mu_{k,2}\mu_{l,2}\\
&\qquad+ 4\frac{1}{8}12\sum_{j=1}^{d}\sum_{\substack{k=1\\k\neq j}}^{d}\sum_{\substack{l=1\\l\neq k\\l\neq j}}^{d} g_{,j}g_{,jk}^{2}g_{,ll}\mu_{j,3}\mu_{k,2}\mu_{l,2} + 4\frac{1}{8}12\sum_{j=1}^{d}\sum_{\substack{k=1\\k\neq j}}^{d}\sum_{\substack{l=1\\l\neq k\\l\neq j}}^{d} g_{,j}g_{,jk}g_{,kk}g_{,ll}\mu_{j,2}\mu_{k,3}\mu_{l,2}\\
&\qquad+ 4\frac{1}{8}24\sum_{j=1}^{d}\sum_{\substack{k=1\\k\neq j}}^{d}\sum_{\substack{l=1\\l\neq k\\l\neq j}}^{d} g_{,j}g_{,jk}g_{,kl}g_{,ll}\mu_{j,2}\mu_{k,2}\mu_{l,3} + 4\frac{1}{8}24\sum_{j=1}^{d}\sum_{\substack{k=1\\k\neq j}}^{d}\sum_{\substack{l=1\\l\neq k\\l\neq j}}^{d} g_{,j}g_{,jk}g_{,kl}g_{,jl}\mu_{j,3}\mu_{k,2}\mu_{l,2}\\
&\qquad+ 4\frac{1}{8}24\sum_{j=1}^{d}\sum_{\substack{k=1\\k\neq j}}^{d}\sum_{\substack{l=1\\l\neq k\\l\neq j}}^{d} g_{,j}g_{,jl}g_{,kl}^{2}\mu_{j,2}\mu_{k,2}\mu_{l,3} + 4\frac{1}{8}3\sum_{j=1}^{d}\sum_{\substack{k=1\\k\neq j}}^{d} g_{,j}g_{,jj}^{2}g_{,kk}\mu_{j,5}\mu_{k,2}\\
&\qquad+ 4\frac{1}{8}6\sum_{j=1}^{d}\sum_{\substack{k=1\\k\neq j}}^{d} g_{,j}g_{,jk}g_{,kk}^{2}\mu_{j,2}\mu_{k,5} + 4\frac{1}{8}12\sum_{j=1}^{d}\sum_{\substack{k=1\\k\neq j}}^{d} g_{,j}g_{,jj}g_{,jk}^{2}\mu_{j,5}\mu_{k,2}\\
&\qquad+ 4\frac{1}{8}3\sum_{j=1}^{d}\sum_{\substack{k=1\\k\neq j}}^{d} g_{,j}g_{,jj}g_{,kk}^{2}\mu_{j,3}\mu_{k,4} + 4\frac{1}{8}12\sum_{j=1}^{d}\sum_{\substack{k=1\\k\neq j}}^{d} g_{,j}g_{,jj}g_{,kk}g_{,jk}\mu_{j,4}\mu_{k,3}\\
&\qquad+ 4\frac{1}{8}12\sum_{j=1}^{d}\sum_{\substack{k=1\\k\neq j}}^{d} g_{,j}g_{,kk}g_{,jk}^{2}\mu_{j,3}\mu_{k,4} + 4\frac{1}{8}8\sum_{j=1}^{d}\sum_{\substack{k=1\\k\neq j}}^{d} g_{,j}g_{,jk}^{3}\mu_{j,4}\mu_{k,3} + 4\frac{1}{8}\sum_{j=1}^{d} g_{,j}g_{,jj}^{3}\mu_{j,7}
\end{aligned}
\tag{A.38p}
$$

Changing in the symmetric terms (with respect to two indexes), the first upper limit $_{d}$ for $_{d-1}$, the second lower limit $\substack{l=1\\l\neq k}$ for $_{l=k+1}$ and multiplying by 2 to compensate the symmetry lost:

$$
\begin{aligned}
&4\frac{1}{8}\sum_{j=1}^{d}\sum_{k=1}^{d}\sum_{l=1}^{d}\sum_{m=1}^{d}\sum_{r=1}^{d}\sum_{s=1}^{d}\sum_{t=1}^{d} g_{,j}g_{,kl}g_{,mr}g_{,st}\mu_{jklmrst}\\
&\quad= 4\frac{1}{8}3\cdot 2\sum_{j=1}^{d}\sum_{\substack{k=1\\k\neq j}}^{d-1}\sum_{\substack{l=k+1\\l\neq j}}^{d} g_{,j}g_{,jj}g_{,kk}g_{,ll}\mu_{j,3}\mu_{k,2}\mu_{l,2} + 4\frac{1}{8}6\cdot 2\sum_{j=1}^{d}\sum_{\substack{k=1\\k\neq j}}^{d-1}\sum_{\substack{l=k+1\\l\neq j}}^{d} g_{,j}g_{,jj}g_{,kl}^{2}\mu_{j,3}\mu_{k,2}\mu_{l,2}\\
&\qquad+ 4\frac{1}{8}12\sum_{j=1}^{d}\sum_{\substack{k=1\\k\neq j}}^{d}\sum_{\substack{l=1\\l\neq k\\l\neq j}}^{d} g_{,j}g_{,jk}^{2}g_{,ll}\mu_{j,3}\mu_{k,2}\mu_{l,2} + 4\frac{1}{8}12\sum_{j=1}^{d}\sum_{\substack{k=1\\k\neq j}}^{d}\sum_{\substack{l=1\\l\neq k\\l\neq j}}^{d} g_{,j}g_{,jk}g_{,kk}g_{,ll}\mu_{j,2}\mu_{k,3}\mu_{l,2}\\
&\qquad+ 4\frac{1}{8}24\sum_{j=1}^{d}\sum_{\substack{k=1\\k\neq j}}^{d}\sum_{\substack{l=1\\l\neq k\\l\neq j}}^{d} g_{,j}g_{,jk}g_{,kl}g_{,ll}\mu_{j,2}\mu_{k,2}\mu_{l,3} + 4\frac{1}{8}24\sum_{j=1}^{d}\sum_{\substack{k=1\\k\neq j}}^{d}\sum_{\substack{l=1\\l\neq k\\l\neq j}}^{d} g_{,j}g_{,jk}g_{,kl}g_{,jl}\mu_{j,3}\mu_{k,2}\mu_{l,2}\\
&\qquad+ 4\frac{1}{8}24\sum_{j=1}^{d}\sum_{\substack{k=1\\k\neq j}}^{d}\sum_{\substack{l=1\\l\neq k\\l\neq j}}^{d} g_{,j}g_{,jl}g_{,kl}^{2}\mu_{j,2}\mu_{k,2}\mu_{l,3} + 4\frac{1}{8}3\sum_{j=1}^{d}\sum_{\substack{k=1\\k\neq j}}^{d} g_{,j}g_{,jj}^{2}g_{,kk}\mu_{j,5}\mu_{k,2}\\
&\qquad+ 4\frac{1}{8}6\sum_{j=1}^{d}\sum_{\substack{k=1\\k\neq j}}^{d} g_{,j}g_{,jk}g_{,kk}^{2}\mu_{j,2}\mu_{k,5} + 4\frac{1}{8}12\sum_{j=1}^{d}\sum_{\substack{k=1\\k\neq j}}^{d} g_{,j}g_{,jj}g_{,jk}^{2}\mu_{j,5}\mu_{k,2}\\
&\qquad+ 4\frac{1}{8}3\sum_{j=1}^{d}\sum_{\substack{k=1\\k\neq j}}^{d} g_{,j}g_{,jj}g_{,kk}^{2}\mu_{j,3}\mu_{k,4} + 4\frac{1}{8}12\sum_{j=1}^{d}\sum_{\substack{k=1\\k\neq j}}^{d} g_{,j}g_{,jj}g_{,kk}g_{,jk}\mu_{j,4}\mu_{k,3}\\
&\qquad+ 4\frac{1}{8}12\sum_{j=1}^{d}\sum_{\substack{k=1\\k\neq j}}^{d} g_{,j}g_{,kk}g_{,jk}^{2}\mu_{j,3}\mu_{k,4} + 4\frac{1}{8}8\sum_{j=1}^{d}\sum_{\substack{k=1\\k\neq j}}^{d} g_{,j}g_{,jk}^{3}\mu_{j,4}\mu_{k,3} + 4\frac{1}{8}\sum_{j=1}^{d} g_{,j}g_{,jj}^{3}\mu_{j,7}
\end{aligned}
\tag{A.38q}
$$

$\boldsymbol{X}$:

This term follows the same strategy as in V.

$$
6g_{\mu}^{2}\sum_{j=1}^{d}\sum_{k=1}^{d} g_{,j}g_{,k}\mu_{jk} = 6g_{\mu}^{2}\sum_{j=1}^{d} g_{,j}^{2}\mu_{j,2} \tag{A.39}
$$

XI:

This term follows the same strategy as in third central moment *skewness* in Subsection A.2.5, independence consideration of $VIII$ term.

$$6g_{\mu}^{2}\frac{1}{4}\sum_{j=1}^{d}\sum_{k=1}^{d}\sum_{l=1}^{d}\sum_{m=1}^{d}g_{,jk}g_{,lm}\mu_{jklm} = 6g_{\mu}^{2}\frac{1}{4}\cdot 2\sum_{j=1}^{d-1}\sum_{k=j+1}^{d}g_{,jj}g_{,kk}\mu_{j,2}\mu_{k,2} + 6g_{\mu}^{2}\frac{1}{4}2 \cdot 2\sum_{j=1}^{d-1}\sum_{k=j+1}^{d}g_{,jk}^{2}\mu_{j,2}\mu_{k,2} + 6g_{\mu}^{2}\frac{1}{4}\sum_{j=1}^{d}g_{,jj}^{2}\mu_{j,4} \tag{A.40}$$

XII:

The sixth mixed or cross central moments between the variables μ_{jklmrs} that $_{j=k\neq l=m\neq r=s}$:

$$6\frac{1}{4}\sum_{j=1}^{d}\sum_{\substack{k=1\\k\neq j}}^{d}\sum_{\substack{l=1\\l\neq k\\l\neq j}}^{d}g_{,j}^{2}g_{,kk}g_{,ll}\mu_{j,2}\mu_{k,2}\mu_{l,2} \tag{A.41a}$$

The sixth mixed or cross central moments between the variables μ_{jklmrs} that $_{j=k\neq l=r\neq m=s}$ and $_{j=k\neq l=s\neq m=r}$ are equivalent. All together reassigning indexes lead to:

$$6\frac{1}{4}2\sum_{j=1}^{d}\sum_{\substack{k=1\\k\neq j}}^{d}\sum_{\substack{l=1\\l\neq k\\l\neq j}}^{d}g_{,j}^{2}g_{,kl}^{2}\mu_{j,2}\mu_{k,2}\mu_{l,2} \tag{A.41b}$$

The sixth mixed or cross central moments between the variables μ_{jklmrs} that:

$$j=l\neq k=m\neq r=s \qquad j=m\neq k=l\neq r=s \qquad j=r\neq k=s\neq l=m \qquad j=s\neq k=r\neq l=m$$

$$6\frac{1}{4}4\sum_{j=1}^{d}\sum_{\substack{k=1\\k\neq j}}^{d}\sum_{\substack{l=1\\l\neq k\\l\neq j}}^{d}g_{,j}g_{,k}g_{,jk}g_{,ll}\mu_{j,2}\mu_{k,2}\mu_{l,2} \tag{A.41c}$$

The sixth mixed or cross central moments between the variables μ_{jklmrs} that:

$$j=l\neq k=r\neq m=s \qquad j=l\neq k=s\neq m=r \qquad j=m\neq k=r\neq l=s \qquad j=m\neq k=s\neq l=r$$
$$j=r\neq k=l\neq m=s \qquad j=r\neq k=m\neq l=s \qquad j=s\neq k=l\neq m=r \qquad j=s\neq k=m\neq l=r$$

$$6\frac{1}{4}8\sum_{j=1}^{d}\sum_{\substack{k=1\\k\neq j}}^{d}\sum_{\substack{l=1\\l\neq k\\l\neq j}}^{d}g_{,j}g_{,k}g_{,jl}g_{,kl}\mu_{j,2}\mu_{k,2}\mu_{l,2} \tag{A.41d}$$

The sixth mixed or cross central moments between the variables μ_{jklmrs} that $j{=}l{=}m{\neq}k{=}r{=}s$ and $j{=}r{=}s{\neq}k{=}l{=}m$ are equivalent. All together reassigning indexes lead to:

$$6\frac{1}{4}2\sum_{j=1}^{d}\sum_{\substack{k=1\\k\neq j}}^{d} g_{,j}g_{,k}g_{,jj}g_{,kk}\mu_{j,3}\mu_{k,3} \tag{A.41e}$$

The sixth mixed or cross central moments between the variables μ_{jklmrs} that:

$$j=k=l\neq m=r=s \qquad j=k=m\neq l=r=s \qquad j=k=r\neq l=m=s \qquad j=k=s\neq l=m=r$$

$$6\frac{1}{4}4\sum_{j=1}^{d}\sum_{\substack{k=1\\k\neq j}}^{d} g_{,j}^2 g_{,jk}g_{,kk}\mu_{j,3}\mu_{k,3} \tag{A.41f}$$

The sixth mixed or cross central moments between the variables μ_{jklmrs} that:

$$j=l=r\neq k=m=s \qquad j=l=s\neq k=m=r \qquad j=m=r\neq k=l=s \qquad j=m=s\neq k=l=r$$

$$6\frac{1}{4}4\sum_{j=1}^{d}\sum_{\substack{k=1\\k\neq j}}^{d} g_{,j}g_{,k}g_{,jk}^2\mu_{j,3}\mu_{k,3} \tag{A.41g}$$

The sixth mixed or cross central moments between the variables μ_{jklmrs} that $j{=}k{\neq}l{=}m{=}r{=}s$:

$$6\frac{1}{4}\sum_{j=1}^{d}\sum_{\substack{k=1\\k\neq j}}^{d} g_{,j}^2 g_{,kk}^2\mu_{j,2}\mu_{k,4} \tag{A.41h}$$

The sixth mixed or cross central moments between the variables μ_{jklmrs} that $j{=}k{=}l{=}m{\neq}r{=}s$ and $j{=}k{=}r{=}s{\neq}l{=}m$ are equivalent. All together reassigning indexes lead to:

$$6\frac{1}{4}2\sum_{j=1}^{d}\sum_{\substack{k=1\\k\neq j}}^{d} g_{,j}^2 g_{,jj}g_{,kk}\mu_{j,4}\mu_{k,2} \tag{A.41i}$$

The sixth mixed or cross central moments between the variables μ_{jklmrs} that:

$$j=k=l=r\neq m=s \qquad j=k=l=s\neq m=r \qquad j=k=m=r\neq l=s \qquad j=k=m=s\neq l=r$$

$$6\frac{1}{4}4\sum_{j=1}^{d}\sum_{\substack{k=1\\k\neq j}}^{d} g_{,j}^2 g_{,jk}^2\mu_{j,4}\mu_{k,2} \tag{A.41j}$$

The sixth mixed or cross central moments between the variables μ_{jklmrs} that:

$j=l=m=r\neq k=s$ $\quad$ $j=l=m=s\neq k=r$ $\quad$ $j=l=r=s\neq k=m$ $\quad$ $j=m=r=s\neq k=l$
$k=l=m=r\neq j=s$ $\quad$ $k=l=m=s\neq j=r$ $\quad$ $k=l=r=s\neq j=m$ $\quad$ $k=m=r=s\neq j=l$

$$6\frac{1}{4}8\sum_{j=1}^{d}\sum_{\substack{k=1\\k\neq j}}^{d}g_{,j}g_{,k}g_{,jk}g_{,jj}\mu_{j,4}\mu_{k,2} \tag{A.41k}$$

The sixth mixed or cross central moments between the variables μ_{jklmrs} that $_{j=k=l=m=r=s}$ lead to the sixth moment $\mu_{j,6}$.

$$6\frac{1}{4}\sum_{j=1}^{d}g_{,j}^{2}g_{,jj}^{2}\mu_{j,6} \tag{A.41l}$$

Summarizing:

$$\begin{aligned}
&6\frac{1}{4}\sum_{j=1}^{d}\sum_{k=1}^{d}\sum_{l=1}^{d}\sum_{m=1}^{d}\sum_{r=1}^{d}\sum_{s=1}^{d}g_{,j}g_{,k}g_{,lm}g_{,rs}\mu_{jklmrs}\\
&=6\frac{1}{4}\sum_{j=1}^{d}\sum_{\substack{k=1\\k\neq j}}^{d}\sum_{\substack{l=1\\l\neq k\\l\neq j}}^{d}g_{,j}^{2}g_{,kk}g_{,ll}\mu_{j,2}\mu_{k,2}\mu_{l,2}+6\frac{1}{4}2\sum_{j=1}^{d}\sum_{\substack{k=1\\k\neq j}}^{d}\sum_{\substack{l=1\\l\neq k\\l\neq j}}^{d}g_{,j}^{2}g_{,kl}^{2}\mu_{j,2}\mu_{k,2}\mu_{l,2}\\
&\quad+6\frac{1}{4}4\sum_{j=1}^{d}\sum_{\substack{k=1\\k\neq j}}^{d}\sum_{\substack{l=1\\l\neq k\\l\neq j}}^{d}g_{,j}g_{,k}g_{,jk}g_{,ll}\mu_{j,2}\mu_{k,2}\mu_{l,2}+6\frac{1}{4}8\sum_{j=1}^{d}\sum_{\substack{k=1\\k\neq j}}^{d}\sum_{\substack{l=1\\l\neq k\\l\neq j}}^{d}g_{,j}g_{,k}g_{,jl}g_{,kl}\mu_{j,2}\mu_{k,2}\mu_{l,2}\\
&\quad+6\frac{1}{4}2\sum_{j=1}^{d}\sum_{\substack{k=1\\k\neq j}}^{d}g_{,j}g_{,k}g_{,jj}g_{,kk}\mu_{j,3}\mu_{k,3}+6\frac{1}{4}4\sum_{j=1}^{d}\sum_{\substack{k=1\\k\neq j}}^{d}g_{,j}^{2}g_{,jk}g_{,kk}\mu_{j,3}\mu_{k,3}\\
&\quad+6\frac{1}{4}4\sum_{j=1}^{d}\sum_{\substack{k=1\\k\neq j}}^{d}g_{,j}g_{,k}g_{,jk}^{2}\mu_{j,3}\mu_{k,3}+6\frac{1}{4}\sum_{j=1}^{d}\sum_{\substack{k=1\\k\neq j}}^{d}g_{,j}^{2}g_{,kk}^{2}\mu_{j,2}\mu_{k,4}\\
&\quad+6\frac{1}{4}2\sum_{j=1}^{d}\sum_{\substack{k=1\\k\neq j}}^{d}g_{,j}^{2}g_{,jj}g_{,kk}\mu_{j,4}\mu_{k,2}+6\frac{1}{4}4\sum_{j=1}^{d}\sum_{\substack{k=1\\k\neq j}}^{d}g_{,j}^{2}g_{,jk}^{2}\mu_{j,4}\mu_{k,2}\\
&\quad+6\frac{1}{4}8\sum_{j=1}^{d}\sum_{\substack{k=1\\k\neq j}}^{d}g_{,j}g_{,k}g_{,jk}g_{,jj}\mu_{j,4}\mu_{k,2}+6\frac{1}{4}\sum_{j=1}^{d}g_{,j}^{2}g_{,jj}^{2}\mu_{j,6}
\end{aligned} \tag{A.41m}$$

Changing in the symmetric terms (with respect to two indexes), the first upper limit d for $d-1$, the second lower limit $\overset{k=1}{k\neq j}$ for $k=j+1$ and multiplying by 2 to compensate the symmetry lost:

$$
\begin{aligned}
&6\frac{1}{4}\sum_{j=1}^{d}\sum_{k=1}^{d}\sum_{l=1}^{d}\sum_{m=1}^{d}\sum_{r=1}^{d}\sum_{s=1}^{d} g_{,j}g_{,k}g_{,lm}g_{,rs}\mu_{jklmrs} \\
&= 6\frac{1}{4}\cdot 2\sum_{j=1}^{d}\sum_{\substack{k=1\\k\neq j}}^{d-1}\sum_{\substack{l=k+1\\l\neq j}}^{d} g_{,j}^2 g_{,kk}g_{,ll}\mu_{j,2}\mu_{k,2}\mu_{l,2} + 6\frac{1}{4}2\cdot 2\sum_{j=1}^{d}\sum_{\substack{k=1\\k\neq j}}^{d-1}\sum_{\substack{l=k+1\\l\neq j}}^{d} g_{,j}^2 g_{,kl}^2\mu_{j,2}\mu_{k,2}\mu_{l,2} \\
&\quad + 6\frac{1}{4}4\cdot 2\sum_{j=1}^{d-1}\sum_{k=j+1}^{d}\sum_{\substack{l=1\\l\neq k\\l\neq j}}^{d} g_{,j}g_{,k}g_{,jk}g_{,ll}\mu_{j,2}\mu_{k,2}\mu_{l,2} + 6\frac{1}{4}8 \\
&\quad \cdot 2\sum_{j=1}^{d-1}\sum_{k=j+1}^{d}\sum_{\substack{l=1\\l\neq k\\l\neq j}}^{d} g_{,j}g_{,k}g_{,jl}g_{,kl}\mu_{j,2}\mu_{k,2}\mu_{l,2} + 6\frac{1}{4}2\cdot 2\sum_{j=1}^{d-1}\sum_{k=j+1}^{d} g_{,j}g_{,k}g_{,jj}g_{,kk}\mu_{j,3}\mu_{k,3} \\
&\quad + 6\frac{1}{4}4\sum_{j=1}^{d}\sum_{\substack{k=1\\k\neq j}}^{d} g_{,j}^2 g_{,jk}g_{,kk}\mu_{j,3}\mu_{k,3} + 6\frac{1}{4}4\sum_{j=1}^{d-1}\sum_{k=j+1}^{d} g_{,j}g_{,k}g_{,jk}^2\mu_{j,3}\mu_{k,3} \\
&\quad + 6\frac{1}{4}\sum_{j=1}^{d}\sum_{\substack{k=1\\k\neq j}}^{d} g_{,j}^2 g_{,kk}^2\mu_{j,2}\mu_{k,4} + 6\frac{1}{4}2\sum_{j=1}^{d}\sum_{\substack{k=1\\k\neq j}}^{d} g_{,j}^2 g_{,jj}g_{,kk}\mu_{j,4}\mu_{k,2} \\
&\quad + 6\frac{1}{4}4\sum_{j=1}^{d}\sum_{\substack{k=1\\k\neq j}}^{d} g_{,j}^2 g_{,jk}^2\mu_{j,4}\mu_{k,2} + 6\frac{1}{4}8\sum_{j=1}^{d}\sum_{\substack{k=1\\k\neq j}}^{d} g_{,j}g_{,k}g_{,jk}g_{,jj}\mu_{j,4}\mu_{k,2} + 6\frac{1}{4}\sum_{j=1}^{d} g_{,j}^2 g_{,jj}^2\mu_{j,6}
\end{aligned}
\tag{A.41n}
$$

XIII:

This term follows the same strategy as in VI.

$$
12g_{\mu}^2\frac{1}{2}\sum_{j=1}^{d}\sum_{k=1}^{d}\sum_{l=1}^{d} g_{,j}g_{,kl}\mu_{jkl} = 12g_{\mu}^2\frac{1}{2}\sum_{j=1}^{d} g_{,j}g_{,jj}\mu_{j,3} \tag{A.42}
$$

XIV:

This term follows the same strategy as in third central moment *skewness* in Subsection A.2.5, independence consideration of the VII term.

$$\begin{aligned} 12g_{\mu}\frac{1}{2}\sum_{j=1}^{d}\sum_{k=1}^{d}\sum_{l=1}^{d}\sum_{m=1}^{d} g_{,j}g_{,k}g_{,lm}\mu_{jklm} = {} & 12g_{\mu}\frac{1}{2}\sum_{j=1}^{d}\sum_{\substack{k=1\\k\neq j}}^{d} g_{,j}^{2}g_{,kk}\mu_{j,2}\mu_{k,2} \\ & + 12g_{\mu}\frac{1}{2}2\cdot 2\sum_{j=1}^{d-1}\sum_{k=j+1}^{d} g_{,j}g_{,k}g_{,jk}\mu_{j,2}\mu_{k,2} \\ & + 12g_{\mu}\frac{1}{2}\sum_{j=1}^{d} g_{,j}^{2}g_{,jj}\mu_{j,4} \end{aligned} \tag{A.43}$$

XV:

This term follows the same strategy as in third central moment *skewness* in Subsection A.2.5, independence consideration of the IX term.

$$\begin{aligned} 12g_{\mu}\frac{1}{4}\sum_{j=1}^{d}\sum_{k=1}^{d}\sum_{l=1}^{d}\sum_{m=1}^{d}\sum_{r=1}^{d} g_{,j}g_{,kl}g_{,mr}\mu_{jklmr} = {} & 12g_{\mu}\frac{1}{4}4\sum_{j=1}^{d}\sum_{\substack{k=1\\k\neq j}}^{d} g_{,j}g_{,jk}g_{,kk}\mu_{j,2}\mu_{k,3} \\ & + 12g_{\mu}\frac{1}{4}2\sum_{j=1}^{d}\sum_{\substack{k=1\\k\neq j}}^{d} g_{,j}g_{,jj}g_{,kk}\mu_{j,3}\mu_{k,2} \\ & + 12g_{\mu}\frac{1}{4}4\sum_{j=1}^{d}\sum_{\substack{k=1\\k\neq j}}^{d} g_{,j}g_{,jk}^{2}\mu_{j,3}\mu_{k,2} \\ & + 12g_{\mu}\frac{1}{4}\sum_{j=1}^{d} g_{,j}g_{,jj}^{2}\mu_{j,5} \end{aligned} \tag{A.44}$$

In the following equation, the terms III, IX and XII are referenced owing to space limitations as they are too long expressions to be transcribed here entirely. As a result, the second order approximation for the fourth central moment assuming independence leads to:

$$
\begin{aligned}
&\mu_4(Y,Y,Y,Y) = \mu_{Y,4} \\
&\approx \underbrace{g_\mu^4}_{I} + \underbrace{\sum_{j=1}^{d} g_{,j}^4 \mu_{j,4}}_{II} + \underbrace{(\text{Eq. (A.33u)})}_{III} + \underbrace{0}_{IV} + \underbrace{2g_\mu^3 \sum_{j=1}^{d} g_{,jj}\mu_{j,2}}_{V} \\
&\quad \underbrace{+4g_\mu \sum_{j=1}^{d} g_{,j}^3 \mu_{j,3} + 2\sum_{j=1}^{d}\sum_{\substack{k=1\\k\neq j}}^{d} g_{,j}^3 g_{,kk}\mu_{j,3}\mu_{k,2}}_{VII} \\
&\quad \underbrace{+6\sum_{j=1}^{d}\sum_{\substack{k=1\\k\neq j}}^{d} g_{,j}^2 g_{,k} g_{,kk}\mu_{j,2}\mu_{k,3} + 12\sum_{j=1}^{d}\sum_{\substack{k=1\\k\neq j}}^{d} g_{,j}^2 g_{,k} g_{,jk}\mu_{j,3}\mu_{k,2} + 2\sum_{j=1}^{d} g_{,j}^3 g_{,jj}\mu_{j,5}}_{VII} \\
&\quad \underbrace{+3g_\mu \sum_{j=1}^{d-2}\sum_{k=j+1}^{d-1}\sum_{l=k+1}^{d} g_{,jj} g_{,kk} g_{,ll}\mu_{j,2}\mu_{k,2}\mu_{l,2} + 6g_\mu \sum_{j=1}^{d}\sum_{\substack{k=1\\k\neq j}}^{d-1}\sum_{\substack{l=k+1\\l\neq j}}^{d} g_{,jj} g_{,kl}^2 \mu_{j,2}\mu_{k,2}\mu_{l,2}}_{VIII} \\
&\quad \underbrace{+24g_\mu \sum_{j=1}^{d-2}\sum_{k=j+1}^{d-1}\sum_{l=k+1}^{d} g_{,jk} g_{,jl} g_{,kl}\mu_{j,2}\mu_{k,2}\mu_{l,2} + 6g_\mu \sum_{j=1}^{d-1}\sum_{k=j+1}^{d} g_{,jj} g_{,jk} g_{,kk}\mu_{j,3}\mu_{k,3}}_{VIII} \\
&\quad \underbrace{+4g_\mu \sum_{j=1}^{d-1}\sum_{k=j+1}^{d} g_{,jk}^3 \mu_{j,3}\mu_{k,3} + \frac{3}{2}g_\mu \sum_{j=1}^{d}\sum_{\substack{k=1\\k\neq j}}^{d} g_{,jj} g_{,kk}^2 \mu_{j,2}\mu_{k,4} + 6g_\mu \sum_{j=1}^{d}\sum_{\substack{k=1\\k\neq j}}^{d} g_{,jk}^2 g_{,kk}\mu_{j,2}\mu_{k,4}}_{VIII} \\
&\quad \underbrace{+\frac{1}{2}g_\mu \sum_{j=1}^{d} g_{,jj}^3 \mu_{j,6}}_{VIII} + \underbrace{(\text{Eq. (A.38q)})}_{IX} + \underbrace{6g_\mu^2 \sum_{j=1}^{d} g_{,j}^2 \mu_{j,2}}_{X} + \underbrace{3g_\mu^2 \sum_{j=1}^{d-1}\sum_{k=j+1}^{d} g_{,jj} g_{,kk}\mu_{j,2}\mu_{k,2}}_{XI} \\
&\quad \underbrace{+6g_\mu^2 \sum_{j=1}^{d-1}\sum_{k=j+1}^{d} g_{,jk}^2 \mu_{j,2}\mu_{k,2} + \frac{3}{2}g_\mu^2 \sum_{j=1}^{d} g_{,jj}^2 \mu_{j,4}}_{XI} + \underbrace{(\text{Eq. (A.41n)})}_{XII} + \underbrace{6g_\mu^2 \sum_{j=1}^{d} g_{,j} g_{,jj}\mu_{j,3}}_{XIII} \\
&\quad \underbrace{+6g_\mu \sum_{j=1}^{d}\sum_{\substack{k=1\\k\neq j}}^{d} g_{,j}^2 g_{,kk}\mu_{j,2}\mu_{k,2} + 24g_\mu \sum_{j=1}^{d-1}\sum_{k=j+1}^{d} g_{,j} g_{,k} g_{,jk}\mu_{j,2}\mu_{k,2} + 6g_\mu \sum_{j=1}^{d} g_{,j}^2 g_{,jj}\mu_{j,4}}_{XIV} \\
&\quad \underbrace{+12g_\mu \sum_{j=1}^{d}\sum_{\substack{k=1\\k\neq j}}^{d} g_{,j} g_{,jk} g_{,kk}\mu_{j,2}\mu_{k,3} + 6g_\mu \sum_{j=1}^{d}\sum_{\substack{k=1\\k\neq j}}^{d} g_{,j} g_{,jj} g_{,kk}\mu_{j,3}\mu_{k,2}}_{XV} \\
&\quad \underbrace{+12g_\mu \sum_{j=1}^{d}\sum_{\substack{k=1\\k\neq j}}^{d} g_{,j} g_{,jk}^2 \mu_{j,3}\mu_{k,2} + 3g_\mu \sum_{j=1}^{d} g_{,j} g_{,jj}^2 \mu_{j,5} - 4\mu_Y \mu_{Y,3} - 6\mu_Y^2 \sigma_Y^2 - \mu_Y^4}_{XV}
\end{aligned}
\tag{A.45}
$$

A.2.8 Fourth central moment *kurtosis* first-order

The fourth central moment *kurtosis* first-order approximation for independent random variables is derived from Eq. (2.123) and Eq. (A.45) leading to:

$$\mu_4\left(Y,Y,Y,Y\right) = \mu_{Y,4} \approx \underbrace{\sum_{j=1}^{d} g_{,j}^{4} \mu_{j,4}}_{II} \tag{A.46}$$

B

Variance of the sum of random variables

This appendix presents the succinct derivation of the formula for the variance of the sum of random variables in Eq. (B.1), applying basic properties of sums, the linearity of expectation, and definitions of variance and covariance.

B.1 Proof

$$
\begin{aligned}
\operatorname{Var}\left(\sum_{i=1}^{ns} X^i\right) &= \mathrm{E}\left[\left(\sum_{i=1}^{ns} X^i\right)^2\right] - \left(\mathrm{E}\left[\sum_{i=1}^{ns} X^i\right]\right)^2 && \text{definition of variance Eq. (2.9)} \\
&= \mathrm{E}\left[\sum_{i_1=1}^{ns}\sum_{i_2=1}^{ns} X^{i_1}X^{i_2}\right] - \left(\mathrm{E}\left[\sum_{i_1=1}^{ns} X^{i_1}\right]\right)^2 && \text{basic properties of sums} \\
&= \sum_{i_1=1}^{ns}\sum_{i_2=1}^{ns} \mathrm{E}[X^{i_1}X^{i_2}] - \left(\sum_{i_1=1}^{ns} \mathrm{E}[X^{i_1}]\right)^2 && \text{linearity of expectation} \\
&= \sum_{i_1=1}^{ns}\sum_{i_2=1}^{ns} \mathrm{E}[X^{i_1}X^{i_2}] - \sum_{i_1=1}^{ns}\sum_{i_2=1}^{ns} \mathrm{E}[X^{i_1}]\,\mathrm{E}[X^{i_2}] && \text{basic properties of sums} \\
&= \sum_{i_1=1}^{ns}\sum_{i_2=1}^{ns} \left(\mathrm{E}[X^{i_1}X^{i_2}] - \mathrm{E}[X^{i_1}]\,\mathrm{E}[X^{i_2}]\right) && \text{combine the sums} \\
&= \sum_{i_1=1}^{ns}\sum_{i_2=1}^{ns} \operatorname{Cov}(X^{i_1}, X^{i_2}) && \text{identify the covariance Eq. (2.18)} \\
&= \sum_{i_1=1}^{ns} \operatorname{Var}(X^{i_1}) + \sum_{i_1=1}^{ns}\sum_{\substack{i_2=1 \\ i_2\neq i_1}}^{ns} \operatorname{Cov}(X^{i_1}, X^{i_2}) && \text{rearrange sum} \\
&= \sum_{i_1=1}^{ns} \operatorname{Var}(X^{i_1}) + 2\sum_{i_1=1}^{ns-1}\sum_{i_2=i_1+1}^{ns} \operatorname{Cov}(X^{i_1}, X^{i_2}) && \text{symmetric terms}
\end{aligned}
\tag{B.1}
$$

Note that in the rearrange sum stage, the covariances that $_{i_1=i_2}$ lead to the variance $\operatorname{Var}\left(X^{i_1}\right)$. Note further that in the symmetric terms, the first upper limit $_{ns}$ is changed for $_{ns-1}$, the second lower limit $\substack{i_2=1 \\ i_2\neq i_1}$ for $_{i_2=i_1+1}$ and the whole term is multiplied by 2 to compensate the symmetry lost with the limits change.

Equivalent derivations can be found for the third and fourth central moments of the sum of random variables.

C

Full second order approach application to NASGRO

This appendix encloses equations to exemplify the prediction of fatigue crack growth life moments according to the NASGRO model. The equations presented here consist of the expected value, the variance, the third central moment, and the fourth central moment, for the consideration of only two random variables, K_{max} and K_{min}, for the sake of simplicity. These formulations are obtained from the FSOA application, therefore, the Taylor approximation up to second order is used. The aim of these mathematical formulations is to better illustrate the methodology presented and to promote the FSOA application when considering a larger number of r.v.s.

The NASGRO system in Fig. C.1 represents the multi-input single-output crack growth propagation.

Figure C.1. Multi-variable NASGRO real-valued function.

Note that from the system in Fig. C.1, the input random variables and the output are evaluated at every crack growth, i.e. at every time increment i. The assumption of two random variables K_{max} and K_{min} implies $d = 2$ in the present case.

C.1 Taylor approximation up to second order

Starting from the dN^i function Eq. (3.12), with two random input variables K^i_{max} and K^i_{min} and rewriting it by means of the multivariate Taylor series up to second order about the mean value vector at every i^{th} increment $P^i = \left(\mu_{K^i_{max}}, \mu_{K^i_{min}}\right)$ leads to Eq. (C.1).

$$
\begin{aligned}
dN^i \approx & \frac{da^i}{C\left(\frac{1-f^i}{1-R^i}\Delta K^i\right)^n} \frac{\left(1-\frac{K^i_{max}}{K_c}\right)^q}{\left(1-\frac{\Delta K^i_{th}}{\Delta K^i}\right)^p}\Bigg|_{\substack{\mu_{K^i_{max}} \\ \mu_{K^i_{min}}}} + \frac{\partial dN}{\partial K_{max}}\Bigg|_{\substack{\mu_{K^i_{max}} \\ \mu_{K^i_{min}}}} \left(K^i_{max} - \mu_{K^i_{max}}\right) \\
& + \frac{\partial dN}{\partial K_{min}}\Bigg|_{\substack{\mu_{K^i_{max}} \\ \mu_{K^i_{min}}}} \left(K^i_{min} - \mu_{K^i_{min}}\right) + \frac{1}{2}\frac{\partial^2 dN}{\partial {K_{max}}^2}\Bigg|_{\substack{\mu_{K^i_{max}} \\ \mu_{K^i_{min}}}} \left(K^i_{max} - \mu_{K^i_{max}}\right)^2 \\
& + \frac{1}{2}\frac{\partial^2 dN}{\partial {K_{min}}^2}\Bigg|_{\substack{\mu_{K^i_{max}} \\ \mu_{K^i_{min}}}} \left(K^i_{min} - \mu_{K^i_{min}}\right)^2 \\
& + \frac{1}{2}2\frac{\partial^2 dN}{\partial K_{max}\partial K_{min}}\Bigg|_{\substack{\mu_{K^i_{max}} \\ \mu_{K^i_{min}}}} \left(K^i_{max} - \mu_{K^i_{max}}\right)\left(K^i_{min} - \mu_{K^i_{min}}\right)
\end{aligned}
\tag{C.1}
$$

C.2 First moment: expected value

The expected value of dN^i, $\mathrm{E}\left[dN^i\right]$, is obtained by applying the equation developed to obtain the first moment, Eq. (2.62). In the present case, considering the approximated dN^i function Eq. (C.1), it gives the following second order approximation for the expected value Eq. (C.2).

$$\begin{aligned}\mathrm{E}\left[dN^i\right] &= \mu_{dN^i} \\ &\approx \frac{da^i}{C\left(\frac{1-f^i}{1-R^i}\Delta K^i\right)^n} \frac{\left(1-\frac{K^i_{max}}{K_c}\right)^q}{\left(1-\frac{\Delta K^i_{th}}{\Delta K^i}\right)^p}\Bigg|_{\substack{\mu_{K^i_{max}} \\ \mu_{K^i_{min}}}} \\ &\quad + \frac{1}{2}\left[\frac{\partial^2 dN}{\partial {K_{max}}^2}\Big|_{\substack{\mu_{K^i_{max}} \\ \mu_{K^i_{min}}}} \mathrm{Cov}\left(K^i_{max}, K^i_{max}\right) + \frac{\partial^2 dN}{\partial {K_{min}}^2}\Big|_{\substack{\mu_{K^i_{max}} \\ \mu_{K^i_{min}}}} \mathrm{Cov}\left(K^i_{min}, K^i_{min}\right)\right. \\ &\qquad \left. + 2\,\frac{\partial^2 dN}{\partial K_{max}\partial K_{min}}\Big|_{\substack{\mu_{K^i_{max}} \\ \mu_{K^i_{min}}}} \mathrm{Cov}\left(K^i_{max}, K^i_{min}\right)\right]\end{aligned} \tag{C.2}$$

Furthermore, since the $\mathrm{Cov}\left(K^i_{max}, K^i_{max}\right) = \mathrm{Var}\left(K^i_{max}\right)$ and $\mathrm{Cov}\left(K^i_{min}, K^i_{min}\right) = \mathrm{Var}\left(K^i_{min}\right)$, the equation can be rewritten as:

$$\begin{aligned}\mathrm{E}\left[dN^i\right] &= \mu_{dN^i} \\ &\approx \frac{da^i}{C\left(\frac{1-f^i}{1-R^i}\Delta K^i\right)^n} \frac{\left(1-\frac{K^i_{max}}{K_c}\right)^q}{\left(1-\frac{\Delta K^i_{th}}{\Delta K^i}\right)^p}\Bigg|_{\substack{\mu_{K^i_{max}} \\ \mu_{K^i_{min}}}} + \frac{1}{2}\left[\frac{\partial^2 dN}{\partial {K_{max}}^2}\Big|_{\substack{\mu_{K^i_{max}} \\ \mu_{K^i_{min}}}} \mathrm{Var}\left(K^i_{max}\right)\right. \\ &\quad \left. + \frac{\partial^2 dN}{\partial {K_{min}}^2}\Big|_{\substack{\mu_{K^i_{max}} \\ \mu_{K^i_{min}}}} \mathrm{Var}\left(K^i_{min}\right) + 2\,\frac{\partial^2 dN}{\partial K_{max}\partial K_{min}}\Big|_{\substack{\mu_{K^i_{max}} \\ \mu_{K^i_{min}}}} \mathrm{Cov}\left(K^i_{max}, K^i_{min}\right)\right]\end{aligned} \tag{C.3}$$

C.3 Second central moment: variance

Likewise, the variance of dN^i, $\mathrm{Var}\left(dN^i\right)$, is calculated by applying the equation developed to obtain the second central moment, Eq. (2.77). The full second order approximation of the variance in the present case, considering the approximated dN^i function Eq. (C.1), is shown in Eq. (C.4).

For the variance formulation, the following equivalences are directly considered: $\mathrm{Cov}\left(K^i_{max}, K^i_{max}\right) = \mathrm{Var}\left(K^i_{max}\right)$ and $\mathrm{Cov}\left(K^i_{min}, K^i_{min}\right) = \mathrm{Var}\left(K^i_{min}\right)$. Note that in the variance equation, the discretised NASGRO and the partial derivatives are evaluated at $\Big|_{\substack{\mu_{K^i_{max}} \\ \mu_{K^i_{min}}}}$, but it is omitted for brevity. Note further that the $\mathrm{E}\left[dN^i\right]$ is the second order approximation for the expected value.

$$
\begin{aligned}
\mathrm{Var}\left(dN^i\right) = \sigma^2_{dN^i} \approx & \left(\frac{da^i}{C\left(\frac{1-f^i}{1-R^i}\Delta K^i\right)^n} \frac{\left(1-\frac{K^i_{max}}{K_c}\right)^q}{\left(1-\frac{\Delta K^i_{th}}{\Delta K^i}\right)^p} \right)^2 + \left(\frac{\partial dN}{\partial K_{max}}\right)^2 \mathrm{Var}\left(K^i_{max}\right) \\
& + 2\left(\frac{\partial dN}{\partial K_{max}}\right)\left(\frac{\partial dN}{\partial K_{min}}\right)\mathrm{Cov}\left(K^i_{max}, K^i_{min}\right) + \left(\frac{\partial dN}{\partial K_{min}}\right)^2 \mathrm{Var}\left(K^i_{min}\right) \\
& + \frac{1}{4}\left[\left(\frac{\partial^2 dN}{\partial {K_{max}}^2}\right)^2 \mu_4\left(K^i_{max}, K^i_{max}, K^i_{max}, K^i_{max}\right)\right. \\
& + 4\left(\frac{\partial^2 dN}{\partial {K_{max}}^2}\right)\left(\frac{\partial^2 dN}{\partial K_{max}\partial K_{min}}\right)\mu_4\left(K^i_{max}, K^i_{max}, K^i_{max}, K^i_{min}\right) \\
& + 2\left(\frac{\partial^2 dN}{\partial {K_{max}}^2}\right)\left(\frac{\partial^2 dN}{\partial {K_{min}}^2}\right)\mu_4\left(K^i_{max}, K^i_{max}, K^i_{min}, K^i_{min}\right) \\
& + 4\left(\frac{\partial^2 dN}{\partial K_{max}\partial K_{min}}\right)\left(\frac{\partial^2 dN}{\partial K_{max}\partial K_{min}}\right)\mu_4\left(K^i_{max}, K^i_{min}, K^i_{max}, K^i_{min}\right) \\
& + 4\left(\frac{\partial^2 dN}{\partial K_{max}\partial K_{min}}\right)\left(\frac{\partial^2 dN}{\partial {K_{min}}^2}\right)\mu_4\left(K^i_{max}, K^i_{min}, K^i_{min}, K^i_{min}\right) \\
& \left. + \left(\frac{\partial^2 dN}{\partial {K_{min}}^2}\right)^2 \mu_4\left(K^i_{min}, K^i_{min}, K^i_{min}, K^i_{min}\right)\right] \\
& + \left(\frac{da^i}{C\left(\frac{1-f^i}{1-R^i}\Delta K^i\right)^n} \frac{\left(1-\frac{K^i_{max}}{K_c}\right)^q}{\left(1-\frac{\Delta K^i_{th}}{\Delta K^i}\right)^p} \right)\left[\left(\frac{\partial^2 dN}{\partial {K_{max}}^2}\right)\mathrm{Var}\left(K^i_{max}\right)\right. \\
& \left. + 2\left(\frac{\partial^2 dN}{\partial K_{max}\partial K_{min}}\right)\mathrm{Cov}\left(K^i_{max}, K^i_{min}\right) + \left(\frac{\partial^2 dN}{\partial {K_{min}}^2}\right)\mathrm{Var}\left(K^i_{min}\right)\right] \\
& + \left(\frac{\partial dN}{\partial K_{max}}\right)\left(\frac{\partial^2 dN}{\partial {K_{max}}^2}\right)\mu_3\left(K^i_{max}, K^i_{max}, K^i_{max}\right) \\
& + 2\left(\frac{\partial dN}{\partial K_{max}}\right)\left(\frac{\partial^2 dN}{\partial K_{max}\partial K_{min}}\right)\mu_3\left(K^i_{max}, K^i_{max}, K^i_{min}\right) \\
& + \left(\frac{\partial dN}{\partial K_{max}}\right)\left(\frac{\partial^2 dN}{\partial {K_{min}}^2}\right)\mu_3\left(K^i_{max}, K^i_{min}, K^i_{min}\right) \\
& + \left(\frac{\partial dN}{\partial K_{min}}\right)\left(\frac{\partial^2 dN}{\partial {K_{max}}^2}\right)\mu_3\left(K^i_{min}, K^i_{max}, K^i_{max}\right) \\
& + 2\left(\frac{\partial dN}{\partial K_{min}}\right)\left(\frac{\partial^2 dN}{\partial K_{max}\partial K_{min}}\right)\mu_3\left(K^i_{min}, K^i_{min}, K^i_{max}\right) \\
& + \left(\frac{\partial dN}{\partial K_{min}}\right)\left(\frac{\partial^2 dN}{\partial {K_{min}}^2}\right)\mu_3\left(K^i_{min}, K^i_{min}, K^i_{min}\right) - \left(\mathrm{E}\left[dN^i\right]\right)^2
\end{aligned}
\tag{C.4}
$$

C.4 Third central moment: *skewness*

Recall that the skewness of dN^i can be determined from the third central moment $\mu_3\left(dN^i, dN^i, dN^i\right) = \mu_{dN^i,3}$ divided by the standard deviation raised to the third power. Then, the moment μ_3 of dN^i is obtained by applying the equation developed to obtain the third central moment, Eq. (2.96). The full second order approximation of the third central moment in the present case, considering the approximated dN^i function Eq. (C.1), is shown in Eq. (C.5).

$$
\begin{aligned}
\mu_3\left(dN^i, dN^i, dN^i\right) = \mu_{dN^i,3} \approx & \underbrace{\left(\frac{da^i}{C\left(\frac{1-f^i}{1-R^i}\Delta K^i\right)^n}\frac{\left(1-\frac{K^i_{max}}{K_c}\right)^q}{\left(1-\frac{\Delta K^i_{th}}{\Delta K^i}\right)^p}\right)^3}_{I} \\
& + \underbrace{\left(\frac{\partial dN}{\partial K_{max}}\right)^3 \mu_3\left(K^i_{max}, K^i_{max}, K^i_{max}\right) + 3\left(\frac{\partial dN}{\partial K_{max}}\right)^2\left(\frac{\partial dN}{\partial K_{min}}\right)\mu_3\left(K^i_{max}, K^i_{max}, K^i_{min}\right)}_{II} \\
& + \underbrace{3\left(\frac{\partial dN}{\partial K_{max}}\right)\left(\frac{\partial dN}{\partial K_{min}}\right)^2 \mu_3\left(K^i_{max}, K^i_{min}, K^i_{min}\right) + \left(\frac{\partial dN}{\partial K_{min}}\right)^3 \mu_3\left(K^i_{min}, K^i_{min}, K^i_{min}\right)}_{II} \\
& + \underbrace{\frac{1}{8}\sum_{j=1}^{d}\sum_{k=1}^{d}\sum_{l=1}^{d}\sum_{m=1}^{d}\sum_{r=1}^{d}\sum_{s=1}^{d} g_{,jk}g_{,lm}g_{,rs}\mu_{jklmrs}}_{III} + \underbrace{0}_{IV} + \underbrace{3g_\mu^2\frac{1}{2}\sum_{j=1}^{d}\sum_{k=1}^{d} g_{,jk}\mu_{jk}}_{V} \\
& + \underbrace{3g_\mu\sum_{j=1}^{d}\sum_{k=1}^{d} g_{,j}g_{,k}\mu_{jk}}_{VI} + \underbrace{3\frac{1}{2}\sum_{j=1}^{d}\sum_{k=1}^{d}\sum_{l=1}^{d}\sum_{m=1}^{d} g_{,j}g_{,k}g_{,lm}\mu_{jklm}}_{VII} \\
& + \underbrace{3g_\mu\frac{1}{4}\sum_{j=1}^{d}\sum_{k=1}^{d}\sum_{l=1}^{d}\sum_{m=1}^{d} g_{,jk}g_{,lm}\mu_{jklm}}_{VIII} + \underbrace{3\frac{1}{4}\sum_{j=1}^{d}\sum_{k=1}^{d}\sum_{l=1}^{d}\sum_{m=1}^{d}\sum_{r=1}^{d} g_{,j}g_{,kl}g_{,mr}\mu_{jklmr}}_{IX} \\
& + \underbrace{6g_\mu\frac{1}{2}\sum_{j=1}^{d}\sum_{k=1}^{d}\sum_{l=1}^{d} g_{,j}g_{,kl}\mu_{jkl}}_{X} - 3\mathrm{E}\left[dN^i\right]\mathrm{Var}\left(dN^i\right) - \left(\mathrm{E}\left[dN^i\right]\right)^3
\end{aligned}
\tag{C.5}
$$

Again, in the third central moment equation, the discretised NASGRO and the partial derivatives are evaluated at $\Big|_{K^i_{min}}^{K^i_{max}}$, but it is omitted for brevity. Note that $\mathrm{E}\left[dN^i\right]$ and the $\mathrm{Var}\left(dN^i\right)$ are the second order approximations for the expected value and for the variance respectively. Note further that only the I, II and last terms have been replaced here for the sake of brevity.

C.5 Fourth central moment: *kurtosis*

Recall that the kurtosis of dN^i can be determined from the fourth central moment $\mu_4\left(dN^i, dN^i, dN^i, dN^i\right) = \mu_{dN^i,4}$ divided by the standard deviation raised to the fourth power. Then, the moment μ_4 of dN^i is obtained by applying the equation developed to obtain the fourth central moment, Eq. (2.120). The full second order approximation of the fourth central moment in the present case, considering the approximated dN^i function Eq. (C.1), is shown in Eq. (C.6).

Once again, in the fourth central moment equation, the discretised NASGRO and the partial derivatives are evaluated at $\Big|_{\mu_{K^i_{min}}}^{\mu_{K^i_{max}}}$ but it is omitted for brevity. Note that $\mathrm{E}\left[dN^i\right]$, the $\mathrm{Var}\left(dN^i\right)$, and the $\mu_3\left(dN^i, dN^i, dN^i\right)$ are the second order approximations for the expected value, for the variance and for the third central moment respectively. Note further that only the I, II and last terms have been replaced here for the sake of brevity.

$$\mu_4\left(dN^i,dN^i,dN^i,dN^i\right)=\mu_{dN^i,4}\approx \underbrace{\left(\frac{da^i}{C\left(\frac{1-f^i}{1-R^i}\Delta K^i\right)^n}\frac{\left(1-\frac{K^i_{max}}{K_c}\right)^q}{\left(1-\frac{\Delta K^i_{th}}{\Delta K^i}\right)^p}\right)^4}_{I} \tag{C.6}$$

$$+\underbrace{\left(\frac{\partial dN}{\partial K_{max}}\right)^4\mu_4\left(K^i_{max},K^i_{max},K^i_{max},K^i_{max}\right)+4\left(\frac{\partial dN}{\partial K_{max}}\right)^3\left(\frac{\partial dN}{\partial K_{min}}\right)\mu_4\left(K^i_{max},K^i_{max},K^i_{max},K^i_{min}\right)}_{II}$$

$$+\underbrace{6\left(\frac{\partial dN}{\partial K_{max}}\right)^2\left(\frac{\partial dN}{\partial K_{min}}\right)^2\mu_4\left(K^i_{max},K^i_{max},K^i_{min},K^i_{min}\right)}_{II}$$

$$+\underbrace{4\left(\frac{\partial dN}{\partial K_{max}}\right)\left(\frac{\partial dN}{\partial K_{min}}\right)^3\mu_4\left(K^i_{max},K^i_{min},K^i_{min},K^i_{min}\right)+\left(\frac{\partial dN}{\partial K_{min}}\right)^4\mu_4\left(K^i_{min},K^i_{min},K^i_{min},K^i_{min}\right)}_{II}$$

$$+\underbrace{\frac{1}{16}\sum_{j=1}^{d}\sum_{k=1}^{d}\sum_{l=1}^{d}\sum_{m=1}^{d}\sum_{r=1}^{d}\sum_{s=1}^{d}\sum_{t=1}^{d}\sum_{u=1}^{d}g_{,jk}g_{,lm}g_{,rs}g_{,tu}\mu_{jklmrstu}}_{III}+\underbrace{0}_{IV}$$

$$+\underbrace{4g_\mu^3\frac{1}{2}\sum_{j=1}^{d}\sum_{k=1}^{d}g_{,jk}\mu_{jk}}_{V}+\underbrace{4g_\mu\sum_{j=1}^{d}\sum_{k=1}^{d}\sum_{l=1}^{d}g_{,j}g_{,k}g_{,l}\mu_{jkl}}_{VI}$$

$$+\underbrace{4\frac{1}{2}\sum_{j=1}^{d}\sum_{k=1}^{d}\sum_{l=1}^{d}\sum_{m=1}^{d}\sum_{r=1}^{d}g_{,j}g_{,k}g_{,l}g_{,mr}\mu_{jklmr}}_{VII}$$

$$+\underbrace{4g_\mu\frac{1}{8}\sum_{j=1}^{d}\sum_{k=1}^{d}\sum_{l=1}^{d}\sum_{m=1}^{d}\sum_{r=1}^{d}\sum_{s=1}^{d}g_{,jk}g_{,lm}g_{,rs}\mu_{jklmrs}}_{VIII}$$

$$+\underbrace{4\frac{1}{8}\sum_{j=1}^{d}\sum_{k=1}^{d}\sum_{l=1}^{d}\sum_{m=1}^{d}\sum_{r=1}^{d}\sum_{s=1}^{d}\sum_{t=1}^{d}g_{,j}g_{,kl}g_{,mr}g_{,st}\mu_{jklmrst}}_{IX}$$

$$+\underbrace{6g_\mu^2\sum_{j=1}^{d}\sum_{k=1}^{d}g_{,j}g_{,k}\mu_{jk}}_{X}+\underbrace{6g_\mu^2\frac{1}{4}\sum_{j=1}^{d}\sum_{k=1}^{d}\sum_{l=1}^{d}\sum_{m=1}^{d}g_{,jk}g_{,lm}\mu_{jklm}}_{XI}$$

$$+\underbrace{6\frac{1}{4}\sum_{j=1}^{d}\sum_{k=1}^{d}\sum_{l=1}^{d}\sum_{m=1}^{d}\sum_{r=1}^{d}\sum_{s=1}^{d}g_{,j}g_{,k}g_{,lm}g_{,rs}\mu_{jklmrs}}_{XII}+\underbrace{12g_\mu^2\frac{1}{2}\sum_{j=1}^{d}\sum_{k=1}^{d}\sum_{l=1}^{d}g_{,j}g_{,kl}\mu_{jkl}}_{XIII}$$

$$+\underbrace{12g_\mu\frac{1}{2}\sum_{j=1}^{d}\sum_{k=1}^{d}\sum_{l=1}^{d}\sum_{m=1}^{d}g_{,j}g_{,k}g_{,lm}\mu_{jklm}}_{XIV}+\underbrace{12g_\mu\frac{1}{4}\sum_{j=1}^{d}\sum_{k=1}^{d}\sum_{l=1}^{d}\sum_{m=1}^{d}\sum_{r=1}^{d}g_{,j}g_{,kl}g_{,mr}\mu_{jklmr}}_{XV}$$

$$-4\mathrm{E}\left[dN^i\right]\mu_3\left(dN^i,dN^i,dN^i\right)-6\left(\mathrm{E}\left[dN^i\right]\right)^2\mathrm{Var}\left(dN^i\right)-\left(\mathrm{E}\left[dN^i\right]\right)^4$$

Bibliography

[1] *CAF MiiRA - Mercancías - Ejes*. CAF MiiRA. 2022. URL: http://www.cafmiira.com/es/mercancias/ejes_p80.html (visited on 07/03/2022).

[2] *CAF MiiRA - Mercancías - Ejes Montados*. CAF MiiRA. 2022. URL: http://www.cafmiira.com/es/mercancias/ejes-montados_p72.html (visited on 07/03/2022).

[3] *EU Transport in Figures: Statistical Pocketbook 2020*. Directorate-General for Mobility and Transport, European Commission, 2020.

[4] *List of Countries by Rail Transport Network Size*. Wikipedia. 2022. URL: https://en.wikipedia.org/wiki/List_of_countries_by_rail_transport_network_size (visited on 07/03/2022).

[5] *Informe 2019 Observatorio Del Ferrocarril En España*. Ministerio de Transportes, Movilidad y Agenda Urbana, 2019.

[6] R. Smith. 'Fatigue of Railway Axles: A Classic Problem Revisited'. In: *European Structural Integrity Society*. Ed. by M. Fuentes, M. Elices, A. Martín-Meizoso and J. Martínez-Esnaola. Vol. 26. Supplement C vols. Elsevier, 2000. 173–181.

[7] U. Zerbst, M. Schödel and H. T. Beier. Parameters Affecting the Damage Tolerance Behaviour of Railway Axles. *Eng Fract Mech*, 78: 793–809, 2011.

[8] R. A. Smith and S. Hillmansen. A Brief Historical Overview of the Fatigue of Railway Axles. *Proc Inst Mech Eng Part F J Rail Rapid Transit*, 218: 267–277, 2004.

[9] *Bibliotheque nationale de France*. BnF. 2022. URL: https://www.bnf.fr/fr/node (visited on 07/03/2022).

[10] A. Bracciali. Railway Wheelsets: History, Research and Developments. *Int J Railw Tech*, 5: 23–52, 2016.

[11] *European Union Agency for Railways*. ERA. 2021. URL: https://www.era.europa.eu/node_en (visited on 16/11/2021).

[12] *Final Report on the Activities of the Task Force Freight Wagon Maintenance.* ERA Safety Unit Safe Cert Sector, 2010.

[13] W. Schütz. A History of Fatigue. *Eng Fract Mech*, 54: 263–300, 1996.

[14] S. Timoshenko. *History of Strength of Materials.* Dover Publications, 1983.

[15] *EN 13103-1:2017. Railway Applications. Wheelsets and Bogies. Part 1: Design Method for Axles with External Journals.* European Committee for Standardization, 2017.

[16] *EN 13979-1:2020. Railway Applications. Wheelsets and Bogies. Monobloc Wheels. Technical Approval Procedure. Part 1: Forged and Rolled Wheels.* European Committee for Standardization, 2020.

[17] *CEN/TS 13979-2:2011. Railway Applications. Wheelsets and Bogies. Monobloc Wheels. Technical Approval Procedure. Part 2: Cast Wheels.* European Committee for Standardization, 2011.

[18] *EN 13260:2020. Railway Applications. Wheelsets and Bogies. Wheelsets. Product Requirements.* European Committee for Standardization, 2020.

[19] *EN 13261:2020. Railway Applications. Wheelsets and Bogies. Axles. Product Requirements.* European Committee for Standardization, 2020.

[20] *EN 15313:2016. Railway Applications. In-service Wheelset Operation Requirements. In-service and off-Vehicle Wheelset Maintenance.* European Committee for Standardization, 2016.

[21] U. Zerbst, K.-H. Schwalbe and R. A. Ainsworth. '7.01 - An Overview of Failure Assessment Methods in Codes and Standards'. In: *Comprehensive Structural Integrity.* Ed. by I. Milne, R. O. Ritchie and B. Karihaloo. Pergamon, 2003. 1–48.

[22] U. Zerbst et al. Safe Life and Damage Tolerance Aspects of Railway Axles - A Review. *Eng Fract Mech*, 98: 214–271, 2013.

[23] V. Grubisic and G. Fischer. Procedure for Reliable Durability Validation of Train Axles. *Materwiss Werksttech*, 37: 973–982, 2006.

[24] C. M. Sonsino. Course of SN-curves Especially in the High-Cycle Fatigue Regime with Regard to Component Design and Safety. *Int J Fatigue*, 29: 2246–2258, 2007.

[25] S. Beretta and D. Regazzi. Probabilistic Fatigue Assessment for Railway Axles and Derivation of a Simple Format for Damage Calculations. *Int J Fatigue*, 86: 13–23, 2016.

[26] E. Haibach. *Analytical Strength Assessment of Components in Mechanical Engineering: FKM-Guideline.* VDMA, 2003.

[27] M. A. Miner. Cumulative Damage in Fatigue. *J of Appl Mech*, 12: A159–A164, 2021.

[28] R. Jones. Fatigue Crack Growth and Damage Tolerance. *Fatigue Fract Eng Mater Struct*, 37: 463–483, 2014.

[29] R. Morgan, K. Gonzales, E. Smith and B. Smith. *Remotely Detecting Cracks in Moving Freight Railcar Axles. Safety IDEA Project 08, Final Report*. 2006.

[30] R. W. Ngigi, C. Pislaru, A. Ball and F. Gu. Modern Techniques for Condition Monitoring of Railway Vehicle Dynamics. *J. Phys.: Conf. Ser.*, 364: 012016, 2012.

[31] W. Verhelst. *D6.1.1 Report on Compensated Resonance Inspection Method.* In: D6.1 - Development of compensated resonance inspection prototype for wheelsets. EU project WIDEM: Wheelset integrated design and effective maintenance, 2008, 3–59.

[32] J. Prager and M. Grzeszkowski. 'Online-Überwachung des Bauteilzustandes von Eisenbahn-Radsatzwellen mitels geführter Ultraschallwellen'. In: DACH-Jahrestagung 2015. Deutsche Gesellschaft für Zerstörungsfreie Prüfung, 2015. Poster 61, 1–2.

[33] P. Miedlar, A. Berens, A. Gunderson and J. Gallagher. Analysis and Support Initiative for Structural Technology (ASIST) Delivery Order 0016: USAF Damage Tolerant Design Handbook: Guidelines For the Analysis and Design of Damage Tolerant Aircraft Structures. 835, 2002.

[34] T. L. Anderson. *Fracture Mechanics: Fundamentals and Applications*. CRC press, 2017.

[35] A. A. Griffith. The Phenomena of Rupture and Flow in Solids. *Phil. Trans. R. Soc. Lond. A*, 221: 163–198, 1921.

[36] G. R. Irwin. *Onset of Fast Crack Propagation in High Strength Steel and Aluminum Alloys*. Naval Research Lab Washington DC, 1956.

[37] G. R. Irwin. Analysis of Stresses and Strains Near the End of a Crack Traversing a Plate. *J of Appl Mech*, 24: 361–364, 1957.

[38] H. Tada, P. C. Paris and G. R. Irwin. *The Stress Analysis of Cracks Handbook*. Vol. 34. ASME, 1973.

[39] A. F. Bower. *Applied Mechanics of Solids*. CRC press, 2009.

[40] I. Raju and J. Newman. Stress-Intensity Factors for a Wide Range of Semi-Elliptical Surface Cracks in Finite-Thickness Plates. *Eng Fract Mech*, 11: 817–829, 1979.

[41] M. Shiratori and T. Miyoshi. Analysis of Stress Intensity Factors for Surface Cracks Subjected to Arbitrarily Distributed Stresses. *Comput. Mech.*, 1027–1032, 1986.

[42] *ASTM E647 - 13a. Standard Test Method for Measurement of Fatigue Crack Growth Rates.* ASTM International, 2014.

[43] G. Shen and G. Glinka. Weight Functions for a Surface Semi-Elliptical Crack in a Finite Thickness Plate. *Theor Appl Fract Mech*, 15: 247–255, 1991.

[44] X. Wang and S. B. Lambert. Stress Intensity Factors for Low Aspect Ratio Semi-Elliptical Surface Cracks in Finite-Thickness Plates Subjected to Nonuniform Stresses. *Eng Fract Mech*, 51: 517–532, 1995.

[45] X. Wang and S. B. Lambert. Stress Intensity Factors and Weight Functions for High Aspect Ratio Semi-Elliptical Surface Cracks in Finite-Thickness Plates. *Eng Fract Mech*, 57: 13–24, 1997.

[46] A. Carpinteri, R. Brighenti and A. Spagnoli. Surface Flaws in Cylindrical Shafts under Rotary Bending. *Fatigue Fract Eng Mater Struct*, 21: 1027–1035, 1998.

[47] A. Carpinteri, R. Brighenti and A. Spagnoli. Fatigue Growth Simulation of Part-through Flaws in Thick-Walled Pipes under Rotary Bending. *Int J Fatigue*, 22: 1–9, 2000.

[48] A. Carpinteri, R. Brighenti and S. Vantadori. Surface Cracks in Notched Round Bars under Cyclic Tension and Bending. *Int J Fatigue*, 28: 251–260, 2006.

[49] M. Madia, S. Beretta and U. Zerbst. An Investigation on the Influence of Rotary Bending and Press Fitting on Stress Intensity Factors and Fatigue Crack Growth in Railway Axles. *Eng Fract Mech*, 75: 1906–1920, 2008.

[50] M. Madia, S. Beretta, M. Schödel, U. Zerbst, M. Luke and I. Varfolomeev. Stress Intensity Factor Solutions for Cracks in Railway Axles. *Eng Fract Mech*, 78: 764–792, 2011.

[51] *ASTM E399 - 12. Standard Test Method for Linear-Elastic Plane-Strain Fracture Toughness KIc of Metallic Materials.* ASTM International, 2014.

[52] M. Sánchez, C. Mallor, M. Canales, S. Calvo and J. L. Núñez. Digital Image Correlation Parameters Optimized for the Characterization of Fatigue Crack Growth Life. *Measurement*, 174: 109082, 2021.

[53] I. Varfolomeev, M. Luke and M. Burdack. Effect of Specimen Geometry on Fatigue Crack Growth Rates for the Railway Axle Material EA4T. *Eng Fract Mech*, 78: 742–753, 2011.

[54] S. Beretta, A. Ghidini and F. Lombardo. Fracture Mechanics and Scale Effects in the Fatigue of Railway Axles. *Eng Fract Mech*, 72: 195–208, 2005.

[55] S. Beretta and M. Carboni. Experiments and Stochastic Model for Propagation Lifetime of Railway Axles. *Eng Fract Mech*, 73: 2627–2641, 2006.

[56] U. Zerbst, K. Mädler and H. Hintze. Fracture Mechanics in Railway Applications – an Overview. *Eng Fract Mech*, 72: 163–194, 2005.

[57] P. C. Paris, M. P. Gomez and W. E. Anderson. A Rational Analytic Theory of Fatigue. *The Trend in Engineering*, 13: 9–14, 1961.

[58] P. C. Paris and F. Erdogan. A Critical Analysis of Crack Propagation Laws. *J Basic Eng*, 85: 528–533, 1963.

[59] R. J. Allen, G. S. Booth and T. Jutla. A Review of Fatigue Crack Growth Characterisation by Linear Elastic Fracture Mechanics (LEFM). Part II - Advisory Documents and Applications within National Standards. *Fatigue Fract Eng Mater Struct*, 11: 71–108, 1988.

[60] R. G. Forman, V. E. Kearney and R. M. Engle. Numerical Analysis of Crack Propagation in Cyclic-Loaded Structures. *J Basic Eng*, 89: 459–463, 1967.

[61] A. J. McEvily and J. Groeger. 'On the Threshold for Fatigue Crack Growth'. In: ICF4, Waterloo. 1977.

[62] K. Walker. 'The Effect of Stress Ratio during Crack Propagation and Fatigue for 2024-T3 and 7075-T6 Aluminum'. In: *Effects of Environment and Complex Load History on Fatigue Life*. ASTM International, 1970.

[63] W. Elber. 'The Significance of Fatigue Crack Closure'. In: *Damage Tolerance in Aircraft Structures*. ASTM International, 1971.

[64] R. G. Forman and S. R. Mettu. Behavior of Surface and Corner Cracks Subjected to Tensile and Bending Loads in Ti-6Al-4V Alloy. *ASTM STP 1131 Am Soc Test Mater Phila PA*, 519–546, 1990.

[65] *NASGRO. Fracture Mechanics and Fatigue Crack Growth Analysis Software. Reference Manual*. Southwest Research Institute, 2002.

[66] U. Zerbst, M. Vormwald, C. Andersch, K. Mädler and M. Pfuff. The Development of a Damage Tolerance Concept for Railway Components and Its Demonstration for a Railway Axle. *Eng Fract Mech*, 72: 209–239, 2005.

[67] S. Beretta and A. Villa. A RV Approach for the Analysis of Fatigue Crack Growth with NASGRO Equation. *4th Int ASRANAT Colloq*, 1–7, 2008.

[68] S. Cantini, S. Cervello and R. Gallo. *A Modern Approach to Wheelset Maintenance Plan Optimisation*. Vol. 9. LRS-techno. Lucchini RS, 2016.

[69] R. Gallo, S. Cantini and D. Minini. A New Wheelset Maintenance Concept. *World Congress on Railway Research*, 9, 2013.

[70] J. A. Bea. *Simulación Del Crecimiento de Grietas Por Fatiga Aleatoria Mediante Elementos Probabilistas.* PhD thesis. Universidad de Zaragoza, 1997.

[71] J. L. Núñez. *Análisis Del Fenómeno de La Fatiga En Metales En Etapa de Nucleación Mediante La Utilización de Modelos Estadísticos de Daño Acumulado y Elementos Finitos Probabilistas.* PhD thesis. Universidad de Zaragoza, 2003.

[72] J. Grasa. *Métodos Probabilistas En Mecánica de Sólidos Deformables. Aplicaciones En Biomecánica.* PhD thesis. Universidad de Zaragoza, 2006.

[73] S. Calvo. *Determinación de La Probabilidad de Fallo En Componentes Métalicos Sometidos a Estados Multiaxiales de Tensión Mediante La Utilización de Elementos Finitos Probabilistas y Modelos Estadísticos de Daño Acumulado.* PhD thesis. Universidad de Zaragoza, 2008.

[74] M. Prados-Privado. *Una nueva aproximación al análisis de la fatiga en implantología dental basado en cadenas de Markov*. PhD thesis. Universidad de Zaragoza, 2017.

[75] P. S. Laplace. *Essai Philosophique Sur Les Probabilités*. Paris: Courcier, 1814.

[76] M. Mayer. *Die Sicherheit der Bauwerke und ihre Berechnung nach Grenzkräften anstatt nach zulässigen Spannungen.* Berlin: Springer, 1926.

[77] M. Mayer. *La Seguridad En Las Construcciones y Su Cálculo Aplicando Los Esfuerzos Límite En Lugar de Las Tensiones Admisibles = Safety in Constructional Works and Its Design According to Limit States Instead of Permissible Stresses.* Madrid: INTEMAC, 1975.

[78] D. A. Virkler, B. M. Hillberry and P. K. Goel. The Statistical Nature of Fatigue Crack Propagation. *J Eng Mater Technol*, 101: 148–153, 1979.

[79] K. Ortiz and A. S. Kiremidjian. Stochastic Modeling of Fatigue Crack Growth. *Eng Fract Mech*, 29: 317–334, 1988.

[80] S. Cervello. Fatigue Properties of Railway Axles: New Results of Full-Scale Specimens from Euraxles Project. *Int J Fatigue*, 86: 2–12, 2016.

[81] M. Novosad, R. Fajkoš, B. Řeha and R. Řezníček. Fatigue Tests of Railway Axles. *Proc Eng*, 2: 2259–2268, 2010.

[82] S. Beretta and M. Carboni. Variable Amplitude Fatigue Crack Growth in a Mild Steel for Railway Axles: Experiments and Predictive Models. *Eng Fract Mech*, 78: 848–862, 2011.

[83] K. Mädler, T. Geburtig and D. Ullrich. An Experimental Approach to Determining the Residual Lifetimes of Wheelset Axles on a Full-Scale Wheel-Rail Roller Test Rig. *Int J Fatigue*, 86: 58–63, 2016.

[84] *UIC B 169 RP 36:2013-12 Defect Tolerance Concept (DTC) Permitted Defects and Surface Properties for Axles under Maintenance.* UIC Standard, 2013.

[85] P. Pokorný, L. Náhlík and P. Hutař. Comparison of Different Load Spectra on Residual Fatigue Lifetime of Railway Axle. *Proc Eng*, 74: 313–316, 2014.

[86] P. Pokorný, P. Hutař and L. Náhlík. Residual Fatigue Lifetime Estimation of Railway Axles for Various Loading Spectra. *Theor Appl Fract Mech*, 82: 25–32, 2016.

[87] M. Traupe and A. Landaberea. EURAXLES - A Global Approach for Design, Production and Maintenance of Railway Axles: WP2 - Development of Numerical Models for the Analysis of Railway Axles. *Materwiss Werksttech*, 48: 687–698, 2017.

[88] W. S. Johnson and B. M. Hillberry. *Probabilistic Aspects of Life Prediction*. 1450. ASTM International, 2004.

[89] J. Maierhofer, H.-P. Gänser, D. Simunek, M. Leitner, R. Pippan and M. Luke. Fatigue Crack Growth Model Including Load Sequence Effects - Model Development and Calibration for Railway Axle Steels. *Int J Fatigue*, 105377, 2019.

[90] L. Wei. *D7.1.8 Results of Probabilistic Analysis*. In: D7.1 - Procedure to define NDT periodicity as function of vehicle service profile. EU project WIDEM: Wheelset integrated design and effective maintenance, 2008, 70–78.

[91] C. Annis. 'Probabilistic Life Prediction Isn't as Easy as It Looks'. In: *Probabilistic Aspects of Life Prediction*. Ed. by W. S. Johnson and B. M. Hillberry. 1450. ASTM International, 2004.

[92] D. S. Paolino and M. P. Cavatorta. Sigmoidal Crack Growth Rate Curve: Statistical Modelling and Applications. *Fatigue Fract Eng Mater Struct*, 36: 316–326, 2013.

[93] S. Beretta and M. Carboni. *D5.1.3 Design Procedure for Axles.* In: D5.1 - Endurance design procedure of wheelsets based on reliable load spectra and reliable Wohler curves. EU project WIDEM: Wheelset integrated design and effective maintenance, 2008, 21–39.

[94] M. Sander and H. Richard. Investigations on Fatigue Crack Growth under Variable Amplitude Loading in Wheelset Axles. *Eng Fract Mech*, 78: 754–763, 2011.

[95] M. Luke, I. Varfolomeev, K. Lütkepohl and A. Esderts. Fatigue Crack Growth in Railway Axles: Assessment Concept and Validation Tests. *Eng Fract Mech*, 78: 714–730, 2011.

[96] S. Beretta, M. Carboni, S. Cantini and A. Ghidini. Application of Fatigue Crack Growth Algorithms to Railway Axles and Comparison of Two Steel Grades. *Proc Inst Mech Eng Part F J Rail Rapid Transit*, 218: 317–326, 2004.

[97] A. Watson and K. Timmis. A Method of Estimating Railway Axle Stress Spectra. *Eng Fract Mech*, 78: 836–847, 2011.

[98] D. Regazzi, S. Beretta and M. Carboni. An Investigation about the Influence of Deep Rolling on Fatigue Crack Growth in Railway Axles Made of a Medium Strength Steel. *Eng Fract Mech*, 131: 587–601, 2014.

[99] M. Traupe, S. Jenne, K. Lütkepohl and I. Varfolomeev. Experimental Validation of Inspection Intervals for Railway Axles Accompanying the Engineering Process. *Int J Fatigue*, 86: 44–51, 2016.

[100] A. S. Watson. 'Implications of Impact Damage on the Structural Integrity of Axles'. Fatigue Strength and Fatigue Life of Railway Axles. BAM - Federal Institute for Materials Research and Testing (Berlin). 2010.

[101] N. Gravier, J. Viet and A. Leluan. Predicting the Life of Railway Vehicle Axles. *Proceedings of the 12th International Wheelset Congress*, 133–146, 1998.

[102] S. Cantini and S. Beretta. *Structural Reliability Assessment of Railway Axles*. Vol. 4. LRS-Techno. Lucchini RS, 2011.

[103] *Handbook of Service Faults*. LRS-Techno. Lucchini RS, 2016.

[104] S. Beretta, M. Carboni, A. L. Conte and E. Palermo. An Investigation of the Effects of Corrosion on the Fatigue Strength of AlN Axle Steel. *Proc Inst Mech Eng Part F J Rail Rapid Transit*, 222: 129–143, 2008.

[105] N. Gravier, J. Viet and A. Leluan. Prédiction de La Durée de Vie Des Essieux-Axes Ferroviaires. *Revue générale des chemins de fer*, 1999: 33–62, 1999.

[106] J. A. Benyon and A. S. Watson. 'The Use of Monte-Carlo Analysis to Increase Axle Inspection Interval'. In: *Proceedings of the 13th International Wheelset Congress*. Rome, 2001. 17–21.

[107] A. Watson, M. Burstow and A. James. *Modern Methods of Axle Assesment*. The Arup Campus, 2003.

[108] U. Zerbst, C. Klinger and D. Klingbeil. Structural Assessment of Railway Axles - A Critical Review. *Eng Fail Anal*, 35: 54–65, 2013.

[109] M. Carboni and S. Beretta. Effect of Probability of Detection upon the Definition of Inspection Intervals for Railway Axles. *Proc Inst Mech Eng Part F J Rail Rapid Transit*, 221: 409–417, 2007.

[110] C. R. Sundararajan. *Probabilistic Structural Mechanics Handbook: Theory and Industrial Applications*. Springer, 2012.

[111] V. Giannella. Stochastic Approach to Fatigue Crack-Growth Simulation for a Railway Axle under Input Data Variability. *Int J Fatigue*, 144: 106044, 2021.

[112] K. Pearson. Asymmetrical Frequency Curves. *Nature*, 48: 615–616, 1893.

[113] S. Calvo, M. Canales, C. Gómez, J. R. Valdés and J. L. Núñez. Probabilistic Formulation of the Multiaxial Fatigue Damage of Liu. *Int J Fatigue*, 33: 460–465, 2011.

[114] Z. Qiu and Z. Zhang. Fatigue Crack Propagation Analysis in Structures with Random Parameters Based on Polynomial Chaos Expansion Method. *Theor Appl Fract Mech*, 105: 102404, 2020.

[115] S. Rahman and D. Wei. A Univariate Approximation at Most Probable Point for Higher-Order Reliability Analysis. *Int J Solids Struct*, 43: 2820–2839, 2006.

[116] X. Wang. *Frequentist and Bayesian Approaches for Probabilistic Fatigue Life Assessment of High-Speed Train Using in-Service Monitoring Data*. PhD thesis. Hong Kong Polytechnic University, 2018.

[117] N. O'Dowd, R. Madarshahian, M. Leung, J. Achenbach and M. Todd. A Probabilistic Estimation Approach for the Failure Forecast Method Using Bayesian Inference. *Int J Fatigue*, 142: 105943, 2021.

[118] *A European Green Deal*. European Commission. 2019. URL: https://ec.europa.eu/info/strategy/priorities-2019-2024/european-green-deal_en (visited on 16/11/2021).

[119] *Delivering the European Green Deal*. European Commission. 2021. URL: https://ec.europa.eu/info/strategy/priorities-2019-2024/european-green-deal/delivering-european-green-deal_en (visited on 16/11/2021).

[120] *European Year of Rail*. European Commission. 2021. URL: https://europa.eu/year-of-rail/index_en (visited on 16/11/2021).

[121] *Shift2Rail*. Shift2Rail. 2021. URL: https://shift2rail.org:443/ (visited on 16/11/2021).

[122] *Europe's Rail Joint Undertaking*. Shift2Rail. 2021. URL: https://shift2rail.org:443/shift2rail-successor/ (visited on 16/11/2021).

[123] *EU Project WIDEM: Wheelset Integrated Design and Effective Maintenance.* 6th Framework Programme, Project ID: 516196. 2005.

[124] *EU Project EURAXLES: Minimizing the Risk of Fatigue Failure of Railway Axles.* 7th Framework Programme, Project ID: 265706. 2010.

[125] *EU Project WOLAXIM: Whole Life Rail Axle Assessment and Improvement.* 7th Framework Programme, Project ID: 262242. 2010.

[126] *EU Project SUSTRAIL: The Sustainable Freight Railway: Designing the Freight Vehicle Track System for Higher Delivered Tonnage with Improved Availability at Reduced Cost.* 7th Framework Programme, Project ID: 730617. 2011.

[127] *EU Project FR8RAIL: Development of Functional Requirements for Sustainable and Attractive European Rail Freight.* H2020-EU, Project ID: 730617. 2016.

[128] C. A. Cornell. A Probability-Based Structural Code. *ACI J Proc*, 66: 974–985, 1969.

[129] C. A. Cornell. Structural Safety Specifications Based on Second-Moment Reliability Analysis. *IABSE Symposium on Concepts of Safety of Structures and Methods of Design*, 1969.

[130] S. C. Wu, Z. W. Xu, G. Z. Kang and W. F. He. Probabilistic Fatigue Assessment for High-Speed Railway Axles Due to Foreign Object Damages. *Int J Fatigue*, 117: 90–100, 2018.

[131] M. Akama and H. Ishizuka. Reliability Analysis of Shinkhansen Vehicle Axle Using Probabilistic Fracture Mechanics. *JSME Int J Ser Mech Mater Eng*, 38(3): 378–383, 1995.

[132] J. A. Bea, M. Doblaré and L. Gracia. Evaluation of the Probability Distribution of Crack Propagation Life in Metal Fatigue by Means of Probabilistic Finite Element Method and B-models. *Eng Fract Mech*, 63: 675–711, 1999.

[133] S. Hillmansen and R. A. Smith. The Management of Fatigue Crack Growth in Railway Axles. *Proc Inst Mech Eng Part F J Rail Rapid Transit*, 218: 327–336, 2004.

[134] Y. J. Hong, J. Xing and J. B. Wang. A Second-Order Third-Moment Method for Calculating the Reliability of Fatigue. *Int J Press Vessel Pip*, 76: 567–570, 1999.

[135] L. Náhlík, P. Pokorný, M. Ševčík, R. Fajkoš, P. Matušek and P. Hutař. Fatigue Lifetime Estimation of Railway Axles. *Eng Fail Anal*, 73: 139–157, 2017.

[136] L. Wang, J. Liang, Y. Yang and Y. Zheng. Time-Dependent Reliability Assessment of Fatigue Crack Growth Modeling Based on Perturbation Series Expansions and Interval Mathematics. *Theor Appl Fract Mech*, 95: 104–118, 2018.

[137] O. Yasniy, Y. Lapusta, Y. Pyndus, A. Sorochak and V. Yasniy. Assessment of Lifetime of Railway Axle. *Int J Fatigue*, 50: 40–46, 2013.

[138] S.-P. Zhu, Q. Liu and H.-Z. Huang. Probabilistic Modeling of Damage Accumulation for Fatigue Reliability Analysis. *Procedia Struct Integr*, 4: 3–10, 2017.

[139] C. Mallor, S. Calvo, J. L. Núñez, R. Rodríguez-Barrachina and A. Landaberea. Full Second-Order Approach for Expected Value and Variance Prediction of Probabilistic Fatigue Crack Growth Life. *Int J Fatigue*, 133: 105454, 2020.

[140] M. Corbetta, C. Sbarufatti, A. Manes and M. Giglio. On Dynamic State-Space Models for Fatigue-Induced Structural Degradation. *Int J Fatigue*, 61: 202–219, 2014.

[141] K. Pearson. X. Contributions to the Mathematical Theory of Evolution. II. Skew Variation in Homogeneous Material. *Phil. Trans. R. Soc. Lond. A*, 186: 343–414, 1895.

[142] D. Broek. *The Practical Use of Fracture Mechanics*. Kluwer Academic Publishers, 1989.

[143] F. Cocheteux and T. Pouillart. Design, Manufacture and Maintenance of Wheelset at SNCF. *Int J Railw*, 2: 8–17, 2009.

[144] M. Carboni and S. Cantini. Advanced Ultrasonic "Probability of Detection" Curves for Designing in-Service Inspection Intervals. *Int J Fatigue*, 86: 77–87, 2016.

[145] C. Mallor, S. Calvo, J. L. Núñez, R. Rodríguez-Barrachina and A. Landaberea. Uncertainty Propagation Using the Full Second-Order Approach for Probabilistic Fatigue Crack Growth Life. *International Journal of Numerical Methods for Calculation and Design in Engineering (RIMNI)*, 36: 37, 2020.

[146] C. Mallor, S. Calvo, J. L. Núñez, R. Rodríguez-Barrachina and A. Landaberea. Propagation of Uncertainty in Fatigue Crack Growth for Probabilistic Life Estimation. *Procedia Struct Integr*, 28: 619–626, 2020.

[147] C. Mallor, S. Calvo, J. L. Núñez, R. Rodríguez-Barrachina and A. Landaberea. On the Use of Probabilistic Fatigue Life Estimation in Defining Inspection Intervals for Railway Axles. *Procedia Struct Integr*, 33: 391–401, 2021.

[148] C. Mallor, S. Calvo, J. L. Núñez, R. Rodríguez-Barrachina and A. Landaberea. A Probabilistic Fatigue Crack Growth Life Approach to the Definition of Inspection Intervals for Railway Axles. *Frattura ed Integrità Strutturale - Fracture and Structural Integrity*, 59: 359–373, 2022.

[149] N. L. Johnson, S. Kotz and N. Balakrishnan. *Continuous Univariate Distributions*. Vol. 1–2. Wiley-Interscience, 1994.

[150] M. El Haddad, T. Topper and K. Smith. Prediction of Non Propagating Cracks. *Eng Fract Mech*, 11: 573–584, 1979.

[151] *ABAQUS 2016 Documentation Collection*. 2016.

[152] P. R. Garvey, S. A. Book and R. P. Covert. *PROBABILITY METHODS FOR COST UNCERTAINTY ANALYSIS: A Systems Engineering Perspective*. CRC Press. 2016.

[153] R. D'Agostino and E. S. Pearson. Tests for Departure from Normality. Empirical Results for the Distributions of B2 and B1,1/2. *Biometrika*, 60: 613–622, 1973.

[154] A. Haldar and S. Mahadevan. *Probability, Reliability, and Statistical Methods in Engineering Design*. John Wiley, 2000.

[155] *EN 1990:2002. Eurocode. Basis of Structural Design*. European committee for standardization, 2002.

[156] *CEN/TR 17469:2020. Railway Applications. Axle Design Method*. European Committee for Standardization, 2020.

[157] J. J. Thomas, G. Perroud, A. Bignonnet and D. Monnet. 'Fatigue Design and Reliability in the Automotive Industry'. In: *European Structural Integrity Society*. Ed. by G. Marquis and J. Solin. Vol. 23. Fatigue Design and Reliability. Elsevier, 1999. 1–11.

[158] T. M. L. Nguyen-Tajan and X. Lorang. EURAXLES - A Global Approach for Design, Production and Maintenance of Railway Axles: WP1 - Advances in Fatigue Load Analysis and Reliability Assessment of Railway Axles. *Materwiss Werksttech*, 48: 666–686, 2017.

[159] *Commission Implementing Regulation (EU) No 402/2013 of 30 April 2013 on the Common Safety Method for Risk Evaluation and Assessment and Repealing Regulation (EC) No 352/2009*. Official Journal of the European Union, 2013.